Journal of Healthcare Engineering

Intelligent Fog/Edge Computing-Assisted Healthcare Informatics

Lead Guest Editor: Shengrong Gong
Guest Editors: Xiaoqing Gu and Maozhen Li

Intelligent Fog/Edge Computing-Assisted Healthcare Informatics

Journal of Healthcare Engineering

Intelligent Fog/Edge Computing-Assisted Healthcare Informatics

Lead Guest Editor: Shengrong Gong
Guest Editors: Xiaoqing Gu and Maozhen Li

Contents

Retracted: Comparison of Two Surgical Approaches to Supination-External Rotation-Type Ankle Fractures
Journal of Healthcare Engineering
Retraction (1 page), Article ID 9840241, Volume 2023 (2023)

Retracted: A Novel Method of Clinical Nursing under the Medical Internet of Things Technology
Journal of Healthcare Engineering
Retraction (1 page), Article ID 9835083, Volume 2023 (2023)

Retracted: Analysis on the Influence of Students' Health Quality Based on Intelligent Optimization of Sports Facilities and Equipment
Journal of Healthcare Engineering
Retraction (1 page), Article ID 9810863, Volume 2023 (2023)

Retracted: To Analyze the Influencing Factors of Senile Coronary Heart Disease Patients Complicated with Frailty Syndrome
Journal of Healthcare Engineering
Retraction (1 page), Article ID 9785980, Volume 2023 (2023)

Retracted: The Investigation of Pulmonary Function Changes of COVID-19 Patients in Three Months
Journal of Healthcare Engineering
Retraction (1 page), Article ID 9757682, Volume 2023 (2023)

Retracted: Controlled Hypotension Combined with Femoral Nerve Block for Knee Replacement without Tourniquet
Journal of Healthcare Engineering
Retraction (1 page), Article ID 9826214, Volume 2023 (2023)

[Retracted] Comparison of Two Surgical Approaches to Supination-External Rotation-Type Ankle Fractures
Bingqian Chen, Zhengfei Wang, Zhi Chen, Xiaohong Qu, Xiaowen Fang, Xuesong Wang, and Guoxiu Ke
Research Article (8 pages), Article ID 7726726, Volume 2022 (2022)

[Retracted] Deep Scale-Variant Network for Femur Trochanteric Fracture Classification with HP Loss
Yuxiang Kang, Zhipeng Ren, Yinguang Zhang, Aiming Zhang, Weizhe Xu, Guokai Zhang, and Qiang Dong
Research Article (7 pages), Article ID 1560438, Volume 2022 (2022)

[Retracted] The Investigation of Pulmonary Function Changes of COVID-19 Patients in Three Months
Lingyan Ye, Guifei Yao, Shuangxiang Lin, Yicheng Fang, Xi Chen, Liangxing Wang, and Susu He
Research Article (6 pages), Article ID 9028835, Volume 2022 (2022)

Contents

[Retracted] Heart Disease Prediction Based on the Embedded Feature Selection Method and Deep Neural Network
Dengqing Zhang, Yunyi Chen, Yuxuan Chen, Shengyi Ye, Wenyu Cai, Junxue Jiang, Yechuan Xu, Gongfeng Zheng, and Ming Chen
Research Article (9 pages), Article ID 6260022, Volume 2021 (2021)

[Retracted] An ECG Heartbeat Classification Method Based on Deep Convolutional Neural Network
Dengqing Zhang, Yuxuan Chen, Yunyi Chen, Shengyi Ye, Wenyu Cai, and Ming Chen
Research Article (9 pages), Article ID 7167891, Volume 2021 (2021)

[Retracted] The Evaluation Model of College Students' Mental Health in the Environment of Independent Entrepreneurship Using Neural Network Technology
Xiangmin Meng, Jie Zhang, and Guoyan Ren
Research Article (9 pages), Article ID 4379623, Volume 2021 (2021)

[Retracted] Hippocampus Segmentation Method Based on Subspace Patch-Sparsity Clustering in Noisy Brain MRI
Xiaogang Ren, Yue Wu, and Zhiying Cao
Research Article (10 pages), Article ID 3937222, Volume 2021 (2021)

A PLA2R-IgG4 Antibody-Based Predictive Model for Assessing Risk Stratification of Idiopathic Membranous Nephropathy
Xiaobin Liu, Jing Xue, Xiaoyi Guo, Yijie Ding, Yi Zhang, Xiran Zhang, Yiqing Huang, Biao Huang, Zhigang Hu, Guoyuan Lu, and Liang Wang
Research Article (6 pages), Article ID 1521013, Volume 2021 (2021)

Hindawi
Journal of Healthcare Engineering
Volume 2023, Article ID 9895710, 1 page
https://doi.org/10.1155/2023/9895710

Retraction

Retracted: Deep Scale-Variant Network for Femur Trochanteric Fracture Classification with HP Loss

Journal of Healthcare Engineering

Received 5 December 2023; Accepted 5 December 2023; Published 6 December 2023

This article has been retracted by Hindawi, as publisher, following an investigation undertaken by the publisher [1]. This investigation has uncovered evidence of systematic manipulation of the publication and peer-review process. We cannot, therefore, vouch for the reliability or integrity of this article.

Please note that this notice is intended solely to alert readers that the peer-review process of this article has been compromised.

Wiley and Hindawi regret that the usual quality checks did not identify these issues before publication and have since put additional measures in place to safeguard research integrity.

We wish to credit our Research Integrity and Research Publishing teams and anonymous and named external researchers and research integrity experts for contributing to this investigation.

The corresponding author, as the representative of all authors, has been given the opportunity to register their agreement or disagreement to this retraction. We have kept a record of any response received.

References

[1] Y. Kang, Z. Ren, Y. Zhang et al., "Deep Scale-Variant Network for Femur Trochanteric Fracture Classification with HP Loss," *Journal of Healthcare Engineering*, vol. 2022, Article ID 1560438, 7 pages, 2022.

Hindawi
Journal of Healthcare Engineering
Volume 2023, Article ID 9873297, 1 page
https://doi.org/10.1155/2023/9873297

Retraction

Retracted: Hippocampus Segmentation Method Based on Subspace Patch-Sparsity Clustering in Noisy Brain MRI

Journal of Healthcare Engineering

Received 5 December 2023; Accepted 5 December 2023; Published 6 December 2023

This article has been retracted by Hindawi, as publisher, following an investigation undertaken by the publisher [1]. This investigation has uncovered evidence of systematic manipulation of the publication and peer-review process. We cannot, therefore, vouch for the reliability or integrity of this article.

Please note that this notice is intended solely to alert readers that the peer-review process of this article has been compromised.

Wiley and Hindawi regret that the usual quality checks did not identify these issues before publication and have since put additional measures in place to safeguard research integrity.

We wish to credit our Research Integrity and Research Publishing teams and anonymous and named external researchers and research integrity experts for contributing to this investigation.

The corresponding author, as the representative of all authors, has been given the opportunity to register their agreement or disagreement to this retraction. We have kept a record of any response received.

References

[1] X. Ren, Y. Wu, and Z. Cao, "Hippocampus Segmentation Method Based on Subspace Patch-Sparsity Clustering in Noisy Brain MRI," *Journal of Healthcare Engineering*, vol. 2021, Article ID 3937222, 10 pages, 2021.

Hindawi
Journal of Healthcare Engineering
Volume 2023, Article ID 9845616, 1 page
https://doi.org/10.1155/2023/9845616

Retraction

Retracted: Heart Disease Prediction Based on the Embedded Feature Selection Method and Deep Neural Network

Journal of Healthcare Engineering

Received 5 December 2023; Accepted 5 December 2023; Published 6 December 2023

This article has been retracted by Hindawi, as publisher, following an investigation undertaken by the publisher [1]. This investigation has uncovered evidence of systematic manipulation of the publication and peer-review process. We cannot, therefore, vouch for the reliability or integrity of this article.

Please note that this notice is intended solely to alert readers that the peer-review process of this article has been compromised.

Wiley and Hindawi regret that the usual quality checks did not identify these issues before publication and have since put additional measures in place to safeguard research integrity.

We wish to credit our Research Integrity and Research Publishing teams and anonymous and named external researchers and research integrity experts for contributing to this investigation.

The corresponding author, as the representative of all authors, has been given the opportunity to register their agreement or disagreement to this retraction. We have kept a record of any response received.

References

[1] D. Zhang, Y. Chen, Y. Chen et al., "Heart Disease Prediction Based on the Embedded Feature Selection Method and Deep Neural Network," *Journal of Healthcare Engineering*, vol. 2021, Article ID 6260022, 9 pages, 2021.

Hindawi
Journal of Healthcare Engineering
Volume 2023, Article ID 9836413, 1 page
https://doi.org/10.1155/2023/9836413

Retraction

Retracted: An ECG Heartbeat Classification Method Based on Deep Convolutional Neural Network

Journal of Healthcare Engineering

Received 5 December 2023; Accepted 5 December 2023; Published 6 December 2023

This article has been retracted by Hindawi, as publisher, following an investigation undertaken by the publisher [1]. This investigation has uncovered evidence of systematic manipulation of the publication and peer-review process. We cannot, therefore, vouch for the reliability or integrity of this article.

Please note that this notice is intended solely to alert readers that the peer-review process of this article has been compromised.

Wiley and Hindawi regret that the usual quality checks did not identify these issues before publication and have since put additional measures in place to safeguard research integrity.

We wish to credit our Research Integrity and Research Publishing teams and anonymous and named external researchers and research integrity experts for contributing to this investigation.

The corresponding author, as the representative of all authors, has been given the opportunity to register their agreement or disagreement to this retraction. We have kept a record of any response received.

References

[1] D. Zhang, Y. Chen, Y. Chen, S. Ye, W. Cai, and M. Chen, "An ECG Heartbeat Classification Method Based on Deep Convolutional Neural Network," *Journal of Healthcare Engineering*, vol. 2021, Article ID 7167891, 9 pages, 2021.

Hindawi
Journal of Healthcare Engineering
Volume 2023, Article ID 9875815, 1 page
https://doi.org/10.1155/2023/9875815

Retraction

Retracted: The Evaluation Model of College Students' Mental Health in the Environment of Independent Entrepreneurship Using Neural Network Technology

Journal of Healthcare Engineering

Received 10 October 2023; Accepted 10 October 2023; Published 11 October 2023

This article has been retracted by Hindawi following an investigation undertaken by the publisher [1]. This investigation has uncovered evidence of one or more of the following indicators of systematic manipulation of the publication process:

(1) Discrepancies in scope
(2) Discrepancies in the description of the research reported
(3) Discrepancies between the availability of data and the research described
(4) Inappropriate citations
(5) Incoherent, meaningless and/or irrelevant content included in the article
(6) Peer-review manipulation

The presence of these indicators undermines our confidence in the integrity of the article's content and we cannot, therefore, vouch for its reliability. Please note that this notice is intended solely to alert readers that the content of this article is unreliable. We have not investigated whether authors were aware of or involved in the systematic manipulation of the publication process.

In addition, our investigation has also shown that one or more of the following human-subject reporting requirements has not been met in this article: ethical approval by an Institutional Review Board (IRB) committee or equivalent, patient/participant consent to participate, and/or agreement to publish patient/participant details (where relevant).

Wiley and Hindawi regrets that the usual quality checks did not identify these issues before publication and have since put additional measures in place to safeguard research integrity.

We wish to credit our own Research Integrity and Research Publishing teams and anonymous and named external researchers and research integrity experts for contributing to this investigation.

The corresponding author, as the representative of all authors, has been given the opportunity to register their agreement or disagreement to this retraction. We have kept a record of any response received.

References

[1] X. Meng, J. Zhang, and G. Ren, "The Evaluation Model of College Students' Mental Health in the Environment of Independent Entrepreneurship Using Neural Network Technology," *Journal of Healthcare Engineering*, vol. 2021, Article ID 4379623, 9 pages, 2021.

Hindawi
Journal of Healthcare Engineering
Volume 2023, Article ID 9862937, 1 page
https://doi.org/10.1155/2023/9862937

Retraction

Retracted: A Study of Cloud-Based Remote Clinical Care Technology

Journal of Healthcare Engineering

Received 10 October 2023; Accepted 10 October 2023; Published 11 October 2023

This article has been retracted by Hindawi following an investigation undertaken by the publisher [1]. This investigation has uncovered evidence of one or more of the following indicators of systematic manipulation of the publication process:

(1) Discrepancies in scope
(2) Discrepancies in the description of the research reported
(3) Discrepancies between the availability of data and the research described
(4) Inappropriate citations
(5) Incoherent, meaningless and/or irrelevant content included in the article
(6) Peer-review manipulation

The presence of these indicators undermines our confidence in the integrity of the article's content and we cannot, therefore, vouch for its reliability. Please note that this notice is intended solely to alert readers that the content of this article is unreliable. We have not investigated whether authors were aware of or involved in the systematic manipulation of the publication process.

In addition, our investigation has also shown that one or more of the following human-subject reporting requirements has not been met in this article: ethical approval by an Institutional Review Board (IRB) committee or equivalent, patient/participant consent to participate, and/or agreement to publish patient/participant details (where relevant).

Wiley and Hindawi regrets that the usual quality checks did not identify these issues before publication and have since put additional measures in place to safeguard research integrity.

We wish to credit our own Research Integrity and Research Publishing teams and anonymous and named external researchers and research integrity experts for contributing to this investigation.

The corresponding author, as the representative of all authors, has been given the opportunity to register their agreement or disagreement to this retraction. We have kept a record of any response received.

References

[1] B. Lin and W. Huang, "A Study of Cloud-Based Remote Clinical Care Technology," *Journal of Healthcare Engineering*, vol. 2021, Article ID 8024091, 12 pages, 2021.

Hindawi
Journal of Healthcare Engineering
Volume 2023, Article ID 9842124, 1 page
https://doi.org/10.1155/2023/9842124

Retraction

Retracted: Mechanism of Depression through Brain Function Imaging of Depression Patients and Normal People

Journal of Healthcare Engineering

Received 10 October 2023; Accepted 10 October 2023; Published 11 October 2023

This article has been retracted by Hindawi following an investigation undertaken by the publisher [1]. This investigation has uncovered evidence of one or more of the following indicators of systematic manipulation of the publication process:

(1) Discrepancies in scope
(2) Discrepancies in the description of the research reported
(3) Discrepancies between the availability of data and the research described
(4) Inappropriate citations
(5) Incoherent, meaningless and/or irrelevant content included in the article
(6) Peer-review manipulation

The presence of these indicators undermines our confidence in the integrity of the article's content and we cannot, therefore, vouch for its reliability. Please note that this notice is intended solely to alert readers that the content of this article is unreliable. We have not investigated whether authors were aware of or involved in the systematic manipulation of the publication process.

Wiley and Hindawi regrets that the usual quality checks did not identify these issues before publication and have since put additional measures in place to safeguard research integrity.

We wish to credit our own Research Integrity and Research Publishing teams and anonymous and named external researchers and research integrity experts for contributing to this investigation.

The corresponding author, as the representative of all authors, has been given the opportunity to register their agreement or disagreement to this retraction. We have kept a record of any response received.

References

[1] C. Tang, Y. Zhang, Z. Zhai, X. Zhu, C. Wang, and G. Yang, "Mechanism of Depression through Brain Function Imaging of Depression Patients and Normal People," *Journal of Healthcare Engineering*, vol. 2022, Article ID 1125049, 13 pages, 2022.

Hindawi
Journal of Healthcare Engineering
Volume 2023, Article ID 9825735, 1 page
https://doi.org/10.1155/2023/9825735

Retraction

Retracted: Self-Attention-Guided Recurrent Neural Network and Motion Perception for Intelligent Prediction of Chronic Diseases

Journal of Healthcare Engineering

Received 10 October 2023; Accepted 10 October 2023; Published 11 October 2023

This article has been retracted by Hindawi following an investigation undertaken by the publisher [1]. This investigation has uncovered evidence of one or more of the following indicators of systematic manipulation of the publication process:

(1) Discrepancies in scope
(2) Discrepancies in the description of the research reported
(3) Discrepancies between the availability of data and the research described
(4) Inappropriate citations
(5) Incoherent, meaningless and/or irrelevant content included in the article
(6) Peer-review manipulation

The presence of these indicators undermines our confidence in the integrity of the article's content and we cannot, therefore, vouch for its reliability. Please note that this notice is intended solely to alert readers that the content of this article is unreliable. We have not investigated whether authors were aware of or involved in the systematic manipulation of the publication process.

In addition, our investigation has also shown that one or more of the following human-subject reporting requirements has not been met in this article: ethical approval by an Institutional Review Board (IRB) committee or equivalent, patient/participant consent to participate, and/or agreement to publish patient/participant details (where relevant).

Wiley and Hindawi regrets that the usual quality checks did not identify these issues before publication and have since put additional measures in place to safeguard research integrity.

We wish to credit our own Research Integrity and Research Publishing teams and anonymous and named external researchers and research integrity experts for contributing to this investigation.

The corresponding author, as the representative of all authors, has been given the opportunity to register their agreement or disagreement to this retraction. We have kept a record of any response received.

References

[1] B. Ma, F. Zhang, and B. Ma, "Self-Attention-Guided Recurrent Neural Network and Motion Perception for Intelligent Prediction of Chronic Diseases," *Journal of Healthcare Engineering*, vol. 2021, Article ID 6382619, 7 pages, 2021.

Hindawi
Journal of Healthcare Engineering
Volume 2023, Article ID 9803624, 1 page
https://doi.org/10.1155/2023/9803624

Retraction

Retracted: BJBN: BERT-JOIN-BiLSTM Networks for Medical Auxiliary Diagnostic

Journal of Healthcare Engineering

Received 10 October 2023; Accepted 10 October 2023; Published 11 October 2023

This article has been retracted by Hindawi following an investigation undertaken by the publisher [1]. This investigation has uncovered evidence of one or more of the following indicators of systematic manipulation of the publication process:

(1) Discrepancies in scope
(2) Discrepancies in the description of the research reported
(3) Discrepancies between the availability of data and the research described
(4) Inappropriate citations
(5) Incoherent, meaningless and/or irrelevant content included in the article
(6) Peer-review manipulation

The presence of these indicators undermines our confidence in the integrity of the article's content and we cannot, therefore, vouch for its reliability. Please note that this notice is intended solely to alert readers that the content of this article is unreliable. We have not investigated whether authors were aware of or involved in the systematic manipulation of the publication process.

Wiley and Hindawi regrets that the usual quality checks did not identify these issues before publication and have since put additional measures in place to safeguard research integrity.

We wish to credit our own Research Integrity and Research Publishing teams and anonymous and named external researchers and research integrity experts for contributing to this investigation.

The corresponding author, as the representative of all authors, has been given the opportunity to register their agreement or disagreement to this retraction. We have kept a record of any response received.

References

[1] C. Xu, F. Yuan, and S. Chen, "BJBN: BERT-JOIN-BiLSTM Networks for Medical Auxiliary Diagnostic," *Journal of Healthcare Engineering*, vol. 2022, Article ID 3496810, 7 pages, 2022.

Hindawi
Journal of Healthcare Engineering
Volume 2023, Article ID 9781731, 1 page
https://doi.org/10.1155/2023/9781731

Retraction

Retracted: Applied Research on the Combination of Weighted Network and Supervised Learning in Acupoints Compatibility

Journal of Healthcare Engineering

Received 10 October 2023; Accepted 10 October 2023; Published 11 October 2023

This article has been retracted by Hindawi following an investigation undertaken by the publisher [1]. This investigation has uncovered evidence of one or more of the following indicators of systematic manipulation of the publication process:

(1) Discrepancies in scope
(2) Discrepancies in the description of the research reported
(3) Discrepancies between the availability of data and the research described
(4) Inappropriate citations
(5) Incoherent, meaningless and/or irrelevant content included in the article
(6) Peer-review manipulation

The presence of these indicators undermines our confidence in the integrity of the article's content and we cannot, therefore, vouch for its reliability. Please note that this notice is intended solely to alert readers that the content of this article is unreliable. We have not investigated whether authors were aware of or involved in the systematic manipulation of the publication process.

Wiley and Hindawi regrets that the usual quality checks did not identify these issues before publication and have since put additional measures in place to safeguard research integrity.

We wish to credit our own Research Integrity and Research Publishing teams and anonymous and named external researchers and research integrity experts for contributing to this investigation.

The corresponding author, as the representative of all authors, has been given the opportunity to register their agreement or disagreement to this retraction. We have kept a record of any response received.

References

[1] X. Qiu, X. Zhong, and H. Zhang, "Applied Research on the Combination of Weighted Network and Supervised Learning in Acupoints Compatibility," *Journal of Healthcare Engineering*, vol. 2021, Article ID 4699420, 8 pages, 2021.

Hindawi
Journal of Healthcare Engineering
Volume 2023, Article ID 9840241, 1 page
https://doi.org/10.1155/2023/9840241

Retraction

Retracted: Comparison of Two Surgical Approaches to Supination-External Rotation-Type Ankle Fractures

Journal of Healthcare Engineering

Received 26 September 2023; Accepted 26 September 2023; Published 27 September 2023

This article has been retracted by Hindawi following an investigation undertaken by the publisher [1]. This investigation has uncovered evidence of one or more of the following indicators of systematic manipulation of the publication process:

(1) Discrepancies in scope
(2) Discrepancies in the description of the research reported
(3) Discrepancies between the availability of data and the research described
(4) Inappropriate citations
(5) Incoherent, meaningless and/or irrelevant content included in the article
(6) Peer-review manipulation

The presence of these indicators undermines our confidence in the integrity of the article's content and we cannot, therefore, vouch for its reliability. Please note that this notice is intended solely to alert readers that the content of this article is unreliable. We have not investigated whether authors were aware of or involved in the systematic manipulation of the publication process.

In addition, our investigation has also shown that one or more of the following human-subject reporting requirements has not been met in this article: ethical approval by an Institutional Review Board (IRB) committee or equivalent, patient/participant consent to participate, and/or agreement to publish patient/participant details (where relevant).

Wiley and Hindawi regrets that the usual quality checks did not identify these issues before publication and have since put additional measures in place to safeguard research integrity.

We wish to credit our own Research Integrity and Research Publishing teams and anonymous and named external researchers and research integrity experts for contributing to this investigation.

The corresponding author, as the representative of all authors, has been given the opportunity to register their agreement or disagreement to this retraction. We have kept a record of any response received.

References

[1] B. Chen, Z. Wang, Z. Chen et al., "Comparison of Two Surgical Approaches to Supination-External Rotation-Type Ankle Fractures," *Journal of Healthcare Engineering*, vol. 2022, Article ID 7726726, 8 pages, 2022.

Hindawi
Journal of Healthcare Engineering
Volume 2023, Article ID 9835083, 1 page
https://doi.org/10.1155/2023/9835083

Retraction

Retracted: A Novel Method of Clinical Nursing under the Medical Internet of Things Technology

Journal of Healthcare Engineering

Received 26 September 2023; Accepted 26 September 2023; Published 27 September 2023

This article has been retracted by Hindawi following an investigation undertaken by the publisher [1]. This investigation has uncovered evidence of one or more of the following indicators of systematic manipulation of the publication process:

(1) Discrepancies in scope
(2) Discrepancies in the description of the research reported
(3) Discrepancies between the availability of data and the research described
(4) Inappropriate citations
(5) Incoherent, meaningless and/or irrelevant content included in the article
(6) Peer-review manipulation

The presence of these indicators undermines our confidence in the integrity of the article's content and we cannot, therefore, vouch for its reliability. Please note that this notice is intended solely to alert readers that the content of this article is unreliable. We have not investigated whether authors were aware of or involved in the systematic manipulation of the publication process.

In addition, our investigation has also shown that one or more of the following human-subject reporting requirements has not been met in this article: ethical approval by an Institutional Review Board (IRB) committee or equivalent, patient/participant consent to participate, and/or agreement to publish patient/participant details (where relevant).

Wiley and Hindawi regrets that the usual quality checks did not identify these issues before publication and have since put additional measures in place to safeguard research integrity.

We wish to credit our own Research Integrity and Research Publishing teams and anonymous and named external researchers and research integrity experts for contributing to this investigation.

The corresponding author, as the representative of all authors, has been given the opportunity to register their agreement or disagreement to this retraction. We have kept a record of any response received.

References

[1] T. Ou, X. Cai, M. Wang, F. Guo, and B. Wu, "A Novel Method of Clinical Nursing under the Medical Internet of Things Technology," *Journal of Healthcare Engineering*, vol. 2021, Article ID 2234457, 10 pages, 2021.

Hindawi
Journal of Healthcare Engineering
Volume 2023, Article ID 9810863, 1 page
https://doi.org/10.1155/2023/9810863

Retraction

Retracted: Analysis on the Influence of Students' Health Quality Based on Intelligent Optimization of Sports Facilities and Equipment

Journal of Healthcare Engineering

Received 26 September 2023; Accepted 26 September 2023; Published 27 September 2023

This article has been retracted by Hindawi following an investigation undertaken by the publisher [1]. This investigation has uncovered evidence of one or more of the following indicators of systematic manipulation of the publication process:

(1) Discrepancies in scope
(2) Discrepancies in the description of the research reported
(3) Discrepancies between the availability of data and the research described
(4) Inappropriate citations
(5) Incoherent, meaningless and/or irrelevant content included in the article
(6) Peer-review manipulation

The presence of these indicators undermines our confidence in the integrity of the article's content and we cannot, therefore, vouch for its reliability. Please note that this notice is intended solely to alert readers that the content of this article is unreliable. We have not investigated whether authors were aware of or involved in the systematic manipulation of the publication process.

In addition, our investigation has also shown that one or more of the following human-subject reporting requirements has not been met in this article: ethical approval by an Institutional Review Board (IRB) committee or equivalent, patient/participant consent to participate, and/or agreement to publish patient/participant details (where relevant).

Wiley and Hindawi regrets that the usual quality checks did not identify these issues before publication and have since put additional measures in place to safeguard research integrity.

We wish to credit our own Research Integrity and Research Publishing teams and anonymous and named external researchers and research integrity experts for contributing to this investigation.

The corresponding author, as the representative of all authors, has been given the opportunity to register their agreement or disagreement to this retraction. We have kept a record of any response received.

References

[1] Q. Zhou, "Analysis on the Influence of Students' Health Quality Based on Intelligent Optimization of Sports Facilities and Equipment," *Journal of Healthcare Engineering*, vol. 2022, Article ID 8145127, 8 pages, 2022.

Hindawi
Journal of Healthcare Engineering
Volume 2023, Article ID 9785980, 1 page
https://doi.org/10.1155/2023/9785980

Retraction

Retracted: To Analyze the Influencing Factors of Senile Coronary Heart Disease Patients Complicated with Frailty Syndrome

Journal of Healthcare Engineering

Received 26 September 2023; Accepted 26 September 2023; Published 27 September 2023

This article has been retracted by Hindawi following an investigation undertaken by the publisher [1]. This investigation has uncovered evidence of one or more of the following indicators of systematic manipulation of the publication process:

(1) Discrepancies in scope
(2) Discrepancies in the description of the research reported
(3) Discrepancies between the availability of data and the research described
(4) Inappropriate citations
(5) Incoherent, meaningless and/or irrelevant content included in the article
(6) Peer-review manipulation

The presence of these indicators undermines our confidence in the integrity of the article's content and we cannot, therefore, vouch for its reliability. Please note that this notice is intended solely to alert readers that the content of this article is unreliable. We have not investigated whether authors were aware of or involved in the systematic manipulation of the publication process.

Wiley and Hindawi regrets that the usual quality checks did not identify these issues before publication and have since put additional measures in place to safeguard research integrity.

We wish to credit our own Research Integrity and Research Publishing teams and anonymous and named external researchers and research integrity experts for contributing to this investigation.

The corresponding author, as the representative of all authors, has been given the opportunity to register their agreement or disagreement to this retraction. We have kept a record of any response received.

References

[1] T. Qin, W. Sheng, and G. Hu, "To Analyze the Influencing Factors of Senile Coronary Heart Disease Patients Complicated with Frailty Syndrome," *Journal of Healthcare Engineering*, vol. 2022, Article ID 7619438, 6 pages, 2022.

Hindawi
Journal of Healthcare Engineering
Volume 2023, Article ID 9757682, 1 page
https://doi.org/10.1155/2023/9757682

Retraction

Retracted: The Investigation of Pulmonary Function Changes of COVID-19 Patients in Three Months

Journal of Healthcare Engineering

Received 26 September 2023; Accepted 26 September 2023; Published 27 September 2023

This article has been retracted by Hindawi following an investigation undertaken by the publisher [1]. This investigation has uncovered evidence of one or more of the following indicators of systematic manipulation of the publication process:

(1) Discrepancies in scope
(2) Discrepancies in the description of the research reported
(3) Discrepancies between the availability of data and the research described
(4) Inappropriate citations
(5) Incoherent, meaningless and/or irrelevant content included in the article
(6) Peer-review manipulation

The presence of these indicators undermines our confidence in the integrity of the article's content and we cannot, therefore, vouch for its reliability. Please note that this notice is intended solely to alert readers that the content of this article is unreliable. We have not investigated whether authors were aware of or involved in the systematic manipulation of the publication process.

In addition, our investigation has also shown that one or more of the following human-subject reporting requirements has not been met in this article: ethical approval by an Institutional Review Board (IRB) committee or equivalent, patient/participant consent to participate, and/or agreement to publish patient/participant details (where relevant).

Wiley and Hindawi regrets that the usual quality checks did not identify these issues before publication and have since put additional measures in place to safeguard research integrity.

We wish to credit our own Research Integrity and Research Publishing teams and anonymous and named external researchers and research integrity experts for contributing to this investigation.

The corresponding author, as the representative of all authors, has been given the opportunity to register their agreement or disagreement to this retraction. We have kept a record of any response received.

References

[1] L. Ye, G. Yao, S. Lin et al., "The Investigation of Pulmonary Function Changes of COVID-19 Patients in Three Months," *Journal of Healthcare Engineering*, vol. 2022, Article ID 9028835, 6 pages, 2022.

Hindawi
Journal of Healthcare Engineering
Volume 2023, Article ID 9826214, 1 page
https://doi.org/10.1155/2023/9826214

Retraction

Retracted: Controlled Hypotension Combined with Femoral Nerve Block for Knee Replacement without Tourniquet

Journal of Healthcare Engineering

Received 10 November 2022; Accepted 10 November 2022; Published 18 January 2023

Journal of Healthcare Engineering has retracted the article titled "Controlled Hypotension Combined with Femoral Nerve Block for Knee Replacement without Tourniquet" [1] due to concerns that the peer review process has been compromised.

Following an investigation conducted by the Hindawi Research Integrity team [2], significant concerns were identified with the peer reviewers assigned to this article; the investigation has concluded that the peer review process was compromised. We therefore can no longer trust the peer review process, and the article is being retracted with the agreement of the Chief Editor.

References

[1] L. Wang, Y. Zheng, X. Zhang, and Q. Ke, "Controlled Hypotension Combined with Femoral Nerve Block for Knee Replacement without Tourniquet," *Journal of Healthcare Engineering*, vol. 2021, Article ID 3219337, 8 pages, 2021.

[2] L. Ferguson, "Advancing Research Integrity Collaboratively and with Vigour," 2022, https://www.hindawi.com/post/advancing-research-integrity-collaboratively-and-vigour/.

Hindawi
Journal of Healthcare Engineering
Volume 2023, Article ID 9840241, 1 page
https://doi.org/10.1155/2023/9840241

Retraction

Retracted: Comparison of Two Surgical Approaches to Supination-External Rotation-Type Ankle Fractures

Journal of Healthcare Engineering

Received 26 September 2023; Accepted 26 September 2023; Published 27 September 2023

This article has been retracted by Hindawi following an investigation undertaken by the publisher [1]. This investigation has uncovered evidence of one or more of the following indicators of systematic manipulation of the publication process:

(1) Discrepancies in scope
(2) Discrepancies in the description of the research reported
(3) Discrepancies between the availability of data and the research described
(4) Inappropriate citations
(5) Incoherent, meaningless and/or irrelevant content included in the article
(6) Peer-review manipulation

The presence of these indicators undermines our confidence in the integrity of the article's content and we cannot, therefore, vouch for its reliability. Please note that this notice is intended solely to alert readers that the content of this article is unreliable. We have not investigated whether authors were aware of or involved in the systematic manipulation of the publication process.

In addition, our investigation has also shown that one or more of the following human-subject reporting requirements has not been met in this article: ethical approval by an Institutional Review Board (IRB) committee or equivalent, patient/participant consent to participate, and/or agreement to publish patient/participant details (where relevant).

Wiley and Hindawi regrets that the usual quality checks did not identify these issues before publication and have since put additional measures in place to safeguard research integrity.

We wish to credit our own Research Integrity and Research Publishing teams and anonymous and named external researchers and research integrity experts for contributing to this investigation.

The corresponding author, as the representative of all authors, has been given the opportunity to register their agreement or disagreement to this retraction. We have kept a record of any response received.

References

[1] B. Chen, Z. Wang, Z. Chen et al., "Comparison of Two Surgical Approaches to Supination-External Rotation-Type Ankle Fractures," *Journal of Healthcare Engineering*, vol. 2022, Article ID 7726726, 8 pages, 2022.

Hindawi
Journal of Healthcare Engineering
Volume 2022, Article ID 7726726, 8 pages
https://doi.org/10.1155/2022/7726726

Research Article

Comparison of Two Surgical Approaches to Supination-External Rotation-Type Ankle Fractures

Bingqian Chen, Zhengfei Wang, Zhi Chen, Xiaohong Qu, Xiaowen Fang, Xuesong Wang, and Guoxiu Ke

Department of Orthopaedics, Changshu Hospital Affiliated to Soochow University, First Peoples' Hospital of Changshu City, Changshu 215500, Jiangsu, China

Correspondence should be addressed to Guoxiu Ke; kgx2327@suda.edu.cn

Received 7 December 2021; Revised 12 March 2022; Accepted 15 March 2022; Published 11 April 2022

Academic Editor: Gu Xiaoqing

Objective. To compare the clinical outcome and postoperative complications of the treatment of supination-external rotation-type ankle fractures using the posterolateral approach in the prone position and the lateral approach in the supine position. *Methods*. A retrospective cohort study was conducted in our hospital, including a total of 66 patients ranging from January 2013 to February 2016, regardless of age or sex. All the patients were classified as Lauge-Hansen supination-external rotation (SER)-type ankle fractures and were assigned to receive an open reduction and internal fixation (ORIF) through a posterolateral approach performed in the prone position (the "posterolateral approach group," 32 patients), or a lateral approach performed in the supine position (the "Lateral Approach Group," 34 patients). In the posterolateral approach group, 5 patients had Grade II fractures, 8 had Grade III fractures, and 19 had Grade IV fractures; among whom, 12 underwent fixation of the posterior malleolus with hollow screws and 6 with plates, and none of them had fixation of the distal tibiofibular syndesmosis; in the lateral approach group, 4 patients had Grade II fractures, 12 had Grade III fractures, and 18 had Grade IV fractures; among whom, 21 received fixation of the posterior malleolus, and 5 received fixation of the distal tibiofibular syndesmosis. The postoperative complications and ankle scores were recorded. *Results*. After 1 year of follow-up, in the posterolateral approach group, the incision healed by primary intention and sutures were removed 2 weeks after the operation in all patients; 1 patient had pain in the region posterior to the fibula, presumably peroneal tendon irritation induced by internal fixation, which disappeared after fracture union and fixation device removal; no loosening or breakage of the internal fixation device was reported; the rate of good to excellent results was 96.8% at 12 months. In the lateral approach group: 1 case of wound infection, 1 case of necrosis of lateral skin flap, and 3 cases of lateral skin irritation were reported; the rate of good to excellent results was 94.6% at 12 months. *Conclusion*. Compared with the traditional lateral approach, the posterolateral approach for the reduction and internal fixation of supination-external rotation-type ankle fractures performed in the prone position has more satisfactory clinical outcomes, with better reduction, more secure fixation, and smaller wound.

1. Introduction

In supination-external rotation-type ankle fractures, which may be complicated by posterior and medial malleolus fractures, the fibular fracture line is at the level of the distal tibiofibular syndesmosis, running from anteroinferior to posterosuperior, and the distal fractured bones have a tendency of posterior lateral dislocation [1, 2]. Traditionally, it is treated by reduction and placement of a plate lateral to the fibula through the lateral approach; the concurrent posterior malleolus fractures are usually reduced indirectly and fixed with hollow screws turned anterior to posterior. This approach has significant disadvantages [3]. First, the plate placed laterally to the fibula cannot prevent the tendency of posterolateral dislocation of the distal fractured bones. Also, the approach and position used will not allow direct reduction and effective fixation of posterior malleolus fracture, weakening reduction effect, and fixation strength.

To overcome the aforementioned disadvantages, the posterolateral approach to the ankle is introduced in the treatment of supination-external rotation-type ankle fractures. This approach allows the placement of the plate posterior to the fibula, providing better support. It also allows directly the revealing of the posterior malleolus fractures for secure fixation [4]. We compared the clinical outcome of the treatments using the new posterolateral approach in the prone position and the conventional lateral approach in the supine position performed in our hospital from January 2013 to February 2016 and reported as follows.

The purpose of this study mainly contains 3 aspects. First, from this study, we were able to determine whether the posterior lateral approach in the prone position is more convenient than the traditional lateral approach. Second is which of the two surgical approaches has smaller incision and less trauma. Thirdly, whether the prone posterior lateral approach is more effective and has fewer postoperative complications compared to the traditional lateral approach. These three points are the most important concerns of surgeons. Through this study, it can be concluded that surgical procedure is more suitable for the treatment of supination and external rotation fracture and is more worthy of clinical promotion. At the same time, we hope to find the advantages and disadvantages of this new technology and find the details that need to be paid attention to during the operation. This is conducive to the application and promotion of the new technology and the improvement of the treatment level of ankle fractures.

2. Materials and Methods

2.1. General Information. A total of 66 patients with Lauge-Hansen supination-external rotation (SER)-type ankle fractures were included in this study. The inclusion criteria include ① aging from 25 years old to 70 years old; ② no serious medical diseases, such as hypertension and diabetes, can tolerate surgery; ③ complete medical records and follow-up data were available. The exclusion criteria include ① age under 25 years old and over 70 years old; ② patients with severe medical conditions who are unable to tolerate surgery; ③ lack of complete medical records and missing visitors. Of which 32 patients, 18 males and 14 females, aged 34–66 years (mean age 43 years), were assigned to the posterolateral approach group, of whom, 5 were classified as Grade II fractures, 8 were Grade III fractures, and 19 were Grade IV fractures. The remaining 34 patients, 16 males, and 13 females, aged 27–61 years (mean age 42 years), were assigned to the lateral approach group, of whom 4 were Grade II fractures, 12 were Grade III fractures, and 18 were Grade IV fractures.

The patients were given symptomatic treatment, such as elevation of the fractured ankle and application of an ice pack. Routine anteroposterior and lateral radiographs and CT scanning of the ankle were performed prior to the surgery, to determine the morphology and dislocation of the fractured ankle. The surgeries were performed 5–10 days after the injury when the swelling had significantly improved, and local dermatoglyphic appeared.

2.2. Operation Methods. Spinal anesthesia or epidural anesthesia is administered, and a tourniquet is applied at the root of the thigh. For patients in the posterolateral approach group, the patient was placed in the prone position, with cushions placed under the hip and knees. After routine disinfection and draping, a longitudinal incision was made at the midline between the posterior border of the fibula and the lateral border of Achilles's tendon, extended beyond the tip of the lateral malleolus distally. The skin was carefully cut open to protect the sural nerve and small saphenous vein in the subcutaneous fascia. Then, the deep fascia was incised, and the insertion of flexor hallucis longus on the fibula was dissected sharply and pulled medially to reveal the posterior malleolus and distal posterior tibiofibular ligament. A blunt dissection was made lateral to the tendon of peroneus longus and peroneus brevis, and the muscle was pulled medially to reveal the underlying fibula, which was done carefully to protect the peroneal retinacula located on the distal aspect of the fibula. The posterior malleolus fracture was reduced first and fixed with hollow screws or a support plate (with hollow screws in 21 patients and with plate in 6 patients); then, the fibula was reduced and fixed with a highly plastic reconstruction plate placed posteriorly to the fibula. For patients with concurrent medial malleolus fractures, an arc-shaped incision was made in the medial aspect of the ankle to reveal the medial malleolus fracture, which was reduced and fixed with hollow screws (Figures 1 and 2).

For patients in the lateral approach group, the patient was placed in the supine position, with a sandbag placed under the hip on the affected side. After routine disinfection and draping, a longitudinal incision was made laterally to the fibula, and advanced layer by layer, to reveal the fibula fracture. After removing the soft tissues in the fractured bone, the manual reduction was performed followed by temporary fixation with Kirschner wires, and then, a highly plastic reconstruction plate was placed laterally to the fibula and fixed with screws. For patients with concurrent medial malleolus fractures, an arc-shaped medial incision was made to reveal the medial malleolus fracture, and then, the anatomical reduction was performed followed by fixation with 1–2 hollow screws. For posterior malleolus fractures involving >1/4 of the joint (20 patients), fixation with 1–2 hollow screws placed from posterior to anterior was performed (Figure 3).

A hook test was performed for patients from both groups. For patients identified with the instability of the distal tibiofibular syndesmosis (5 in the lateral approach group and 0 in the posterolateral approach group), the distal tibiofibular syndesmosis was reduced using reduction forceps and fixed with 1–2 cortical bone screws placed from the fibula during ankle dorsiflexion.

After the surgery, patients were given the elevation of the fractured ankle and the application of an ice pack for 48 hours. They started functional training after the removal of vacuum drains the next day and had sutures removed at 2 weeks when their wounds healed. At 2 months, the screws for fixation of distal tibiofibular syndesmosis were removed. Radiographs were obtained, and ankle function scores

Figure 1: (a–h) The procedure of posterolateral approach for pronation-extorsion fractures of the ankle. (a) Patients took a prone position. (b) The sural nerve lies on the posterolateral side of the ankle under the skin, usually crossing the lower segment of the incisions from posterior to anterior. (c) Pulled flexor hallucis longus medially to reveal the posterior malleolus. (d) The tendon of peroneus longus and peroneus brevis was pulled medially to reveal the underlying fibula. (e) The fibula was reduced and fixed with a highly plastic reconstruction plate placed posteriorly to the fibula. (f, g) The posterior malleolus fracture was reduced and fixed with a support plate or a hollow screw. (h) An arc-shaped incision was made in the medial aspect of the ankle to reveal the medial malleolus fracture, which was reduced and fixed with hollow screws.

(American Orthopedic Foot and Ankle Society, AOFAS) and complications were recorded during the follow-up visits at 3, 6, and 12 months.

AOFAS: in 1994, the American Association of Foot and Ankle Society (AOFAS) developed and recommended the AOFAS Ankle-Hindfoot Scale, including the fill and physician examination, a total of nine projects: indicators have pain, function and autonomic activities, support conditions, the biggest walking distance, ground to walk, before and after the abnormal gait, activity (flexing and stretching), hind activities (varus and valgus), ankle—after sufficient stability (and varus and valgus) before and after, the foot line of force. Grading standard: >90, excellent; 75–89, good; 50–74, fair; <50, poor.

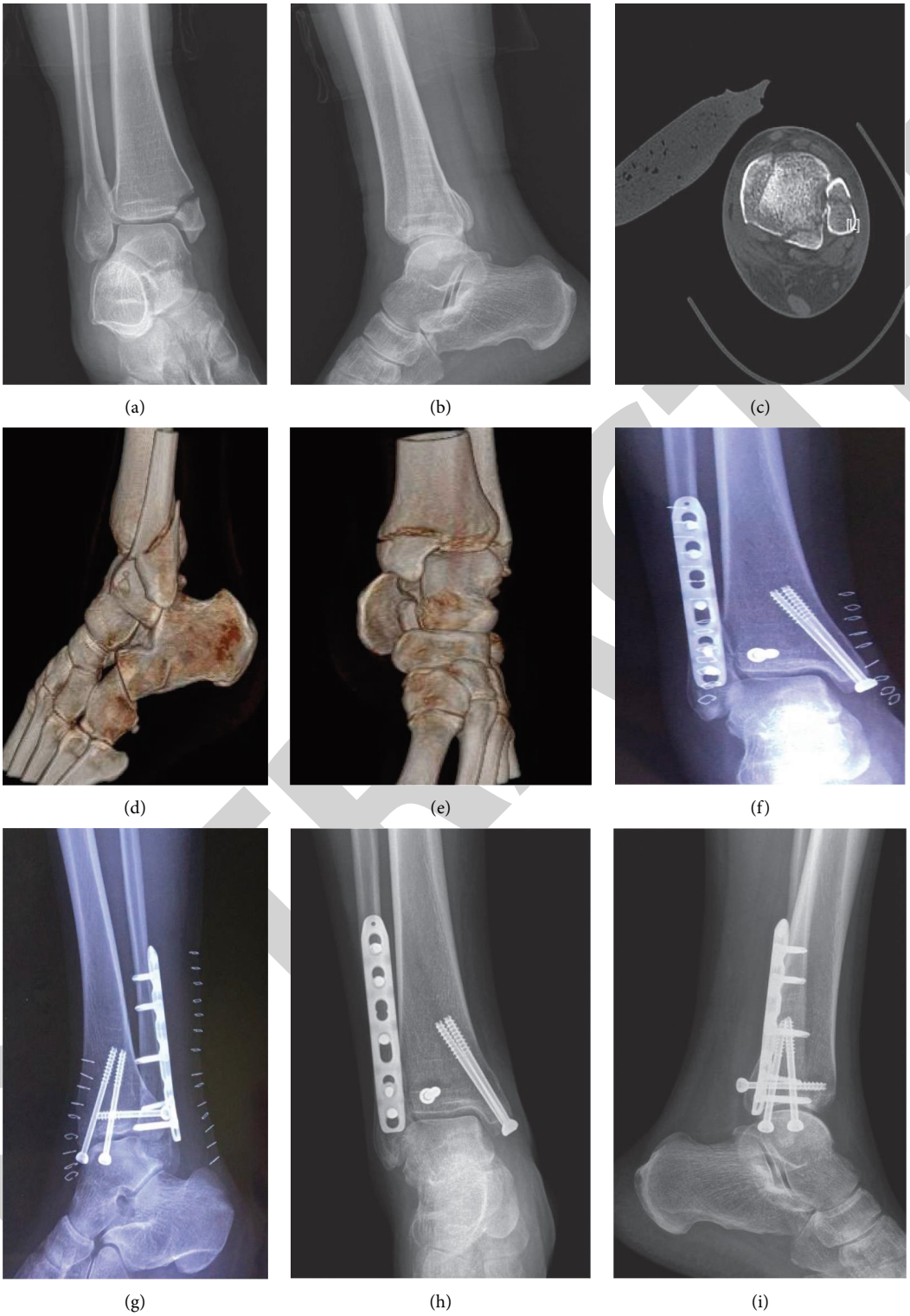

Figure 2: (a, b) 45-year-old female patients with right ankle fracture caused by trauma. (c–h) CT scan shows that the fracture involves medial, lateral, and posterior malleolus. The fracture belongs to the supination-external rotation-type (Grade IV). (c–f) The prone position and posterolateral approach were used. The fibula was fixed by a plate, the posterior malleolus was fixed by a lag screw, and the medial malleolus was fixed by two hollow screws. (h, i) One year after surgery, the X radiographs show that the fractures were healed well and the ankle function recovered excellently.

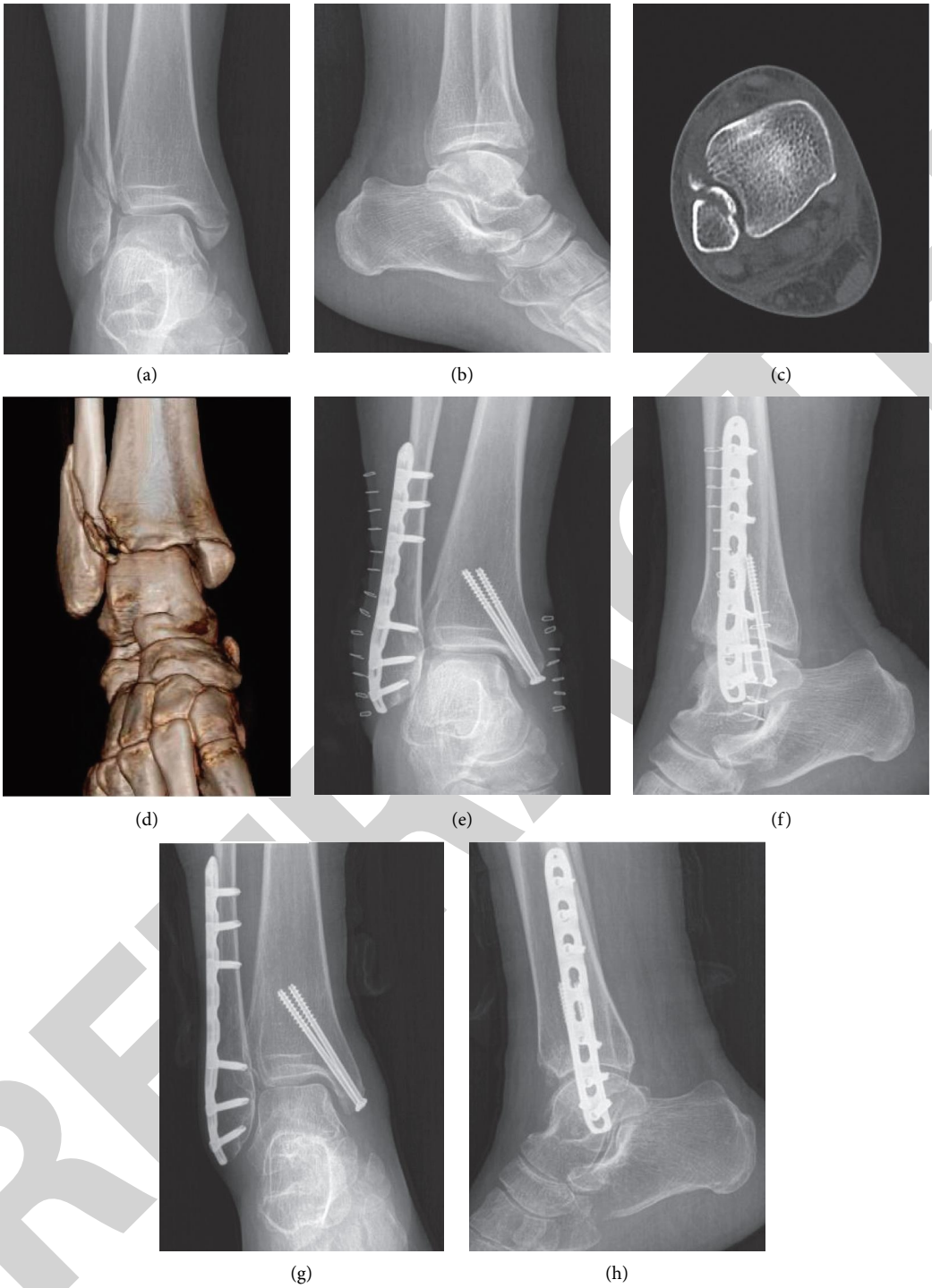

Figure 3: (a, b) A 47-year-old male patients with a right ankle fracture caused by trauma. (c, d) CT scan shows that the fracture involves medial-lateral and lateral malleolus. The fracture belongs to the supination-external rotation-type (GradeIII). (e, f) The supine position and lateral approach were used, a plate was used to fix the lateral malleolus, and two lag screws were used to fix the medial malleolus. (g, h) One year after surgery, the X radiographs show that the fractures were healed well, and the ankle function recovered excellently.

2.3. Statistical Analysis. Statistical analysis was performed using SPSS 21.0 (Statistical Package for Social Sciences. SPSS Inc. Released 2010, SPSS Statistics for Windows, Version 21.0, Chicago: SPSS Inc.). Measurement data were present as $\bar{x} \pm s$. The mean AOFAS scores and standard deviations of each group were calculated and compared with each other using the Mann–Whitney U test. Logistic regression was used to see if a combination of factors including sex, fracture type, and classification of the fracture might have influenced the AOFAS scores for each group. Statistical significance was defined as $P < 0.05$.

3. Results

All patients were followed up for at least one year, both in the clinic and by telephone. Follow-up mainly included wound healing, postoperative pain, and ankle function recovery. In the posterolateral approach group, the incision healed by primary intention and sutures were removed 2 weeks after the operation in all patients. In the lateral approach group, 1 patient had a wound infection at 1 week and was treated with debridement with continuous closed irrigation, and the sutures were removed 2 weeks later when the wound healed; 1 patient developed necrosis of lateral skin flaps, and with increased frequency of dressing changes, the wound healed under scabbing.

All patients were followed up for 12 months, during which, 1 patient from the posterolateral approach group felt mild pain in the region posterior to the fibula, possibly due to irritation of the peroneal tendon by the fixation plate, which disappeared after fracture union and fixation device removal; 3 patients reported pain and discomfort in the lateral skin due to irritation by the plates, which disappeared after the removal of the plates; no loosening or breakage of the internal fixation device or redisplacement of fractures was reported.

The ankle function scoring (AOFAS) at 12 months showed 23 excellent results, 8 good results, and 1 poor result, with a rate of good to excellent results of 96.8%, in the posterolateral approach group; and The ankle function scoring (AOFAS) at 12 months showed 22 excellent results, 10 good results, and 2 poor results, with a rate of good to excellent results of 94.1%, in the lateral approach group (Tables 1 and 2).

4. Discussion

4.1. Characteristics of Supination-External Rotation-Type Ankle Fractures. Supination-external rotation-type ankle fractures are commonly seen in clinical practice, accounting for about 85% of all ankle fractures [5]. It has the following characteristics [1, 2]: first, the broken end of the fibula is located in the distal tibiofibular syndesmosis, the fracture line running obliquely from anteroinferior to posterosuperior; second, the distal fractured bones have the tendency of posterior lateral dislocation.

Supination-external rotation-type ankle fractures are usually complicated by posterior malleolus fractures. The posterior malleolus is an important part of the articular facet on the tibia, whose displacement may lead to a decreased area of the articular surface, and concentration of joint stress [6, 7]. Also, it gives attachment to the distal posterior tibiofibular ligament. Therefore, the normal attachment of the distal posterior tibiofibular ligament relies on a normal anatomical position of the posterior malleolus, and maintaining the distal posterior tibiofibular ligament tension is essential for the stability of distal tibiofibular syndesmosis, especially when the medial ankle is injured [8, 9]. In conclusion, the posterior malleolus is important for the integrity and stability of the ankle [10–12]. In this study, hollow screw or reconstruction plate fixation following routine revealing and reduction of posterior malleolus fracture was performed for patients in the posterolateral approach group, and indirect reduction and fixation of posterior malleolus fracture were performed for 21 patients from the lateral approach group, and no case of instable distal tibiofibular syndesmosis was reported.

Posterior malleolus fracture can be fixed with hollow screws or support plates in the treatment through a posterolateral approach. In this study, 21 patients had screw fixation, and 6 had plate fixation, both achieved a satisfactory effect, with no case of redislocation reported, and showed no significant difference in 1-year satisfaction with clinical outcomes. However, the screw fixation is better compared to the plate fixation, as it permits smaller wound, simpler operation, and lower cost. Therefore, we recommend the screw fixation for posterior malleolus fracture.

4.2. Two Treatment Options and Their Advantages and Disadvantages. The lateral approach in the supine position, which allows the surgeon to reach the fracture site from a lateral incision, and placement of plates lateral to the fibula, is currently widely used in the surgical treatment of ankle fractures, as it is easy to learn and convenient for the management of medial malleolus fractures [13]. However, it has many disadvantages. First, through this approach, the posterior malleolus is not revealed and can only be reduced indirectly and fixed with hollow screws turned anterior to posterior, producing poor reduction and fixation. Second, this approach does not allow the placement of a plate posterior to the fibula, which provides better support. Finally, the plate placed underneath the skin lateral to the fibula may cause irritation of the skin, or even necrosis of flaps. In this study, 3 patients from the lateral approach group experienced skin irritation from the plates, which was relieved after the removal of the plates.

The posterolateral approach in the prone position allows the revealing of the lateral and posterior malleolus through an incision, facilitating better management of supination-external rotation-type ankle fractures [14, 15]. First of all, it allows the placement of a lateral plate posterior to the fibula, which provides better support and is more conformable to the principle of biomechanics [4]. Second, posterior malleolus fracture is revealed from the same incision, allowing better reduction and more secure plate or screw fixation. Also, the placement of a plate deep in the soft tissues helps to avoid skin irritation and reduce the risk of flap necrosis. As evidence, in this study, no patient from the posterolateral approach group experienced flap necrosis, while 1 case of flap necrosis and 1 case of wound infection were reported in the lateral approach group. In addition, with the posterior plate placement and anterior-to-posterior screw fixation, there is no concern about screws in the articular cavity, allowing for bicortical fixation with long screws, which has a higher resistance to pull-out and is particularly suitable for osteoporotic elderly patients [16]. Finally, the prone position is helpful for the reduction of fractures. We noticed a phenomenon in clinic practice that the fracture block of lateral malleolus, even if comminuted, has had a good

Table 1: Personal information and rates of excellent results in both groups.

Group	*n*	Mean age	Presence of concurrent posterior malleolus fracture	Use of screws at the distal tibiofibular syndesmosis	Rates of excellent results (%)
Posterolateral approach group	32	43	27	0	96.8
Lateral approach group	34	42	30	5	94.1

Table 2: Rates of excellent results of different treatments of posterior malleolus fractures through a posterolateral approach.

Group	*N*	Mean age	Male	Female	Rates of excellent results (%)
Hollow crew fixation	21	46	7	5	95.4
Plate fixation	6	43	3	4	94.6

reduction when revealed through the posterolateral approach,which is possibly due to the action of gravity, which places the ankle in dorsiflexion and a neutral position, and corrects external rotation and dislocation.

The results of this study showed that, although the posterolateral approach was more beneficial for the reduction and fixation of fractures, and the posterolateral approach group reported fewer cases of complications than the lateral approach group, there was no significant difference in the 1-year satisfaction with clinical outcomes between the two groups.

4.3. Considerations for Surgeries through Posterolateral Approach. First, the sural nerve shall be carefully protected during the operation. The sural nerve lies on the posterolateral side of the ankle under the skin, usually crossing the lower segment of the incisions from posterior to anterior, and thus shall be protected when dissecting the fat layer [17, 18]. Second, note that the insertion of flexor hallucis longus on the fibula should be dissected and pulled medially, to reveal the posterior malleolus fractures, during which the posterior tibial vessels and nerves immediately medial to it shall be protected [19]. Third, when revealing the posterior malleolus fracture, be careful not to cut the distal tibiofibular ligament attached to it. In addition, the plates shall not be placed too low but placed above the groove for the peroneal tendon, or irritation of the tendon will occur [20]. In this study, a patient from the posterolateral approach group experienced pain in the region posterior to the fibula, which is possibly caused by irritation of the peroneal tendon by the fixation plate placed too low. What's more, a thin plate with good plasticity shall be chosen to reduce the risk of tendon irritation. Usually, a 3.5 mm reconstruction plate or 1/3tubular plate is preferred. Finally, a hook test before the end of the surgery is necessary for determining whether the distal tibiofibular syndesmosis is stable enough. If the distal tibiofibular syndesmosis is unstable despite the fixation of posterior malleolus, which is more common in cases complicated by medial collateral ligament rupture, screw fixation of the distal tibiofibular syndesmosis is required. In this study, 5 patients from the lateral approach group, who did not receive the fixation of posterior malleolus due to small sizes, were identified with unstable distal tibiofibular syndesmosis in the hook test, which was corrected by screw fixation of the distal tibiofibular syndesmosis.

5. Conclusion

Compared with the traditional lateral approach, the posterolateral approach in the prone position allows the revealing of the lateral and posterior malleolus through an incision and better reduction and fixation of the posterior malleolus. It also allows the placement of the lateral plate posterior to the fibula, which provides better mechanical support and helps to avoid skin irritation. This is a safe and excellent surgical technique to treat supination-external rotation-type ankle fractures and has more satisfactory clinical outcomes, with better reduction, more secure fixation, and safer wound than the traditional lateral approach, though there is no significant difference in 1-year satisfaction rate. In the posterolateral approach group, there was no significant difference in clinical efficacy and complication rates between the lag screw and the plate fixation for posterior malleolus. However, the use of hollow screws permits smaller wound, simpler operation, and lower cost.

In future work, we will strive to constantly improve the technology of the posterolateral approach in prone position to treat supination-external rotation-type ankle fractures. At the same time, we will also apply this technology to other types of ankle fractures, compare it with the traditional surgical methods, and analyze the advantages and disadvantages of the technology.

Data Availability

The dataset used to support the findings of this study is available from the corresponding author upon request.

Ethical Approval

This study was reviewed and approved by the Ethics Management Committee of Changshu First People's hospital. The clinical registration number was 2017 Lun Shen (Shen Bao) batch No. 20.

Conflicts of Interest

The authors declare that they have no conflicts of interest.

Acknowledgments

This work was supported by the Changshu Hospital Affiliated to Soochow University.

Hindawi
Journal of Healthcare Engineering
Volume 2023, Article ID 9895710, 1 page
https://doi.org/10.1155/2023/9895710

Retraction

Retracted: Deep Scale-Variant Network for Femur Trochanteric Fracture Classification with HP Loss

Journal of Healthcare Engineering

Received 5 December 2023; Accepted 5 December 2023; Published 6 December 2023

This article has been retracted by Hindawi, as publisher, following an investigation undertaken by the publisher [1]. This investigation has uncovered evidence of systematic manipulation of the publication and peer-review process. We cannot, therefore, vouch for the reliability or integrity of this article.

Please note that this notice is intended solely to alert readers that the peer-review process of this article has been compromised.

Wiley and Hindawi regret that the usual quality checks did not identify these issues before publication and have since put additional measures in place to safeguard research integrity.

We wish to credit our Research Integrity and Research Publishing teams and anonymous and named external researchers and research integrity experts for contributing to this investigation.

The corresponding author, as the representative of all authors, has been given the opportunity to register their agreement or disagreement to this retraction. We have kept a record of any response received.

References

[1] Y. Kang, Z. Ren, Y. Zhang et al., "Deep Scale-Variant Network for Femur Trochanteric Fracture Classification with HP Loss," *Journal of Healthcare Engineering*, vol. 2022, Article ID 1560438, 7 pages, 2022.

Hindawi
Journal of Healthcare Engineering
Volume 2022, Article ID 1560438, 7 pages
https://doi.org/10.1155/2022/1560438

Research Article

Deep Scale-Variant Network for Femur Trochanteric Fracture Classification with HP Loss

Yuxiang Kang,[1] Zhipeng Ren,[1] Yinguang Zhang,[1] Aiming Zhang,[2] Weizhe Xu,[3] Guokai Zhang,[2] and Qiang Dong[1]

[1]*Department of Orthopaedics, Tianjin Hospital, Tianjin 300211, China*
[2]*School of Optical-Electrical and Computer Engineering, University of Shanghai for Science and Technology, Shanghai 200093, China*
[3]*School of Computer Science, The University of Manchester, M14 5ta, Manchester, UK*

Correspondence should be addressed to Guokai Zhang; zhangguokai_01@163.com and Qiang Dong; dongqiangtianjin@126.com

Received 16 December 2021; Revised 22 January 2022; Accepted 17 February 2022; Published 27 March 2022

Academic Editor: Xiaoqing Gu

Achieving automatic classification of femur trochanteric fracture from the edge computing device is of great importance and value for remote diagnosis and treatment. Nevertheless, designing a highly accurate classification model on 31A1/31A2/31A3 fractures from the X-ray is still limited due to the failure of capturing the scale-variant and contextual information. As a result, this paper proposes a deep scale-variant (DSV) network with a hybrid and progressive (HP) loss function to aggregate more influential representations of the fracture regions. More specifically, the DSV network is based on the ResNet and integrated with the designed scale-variant (SV) layer and HP loss, where the SV layer aims to enhance the representation ability to extract the scale-variant features, and HP loss is intended to force the network to condense more contextual clues. Furthermore, to evaluate the effect of the proposed DSV network, we carry out a series of experiments on the real X-ray images for comparison and evaluation, and the experimental results demonstrate that the proposed DSV network could outperform other classification methods on this classification task.

1. Introduction

Femur trochanteric fracture has been a common healthcare problem for elderly people, which severely influences the daily life of the injured people. Currently, the most effective way to assist the radiologist in diagnosing this disease is by adopting X-ray or computed tomography (CT) to examine the injured parts and then undergoing reasonable treatments. Especially, in clinical diagnosis, the most commonly used classification criterion for the fracture is the OA/OTA, which divides the fracture into three types: 31/A1, 31/A2, and 31/A3, based on the conditions of the different fractures [1]. In the type of 31/A1, it always comes with pertrochanteric fracture, and in 31/A2, it defines the multifragmentary pertrochanteric fracture, while in 31/A3, it usually represents the reverse obliquity (as shown in Figure 1). Based on this criterion, the orthopaedic surgeon could diagnose the fracture types more precisely and then make the follow-up treatment plan according to different fracture types to achieve the personalized diagnosis. However, in clinical practice, the manual examination for each patient's images is usually a tedious and labor-intensive job. In addition, due to the different clinical experiences of radiologists, the final diagnosis result could be slightly diverse which may be a handicap for the subsequent treatment. Thus, to address those challenges, many attempts of designing the algorithms for the computer-aided system to achieve the automatic classification of the OA/OTA are widely proposed. For example, Aruse et al. [2] designed a three-dimensional computer model which computed the four scaphoid axes to measure the direction and angle of the fracture and then calculated the correlation of different fracture angles to prove that the direction of the fracture inclination was less influential in scaphoid fractures. Basha

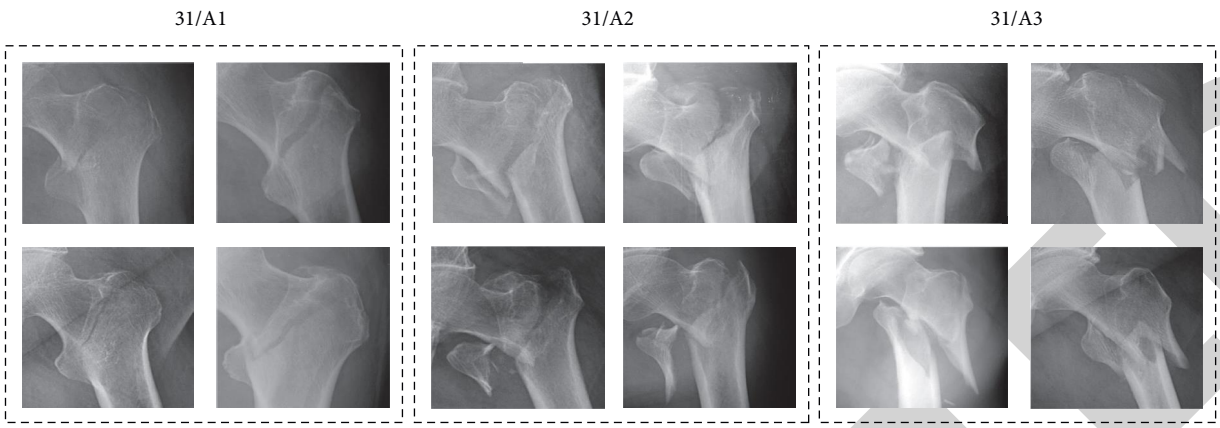

Figure 1: The data samples of 31/A1, 31/A2, and 31/A3.

et al. [3] designed an efficient and automatic bone fracture detection system which combined the enhanced Haar wavelet transform with scale-invariant feature transform (SIFT) to extract the image features and then input them to a neural network for bone fracture classification; the final experimental results indicated that the designed model could gain better classification performance compared with the SIFT method. Yin et al. [4] explored the Tang classification system which was based on the three-dimensional image analysis system to achieve the automatic classification of the femoral intertrochanteric fracture, and it demonstrated that the proposed Tang classification system could be more reliable than other ones in this task. Moreover, in the work [5], it proposed an exemplar pyramid architecture that learned different image features and then classified the fracture types by adopting the classical classifiers. Burns et al. [6] utilized the machine learning approach to create an automated detection and localization computer-aided system by extracting high-level vertebral compression fracture features to gain a high sensitivity classification performance. In [7], the authors extracted the texture and shape features of the vertebral bodies from the median sagittal planes of lumbar spine images and applied different classifiers to classify the osteoporosis or vertebral metastasis fractures. Although those designed methods could effectively improve the efficiency of the diagnosis process and alleviate the workload of the radiologist, the subjective feature definition and selection of those hand-crafted based methods is still a challenging problem.

In recent years, the deep neural network (DNN) has gained promising performance in various computer vision fields and applications [8–14]. Especially, the convolutional neural network (CNN) has been the most prevalent approach in regard to the image classification task. For example, the method in [15] proposed a deep learning architecture that was able to help doctors detect the bone fractures based on the OA/OTA criterion, and the proposed classification model could gain the improvement on average accuracy by 14%. Chung et al. [16] employed a deep learning algorithm to detect and classify proximal humerus fractures on plain anteroposterior shoulder images; it then compared the results with human groups and indicated that the proposed method could obtain superior performance compared with the general physicians and orthopedists. Pranata et al. [17] developed an automatic computer-aided system for fracture detection and classification from the calcaneus CT images; in this system, it extracted the features from coronal, sagittal, and transverse views by adopting CNN, ResNet, and VGG, respectively, and then using the SURF algorithm to classify the bone fracture types. Anami et al. [18] presented a novel architecture to classify diaphyseal tibial fractures by the neural network; it had two main stages, and the first stage aimed to classify the normal and abnormal ones, while the second stage was used to classify the simple, wedge, and complex type of the fracture. Farda et al. [19] used the principle component analysis (PCA) to process the input image and employed the deep neural network to extract the features to gain a better classification performance of calcaneal fracture types. In [20], an artificial intelligence (AI) system was reported to evaluate the performance of classifying knee fractures based on the AO/OTA criterion, and the comparison results demonstrate that the CNN could be utilized for both fracture identification and classification. To achieve the automatic segmentation of fracture regions, the previous work [21] exploited a segmentation model by adopting the Unet structure to segment the wrist fractures, which performed competitive performance at that time. Furthermore, in [22, 23], the authors tried the Inception V3 and Inception-ResNet for efficiently extracting the high-level representations from the fracture regions. After that, Krogue et al. [24] explored the dense network to achieve the placement of the hip fractures and evaluated the performance on the 100-image subset.

In spite of those previous methods having gained promising results on this classification task, those ones are mainly suffering from failing to learn the scale-variant and contextual information from the feature space, which leads to a handicap for achieving a better classification performance. Note that since edge computing device is widely used in healthcare diagnosis or treatment, herein, developing an accurate and timely classification model is essential and valuable to achieve a remote and intelligent diagnosis. To address those above challenges, in this paper, we propose a deep scale-variant network with a hybrid progressive loss

function to achieve the automatic classification of the femur trochanteric fracture from X-ray images. Unlike those previous works, our DSV network is based on the ResNet which is widely used in the computer vision field. At the beginning, to capture the scale-variant feature representations, we design a scale-variant (SV) layer, which uses the adaptive convolution layers with the channel attention mechanism to enhance the scale-variant feature learning ability of the network. Furthermore, providing sufficient contextual information or clues of the fracture regions could also be of great importance in the classification of 31A1/31A2/31A3. Thereby, we design a hybrid and progressive (HP) loss for strengthening the influence of the contextual features, which in turn gain a more accurate classification performance. Finally, we conduct a series of exhaustive experiments on the real X-ray images and report the comparison results to effectively validate the effectiveness of the DSV network.

In the following sections, we first introduce the proposed method in Section 2 and then give the descriptions of the experimental data and evaluation metrics in Section 3. Lastly, the comprehensive conclusion is discussed in Section 4.

2. Methodology

In this paper, we propose a scale-variant network that could efficiently learn the contextual and scale features from the femur trochanteric region. As illustrated in Figure 2, the whole network is based on the ResNet, which has been widely used in many computer vision fields. Especially, to capture the scale-variant representations, a scaled variant (SV) layer is developed to enhance the feature learning ability of the network. Moreover, a hybrid and progressive (HP) loss function is employed to obtain the highly discriminative deep features from different network levels. In the following sections, we elaborate on the details of SV layer and HP loss.

2.1. Network Architecture. Figure 2 shows the overview architecture of the proposed DSV network. Especially, the main backbone of the network is based on ResNet, and we omit the repeated layers for concise display. Compared with the ResNet, the DSV network mainly contains two different parts. Specifically, the first part is the SV layer, which extracts the deep scale-variant features consecutively. The second part is the HP loss, which is calculated to emphasize the contextual and discriminative regions. With the help of those two parts, inputting an X-ray image of the femur trochanteric, it first generates the coarse feature map through each residual feature learning part and then delivers the generated one to SV layer for obtaining the scale-variant representations. Note that considering the complexities of the network, we only deploy SV layer before each residual learning phase. Finally, the extracted high-level features enter into a fully connected (FC) layer with the cross-entropy loss to impel the network focus on the universal parts. The proposed HP loss calculates the diversities from different network levels to highlight the discriminative contextual regions.

2.2. Scale-Variant Layer. Although the hierarchical layers of the network enable it to extract the deep features, it is still limited by the fixed filter size, which leads to incorrect classification of the fracture regions. To address this challenge, in our DSV network, we develop an SV layer, which deploys it before each residual learning phase to adaptively and progressively extract the scale-variant representations. The detailed structure of the SV layer is shown in Figure 3; it obeys the residual connection to facilitate the training process. Specifically, we denote the input feature from the previous residual learning phase as $\mathbb{F} \in \mathbb{R}^{H\times W\times C}$ where H, W, C denote the height, width, and channel numbers of $\mathbb{F}$, respectively. Then, in the SV layer, it first passes $\mathbb{F}$ into three separate 1×1 layers to compress the feature maps, which denotes the output feature map as $\mathbb{F}_1 \in \mathbb{R}^{H\times W\times c/2}$, $\mathbb{F}_2 \in \mathbb{R}^{H\times W\times c/2}$, and $\mathbb{F}_3 \in \mathbb{R}^{H\times W\times c/2}$, respectively. Subsequently, $\mathbb{F}_1$ is directly delivered into the channel attention (CA) module, which aims to further prune the feature map from the channel level. Mathematically, split $\mathbb{F}_1$ into channel level expression, which can be denoted as

$$\mathbb{F}_1 = \left[\mathbb{F}_1(1), \mathbb{F}_1(2), \ldots, \mathbb{F}_1(c), \ldots, \mathbb{F}_1(C/2)\right], \tag{1}$$

where $\mathbb{F}_1(c)$ indicates the c-th channel feature map of $\mathbb{F}$, $c \in \{1, 2, \ldots, C/2\}$. Then, the $\mathbb{F}_1(c)$ is first applied by a global average pooling over the full channel feature map, and the operation of GAP could be given as

$$t_c = \frac{1}{H \times W} \sum^{H} \sum^{W} \mathbb{F}_c, \tag{2}$$

where the parameter of t_c represents the overall factor value of c-th feature map channel. Then, a gating mechanism is utilized to learn the dependencies of each feature channel, which can be formulated as

$$t' = \sigma\left(\mathbb{W}\delta\left(\mathbb{W}' t\right)\right), \tag{3}$$

where t' indicates the importance factor, $\mathbb{W}$ and $\mathbb{W}'$ are the weights of two fully connected layers, separately, and $\delta(\cdot)$ represents the ReLU activation which could be given as

$$\delta(x) = \max(0, x), \tag{4}$$

where $\sigma(\cdot)$ denotes the sigmoid activation function, and it can be defined as

$$\sigma(x) = \frac{1}{1 + e^{-x}}. \tag{5}$$

After that, the gained importance factor $t_c{}'$ multiplies with $\mathbb{F}$ to obtain the enhanced feature map $\mathbb{F}'$:

$$\mathbb{F}_1' = \mathbb{F}_1 \cdot t'. \tag{6}$$

Notably, in order to learn the scale-variant features more efficiently, before applying the CA to $\mathbb{F}_2$ and $\mathbb{F}_3$, we deliver $\mathbb{F}_2$ to a 3×3 convolution layer and feed $\mathbb{F}_3$ through two 3×3 convolution layers, respectively. Afterwards, denote the outputs of CA module of $\mathbb{F}_2$ and $\mathbb{F}_3$ as $\mathbb{F}_2'$ and $\mathbb{F}_3'$, and then those three scale-variant representations ($\mathbb{F}_1'$, $\mathbb{F}_2'$, $\mathbb{F}_3'$) are fused as follows:

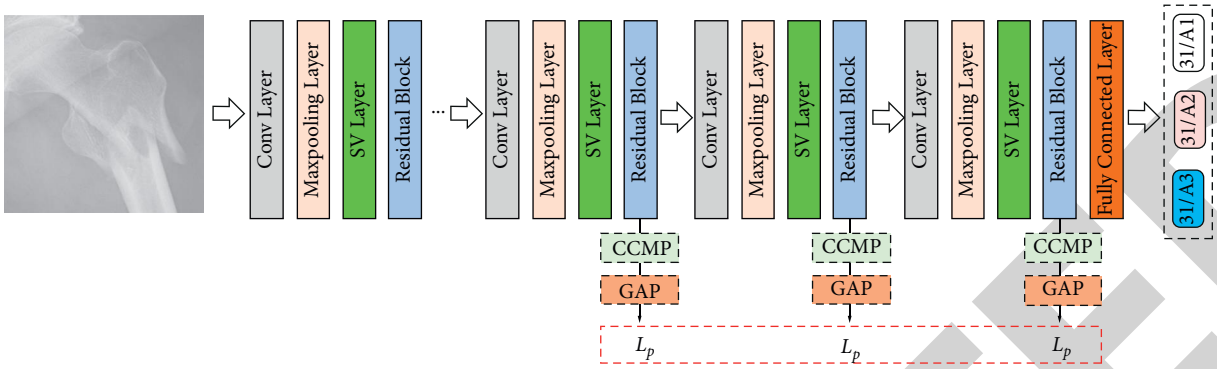

Figure 2: The main architecture of the DSV network: L_p is one part of the HP loss, and CCMP and GAP denote the cross channel max-pooling layer and global average-pooling layer, respectively.

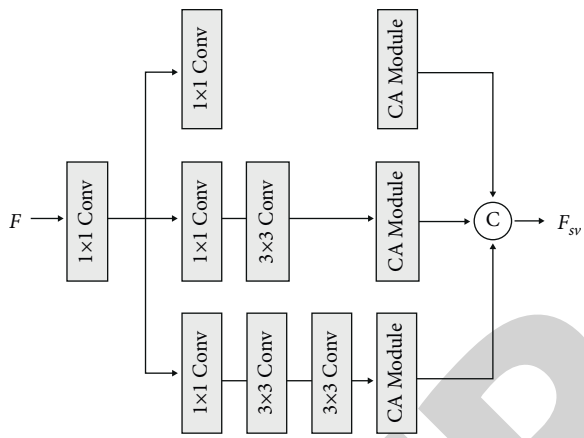

Figure 3: The structure of the SA layer.

$$\mathbb{F}_{sv} = \tau\{\mathbb{F}_1', \mathbb{F}_2', \mathbb{F}_3'\}, \tag{7}$$

where $\tau(\cdot)$ represents the concatenation operation. By adopting the SV layer, the network is more effective to extract the scale-variant features, which is able to further improve the classification performance of the DSV network. Moreover, to further explore the contextual information of the image, we employ a hybrid and progressive loss, which could efficiently enhance the network to spotlight the discriminative femur trochanteric fracture regions.

2.3. Hybrid and Progressive Loss. To efficiently extract more contextual information from the femur trochanteric fracture regions, we develop a hybrid and progressive loss function L_{HP}:

$$\mathscr{L}_{HP} = \mathscr{L}_{ce} + \mu \times \mathscr{L}_{sp}, \tag{8}$$

where L_{ce} denotes the cross-entropy loss function, L_{sp} is the side progressive loss function, and μ is a weighting hyper-parameter to balance those two loss functions. More specifically, L_{ce} could be defined as

$$\mathscr{L}_{\text{ce}} = \sum_{k=1}^{N} y_k \log\, p_k + \sum_{j=k}^{N} (1 - y_k)\log(1 - p_k), \tag{9}$$

where p_k is the predicted probability for class k, y_k is the true label, and the value of N is 3. Note that the value of p_k is calculated from the FC layer with the softmax activation function:

$$\psi(\mathbf{s})_i = \frac{e^{s_i}}{\sum_{n=1}^{3} e^{s_n}}, \tag{10}$$

where s_i is the output feature map from the FC layer. Furthermore, L_{sp} is a combined one which is formulated as

$$\mathscr{L}_{sp} = \sum_{m=1}^{M} \mathscr{L}_p, \tag{11}$$

where the value of M is set as 3; considering the trade-off between network complexity and efficiency, $\mathscr{L}_p$ is gained by

$$\mathscr{L}_p = \rho(\gamma(\mathscr{F}_m)), \tag{12}$$

where $\gamma(\cdot)$ is the cross channel max-pooling [25] to merge the feature map to the dimension of $H \times W \times 3$, ρ is the global average pooling, and $\mathscr{F}_m$ is the feature map from last m-th residual block of the network. By aggregating the contextual clues with a progressive learning mode, it forces the network to produce more abstract and essential information, thus leading to a better classification performance.

3. Experiment

To demonstrate the effectiveness of the proposed model, in this section, we validate our proposed model with real femur trochanteric fracture images. Besides, we carry out a series of experiments to explore the influence of different configurations on classification performance. Extensive experimental results demonstrate that the proposed DSV network could gain competitive classification performance compared with other state-of-the-art approaches. In the following content, we will provide detailed descriptions of the experimental dataset, implementation details, evaluation metrics, and experimental results.

3.1. Dataset. For the evaluation dataset, we adopt three types of data (31/A1, 31/A2, and 31/A3), with the amount of 117, 125, and 128, separately. Especially, the max/min age of the

evaluated dataset is 91 and 26, respectively, and the mean age of the dataset is 65. For accurate evaluation of the proposed model, the types of the experimental dataset are confirmed by three orthopaedic specialists with experience over 5 years based on the AO/OTA criterion. Notably, the input image is resized to 512×512 and the region of interest (ROI) of the original image is cropped for reducing the computational complexity.

3.2. Implementation Details. In our validation experiments, we implemented the network by the PyTorch platform with the NVIDIA GTX2070 graphics processing unit (GPU). For the network training, we use the Adam optimizer and set the initial learning rate as 0.001 in the first 60 epochs and then decay the value by 0.01 for the following 30 epochs. To increase the amount of the data, we use data augmentation such as random flipping, rotation, cropping, and padding to generate more training data. Particularly, the batch size of our model is 5, and before inputting the ROI image to the network, we resize them to 512×512.

3.3. Evaluation Metrics. In this section, we evaluate our model by employing accuracy, sensitivity, specificity, and the area under the curve (AUC) score. The accuracy is the measurement of the true predicted values, which can be formulated as

$$\text{accuracy} = \frac{TP + TN}{TP + FP + TN + FN}, \tag{13}$$

where TP, TN, FP, and FN represent the true positive, false positive, true negative, and false negative, respectively. The sensitivity denotes the ability to identify the true positives, and it can be defined as

$$\text{sensitivity} = \frac{TP}{TP + FN}, \tag{14}$$

while the specificity indicates the ability to identify the true negatives, which could be given as

$$\text{specificity} = \frac{TN}{TN + FP}. \tag{15}$$

Specifically, the AUC score is the classical metric to evaluate the performance of the classifier; the higher the score of the AUC is, the better performance the model would gain.

3.4. Impact of Different Data Samples. Table 1 reports the comparison results on different data samples, where it is divided into 20%, 40%, 60%, 80%, and 100% of the total data samples. Note that we do not test smaller percent (<20%) of the data samples, since it could be hard for the network to be convergent. From the comparison results, we can observe that the best performance is achieved by adopting 100% of data samples, which could be explained that more data samples could provide more robust representations that further boost the classification performance. Moreover, with the increasing number of data samples, the classification performance is stably improving which is also consistent with the prementioned hypothesis.

Table 1: The impact of different data samples.

Data samples (%)	Accuracy (%)	Sensitivity (%)	Specificity (%)	AUC
20	85.2	85.1	82.0	0.83
40	85.6	86.1	83.1	0.85
60	86.7	86.9	83.6	0.88
80	88.8	87.3	85.3	0.94
100	90.2	88.9	86.5	0.98

3.5. Ablation Study of Different Components. In this section, we employ extensive experiments to conduct the ablation study of different components. As illustrated in Table 2, we explore three comparisons which are "ResNet," "ResNet + SV," "ResNet + HP," "ResNet + SV + HP," respectively. Here, "+ SV," "+ HP," and "+ SV + HP" denote the network with the scale-variant layer, hybrid and progressive loss, and simultaneous two parts. From the results, we observe that the best performance is obtained by "ResNet + SV + HP" with a score of 90.2%, 88.9%, 86.5%, and 0.98 on the accuracy, sensitivity, specificity, and AUC, respectively. Moreover, compared with different network settings, "ResNet + SV" could achieve better performance than "ResNet + HP," which indicates that the scale-variant features could have more significant impact compared with the contextual clues on this classification task.

3.6. The Influence of Different Branch Numbers of SV Layer. In our SV layer, we utilize three branches to capture the scale-variant features; however, it could be flexible to select the numbers of the branches. Therefore, in this section, we carry out experiments to evaluate the influence of different branches of the SV layer. The comparison result is shown in Table 3, and there are four branch numbers (1, 2, 3, 4) for comparison. At the beginning, it is obvious that using more branches could improve the classification performance; however, when the number of the branch is bigger than 3, the performance is not efficiently improved on those four metrics. Therefore, to balance the trade-off between the complexity and performance, we still adopt the 3 branches as the final set of SV layer. In summary, the final performance of applying 3 branches is 90.2%, 88.9%, 86.5%, and 0.98 on the accuracy, sensitivity, specificity, and AUC, separately.

3.7. The Performance of Various HP Loss Settings. In order to further evaluate the influence of HP loss, especially the calculated location on the network, in this section, we conduct a series of experiments to validate its effect. Since we only calculate the outputs of the last three residual blocks of the DSV network, here we denote "HP-1," "HP-2," and "HP-3" as the third to last, next to last, and last of the residual block, while "HP-o" and "HP-123" represent the DSV network without or with the HP loss. As illustrated in Table 4, the comparison result demonstrates that using the HP loss with any location of the DSV network could boost its classification performance compared with "HP-o," and furthermore, it is obvious that the best performance is achieved by "HP-123."

Table 2: The comparison results of different components of DSV network.

Components	Accuracy (%)	Sensitivity (%)	Specificity (%)	AUC
ResNet	87.5	86.7	81.9	0.87
ResNet + SV	89.3	87.5	85.6	0.95
ResNet + HP	88.9	87.3	85.4	0.94
ResNet + SV + HP	90.2	88.9	86.5	0.98

Table 3: The comparison results of different branch numbers of SV layer.

Branch numbers (BNs)	Accuracy (%)	Sensitivity (%)	Specificity (%)	AUC
ResNet	87.5	86.7	81.9	0.87
BNs = 1	88.7	87.5	85.3	0.94
BNs = 2	88.9	88.2	85.5	0.96
BNs = 3	90.2	88.9	86.5	0.98
BNs = 4	90.2	88.6	86.4	0.97

Table 4: The performance of various HP loss settings.

	Accuracy (%)	Sensitivity (%)	Specificity (%)	AUC
HP-o	89.3	87.5	85.6	0.95
HP-1	89.3	87.8	85.3	0.95
HP-2	89.7	88.2	85.7	0.96
HP-3	89.8	88.7	85.8	0.97
HP-123	90.2	88.9	86.5	0.98

Table 5: The comparison results with other methods.

Method	Accuracy (%)	Sensitivity (%)	Specificity (%)	AUC
Inception V4 [26]	87.8	86.1	82.3	0.86
ResNet [27]	87.5	86.7	81.9	0.87
DenseNet [28]	87.2	86.3	83.4	0.91
SKNet [29]	87.1	86.8	83.6	0.92
Res2Net [30]	88.2	87.7	85.7	0.95
DDA [31]	88.9	87.6	85.9	0.97
DSV	90.2	88.9	86.5	0.98

3.8. Comparison with Other Methods. In this section, we compare our proposed DSV network with other classification methods to evaluate its effectiveness. Table 5 lists the comparison results, and here we employ some baseline methods such as Inception V4 [26], ResNet [27], DenseNet [28], SKNet [29], Res2Net [30], and DDA [31]. It is evident that compared with other classification methods, our DSV network gains more accurate classification on the four evaluation metrics. It could be explained that with the designed SV layer and HP loss, the DSV network has more powerful feature ability on the scale-variant and contextual clues, which leads to better classification performance.

4. Conclusion

In this paper, we have proposed a DSV network for the automatic classification of the femur trochanteric fracture. The DSV network aggregates the scale-variant representation through the SV layer and learns the contextual clues by the HP loss from different depths of layers. To evaluate the effectiveness of the DSV network, we perform extensive experiments on the real femur trochanteric fracture of X-ray images, and the exhaustive comparison results demonstrate that the proposed DSV network could be superior to other recent image classification methods with higher classification performance. In the future work, we will mainly focus on employing our model on different modalities images such as magnetic resonance imaging (MRI) and computed tomography (CT) to explore the effectiveness of the proposed model. Moreover, we would try to deploy our model with lighter one on the edge computing device to help achieve the remote diagnosis efficiently.

Conflicts of Interest

The authors declare that they have no conflicts of interest.

Acknowledgments

This research was sponsored by the Science and Technology Talent Cultivation Project of Tianjin Health Commission (KJ20215) and Research Project of Tianjin Sports Bureau (21DY014).

References

[1] E. Meinberg, J. Agel, C. Roberts, M. Karam, and J. Kellam, "Fracture and dislocation classification compendium-2018," *Journal of Orthopaedic Trauma*, vol. 32, no. 1, pp. S1–S10, 2018.

[2] O. Aruse, I. Immerman, and O. Badir, "Scaphoid fracture displacement is not correlated with the fracture angle," *Journal of Hand Surgery*, vol. 46, Article ID 17531934211004434, 2021.

[3] C. Z. Basha, T. M. Padmaja, and G. N. Balaji, "An effective and reliable computer automated technique for bone fracture detection[J," *J. EAI Endorsed Trans. Pervasive Health Technol.*vol. 5, no. 18, p. e2, 2019.

[4] B. Yin, Y. He, D. Wang, and J. Zhou, "Classification of femur trochanteric fracture: evaluating the reliability of Tang classification," *Injury*, vol. 52, no. 6, pp. 1500–1505, 2021.

[5] S. Demir, S. Key, T. Tuncer, and S. Dogan, "An exemplar pyramid feature extraction based humerus fracture classification method," *Medical Hypotheses*, vol. 140, Article ID 109663, 2020.

Hindawi
Journal of Healthcare Engineering
Volume 2023, Article ID 9757682, 1 page
https://doi.org/10.1155/2023/9757682

Retraction

Retracted: The Investigation of Pulmonary Function Changes of COVID-19 Patients in Three Months

Journal of Healthcare Engineering

Received 26 September 2023; Accepted 26 September 2023; Published 27 September 2023

This article has been retracted by Hindawi following an investigation undertaken by the publisher [1]. This investigation has uncovered evidence of one or more of the following indicators of systematic manipulation of the publication process:

(1) Discrepancies in scope
(2) Discrepancies in the description of the research reported
(3) Discrepancies between the availability of data and the research described
(4) Inappropriate citations
(5) Incoherent, meaningless and/or irrelevant content included in the article
(6) Peer-review manipulation

The presence of these indicators undermines our confidence in the integrity of the article's content and we cannot, therefore, vouch for its reliability. Please note that this notice is intended solely to alert readers that the content of this article is unreliable. We have not investigated whether authors were aware of or involved in the systematic manipulation of the publication process.

In addition, our investigation has also shown that one or more of the following human-subject reporting requirements has not been met in this article: ethical approval by an Institutional Review Board (IRB) committee or equivalent, patient/participant consent to participate, and/or agreement to publish patient/participant details (where relevant).

Wiley and Hindawi regrets that the usual quality checks did not identify these issues before publication and have since put additional measures in place to safeguard research integrity.

We wish to credit our own Research Integrity and Research Publishing teams and anonymous and named external researchers and research integrity experts for contributing to this investigation.

The corresponding author, as the representative of all authors, has been given the opportunity to register their agreement or disagreement to this retraction. We have kept a record of any response received.

References

[1] L. Ye, G. Yao, S. Lin et al., "The Investigation of Pulmonary Function Changes of COVID-19 Patients in Three Months," *Journal of Healthcare Engineering*, vol. 2022, Article ID 9028835, 6 pages, 2022.

Hindawi
Journal of Healthcare Engineering
Volume 2022, Article ID 9028835, 6 pages
https://doi.org/10.1155/2022/9028835

Research Article

The Investigation of Pulmonary Function Changes of COVID-19 Patients in Three Months

Lingyan Ye,[1] **Guifei Yao**,[1] **Shuangxiang Lin**,[2] **Yicheng Fang**,[2] **Xi Chen**,[1] **Liangxing Wang**,[3] **and Susu He**[1]

[1]*Department of Respiratory Medicine, Taizhou Hospital of Zhejiang Province Affiliated to Wenzhou Medical University, Linhai, Zhejiang, China*
[2]*Department of Radiology, Taizhou Hospital of Zhejiang Province Affiliated to Wenzhou Medical University, Linhai, Zhejiang, China*
[3]*Department of Respiratory Medicine, The First Affiliated Hospital of Wenzhou Medical University, Wenzhou, Zhejiang, China*

Correspondence should be addressed to Liangxing Wang; wzyxywlx@163.com and Susu He; hess1555@enzemed.com

Received 10 November 2021; Accepted 8 December 2021; Published 17 January 2022

Academic Editor: Gu Xiaoqing

Background. Novel coronavirus disease 2019 (COVID-19) was discovered in December 2019 and has infected more than 80 million people worldwide, and more than 50 million people have achieved a clinical cure. In this study, the pulmonary function results of patients after clinical medicine for three months were reported. *Objective*. To investigate the effect of COVID-19 on lung function in patients. *Methods*. A retrospective analysis was performed on 56 COVID-19-infected patients who were cured after the clinical treatment at Taizhou Public Health Medical Center in Zhejiang Province from January 31, 2020, to March 10, 2020. At discharge and three months after discharge, lung function was measured, including inspiratory vital capacity (IVC), forced vital capacity (FVC), forced expiratory volume in first second (FEV1), forced expiratory volume in first second to inspiratory vital capacity (FEV1/IVC), maximum mid-expiratory flow rate (MEF), peak expiratory flow rate (PEF), and carbon monoxide dispersion (DLCO). *Results*. At discharge, there were 37 patients (66.1%) with pulmonary dysfunction, 22 patients (39.3%) with ventilation dysfunction, 31 cases (55.4%) with small airway dysfunction, and 16 cases (28.6%) with restricted ventilation dysfunction combined with small airway dysfunction. At 3 months after discharge, 24 of the 56 patients still had pulmonary dysfunction and all of them had small airway dysfunction, of which 10 patients (17.9%) were restricted ventilation dysfunction combined with small airway dysfunction. DLCO was measured three months after discharge. Twenty-nine patients (51.8%) had mild to moderate diffuse dysfunction. All pulmonary function indexes of 56 patients recovered gradually after 3 months after release, except FEV1/IVC, and the difference was statistically significant ($P < 0.05$). There were 41 patients of normal type (73.2%) and 15 patients of severe type (26.8%). Among the 15 severe patients, 8 patients (53.3%) had ventilation dysfunction at discharge, 9 patients (60%) had small airway dysfunction, 4 patients (26.7%) still had ventilation dysfunction 3 months after discharge, 7 patients (46.7%) had small airway dysfunction, and 10 patients (66.7%) had diffuse dysfunction. Among the 41 common type patients, 14 patients (34.1%) had ventilation dysfunction at discharge, 22 patients (53.7%) had small airway dysfunction, 6 patients (14.6%) still had ventilation dysfunction 3 months after discharge, 17 patients (41.5%) had small airway dysfunction, and 19 patients (46.3%) had diffuse dysfunction. Patients with severe COVID-19 had more pulmonary impairment and improved pulmonary function than normal patients. *Conclusion*. COVID-19 infection can cause lung function impairment, manifested as restricted ventilation dysfunction, small airway dysfunction, and diffuse dysfunction. The pulmonary function of most patients was improved 3 months after clinical cure and discharge, and some patients remained with mild to moderate diffuse dysfunction and small airway dysfunction.

1. Introduction

Since December 2019, COVID-19, first discovered in Wuhan, has rapidly spread to many countries and regions worldwide, and is now a pandemic with high morbidity and mortality that has occurred all over the world [1, 2]. Severe acute respiratory syndrome coronavirus 2 (SARS-CoV-2) is a beta coronavirus. There have been two previous severe worldwide beta coronavirus infections: severe acute respiratory syndrome (SARS) and Middle East respiratory syndrome (MERS) [3, 4]. This kind of virus mainly leads to respiratory tract infection in humans, which can occur in patients with severe pneumonia, pulmonary edema, ARDS or multiple organ failure, and death, and lung dysfunction is a common complication [5].

There have been several recent literature reports [5–8], which indicate that most of the patients with COVID-19 mainly represented with fever, dry cough, and sputum in some patients. With the progress of the disease, some patients may show shortness of breath one week after onset. Prior study has reported [9] that, the infection of SARS, which is also one kind of beta coronavirus, can result in some patients with pulmonary fibrosis. Lung function impairment in survival patients is found in the clinical lung function follow-up, including obstructive ventilatory function, restrictive ventilatory function, and dispersion function obstacles [10, 11]. There is an obvious correlation between patients with residual lesions in the lung and lung function impairment [11].

At present, there are few reports on the recovery of lung function in COVID-19 patients after recovery. So will the infection of COVID-19 patients lead to impaired lung function or even left pulmonary fibrosis? Our study aims at elucidating the effect of novel COVID-19 infection on the lung function of patients and providing clues for the later pulmonary rehabilitation therapy of clinically cured patients with COVID-19.

2. Methods

2.1. Patients. This study retrospectively collected 56 patients with COVID-19 who met the clinical cure criteria after hospitalization in Taizhou Public Health Center of Zhejiang Province from January 31, 2020, to March 10, 2020 [12]; that is, respiratory symptoms were significantly improved, two pharyngeal swabs for novel coronavirus nucleic acid tests were both negative, longer than 24 h, and lung CT showed significant absorption of lesions. The respiratory secretions obtained by nasopharyngeal swabs were detected by RT-PCR for novel coronavirus positive before admission, and the patients were diagnosed as COVID-19 according to the Chinese COVID-19 protocol [12]. The diagnostic criteria for patients with severe COVID-19 were as follows: (1) respiratory distress, respiratory rate (RR) > 30 times/min; (2) average oxygen saturation ≤93%, arterial oxygen partial pressure/oxygen concentration (PaO_2/FiO_2) ≤ 300; and (3) chest imaging lesion progression [13] within 24–48 hours > 50%. We collected the age, sex, and smoking history of the enrolled patients, and performed pulmonary function tests at discharge and follow-up three months after release. This study was approved by the Ethics Committee of Taizhou Hospital of Taizhou Medical Group (Center) of Zhejiang Province, and patients' written informed consent was obtained after retrospective data collection.

2.2. Lung Function Test. All patients were examined for pulmonary function after reaching clinical cure. The detection indexes included inspiratory vital capacity (IVC), forced vital capacity (FVC), forced expiratory volume in 1s (FEV1), and the ratio of forced expiratory volume in the first second to inhaled vital volume FEV1/IVC. The maximum expiratory flow at 25% of vital capacity is denoted by MEF 25, maximum expiratory flow at 50% of vital capacity is denoted by MEF 50, maximum expiratory flow at 75% of vital capacity is denoted by MEF 75, peak expiratory flow is denoted as PEF, and diffusion capacity for carbon monoxide is denoted as DLCO. All of the patients tested for lung function were seated comfortably in separate and enclosed rooms, and were tested for lung function three times, with the highest FEV1 value. Except FEV1/IVC and FEV1/FVC, other pulmonary function indexes were expressed as the percentage of measured values to predicted values. The lung function tester used in this study was Powercube Body BF lung function tester produced by Ganshorn Medizin Ectronic (Germany). All lung function tests were performed by the same technician. All practices are performed and assessed in accordance with the new standards issued by the European Respiratory Society/American Thoracic Society (ERS/ATS) in 2017 [14, 15]. Pulmonary function criteria include the following: (1) pulmonary ventilation function—FVC% <80%, FEV1% < 80%, FEV1/FVC > 70%, indicating restrictive ventilation dysfunction; FVC% >80%, FEV1% < 80%, and FEV1/FVC < 70% were obstructive ventilation dysfunction. The degree of pulmonary ventilation dysfunction was expressed by FEV1%, which was divided into mild damage (≥70%), moderate damage (50% ≤ FEV1% < 70%), severe damage (35% ≤ FEV1% < 50%), and very severe damage (<35%) [15, 16]; (2) pulmonary diffusion function—DLCO% ≥ 80% was normal, mild disorder (60% ≤DLCO% < 80%), moderate disorder (40% ≤ DLCO % < 60%), and severe disorder (DLCO% < 40%) [14, 15]; And (3) small airway function—MEF25%, MEF 50% ≥ 70% is normal, mild impairment (60% ≤ MEF25%, MEF 50% < 70%), moderate impairment (40% ≤ MEF25%, MEF 50% < 60%), and severe impairment (MEF25%, MEF 50% < 40%) [15].

2.3. Statistical Analysis. All statistical analyses were carried out using SPSS (v20.0). Categorical variables were described as frequency rates and percentages, and continuous variables were described using mean and median.

3. Results

The median age of 56 patients was 44.13 ± 10.15 years (range, 23–79 years old), and 50 percent of them were male; 4 patients (7.14%) had a history of smoking; and 2 patients (3.57%) had a history of COPD (chronic obstructive

pulmonary disease). There were 41 patients of normal type (73.2%) and 15 patients of severe type (26.8%) (Table 1).

At discharge, 37 (66.1%) of the 56 COVID-19 patients had pulmonary dysfunction: 22 (39.3%) showed ventilation dysfunction, including 15 (26.8%) with mild and 7 (12.5%) with moderate, 1 (1.8%) with obstructive ventilation dysfunction, and 21 (37.5%) with restrictive ventilation dysfunction. Thirty-one patients (55.4%) presented small airway dysfunction, of which 16 patients (28.6%) were restricted ventilation dysfunction combined with small airway dysfunction. Three months after discharge, 24 patients (42.9%) remained with pulmonary dysfunction, all of which were presented as small airway dysfunction, and 10 patients (17.9%) were restricted ventilation dysfunction combined with small airway dysfunction. Fifty-six patients with COVID-19 were tested by DLCO 3 months after cure and discharge, 29 patients (51.8%) had diffuse dysfunction, 10 patients (17.9%) had restricted ventilation dysfunction and small airway dysfunction, of which 23 patients (41.1%) had mild diffuse dysfunction, and 6 patients (10.7%) had moderate diffuse dysfunction (Table 2). Lung function indexes of 56 patients at discharge such as IVC, FEV1, FVC, MEF 25, MEF 50, MEF 75, and PEF were 62.5 ± 14.4, 83.4 ± 12.3, 84.8 ± 12.9, 71.1 ± 37.6, 79.6 ± 25.1, 87.3 ± 18.7, and 85.2 ± 18.6, respectively, and three months after discharge, indexes improved to 83.1 ± 19.0, 92.7 ± 15.0, 92.9 ± 12.8, 78.6 ± 34.8, 92.0 ± 31.0, 101 ± 22.4, and 102 ± 18.6. So the pulmonary function indexes of 56 patients (IVC, FEV1, FVC, MEF 25, MEF 50, MEF 75, PEF) changed significantly on the day of discharge and 3 months after discharge, and the difference was statistically significant ($P < 0.05$) (as shown in Table 3), which indicated that the pulmonary function impairment of COVID-19 patients was gradually recovered 3 months after discharge compared with that at discharge, and the pulmonary function of most patients had basically returned to normal. The decreasing trend of FEV1/IVC may be related to the faster recovery rate of IVC than that of FEV1 over time.

Pulmonary function in mild and severe COVID-19 patients: Among the 15 severe patients, 8 patients (53.3%) had ventilation dysfunction at discharge, 9 patients (60%) had small airway dysfunction, 4 patients (26.7%) still had ventilation dysfunction 3 months after discharge, 7 patients (46.7%) had small airway dysfunction, and 10 patients (66.7%) had diffuse dysfunction. Among the 41 common type patients, 14 patients (34.1%) had ventilation dysfunction at discharge, 22 patients (53.7%) had small airway dysfunction, 6 patients (14.6%) still had ventilation dysfunction 3 months after discharge, 17 patients (41.5%) had small airway dysfunction, and 19 patients (46.3%) had diffuse dysfunction (Table 2). Lung function injury is more typical in severe patients than in common patients. Three months after clinical cure and discharge, lung function in light and severe patients all recovered well, and the improvement in IVC and MEF25 indexes in severe patients was more obvious (Table 4).

4. Discussion

Novel coronavirus has spread around the world and seriously threatened people's safety and health. The pandemic of COVID-19 has posed a significant challenge to the global health service system. The coronavirus is high transmissible with strong pathogenicity, transmitted by respiratory droplets or close contact. With the invasion of the coronavirus in the respiratory tract, the patient could have lung tissue injured directly or get an acute respiratory distress syndrome incurred by the inflammatory immune response, which has a high fatality rate [17, 18]. Even after the clinical cure, there are still patients whose chest CT lesions are not fully absorbed, with remaining pulmonary interstitial changes and the lung function damage, thus affecting the life quality of these patients [19]. Recent studies have shown that COVID-19 survivors may have long-term pulmonary dysfunction [20].

The sequela of some SARS patients is pulmonary fibrosis [9]. Recent studies have shown that the pathological features of COVID-19 are similar to those of SARS. Interstitial mononuclear inflammatory infiltration and alveolar septal fibroblast proliferation can also be found in the lungs of COVID-19 patients [21]. In this study, lung function detection was performed on 56 cured patients on the day of discharge. It showed that 66.1% of the patients had lung function impairment, which was mild and moderate pulmonary dysfunction, and no severe or extremely severe pulmonary dysfunction was observed. The pathophysiological changes after COVID-19 infection mainly were double diffuse lung tissue damage associated with cellular fiber mucous exudate, leading to a wide range of interstitial inflammatory change [22], whose manifestations after the invasion of the coronavirus in the airway were bronchial epithelial basement membrane thickening, alveolar walls transparent sample, structure of lung tissue damage, extracellular matrix accumulation in great quantities, interstitial fibrosis caused by the inflammation injury of lung tissue, interstitial fibrosis II type alveolar epithelial injury at the same time, and the lack of surface active substance, which leads to the closed small airways, and these pathological changes result in the decrease of lung compliance and abnormal small airway function, thereby seriously affecting

Table 1: Characteristics of the patients infected with COVID-19 ($n = 56$).

Characteristic	Results
Age (years)	
Median	44.13 ± 10.15
Range	23–79
<30	3 (5.4%)
30–49	35 (62.5%)
50–69	16 (28.6%)
>70	2 (3.5%)
Sex	
Men	28 (50%)
Women	28 (50%)
Smoking history	4 (7.14%)
Chronic obstructive pulmonary disease	2 (3.57%)
Type	
Severe	15 (26.8%)
Nonsevere	41 (73.2%)

Data are n (%), n/N (%), and median.

Table 2: Pulmonary function characteristics of COVID-19 patients.

Pulmonary dysfunction	On the day of discharge			Three months after discharge		
	All ($N = 56$)	Severe ($N = 15$)	Nonsevere ($N = 41$)	All ($N = 56$)	Severe ($N = 15$)	Nonsevere ($N = 41$)
Ventilation dysfunction	22 (39.3%)	8 (53.3%)	14 (34.1%)	10 (17.9%)	4 (26.7%)	6 (14.6%)
Mild ventilation dysfunction	15 (26.8%)	5 (33.3%)	10 (24.4%)	5 (8.9%)	2 (13.3%)	3 (7.3%)
Moderate ventilation dysfunction	7 (12.5%)	3 (20%)	4 (9.7%)	5 (8.9%)	2 (13.3%)	33 (7.3%)
Small airway dysfunction	31 (55.4%)	9 (60%)	22 (53.7%)	24 (42.9%)	7 (46.7%)	17 (41.5%)
Ventilation dysfunction with small airway dysfunction	16 (28.6%)	6 (40%)	10 (24.4%)	10 (17.9%)	4 (26.7%)	6 (14.6%)
Disseminated dysfunction				29 (51.8%)	10 (66.7%)	19 (46.3%)

Table 3: Pulmonary function changes of patients infected with COVID-19.

Pulmonary function (%Pred)	On the day of discharge ($N = 56$)	Three months after discharge ($N = 56$)	P value
IVC	62.5 ± 14.4	83.1 ± 19.0	<0.001
FVCex	84.8 ± 12.9	92.9 ± 12.8	0.00115
FEV1	83.4 ± 12.3	92.7 ± 15.0	<0.001
MEF25	71.1 ± 37.6	78.6 ± 34.8	0.0275
MEF50	79.6 ± 25.1	92.0 ± 31.0	0.0222
MEF75	87.3 ± 18.7	101 ± 22.4	<0.001
PEF	85.2 ± 18.6	102 ± 18.6	<0.001
DLCO		84.8 ± 19.2	

Table 4: Pulmonary function changes in patients with different types of COVID-19.

Pulmonary function (%Pred)	On the day of discharge			Three months after discharge		
	Nonsevere ($N = 41$)	Severe ($N = 15$)	P value	Nonsevere ($N = 41$)	Severe ($N = 15$)	P value
FEV1/IVC	112 ± 21.5	114 ± 21.7	0.854	92.4 ± 20.7	82.1 ± 6.71	0.007
IVC	64.4 ± 13.8	57.7 ± 15.2	0.135	82.4 ± 18.9	84.9 ± 19.8	0.689
FVCex	86.9 ± 11.6	79.6 ± 14.9	0.096	94.6 ± 11.8	88.9 ± 14.5	0.176
FEV1	85.3 ± 11.9	78.8 ± 12.5	0.0856	94.0 ± 14.2	89.6 ± 16.9	0.367
MEF25	73.7 ± 41.1	64.6 ± 26.7	0.336	78.0 ± 33.8	80.2 ± 38.2	0.841
MEF50	81.4 ± 26.0	75.3 ± 23.0	0.394	92.8 ± 29.7	89.9 ± 35.1	0.769
MEF75	86.3 ± 17.1	89.6 ± 22.6	0.61	100 ± 20.1	102 ± 27.9	0.79
PEF	82.5 ± 17.7	92.0 ± 19.6	0.105	101 ± 17.9	105 ± 20.5	0.455
DLCO				87.9 ± 16.9	79.6 ± 22.4	0.209

pulmonary gas exchange. The final manifestations were restricted ventilation dysfunction, small airway dysfunction, and diffuse dysfunction [23]. The study results of Wang et al. [24] showed that residual lung injury and lung function impairment in patients with mild symptoms of COVID-19 could last for longer than one month. The pulmonary function results of this study showed that 21 patients (37.5%) met FVC% < 80%, FEV1% < 80%, and FEV1/FVC > 70% and had restricted ventilation dysfunction at discharge; and 31 patients (55.4%) had MEF 25 and MEF 50 < 70% predictive value, and had small airway dysfunction. Three months after discharge, 24 patients (42.9%) still had small airway dysfunction, and 10 of them (17.9%) had restricted ventilation dysfunction. The above results were consistent with pathological changes. The results in Table 4 of this study showed that the indexes of IVC, FEV1, FVC, MEF25, and MEF50 in severe patients were lower than those in normal type patients at discharge. The proportion of severe ventilation dysfunction and small airway dysfunction in severe patients at discharge and three months after discharge was also higher than that in normal type patients, suggesting that lung function injury in severe patients was more common than that in normal type patients. Previous results reported from a series of hospitalized COVID-19 patients showed that impaired lung diffusion function (TLCO <80% prediction) was the most common manifestation, in which obvious lung function deficit was only about one-tenth [25]. At 3 months after discharge, the mean value of DLCO% in 56 patients was (84.8% ± 19.2%), and 29 patients (51.8%) had DLCO% < 80%. Diffuse dysfunction was represented, including 23 patients with mild disorder and 6 patients with moderate disorder. Diffuse dysfunction was more common in severe COVID-19 patients (66.7%).

Our research shows that reaction ventilation dysfunction and pulmonary function index of small airway dysfunction IVC, FEV1 and FVC, MEF 25, and MEF 50 recover gradually over time. The lung function of 57% patients recovers well at three months after cured and discharge, which is consistent with a recent study about the lung injury recovery status of the the SARS patients after 15 years [26]. Therefore, we can

preliminarily infer that the lung function of COVID-19 patients, especially FEV1, FVC, MEF25, and MEF50, could recover gradually over time, suggesting that the interstitial inflammatory changes and interstitial fibrosis caused by or secondary to COVID-19 could be slowly recovered instead of progressive development. Unfortunately, we did not conduct the DLCO test at the time of discharge, so we could not evaluate the recovery of diffusion function. Our research results also show that the lung function damage in severe patients is more serious, with more apparent improvements in IVC (84.9 ± 19.8) and MEF25 indicators (80.2 ± 38.2) compared with that in normal type patients (IVC (82.4 ± 18.9) and MEF25 (78.0 ± 33.8)), indicating that with effective early management for heavy COVID-19 patients, the lung function could get better improvement. In combination with our study, some patients with COVID-19 have mild to moderate impairment in small airway or diffuse function on the day of release and 3 months after discharge, suggesting that the pulmonary function of COVID-19 patients has not been fully recovered in the early stage of rehabilitation. Combined with their pulmonary pathological changes, it is not still clear whether it is related to pulmonary interstitial lesions or pulmonary fibrosis lesions, which we will leave in our future study.

Because the detection of lung function is safe, noninvasive, and easy to be accepted by patients, it can be used as an objective indicator for clinical monitoring and evaluation of the pulmonary outcome of COVID-19 patients during recovery. This study shows that COVID-19 patients have pulmonary function impairment after clinical cure and discharge, mainly in dispersion dysfunction and small airway dysfunction. The pulmonary function could be improved gradually over time, and early pulmonary rehabilitation intervention might be helpful to the recovery of pulmonary function.

Data Availability

Data are available upon request from the corresponding author.

Conflicts of Interest

The authors declare no conflicts of interest.

Acknowledgments

This study was funded by the Medical Science and Technology Project Foundation of Zhejiang Province of China (2021KY1202, 2021KY393, and 2022KY1376), the Scientific Research Fund of Taizhou Science and Technology Agency (1801KY18), and the Scientific Research Foundation of Taizhou Enze Medical Center (Group) (20EZZDB1). The authors thank all patients involved in the study and acknowledge all healthcare workers involved in the diagnosis and treatment of patients in Taizhou, China.

References

[1] J. F.-W. Chan, S. Yuan, K.-H. Kok et al., "A familial cluster of pneumonia associated with the 2019 novel coronavirus indicating person-to-person transmission: a study of a family cluster," *The Lancet*, vol. 395, no. 10223, pp. 514–523, 2020.

[2] J. T. Wu, K. Leung, and G. M. Leung, "Nowcasting and forecasting the potential domestic and international spread of the 2019-nCoV outbreak originating in Wuhan, China: a modelling study," *The Lancet*, vol. 395, no. 10225, pp. 689–697, 2020.

[3] C. Drosten, S. Günther, W. Preiser et al., "Identification of a novel coronavirus in patients with severe acute respiratory syndrome," *New England Journal of Medicine*, vol. 348, no. 20, pp. 1967–1976, 2003.

[4] A. M. Zaki, S. van Boheemen, T. M. Bestebroer, A. D. M. E. Osterhaus, and R. A. M. Fouchier, "Isolation of a novel coronavirus from a man with pneumonia in Saudi Arabia," *New England Journal of Medicine*, vol. 367, no. 19, pp. 1814–1820, 2012.

[5] X. Mo, W. Jian, Z. Su et al., "Abnormal pulmonary function in COVID-19 patients at time of hospital discharge," *European Respiratory Journal*, vol. 55, no. 6, p. 2001217, 2020.

[6] C. Huang, Y. Wang, X. Li et al., "Clinical features of patients infected with 2019 novel coronavirus in Wuhan, China," *The Lancet*, vol. 395, no. 10223, pp. 497–506, 2020.

[7] N. Chen, M. Zhou, X. Dong et al., "Epidemiological and clinical characteristics of 99 cases of 2019 novel coronavirus pneumonia in Wuhan, China: a descriptive study," *The Lancet*, vol. 395, no. 10223, pp. 507–513, 2020.

[8] C. Michael, B. Adam, M. Xueyan et al., "CT imaging features of 2019 novel coronavirus (2019-nCoV)," *Radiology*, vol. 295, no. 1, pp. 202–207, 2020.

[9] G. E. Antonio, K. T. Wong, D. S. C. Hui et al., "Thin-section CT in patients with severe acute respiratory syndrome following hospital discharge: preliminary experience," *Radiology*, vol. 228, no. 3, pp. 810–815, 2003.

[10] D. S. Hui, K. T. Wong, F. W. Ko et al., "The 1-year impact of severe acute respiratory syndrome on pulmonary function, exercise capacity, and quality of life in a cohort of survivors," *Chest*, vol. 28, no. 3, pp. 1393–1400, 2005.

[11] H.-H. Hsu, C. Tzao, C.-P. Wu et al., "Correlation of high-resolution CT, symptoms, and pulmonary function in patients during recovery from severe acute respiratory syndrome," *Chest*, vol. 126, no. 1, pp. 149–158, 2004.

[12] National Health Commission & State Administration of Traditional Chinese Medicine, "Diagnosis and treatment protocol for novel coronavirus pneumonia (trial version 7)," *Chinese Medical Journal*, vol. 133, no. 9, pp. 1087–1095, 2020.

[13] L. Lin and T. S. Li, "Interpretation of guidelines for the diagnosis and treatment of novel coronavirus (2019-nCoV) infection by the national health commission (trial version 5)," *Zhonghua Yixue Zazhi*, vol. 100, pp. 805–807, 2020.

[14] B. L. Graham, V. Brusasco, F. Burgos et al., "2017 ERS/ATS standards for single-breath carbon monoxide uptake in the lung," *European Respiratory Journal*, vol. 49, no. 1, Article ID 1600016, 2017.

[15] B. H. Culver, B. L. Graham, A. L. Coates et al., "Recommendations for a standardized pulmonary function report. An official American thoracic society technical statement," *American Journal of Respiratory and Critical Care Medicine*, vol. 196, no. 11, pp. 1463–1472, 2017.

[16] E. J. Heckman, M. D. Heckman and G. T. O'Connor, Pulmonary function tests for diagnosing lung disease," *JAMA*, vol. 313, no. 22, pp. 2278-2279, 2015.

[17] Y. Gao, T. Li, M. Han et al., "Diagnostic utility of clinical laboratory data determinations for patients with the severe

Hindawi
Journal of Healthcare Engineering
Volume 2023, Article ID 9810863, 1 page
https://doi.org/10.1155/2023/9810863

Retraction

Retracted: Analysis on the Influence of Students' Health Quality Based on Intelligent Optimization of Sports Facilities and Equipment

Journal of Healthcare Engineering

Received 26 September 2023; Accepted 26 September 2023; Published 27 September 2023

This article has been retracted by Hindawi following an investigation undertaken by the publisher [1]. This investigation has uncovered evidence of one or more of the following indicators of systematic manipulation of the publication process:

(1) Discrepancies in scope
(2) Discrepancies in the description of the research reported
(3) Discrepancies between the availability of data and the research described
(4) Inappropriate citations
(5) Incoherent, meaningless and/or irrelevant content included in the article
(6) Peer-review manipulation

The presence of these indicators undermines our confidence in the integrity of the article's content and we cannot, therefore, vouch for its reliability. Please note that this notice is intended solely to alert readers that the content of this article is unreliable. We have not investigated whether authors were aware of or involved in the systematic manipulation of the publication process.

In addition, our investigation has also shown that one or more of the following human-subject reporting requirements has not been met in this article: ethical approval by an Institutional Review Board (IRB) committee or equivalent, patient/participant consent to participate, and/or agreement to publish patient/participant details (where relevant).

Wiley and Hindawi regrets that the usual quality checks did not identify these issues before publication and have since put additional measures in place to safeguard research integrity.

We wish to credit our own Research Integrity and Research Publishing teams and anonymous and named external researchers and research integrity experts for contributing to this investigation.

The corresponding author, as the representative of all authors, has been given the opportunity to register their agreement or disagreement to this retraction. We have kept a record of any response received.

References

[1] Q. Zhou, "Analysis on the Influence of Students' Health Quality Based on Intelligent Optimization of Sports Facilities and Equipment," *Journal of Healthcare Engineering*, vol. 2022, Article ID 8145127, 8 pages, 2022.

Hindawi
Journal of Healthcare Engineering
Volume 2022, Article ID 8145127, 8 pages
https://doi.org/10.1155/2022/8145127

Research Article

Analysis on the Influence of Students' Health Quality Based on Intelligent Optimization of Sports Facilities and Equipment

Qi Zhou

School of Physical Education, Shandong Normal University, Jinan, Shandong 250014, China

Correspondence should be addressed to Qi Zhou; lijw@sdnu.edu.cn

Received 3 December 2021; Revised 28 December 2021; Accepted 29 December 2021; Published 15 January 2022

Academic Editor: Gu Xiaoqing

Physical health promotion has always been a way for schools to pay close attention to and devote resources to their students' development, physical fitness, and social adaptability. To promote the improvement of students' overall physical quality, we must begin with the foundation and school physical education. This study proposes an improved K-means algorithm based on an analysis of the influencing factors of intelligent optimization of sports facilities and equipment on students' health quality. Clustering analysis is carried out based on two groups of data classified as boys and girls, using the improved K-means algorithm. The findings reveal that the average change trend of physical fitness test items in each male cluster is generally similar, with a moderate change. The change in the average score of physical fitness test items for each cluster of girls in the group showed two distinct valleys, and the trend was complicated. This necessitates schools to invest funds to construct venues and purchase equipment in order to increase the number of sporting events.

1. Introduction

As an important part of school education, school physical education is an effective way to improve quality education. It can lay a solid foundation for crazy sports, competitive sports, and lifelong sports and plays an important role in promoting students' health [1]. Sports venue equipment is the basic objective condition of school physical education. Whether the venue equipment is ready to be perfected is the key for teachers to achieve teaching objectives and tasks, and whether the venues and equipment can be reasonably used is an important link to improve teaching quality [2, 3]. The venue is the material guarantee implemented by the physical education class. Without the venue, physical education class will not be able to do it. Without the equipment or equipment shortage, it will not only affect the physical education class but also make students feel bored and reduce their enthusiasm so that physical education class cannot normally do it and cannot achieve the expected effect. Sports venue equipment plays a vital role in school sports [4].

The concept of school education is critical for college students' development [5]. The form, content, and innovative teaching methods of physical education are critical to the development of university physical education in the university curriculum. Currently, there are numerous issues with the construction of sports facilities and equipment, and numerous nuances in the intelligent design of competition venues. The design scheme is mixed up with the intelligent construction of other facilities during construction, causing the specific construction to become disorganized, and changing the construction scheme also delays the construction period and the use effect [6, 7]. In our country's university sports facilities, there are currently some issues, such as a lack of intelligent sports services, unscientific management, and a low level of openness and sharing [8]. As a result, if the country promotes the wide adoption of the internet of things and the development of the sports internet of things, these issues can be solved one by one using the technologies, concepts, and functions of the internet of things.

By understanding students' physical health problems, it is found that students get more physical exercises in their study and life, constantly improve their own health, face life and study with a healthier body, and develop comprehensive

moral, intellectual, and physical qualities. Therefore, this study not only embodies the concrete practical significance but also has certain theoretical value [9]. This study tries to find out the factors that affect students' health quality by investigating the intelligent optimization of sports facilities and equipment. So as to put forward some constructive suggestions, students' health quality should be improved, and a little contribution should be made to the school's physical education.

At present, the number of college students is increasing. Faced with a large number of student data, it is difficult for teachers to design personalized exercise prescriptions for each student, so as to efficiently and scientifically improve students' physical quality. Therefore, it is the focus of this study to use reasonable methods to analyze and evaluate physical test data and reasonably classify students, and how to reasonably recommend prescriptions. In order to solve the above problems, data mining technology is applied to cluster analysis of data samples by the K-L-Hearts algorithm. According to the characteristics of clustering results, some suggestions for improving physical fitness are put forward.

2. Related Work

According to literature [10] through the investigation of some schools, it is found that there is little difference in the quantity, compliance, and usage of essential sports equipment among schools of different sizes. Literature [11] mentioned that the investment in sports funds was insufficient; the number of students in the school is increasing year by year, which leads to the shortage of sports facilities in the school; due to the development of cities, land use is particularly tight; schools lack specialized sports management and maintenance personnel: the degree of socialization is not enough; school leaders do not pay enough attention to sports. Literature [12, 13] point out that the development of school sports cannot be separated from the management of school sports equipment protection and maintenance, which is extremely important. Literature [14–16] found that schools only pay attention to the construction of sports venues that occupy a small area, are easy to carry out sports events, are popular with popular students, have many functions, and have low investment costs. Literature [17] found that as long as sports venues and facilities' equipment are geared toward competitive sports, the degree of openness of sports facilities in schools is not enough, and students are charged for the use of some expensive facilities. The emergence of some problems is related to the development of present sports.

According to literature [18], from the relationship between sports and nutrition, it is discussed that the abnormal phenomenon that most of the quality development levels show a downward trend is closely related to the reduction in physical exercise and extracurricular activities caused by students' heavy learning burden. Literature [19] suggests that aiming at the increase in obesity among students, on the basis of strengthening students' exercise, also publicizes the impact of various food intake on physical fitness and regularly arranges strict physical examination; literature [20] concludes that malnutrition rate, especially severe malnutrition rate, is obviously decreasing, while overweight and obesity rates are increasing, so teenagers should have a reasonable diet, watch less TV, play less computer, strengthen physical exercise, and increase outdoor activities in their spare time. Literature [21] discusses that the reasons for examination-oriented education system, society, and family should pay for the decline of students' physical health. The comparison of before and after improvements in physical fitness test indicators in the literature [22] reveals a lack of health awareness among school leaders and teachers, and sports health has not been elevated to the highest or most important goal of student development. According to the literature [23], senior students are overweight or underweight. Despite the fact that the student's test scores were mostly passing, the excellent rate and the good rate are low, indicating that the student's physical health is not promising. The physical health of female college students was investigated in the literature [24], which discovered and analyzed the differences in physical health between different types of students. [25] According to a survey of college students from various regions of China, there are differences in physical fitness among college students. Shorter students in the Western region have poorer physical fitness, while taller students in the Eastern region have better physical functions.

3. Research Method

3.1. Health Overview. Physical health is our most concerned topic. There is a close relationship between physical fitness and health, and they are highly similar in terms of "good health." Usually, people with good health have healthy bodies, and people with healthy bodies also have good health. But this statement is not absolute, and there are differences in meaning between them.

When evaluating the health and physique of individuals, there are also differences in measurement and evaluation techniques and standards. When evaluating the physique of individuals, the first thing to think about is the health status and then the inductive evaluation of their shape, function, physical quality, sports strength, and psychology.

In order to improve students' physical health, we must first find ways to increase their awareness of physical activity and cultivate healthy sports attitudes. We all know that one of the factors affecting students' physical health is their lack of awareness of physical exercise, so it is critical to increase their awareness of physical exercise. As we all know, the body is the foundation of learning, and scientific and effective physical exercise is the best way for us to get healthy and learn.

Every student is an individual, and their ability to receive education and their ability to receive physical education differ. PE teachers should develop corresponding teaching plans based on individual student characteristics and teach students according to their aptitude when teaching courses, in order to more quickly promote the healthy development of students' physiques. Physical education teachers should make accurate assessments of students' strengths based on their current circumstances so that students can better

showcase their own strengths, address any weaknesses, and boost their self-confidence.

3.2. Intelligent Optimization of Sports Equipment and Facilities. In the twenty-first century, the social competitive pressure is becoming more and more intense. It not only includes superficial intellectual competition but also tests on physical and psychological aspects. These nonintellectual factors determine the success or failure of competition at the same time, and the important factor that determines this aspect is the health status. However, at present, some groups of college students lack the awareness of exercising, and their awareness of exercising is scientifically weak. Therefore, it is the key to effectively and scientifically improve college students' health quality, and exercise prescription is the best way to effectively and scientifically improve their health.

Whether or not the sports facilities and equipment are perfect will have a significant impact not only on teaching but also on the improvement of national competitive sports. Imperfect sports venues and facilities and a lack of good venues and equipment will not pique students' interest in sports learning, limiting their active participation in physical activity and limiting their physical quality improvement. Because they lack adequate venues and equipment, some students become bored with physical education classes. It is possible that they are uninterested, in which case their grades will not improve. Independent modules are used to create dependent modules. Independent modules can determine the built positions of other independent modules by creating and solving models. Dependent modules should be grouped together with the independent modules on which they rely. The model can be established as follows.

Assume that the dependent module X_m depends on the independent module $X_1, X_2, \ldots, X_a; m = n_1 + 1, \ldots, n, a = n_1$. Then, the mathematical model with the least cost for establishing the dependent module is as follows:

$$\min \sum_{i=1}^{a} f_{mi} d_{mi}. \tag{1}$$

The secondary facility planning method is adopted. First, all facilities are sorted in order of importance and area, and the ones with larger importance and area are taken out as independent modules. In this example, the first 8 modules are divided into independent modules and the next 25 modules are divided into dependent modules. The optimized layout model of independent modules is established as follows:

$$\min \sum_{i=1}^{8} \sum_{j=1}^{8} \sum_{k=1}^{8} \sum_{l=1}^{8} C_{ijkl} X_{ik} X_{jl}. \tag{2}$$

When the module i is built in position k, it is $x_{ik} = 1$, and otherwise, it is 0. The distance matrix between locations is D, and the transportation matrix between modules is F. It is required that these eight facility modules must be built at these eight locations to minimize the total cost.

After the independent module is optimized, a simple mathematical model is established for the remaining 25 dependent modules, assuming that the dependent module X_m depends on the independent module $X_1, X_2, \ldots, X_8; m = 9, \ldots, 33$. Then, the mathematical model with the least cost for establishing the dependent module is as follows:

$$\min \sum_{i=1}^{8} f_{mi} \sqrt{(x_m - x_i)^2 = (y_m - y_i)^2}. \tag{3}$$

The development balance of school teaching projects is linked to the irrational allocation of sports equipment. M schools only allocate some sports venues with low costs, multiple functions, and less land occupation, preventing some sports events from taking place; the single content of physical education in schools leads to unbalanced development of teaching items, while the allocation of school sports equipment is solely based on teaching items. Due to a slew of issues, sports facilities are being allocated in an irrational manner. The lack of attention given to school physical education by schools and educational authorities is the primary cause of these phenomena.

3.3. Analysis of College Students' Physical Health. The massive data and powerful analytical abilities of big data will provide more valuable possibilities for the promotion of students' physical health in concept and how to reveal hidden, previously unknown, and potentially practical information from the massive fuzzy and noisy historical data of practical application databases. The goal of clustering analysis is to group things into classes based on some attributes, with the as little similarity between classes as possible and as much similarity within classes as possible.

Clustering analysis is to reasonably divide data, establish classification according to certain principles, and determine the existence of data category by analyzing each record of original data in a historical record database. If the data sample set under study is M, C is defined as a nonempty subset of a sample set M: $C \subset M$ and $C \neq \varnothing$. Clustering is to satisfy the following conditions under the set of class $C_1, C_2, \ldots, C_k$:

$$\begin{cases} C_1 \cup C_2 \cup \cdots C_k = M, \\ C_i \cap C_j = \varnothing. \end{cases} \tag{4}$$

According to the first condition, each sample in the sample set M has a class corresponding to it, while the second condition indicates that each sample of M belongs to at most one class.

K-means algorithm is a typical distance-based clustering algorithm, which uses distance as the evaluation criterion of similarity, that is, the closer the distance between two objects, the greater the similarity. It can well solve the clustering problem of numerical attribute data objects. The algorithm is as follows:

(1) Randomly select k records from n records as centroid

(2) Measure each remaining record, get its distance to each centroid, and classify it to the nearest centroid class

(3) Recalculate the obtained centroid of each class

Iterate for 2 ~ 3 steps until the new centroid is equal to the original centroid or less than the specified threshold; then, the algorithm ends.

The flow of the K-means clustering algorithm is shown in Figure 1.

K-means is widely used because of its simplicity and easy realization. However, this algorithm has some defects. In this section, we will propose an improved algorithm to optimize the K-means algorithm.

The distance is calculated from each cluster center to other cluster centers, and half of the minimum distance is expressed as $d_{e(i)}$, that is, half of the minimum distance from the i th cluster center to other cluster centers. For all data points, the distance to the i th cluster center is calculated and compared with $d_{e(i)}$, respectively.

If the distance is less than or equal to $d_{e(i)}$, the data point is assigned to the i th cluster; otherwise, the distance from the point to other cluster centers is calculated. This process is repeated until the data point is assigned to other clusters. If the data point cannot be assigned to any cluster, it is put in the cluster where the nearest cluster center is located.

The improved algorithm is as follows:

$$d_{e(i)} = \frac{\min\left\{\left|C_i, C_j\right|\right\}}{2}, \tag{5}$$

where $d_{e(i)}$ is 1/2 of the minimum distance from the i th cluster to other clusters.

$$d\left(Z_p, M_j\right) = \sqrt{\sum_{k=1}^{d}\left(Z_{p,k} - M_{j,k}\right)^2}, \tag{6}$$

where Z_p is the p -th data point, M_j is the centroid of the j -th cluster, and d is the dimension.

$$M_j = \frac{1}{n_j}\left(\sum_{\nabla Z_p \in C_j} Z_p\right), \tag{7}$$

where n_j is the number of data points in the cluster j.

According to the requirements of the K-means algorithm, SPSS Modeler software is used to design clustering models for the records of boys and girls, respectively, as shown in Figure 2.

For male students, seven fields including vital capacity score, 50 m score, 1,000 m score, standing long jump score, sitting body flexion score, pull-up score, and total score are selected as input fields. For girls, seven fields, namely, vital capacity score, 50 m score, 800 m score, standing long jump score, sitting body flexion score, one-minute sit-up score, and total score, are selected as input fields.

After clustering, the results are divided into 1–5 categories. The larger the average score in these 5 categories of data, the better the students' sports performance in this index. Then, this value can be used to compare the same items in five types of data and analyze the running model to obtain clustering results.

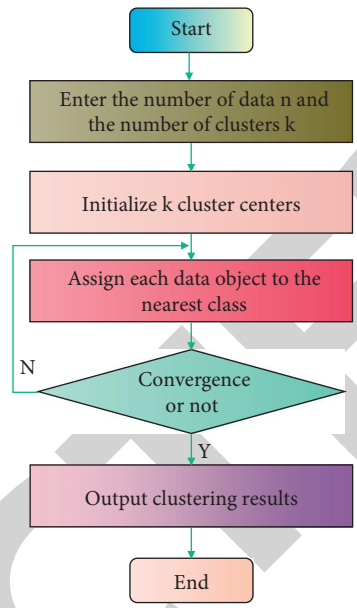

Figure 1: Algorithm flowchart.

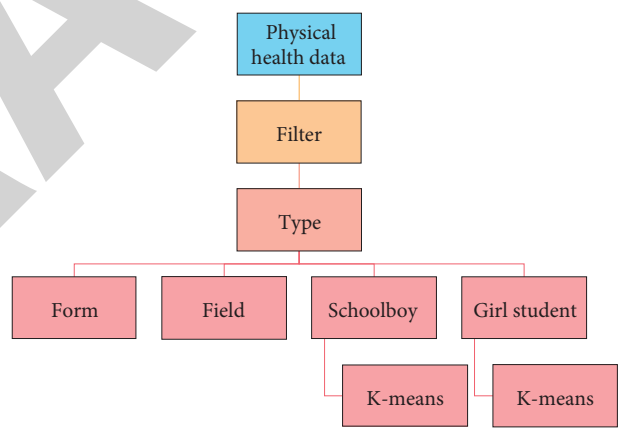

Figure 2: K-means clustering model.

4. Result Analysis and Discussion

4.1. Analysis on the Demand of Sports Venues and Equipment and Students' Participation in Sports Activities. Sporting activities are a way for students to unwind during their free time. The development of sports activities not only helps to relieve brain fatigue, but it also helps to relax the tense mood of the day, which is beneficial to students' health and has an impact on their physical fitness. Currently, all of the district's schools offer sports activities, but the majority of them focus on running, which distorts the concept of sports. The reason for this is that sports facilities are not sufficiently equipped to meet the needs of students.

After-school sports training is an effective means to cultivate students' hobbies, improve sports skills, and train talents for the country. It provides the source power for the development of school sports, is also an important part of China's current sports training system and mechanism, and is the foundation of cultivating outstanding sports talents in China.

Sports training needs to be based on sports venues and equipment. Sufficient sports venues and equipment can better tap their own potential and improve their own quality and skill level. Figure 3 shows the demand analysis of sports venue equipment and after-school sports practice.

Through the questionnaire survey of teachers, 60% of physical education teachers think that they cannot meet the needs of extracurricular physical education training, and 8% even think that they are not satisfied. Through interviews with teachers, the shortage of school sports facilities also directly affects students' training plans, and some students are particularly interested in emerging sports programs. However, due to the lack of sports facilities, such sports programs cannot be developed, which restricts the provision of sports reserve talents.

After a series of sports interventions, the subjects were retested, and it was found that the students' test scores were significantly improved. From the comparison before and after (Figure 4), the excellent rate and good rate of the test were significantly improved, especially the good rate increased by 10 percentage points, and the passing rate of the students was also decreasing. On the whole, the average scores of the students were effectively improved. Therefore, reasonable and scientific physical exercise can obviously improve students' physical quality.

Boys' test scores are steadily improving, as evidenced by the results of girls' tests (Figure 5). Girls' scores also have noticeable improvement. Girls' test pass rate has increased to 100% following the sports intervention, and the excellent and good rates are also improving. The data of the subjects are constantly improving in the above tests of boys and girls, and the effect is visible when students are subjected to aerobic exercises such as variable speed running and endurance running. As a result, students must engage in relevant scientific physical exercises on a regular basis in order to improve their cardiopulmonary function.

4.2. Analysis of Students' Health Quality

4.2.1. Analysis of K-Means Clustering Algorithm. Experiments will prove that the improved K-means algorithm improves the accuracy of clustering and reduces the number of iterations. In this study, Iris, wine, balance, and Pima data from the UCI database are selected as experimental data. The experimental hardware environment is Intel (*R*) Pentium (*R*) dual-core CPU 2.2 GHz, 2 GB memory, and 1 50G hard disk. The environment is Windows XP operating system, MATLAB.

Figure 6 is the experimental result of the average running average accuracy obtained by executing the two algorithms 100 times for these four datasets, respectively.

Figure 3: Analysis of the demand for sports venue equipment and after-school sports practice in mainland China.

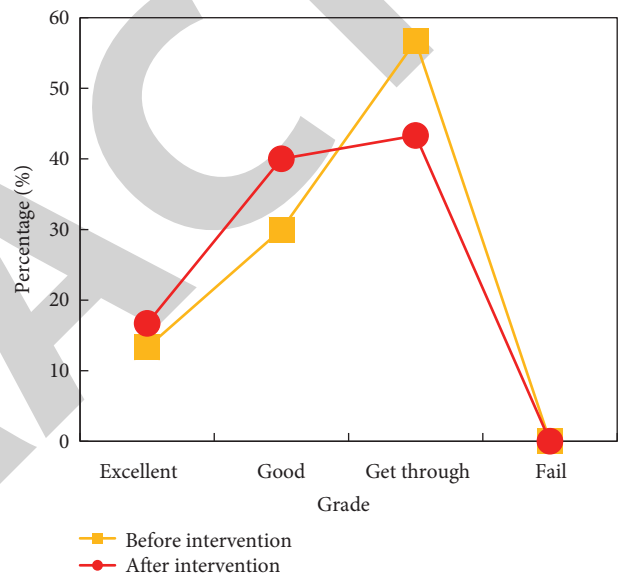

Figure 4: Comparison of male students' vital capacity test.

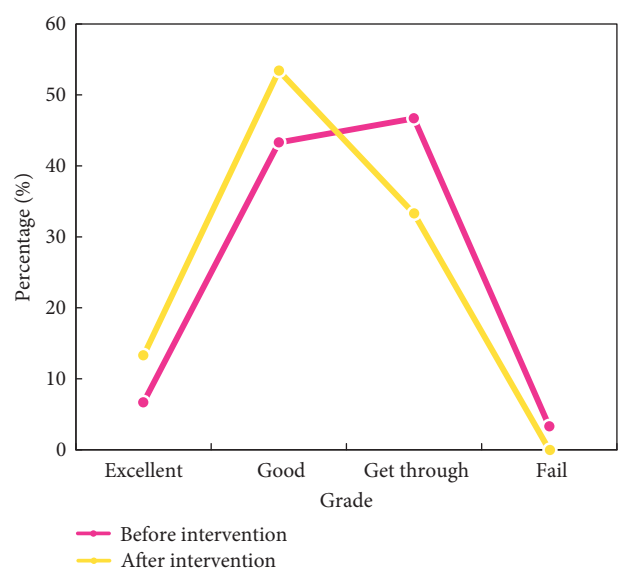

Figure 5: Comparison of girl's vital capacity test.

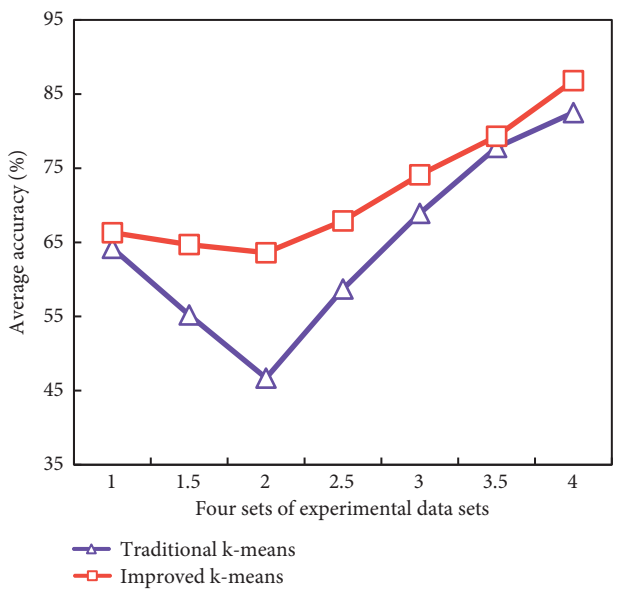

Figure 6: Hundred times average running average accuracy experimental results.

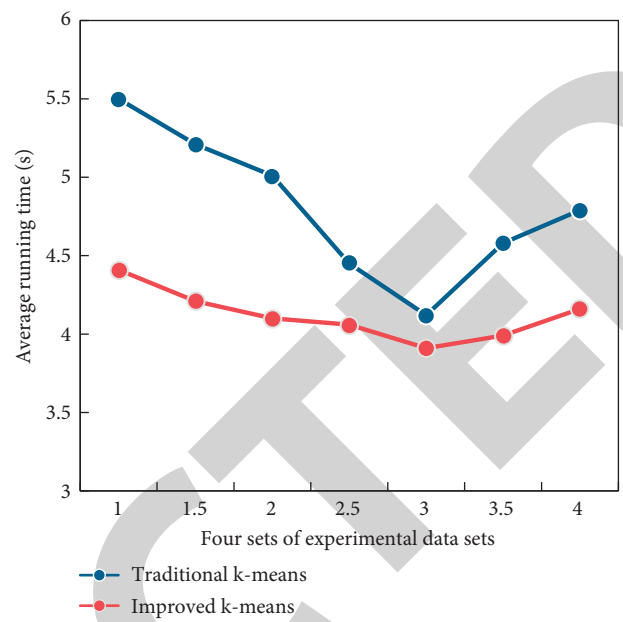

Figure 7: Experimental result chart of 100 times average running time.

From this figure, the improved algorithm avoids the unreasonable division caused by randomness when the original algorithm selects the initial clustering center by selecting the part of the data object set as the initial clustering center. So that the data point objects can be divided into more reasonable clusters. Therefore, the average accuracy of classification can be effectively improved.

Figure 7 is the experimental result of the average running time obtained by executing the two algorithms 100 times for these four datasets, respectively.

From this figure, it can be seen that the improved algorithm first improves the selection of the initial clustering center, thus reducing the running time of the algorithm. Second, because the traditional K-means algorithm needs to calculate the distance between data points and each cluster, the improved algorithm only needs to calculate the distance between data points and one cluster in the best case, so the average running time of the improved algorithm is significantly less than that of the original algorithm.

4.2.2. Results Analysis of Clustering. After summarizing the average scores of each individual physical quality of five types of students in the boys' group and girls' group, it can be seen that each cluster has its own characteristics. The results of clustering and the specific analysis of each cluster are as follows.

(1) The clustering results of boys are shown in Figure 8.

(2) The average total score of each item of cluster 1 boys is the highest and that of cluster 3 boys is the lowest. In 50 m, 1,000 m, standing long jump, sitting forward, and pull-ups, students in cluster 1 scored the highest, while students in cluster 3 scored the lowest except pull-ups. Students in cluster 5 of vital capacity items scored the highest.

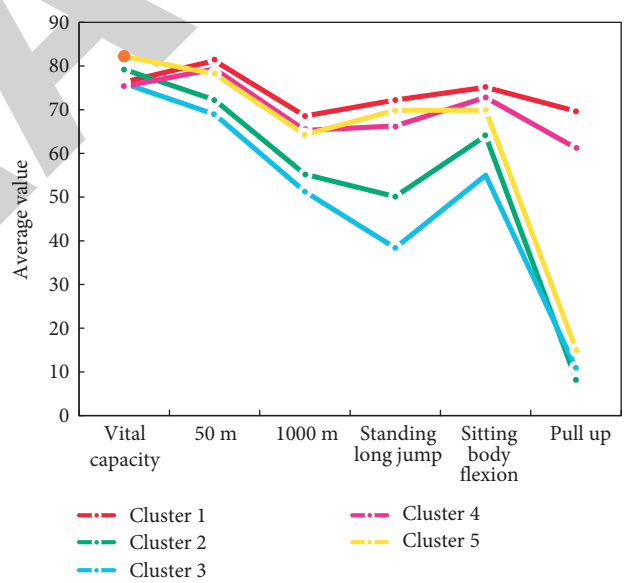

Figure 8: Change trend of average scores of boys after clustering.

(3) Cluster students also have the lowest score; there is little difference between the pull-up scores of boys in cluster 1 and cluster 4, but the pull-up scores of boys in clusters 2, 3, and 5 are extremely poor, especially the average pull-up scores of boys in cluster 2 are in single digits. Generally speaking, the pull-up scores of boys in five categories are the lowest, which also reflects the serious shortage of boys' upper limb strength.

(4) The 50 m, 1,000 m, sitting posture flexion, and pull-up of clustered boys have excellent performances among the five types of students, and the average of these four scores ranks second.

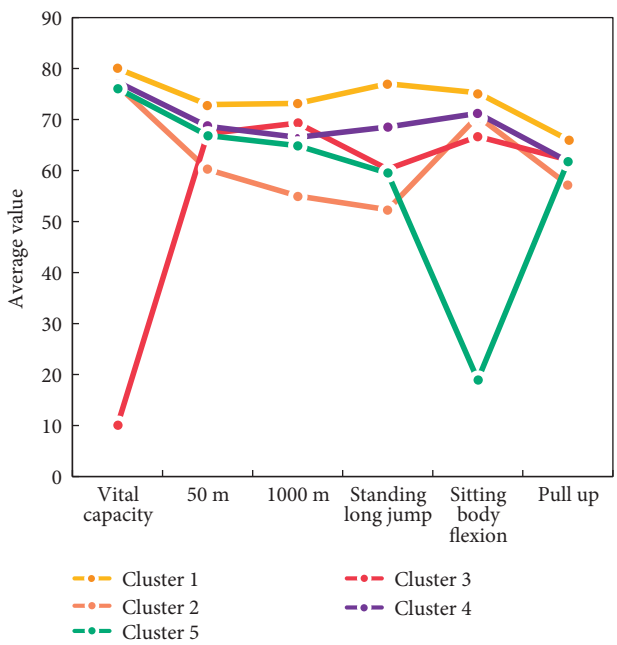

Figure 9: Change trend of average scores of girls after clustering.

Compared with the results of boys' clustering, the change in average scores of different items in each cluster of girls is more complicated. The average scores of girls after clustering are shown in Figure 9.

Cluster 1, 3, and 4 girls' scores of each item have the same changing trend, while cluster 2 and cluster 5 have great contrast between each item. The average score of cluster 1 in the listed seven items is far higher than that of other clusters, and the number of records occupied by cluster L is the highest. The average score of vital capacity of cluster 3 girls is only 10.12, and the average score of sitting body flexion of cluster 5 girls is 18.96, forming two abnormally prominent valleys.

The average total scores of girls in cluster 3 and cluster 5 rank first and second from the bottom, respectively, due to the large differences in these two items' scores. Cluster 2 girls have the lowest scores in the 50 m, 800 m, standing long jump, and sit-ups, but there is little difference between them and the other four clusters, so they are in the middle of the average total score comparison. The change trend of clustered girls' scores eased and remained high, while the average scores of all other scores ranked second, except for 800 m and sit-ups.

4.3. Suggestion. Relevant leaders of the Education Bureau and schools should attach importance to the development of school sports, increase investment in sports facility construction, and equip a set of perfect sports equipment for students to use. The school should be regularly supervised and inspected, especially the sports field equipment, and the school should be urged to strengthen the construction of sports field equipment. To establish a standardized sports equipment room, there should be explicit regulations and requirements for the entrance and exit of equipment. In the absence of sports venues and equipment, the diversity of site and equipment use should be known.

Schools should be people-oriented and meet the needs of students participating in sports activities; as a result, stadiums and facilities must be quickly built, and funds must be invested to purchase appropriate sports equipment. Physical education teachers should use this as a foundation for vigorously developing sports, enriching students' enjoyment of sports activities, allowing more students to participate in sports activities, enriching students' sports lives, and promoting students' athletic development. Physical health tests for students are not only a school requirement but also a good opportunity for students to learn about their physical condition. Students should have a clear and comprehensive understanding of their own physical information and the issues that come with it. The cause should be determined in light of the issue. For example, some common issues in girls include a severe lack of lower limb strength, poor aerobic exercise ability, and boys' weak upper limb strength, among others. When choosing sports events, all types of students should consider improving their physical quality with weak or serious information displays.

To deeply analyze the physique information of physique measurement data, not only the data from the horizontal direction is analyzed, but also the physique information of many years is compared vertically, and the regularity of its presentation is explored, so as to effectively predict the physique quality, which is in the trend of inferior development. From a scientific point of view, it is far from enough to only investigate the status quo of physical health. The reasons for the status quo of physical information should be deeply analyzed, effective intervention to the actual status should be made, and feedback information should be collect in real time to adjust and improve the intervention measures in time to fundamentally solve the actual problems.

5. Conclusions

There is a significant disparity between the school's physical education courses and students' preferred sports, preventing students from improving their physical fitness and mastering their skills. Due to the influence of sports facilities, some sports cannot be offered, resulting in students' lack of enthusiasm for physical education class. Overall, the subject test data are unsatisfactory, and the scores are on the verge of passing. There are few samples with noticeable data, particularly in boys' pull-ups, and many subjects fail the test. Clustering results show that there are obvious deficiencies in upper and lower limb strength levels of male and female students, respectively, based on the overall trend. As a result, it is necessary to investigate the internal relationship between students' physical fitness and indicators based on clustering results in order to promote physical health and in order to significantly improve students' physical health.

The algorithm's time complexity and performance need to be improved further. The improved algorithm will easily degenerate into the traditional K-means algorithm in the worst case or when the amount of data is small, so the next step is to improve the algorithm for these two special cases.

Hindawi
Journal of Healthcare Engineering
Volume 2023, Article ID 9803624, 1 page
https://doi.org/10.1155/2023/9803624

Retraction

Retracted: BJBN: BERT-JOIN-BiLSTM Networks for Medical Auxiliary Diagnostic

Journal of Healthcare Engineering

Received 10 October 2023; Accepted 10 October 2023; Published 11 October 2023

This article has been retracted by Hindawi following an investigation undertaken by the publisher [1]. This investigation has uncovered evidence of one or more of the following indicators of systematic manipulation of the publication process:

(1) Discrepancies in scope
(2) Discrepancies in the description of the research reported
(3) Discrepancies between the availability of data and the research described
(4) Inappropriate citations
(5) Incoherent, meaningless and/or irrelevant content included in the article
(6) Peer-review manipulation

The presence of these indicators undermines our confidence in the integrity of the article's content and we cannot, therefore, vouch for its reliability. Please note that this notice is intended solely to alert readers that the content of this article is unreliable. We have not investigated whether authors were aware of or involved in the systematic manipulation of the publication process.

Wiley and Hindawi regrets that the usual quality checks did not identify these issues before publication and have since put additional measures in place to safeguard research integrity.

We wish to credit our own Research Integrity and Research Publishing teams and anonymous and named external researchers and research integrity experts for contributing to this investigation.

The corresponding author, as the representative of all authors, has been given the opportunity to register their agreement or disagreement to this retraction. We have kept a record of any response received.

References

[1] C. Xu, F. Yuan, and S. Chen, "BJBN: BERT-JOIN-BiLSTM Networks for Medical Auxiliary Diagnostic," *Journal of Healthcare Engineering*, vol. 2022, Article ID 3496810, 7 pages, 2022.

Hindawi
Journal of Healthcare Engineering
Volume 2022, Article ID 3496810, 7 pages
https://doi.org/10.1155/2022/3496810

Research Article

BJBN : BERT-JOIN-BiLSTM Networks for Medical Auxiliary Diagnostic

Chuanjie Xu,[1] **Feng Yuan**,[2] **and Shouqiang Chen**[3]

[1]*Shandong Provincial Key Laboratory for Novel Distributed Computer Software Technology, Jinan, China*
[2]*School of Information Engineering, Shandong Management University, Jinan 250357, China*
[3]*Center of Hear of the Second Affiliated Hospital of Shandong University of Traditional Chinese Medicine, Jinan 250001, China*

Correspondence should be addressed to Feng Yuan; 2019020842@stu.sdnu.edu.cn

Received 8 November 2021; Revised 16 December 2021; Accepted 21 December 2021; Published 11 January 2022

Academic Editor: Gu Xiaoqing

This study proposed a medicine auxiliary diagnosis model based on neural network. The model combines a bidirectional long short-term memory (Bi-LSTM) network and bidirectional encoder representations from transformers (BERT), which can well complete the extraction of local features of Chinese medicine texts. BERT can learn the global information of the text, so use BERT to get the global representation of medical text and then use Bi-LSTM to extract local features. We conducted a large number of comparative experiments on datasets. The results show that the proposed model has significant advantages over the state-of-the-art baseline model. The accuracy of the proposed model is 0.75.

1. Introduction

At present, medical diagnosis is mostly based on the information obtained from the diagnosis of equipment and instruments, combined with the medical knowledge of physicians and years of accumulated experience for diagnosis. However, in the process of diagnosis, the subjectivity of the doctor may cause misdiagnosis in the process of diagnostic reasoning, which reduces the accuracy of manual diagnosis and weakens the confidence of patients in clinical practice [1, 2].

To solve this problem, researchers have proposed auxiliary models for clinical diagnosis and treatment [3, 4]. Specifically, the goal of the model is to predict the final diagnosis based on TCM symptoms as the input; for example, when we input relief of chest tightness but persistent tiredness and sluggishness, the model predicts a diagnosis of chest paralysis. Such a model can help practitioners use medical knowledge to more effectively solve various medical problems and make clinical diagnosis and decision-making faster, avoid omissions, and prevent the loss of relevant information, to find more solutions to intractable diseases [5, 6]. In view of this, this paper studies a new medical-assisted diagnosis model. Due to differences in individual levels of experience and research purposes, the conclusions reached from models can be relatively subjective as well as both time-consuming and difficult to implement in the clinic. Therefore, it is necessary to introduce new technologies and methods to quickly ascertain the doctors' research goals and clinical experience from massive amounts of medical data. In recent years, with the development of artificial intelligence, especially deep learning, more and more neural network technologies are applied to intelligent diagnosis. For example, modelling using neural networks and random forests shows high accuracy in clinical diagnosis with multicategory classification [7–9]. Although these models circumvent some of the problems of traditional methods, they still have great deficiencies in the acquisition of medical text information. So, the model's understanding of medical texts must be strengthened.

In this paper, a medical-assisted diagnosis model based on Bi-LSTM network and BERT was proposed. Bi-LSTM can better capture the information of the sentence and improving the classification performance of the sequence [10, 11]. BERT can generate a deeper two-way language representation; the word vector can contain more contextual

information [12, 13]. The model can complete five categories of classification tasks and can effectively enhance the understanding of the local features of TCM texts, thereby improving the accuracy of the model for predicting diseases.

The main contributions of our work can be summarized as follows:

(1) A model based on Bi-LSTM and BERT was proposed for medical-assisted diagnosis

(2) Incorporating global information into the extraction of local features can obtain more local features of the text

(3) The proposed model can also be fine-tuned to apply it to other professional fields

2. Related Work

At present, there are few studies on auxiliary diagnosis systems for clinical texts and those that do focus on English clinical texts and feature engineering; very little work exists on Chinese clinical texts and deep learning models. The method used for the auxiliary diagnosis model at the beginning is the comprehensive analysis method. Mi et al. [14] combined different data mining technologies and proposed a personal understanding and statistical analysis method to explore the dialectics and treatment rules of TCM-based disease treatment and obtain valuable information from them. With the development of machine learning, especially deep learning, many researchers apply it to auxiliary diagnosis. Chen et al. [15] applied support vector machines and decision trees to the classification of breast cancer texts and achieved good results. Ekong et al. [16] used the fuzzy clustering method to detect liver function patients. Xu et al. [17] designed and implemented a medical information text classification system based on a KNN. In addition, the three main deep learning models for auxiliary diagnosis are convolutional neural networks (CNNs) [18], recurrent neural networks (RNNs) [19], and FastText [20]. Zhang et al. [21] proposed an auxiliary diagnosis method based on a convolutional neural network. This model can diagnose the patient's condition through the wrist pulse. Kale et al. [22] applied a modern LSTM method to large datasets of multiple clinical time series for the first time and achieved certain results. Hu et al. [23] proposed a model that can be used to assist in diagnosis by calculating the Yin and Yang dialectic based on FastText. The input to these models can be words or characters. Although these models have achieved certain results, their understanding of the texts remains insufficient. Our proposed auxiliary diagnosis model can effectively solve this problem.

3. Model

The proposed model is shown in Figure 1. In this model, the bidirectional encoder representations from transformers (BERT) first obtains the global representation of the input text, then integrates the global information into the local information when extracting the local information, and finally performs the feature of the local information integrated into the global information. Extract and output the final prediction results.

3.1. BERT. First, we use BERT to get global information; the model architecture of BERT is based on the original transformer model. The input representation is a concatenation of WordPiece embeddings, positional embedding, and the segment embedding. Specifically, for single sentence classification, the segment embedding has no discrimination. Let W_t be the vector representation of the tth word in a sentence of length n; then, use BERT to encode to get h_t:

$$h_t = \mathrm{BERT}(w_t). \tag{1}$$

The BERT model is pretrained on unlabeled large-scale texts through two strategies, namely, shielding language modelling and next sentence prediction. The pretrained BERT token embedding provides a powerful context-sensitive utterance representation, which can be used in various target models, such as TextCNN and Bi-LSTM. Many natural language processing (NLP) tasks benefit from the use of BERT to achieve state-of-the-art performance and reduce training time. The transformer structure of the component in BERT is shown in Figure 2.

3.2. Bi-LSTM. After obtaining the global information, we use the bidirectional recurrent neural network to extract the local features integrated into the global information, and the LSTM network, which includes a set of memory cells, is able to learn long-term dependencies. The structure of a single memory cell is presented in Figure 3. The LSTM network transmits the input information in two ways, as an output (or hidden) vector (denoted by h) and as a state vector (denoted by c), which are combined using three gates that are explicitly designed to store and propagate long-term dependencies.

Gate i is called the input gate. The value of its output will be updated in the state vector. The gate f is called the "forgotten gate," which can determine which information in the previous state can be discarded. The storage unit uses the output of these two gates to create a new state vector. Finally, gate o, called the output gate, generates the final output vector of the memory cell. H represents the output of the current unit. The following equations are used in each memory cell to generate the output vector and state vector of the torque:

$$\begin{aligned}
i_t &= \delta(w_{xi} \cdot x_t + w_{hi} \cdot h_{t-1} + w_{ci} \cdot c_{t-1} + b_i),\\
f_t &= \delta(w_{xf} \cdot x_t + w_{hf} \cdot h_{t-1} + w_{cf} \cdot c_{t-1} + b_f),\\
c_t &= f_t \cdot c_{t-1} + i_t \cdot \tanh(w_{xc} \cdot x_t + w_{hc} \cdot h_{t-1} + b_c),\\
o_t &= \delta(w_{xo} \cdot x_t + w_{ho} \cdot h_{t-1} + w_{co} \cdot c_t + b_o),\\
h_t &= o_t \cdot \tanh(c_t).
\end{aligned} \tag{2}$$

After inputting all sentences into BERT, all vector representations of the current text can be obtained:

$$H = [h_1; h_2; \ldots h_n]. \tag{3}$$

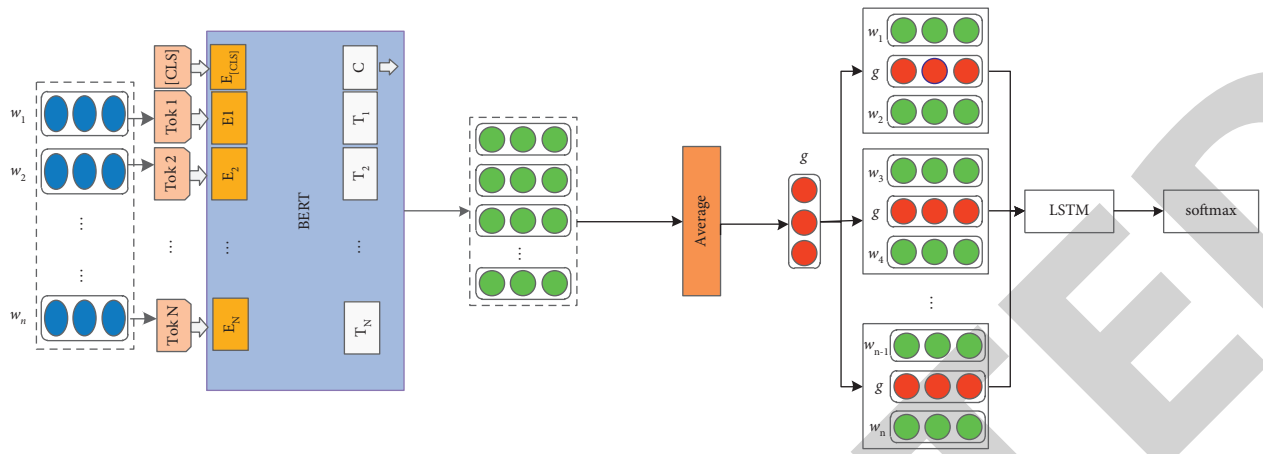

Figure 1: BJBN network model.

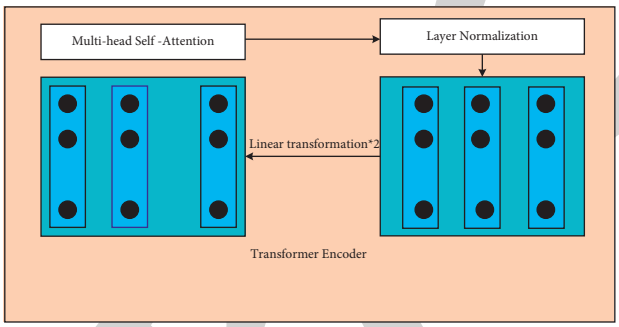

Figure 2: Transformer model structure.

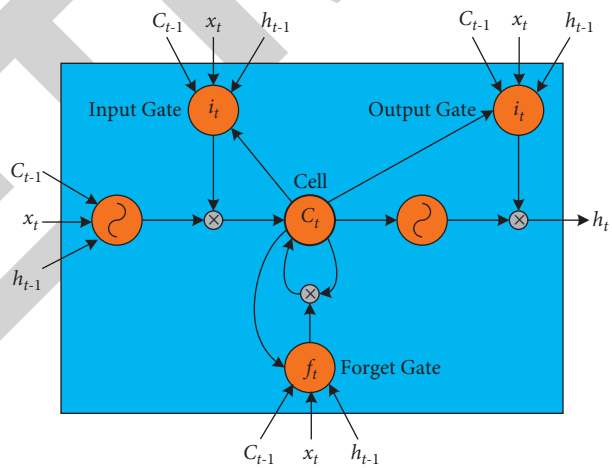

Figure 3: The structure of a memory cell.

Pass the obtained text vector through the average pooling layer to obtain the final global representation g:

$$g = \text{Average}(H). \tag{4}$$

After obtaining g_{-}, blend it into the middle of the local sequence and then use the recurrent neural network to extract its features. After extraction by the convolutional neural network, L is obtained:

$$L = \text{LSTM}(x_{t-1}, g, x_t). \tag{5}$$

After obtaining L through the recurrent neural network, pass it through the softmax layer to obtain the final prediction result PL:

$$\text{PL} = \text{softmax}(L). \tag{6}$$

4. Experiment

Experimental results show that our model achieves state-of-the-art performance. All experiments were performed on an Nvidia GTX 1080 and RTX 2080Ti GPU.

4.1. Data. We used 20,000 TCM medical records collected from the outpatient clinic of the Second Affiliated Hospital of Shandong University of Traditional Chinese Medicine from 2015–2019 as the dataset. For those data that do not meet the writing standards of Chinese medicine and duplicate data, we use manual methods to remove them. Of the 20,000 records obtained, 2333 can be used for this experiment. One of the data samples is as follows: the main cause is suffocation, and patient's legs were swollen for two consecutive months. The patient was diagnosed as coronary heart disease and myocardial infarction due to chest pain and sweating 7 years ago. Medication was taken; CABG surgery was performed in the same year, and medication was persisted thereafter. In the past 3 years, chest tightness during activity occurred again, and nitroglycerin can be relieved quickly. In the past 1 year, shortness of breath and fatigue were caused by exertion, and it was easy to catch a cold. In the past 2 months, edema of both lower extremities occurred. The patient has symptoms such as cough, sputum, abdominal distension, anorexia, nausea, and cold. The complexion is yellow and white, the tongue is pale and dark with ecchymosis and tooth marks, and the pulse is heavy. These data are associated with 5 disease categories (chest paralysis, dysphoria, dizziness, palpitations, and thirst). Figure 4 shows the percentage of various diseases. Table 1 shows the specific number of each disease. The training set contains 1866 records, and the test set contains 467 records. The average number of characters in each record is 316. To ensure proper experimental results, we manually divided the dataset to create the training and test data. The ratio of the incidence of each disease in the training set to that of the test set is 4 : 1.

4.2. Detailed Description of the Experiment. In this study, the natural language toolkit (NLTK) is used in the preprocessing stage to process each question and its corresponding answer in the dataset. The processing includes case conversion, stemming reduction, and stop-word removal. The GloVe model proposed by Pennington et al. [24] was trained to obtain 300-dimensional initial word vectors, while the word vectors of words not in the dictionary were initialized to 300-dimensional zero vectors. Adam is used as the optimizer in this paper, with a first momentum coefficient of 0.9, a second momentum coefficient of 0.999, adaptive learning rates of $[1 \times 10^{-9}, 4 \times 10^{-5}, 1 \times 10^{-7}]$, L2 parameters of $[1 \times 10^{-6}, 4 \times 10^{-7}, 1 \times 10^{-7}]$, and batch sizes of $[64, 128, 256]$. We select the best parameters with the training set and then evaluate the final performance with the test dataset.

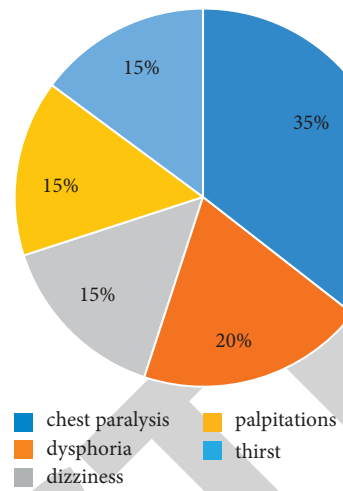

Figure 4: Percentage of the Chinese medical record datasets by symptom.

4.3. Experimental Results and Analysis. To evaluate the performance of the model proposed in this article, three indicators are used: F1-score, accuracy (Acc), and mean average of precision (MAP). We also use these indicators to compare the results of the proposed model with seven pre-existing classification models. These comparisons are shown in Table 2 in which (1), (2), (3), (4), (5), (6), and (7) correspond to [22, 23, 25–29], respectively, and (8) is the proposed method (baseline).

From the results of Table 2, we can draw the following conclusions:

(1) The FastText model, based on n-grams, performs better than the TextCNN and TextRNN models in the three evaluation indexes (MAP, F1-score, and Acc) mainly because there are a large number of medical nouns in the experimental datasets used in this article, which are utilized by the n-grams feature, resulting in a better model performance. These results also prove that it is necessary to train the word vectors in special fields (Row1 vs. Row2 and Row3).

(2) The TextRCNN method is superior to the TextCNN, TextRNN, and FastText models according to the three indicators used in this experiment. The main reason for this is that TextRCNN combines the advantages of the TextCNN and TextRNN models

Table 1: The corpus size of the dataset of Chinese medical records.

Data set	Symptom name	Number of medical records	Number of characters
TCM data	Chest pain	826	261016
	Dysphoria	453	143148
	Dizziness	360	113760
	Palpitations	349	100804
	Thirst	345	109020

Table 2: Experimental results of eight models with TCM data.

Model	Average acc	Average precision	Average recall	Average F1-score
FastText	0.6628	0.7520	0.5866	0.6592
TextCNN	0.6243	0.7362	0.5621	0.6375
TextRNN	0.6521	0.7456	0.5697	0.6459
TextRCNN	0.6957	0.7672	0.6238	0.6881
DPCNN	0.6139	0.6692	0.5873	0.6256
TextRNN_Att	0.7153	0.7749	0.6477	0.7056
Transformer	0.6285	0.6837	0.5891	0.6329
Our model	0.7512	0.8352	0.6818	0.7569

and makes them complementary. This result also proves that although the n-grams feature has an important role in the medical diagnostic process; as the architecture of the deep learning network model becomes more complicated, the effect of the n-grams feature will result in a worse performance than the deep learning model, which is why the deep learning model shines in various natural language processing tasks (Row4 vs. Row1, Row2, and Row3).

(3) Compared with those for the deep pyramid convolutional neural network (DPCNN) method, the results obtained for the previous four methods are poor. This is because the DPCNN model is relatively complicated. At the same time, the datasets used in this article are mostly short text. Not all tasks using deep learning methods can achieve good results; we should choose the model that suits our needs for specific tasks in order to effectively obtain good results (Row5 vs. Row1, Row2, Row3, and Row4).

(4) The TextRNN_Att method outperforms methods (1)–(5) in terms of the three evaluation indicators. This is because TextRNN_Att introduces the attention mechanism into TextRNN; this captures the displayed text sequence features and thus shows good results, further proving that the introduction of the attention mechanism is beneficial for medical auxiliary diagnostic tasks (Row6 vs. Row1, Row2, Row3, Row4, and Row5).

(5) The transformer method only slightly outperforms the DPCNN method and is otherwise outperformed by several of the other models in terms of the three evaluation indicators. This is because most of the datasets used in this article are short text. Transformer is relatively complicated and therefore performs poorly when capturing short text features. These results further prove that the Transformer model is not suitable for medical auxiliary diagnostic tasks (Row7 vs. Row1, Row2, Row3, Row4, Row5, and Row6).

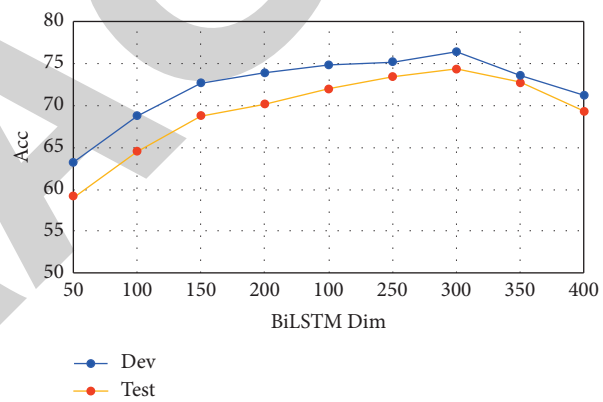

Figure 5: The influence of Bi-LSTM dimensions on experimental results.

(6) The medical-assisted diagnosis method proposed in this paper to enhance local feature extraction has higher MAP, F1, and Acc values than all the above models. It can be seen that the proposed model can effectively use global information to enhance the local information of medical text extraction ability, which also shows that the method proposed in this paper is an effective medical-assisted diagnosis method.

4.4. Parameter Sensitivity. In this section, we evaluate the impact of some parameters such as hidden state dimension of Bi-LSTMs on our dataset.

We investigate the impact of hidden state dimension of LSTMs with results shown in Figure 5. We can see that Acc of our model shows an upward trend when the dimension size is less than 300, especially achieving highest when the dimension size is exactly 300, which indicates that a large

dimension size could contribute to model performance. However, when the dimension size is larger than 300, the accuracy of the model drops on both development sets and test sets possibly due to insufficient training data.

5. Conclusion

In this paper, the medical auxiliary diagnosis model is studied by using a real-world medical dataset, leading to the proposal of a new model to address the shortcomings of existing methods. The experimental results show that our proposed model has certain advantages over previous models in medical auxiliary diagnosis. The main results of this paper can be summarized in two points. (1) A model based on Bi-LSTM and BERT was proposed for medical-assisted diagnosis. (2) Our work of this paper can have an inspirational effect on research in related fields.

Our experimental results show that the proposed auxiliary diagnostic model can obtain better results than the previous classic model, achieving an accuracy of 75.69%, which is very competitive with recently published auxiliary diagnostic models.

Data Availability

The data used to support the findings of this study are available from the corresponding author upon request.

Conflicts of Interest

The authors declare that they have no conflicts of interest.

Authors' Contributions

Chuanjie Xu and Feng Yuan are co-first authors.

Acknowledgments

This work was supported by Shandong Provincial Natural Science Foundation (ZR2019MG022) and Shandong Provincial Key R&D Project (2019GGX101056).

References

[1] F. Cheung, "TCM: m," *Nature*, vol. 480, no. 7378, pp. S82–S83, 2011.

[2] Z. Huang and A. Pan, "Non-local weighted regularization for optical flow estimation," *Optik*, vol. 208, Article ID 164069, 2020.

[3] W. Cai, B. Liu, Z. Wei, M. Li, and J. Kan, "TARDB-Net: triple-attention guided residual dense and BiLSTM networks for hyperspectral image classification," *Multimedia Tools and Applications*, vol. 80, no. 7, Article ID 11291, 2021.

[4] K. Zhong, Y. Wang, J. Pei, S. Tang, and Z. Han, "Super efficiency SBM-DEA and neural network for performance evaluation," *Information Processing & Management*, vol. 58, no. 6, Article ID 102728, 2021.

[5] X. Ning, K. Gong, W. Li, L Zhang, X Bai, and S Tian, "Feature Refinement and Filter Network for Person Re-identification," *IEEE Transactions on Circuits and Systems for Video Technology*, vol. 31, no. 9, 2020.

[6] X. Chen, P. H. Liu, Y. Z. Sun et al., "Research on disease prediction models based on imbalanced medical data sets," *Chinese Journal of Computers*, pp. 1–14, 2017.

[7] J. Wang, R. Wu, and X. Z. Zhou, "Syndrome factors based on SVM from coronary heart disease treated by prominent TCM doctors," *Journal of Beijing University of Traditional Chinese Medicine*, vol. 31, no. 8, pp. 540–543, 2008.

[8] L. Xu, S. Q. Chen, J. H. Hou, W. X. Bi, and F. Yuan, "The research on the construction of the TCM differentiation model based on BP neural network," *World Chinese Medicine*, vol. 11, no. 2, pp. 335–338, 2016.

[9] H. Wang and X. Hu, "Intelligent diagnosis classification on TCM five pathogens produced by five organs," *Jisuanji Gongcheng yu Yingyong(Computer Engineering and Applications)*, vol. 47, no. 6, 2011.

[10] J. Yang, J. Liu, R. Han, and J. Wu, "Generating and restoring private face images for internet of vehicles based on semantic features and adversarial examples," *IEEE Transactions on Intelligent Transportation Systems*, pp. 1–11, 2021.

[11] K Zhong, Y Wang, J Pei, S Tang, and Z Han, "Super efficiency SBM-DEA and neural network for performance evaluation," *Information Processing & Management*, vol. 58, no. 6, 2021.

[12] J. Yang, J. Liu, and R. Han, "Transferable face image privacy protection based on federated learning and ensemble models," *Complex & Intelligent Systems*, vol. 7, no. 5, pp. 2299–2315, 2021.

[13] J. Yang, B. Guo, Z. Wang, and Y. Ma, "Hierarchical prediction based on network-representation-learning-enhanced clustering for bike-sharing system in smart city," *IEEE Internet of Things Journal*, vol. 8, no. 8, pp. 6416–6424, 2021.

[14] M. H. Ying, L. C. Yun, and L. H. Rong, "Analysis Method of Chinese Medical Records," *Chinese Journal of Experimental Traditional Medical Formulae*, 2017.

[15] G. Chen, J. Warren, and P. Riddle, "Semantic space models for classification of consumer webpages on metadata attributes," *Journal of Biomedical Informatics*, vol. 43, no. 5, pp. 725–735, 2010.

[16] V. E. Ekong, E. A. Onibere, and A. A. Imianvan, "Fuzzy cluster means system for the diagnosis of liver diseases," *Journal of Computer Science and Technology*, vol. 2, no. 3, pp. 205–209, 2011.

[17] X. Xu and Q. Zhang, "Research of medical information text categorization based on knn algorithm," *Comput Technol Dev*, vol. 19, no. 4, pp. 206–209, 2009.

[18] Y. Kim, "Convolutional Neural Networks for Sentence classification," 2014, https://arxiv.org/abs/1408.5882.

[19] P. Liu, X. Qiu, and X. Huang, "Recurrent neural network for text classification with multi-task learning," in *Proceedings of the Twenty-Fifth International Joint Conference on Artificial Intelligence*, NY, USA, July 2016.

[20] A. Joulin, G. Edouard, B. Piotr, and M. Tomas, "Bag of tricks for efficient text classification," 2016, https://arxiv.org/abs/1607.01759.

[21] S. R. Zhang and Q. F. Sun, "Human pulse recognition based on convolutional neural networks," in *Proceedings of the 2016 International Symposium on Computer, Consumer and Control (IS3C)*, IEEE, Xi'an, China, July 2016.

[22] Z. C. Lipton, D. C. Kale, and R. C. Wetzell, "Phenotyping of clinical time series with lstm recurrent neural networks," 2015, https://arxiv.org/abs/1510.07641.

[23] Q. Hu, T Yu, L Zhu, J Li, Q Yux, and Y Gux, "A preliminary study on imbalanced syndrome differentiation of cold and heat," in *Proceedings of the International Conference on*

Hindawi
Journal of Healthcare Engineering
Volume 2023, Article ID 9842124, 1 page
https://doi.org/10.1155/2023/9842124

Retraction

Retracted: Mechanism of Depression through Brain Function Imaging of Depression Patients and Normal People

Journal of Healthcare Engineering

Received 10 October 2023; Accepted 10 October 2023; Published 11 October 2023

This article has been retracted by Hindawi following an investigation undertaken by the publisher [1]. This investigation has uncovered evidence of one or more of the following indicators of systematic manipulation of the publication process:

(1) Discrepancies in scope
(2) Discrepancies in the description of the research reported
(3) Discrepancies between the availability of data and the research described
(4) Inappropriate citations
(5) Incoherent, meaningless and/or irrelevant content included in the article
(6) Peer-review manipulation

The presence of these indicators undermines our confidence in the integrity of the article's content and we cannot, therefore, vouch for its reliability. Please note that this notice is intended solely to alert readers that the content of this article is unreliable. We have not investigated whether authors were aware of or involved in the systematic manipulation of the publication process.

Wiley and Hindawi regrets that the usual quality checks did not identify these issues before publication and have since put additional measures in place to safeguard research integrity.

We wish to credit our own Research Integrity and Research Publishing teams and anonymous and named external researchers and research integrity experts for contributing to this investigation.

The corresponding author, as the representative of all authors, has been given the opportunity to register their agreement or disagreement to this retraction. We have kept a record of any response received.

References

[1] C. Tang, Y. Zhang, Z. Zhai, X. Zhu, C. Wang, and G. Yang, "Mechanism of Depression through Brain Function Imaging of Depression Patients and Normal People," *Journal of Healthcare Engineering*, vol. 2022, Article ID 1125049, 13 pages, 2022.

Hindawi
Journal of Healthcare Engineering
Volume 2022, Article ID 1125049, 13 pages
https://doi.org/10.1155/2022/1125049

Research Article

Mechanism of Depression through Brain Function Imaging of Depression Patients and Normal People

Chaozhi Tang,[1] Yuling Zhang,[1] Zihan Zhai,[1] Xiaofeng Zhu,[1] Chaowei Wang,[2] and Ganggang Yang[1]

[1]*College of Life Sciences, Henan Normal University, Xinxiang 453007, Henan, China*
[2]*Department of Neurology, The First Affiliated Hospital of Xinxiang Medical College, Xinxiang 453100, Henan, China*

Correspondence should be addressed to Ganggang Yang; 041128@htu.edu.cn

Received 28 September 2021; Revised 15 November 2021; Accepted 25 November 2021; Published 10 January 2022

Academic Editor: Gu Xiaoqing

In recent years, functional magnetic resonance technology has discovered that abnormal connections in different brain regions of the brain may serve as the pathophysiological mechanism of mental illness. Exploring the mechanism of information flow and integration between different brain regions is of great significance for understanding the pathophysiological mechanism of mental illness. This article aims to analyze the mechanism of depression by comparing human brain images of normal people and patients with depression and conduct research. Fluoxetine, a selective 5-HT reuptake inhibitor (SSRI) widely used in clinical practice, can selectively inhibit 5-HT transporter and block the reuptake of 5-HT by the presynaptic membrane. The effect of 5-HT is prolonged and increased, thereby producing antidepressant effects. It has low affinity for adrenergic, histaminergic, and cholinergic receptors and has a weaker effect, resulting in fewer adverse reactions. This paper uses the comparative experiment method and the Welch method and uses the average shortest path length L to describe the average value of the shortest path length between two nodes in the network. Attention refers to the ability of a person's mental activity to point and to concentrate on something. Sustained attention means that attention is kept on a certain cognitive object or activity for a certain period of time, which is also called the stability of attention. The research on attention of depression patients generally focuses on continuous attention, and the results obtained show inconsistencies. Most studies have shown that the sustained attention of the depression group is significantly worse than that of the healthy control group. An overview of magnetic resonance imaging technology and an analysis of depression based on resting state were carried out. The key brain areas of the sample core network were scanned, and the ALFF results were analyzed. The data showed that the severity of depression in the depression group was negatively correlated with the ReHo value in the posterior left cerebellum ($P = 0.010$). The sense of despair was negatively correlated with the ReHo value in the posterior right cerebellum ($P = 0.013$). The diurnal variation was negatively correlated with the ReHo value of the left ring ($P = 0.014$). It was positively correlated with the ReHo value of the left ventricle ($P = 0.048$). This experiment has better completed the research on the mechanism of depression by analyzing the functional images of patients with depression and normal human brain.

1. Introduction

Inhibition refers to the brain's ability to prevent the input of irrelevant information, suppress the original information or interference information that has nothing to do with the current task, and restrain the activation of inappropriate dominant responses caused by related clues. Research on brain networks related to depression has also become one of the research hotspots in recent years. Some studies use specific tasks to stimulate depression patients and then compare the brain activity of normal controls [1]. It was found that the patient's prefrontal lobe, amygdala, hypothalamus, hippocampus, and other regions had abnormal activities. In addition, studies have also reported that changes in dorsal and frontal lobe activity are positively correlated with depression [2]. The hippocampus is negatively correlated with autocorrelation. The study found that when patients with major depression have negative images related to emotions or text descriptions related to self-processing, the basic nodes of the front and back default

pattern network—the posterior cortex and the ventricular prefrontal cortex—are reduced [3, 4].

Depression is one of the most common mental illnesses. According to the latest report of the World Health Organization, depression affects 4.4% of the world's population and causes the most important nonfatal disease burden. Although the basic research of neuropsychiatry has made great progress in recent years, it is still lagging behind to apply the acquired basic research information of depression to the clinic [5]. This is because our understanding of the pathological mechanism of depression is still very good. Limitations, this is also reflected in the heterogeneity of the concept of depression disease and the limited therapeutic effect. Psychiatrists still rely on DSM, ICD, and other systems to diagnose from a symptomatic point of view and lack objective testing tools, such as imaging scans and serological examinations to help diagnose depression, choose treatment, and manage response to treatment. Therefore, the exploration of the pathological mechanism of depression is still a hot and difficult point in current research. Memory is the basis of various human mental activities. Therefore, memory function is very important for normal human mental activities. Memory decline is also one of the common main complaints of patients with depression. There are abundant researches on memory in patients with depression, involving delayed memory of speech, visuospatial memory, working memory, short-term memory, implicit memory, and explicit memory.

In recent years, many scholars and experts at home and abroad have conducted in-depth thinking and research on this issue. Liu et al. pointed out that delusion is a way for individuals to respond to negative life events. Such people often focus their attention on their own depressive emotions, increase their attention and memory of negative information around them, tend to recall experiences and events related to negative moods, and do not adopt positive attitudes and behaviors. The study did not mention how to solve this problem [6]. Han et al.'s hopelessness theory believes that when individuals experience negative life events, they always view things negatively, thinking that they are incapable and unable to solve problems and often feel helpless and hopeless [7]. Shalini and Sanchita also pointed out those patients with depression have negative biases. Such people always consciously or unconsciously pay attention to negative stimuli in the environment, often have miserable and hopeless thoughts, and often make negative evaluations of themselves and the surrounding environment. This negative bias often affects interpersonal communication and hinders social function [8]. Research by Anusri et al. found that some of the above-mentioned brain areas of the brain have reduced BOLD signal strength when performing some cognitive-related tasks. But his research did not summarize this phenomenon as the concept of negative activation [9]. Stetka mainly used PET technology to extract the BOLD signals of the negatively activated brain regions induced by these tasks and compared them with the signals in the resting state. They found that these brain regions were consistent with the activity level of the whole brain. The brain area is a special activity state in the resting state. However, his research has not confirmed that there is a reliable and stable negative correlation between some active networks and default networks when performing tasks [10]. Perelman compared the activation of the default network of depressed patients and healthy people in the task state and found that the negative activation of the default network increases, that is, patients with depression are more inhibited. However, no specific brain area was pointed out [11]. After Atluri et al. discovered the phenomenon of blood-oxygen-level-dependent signal response, people have new technical means for detecting the brain. But he did not summarize the magnetic resonance imaging technology [12].

PET is the only new imaging technology that can display the metabolism of biomolecules, receptors, and nerve mediators in the living body. It has been widely used in the diagnosis and differential diagnosis of various diseases, disease judgment, curative effect evaluation, organ function research, and new drug development, etc. The innovations of this article are as follows: (1) It mainly summarizes the research methods, technical methods, and related algorithms used in the article. (2) The average aggregation rate of all nodes in the network is expressed by the algorithm, and the MSC is redefined using the smoothing technique (Welch method). (3) Various parts of the human brain are discussed and analyzed.

2. Methods of the Mechanism of Depression through Brain Function Imaging of Depression Patients and Normal People

2.1. Data Research Methods of Functional Magnetic Resonance Imaging. In recent years, since the impairment of cognitive function in depression is directly related to the rehabilitation of the social function of patients with depression, research on cognitive impairment in depression has received extensive attention. Cognitive functions include a variety of mental activities such as perception, attention, memory, thinking, executive function, and language comprehension.

Functional magnetic resonance imaging (functional magnetic resonance imaging (fMRI)) is an emerging neuroimaging method, and its principle is to use magnetic resonance imaging to measure the changes in hemodynamics caused by neuronal activity. Due to its non-invasiveness, no radiation exposure problems, and its wider application, fMRI has occupied a place in the field of brain function positioning since the 1990s. It is mainly used to study the brain or spinal cord of humans and animals. The traditional data research method needs to obtain the information under the task state in advance and then compare and analyze it with the subsequent information, but now, the fMRI imaging technology is combined to collect the fMRI data of the subject, in which we can get the difference through different regions of interest (ROI). ROI feature changes information under different time series, so it is no longer necessary to obtain information for comparison in advance, and this data analysis method is based on the fMRI data analysis method [13–15]. At present, there are many

methods for fMRI data analysis. According to the degree to which the analysis method depends on the stimulus, the analysis techniques are divided into two categories: one is based on model-driven methods, and the other is based on data-driven methods [16]. The model-driven method is a method based on statistical analysis, and its prerequisite is that the time-to-time images of the pre-brain activity are known. This method is suitable for single functional positioning of the brain, predicting the temporal image of brain activity according to the time of stimulation, and then using the predicted temporal image of brain activity for statistical analysis and positioning [17–19]. A sample image of monitoring using fMRI is shown in Figure 1.

The condition of cognitive impairment in patients with depression needs to be explored in depth. In addition, there are not many studies on the factors affecting cognitive impairment in patients with depression, mainly focusing on the impact of a single factor on cognitive impairment in patients with depression. The main factors involved are the severity of depression, the first episode, or relapse, whether to take drugs, and the course of the disease. Therefore, it is necessary to conduct further research on the relationship between related factors and cognitive impairment in patients with depression. However, when it comes to the positioning of complex brain functions, data-driven methods are required. The majority of scientific researchers have also proposed many methods of positioning analysis, mainly the following:

(1) Principal component analysis (PCA) method [20]: in fMRI technology, the spatial resolution is high, and more ROI areas are often selected during data acquisition, resulting in a larger dimensionality of the fMRI data collected, making the processing process more complicated, so it can be based on some of the ROI data. Contact or functional correlation to compress the data (that is, principal component analysis) retains its main information in the compressed data and then selects features with a higher contribution rate as the signal reflection of fMRI data [21–23]. Depression is a kind of mental illness characterized by significant and lasting depression. It is the main type of mood disorder and one of the common mental disorders. Depression has high morbidity, mortality, and public health costs.

(2) Cluster analysis (CA) method [24]: fuzzy cluster analysis technology is an effective method for functional positioning in the research of functional nuclear magnetic resonance data. This method is an exploratory analysis method that can affect the generalization rate of clustering by adjusting the characteristics of the input and then showing the contribution of the input features through the change of the clustering generalization rate [25, 26]. It is an unsupervised analysis method and has good development prospects. Miguel Nicollis calls the brain network a "shared brain-computer interface," that is, this brain-computer interface is operated by multiple people and applies this technology based on a common goal. For example, physical therapists and doctors can use brain-computer interface technology to take care of or take care of patients in different locations. In the process of clustering analysis of fMRI data, the contribution of clustering features to the cluster generalization rate is used to correlate the functional brain network of the brain and to analyze its positioning. Dopamine is the most abundant catecholamine neurotransmitter in the brain. Dopamine acts as a neurotransmitter to regulate various physiological functions of the central nervous system. Dysregulation of the dopamine system involves Parkinson's disease, schizophrenia, Tourette syndrome, attention deficit hyperactivity syndrome, and pituitary tumors.

(3) Independent component analysis (ICA) method: independent component analysis is a type of analysis method used to solve the problem of blind source separation in signal processing [27]. The human brain is a complex system, and different cognitive activities of the brain are often completed by the synergy of multiple brain areas. The fMRI data collected during the experiment has many features that can be extracted but often the data will be mixed with some messy and useless signals. In the process of feature extraction, the interference of these signals is usually removed to find out that can truly reflect the recognition. [28]. The independent component analysis method has a good suppression effect on the influence of noise such as Gaussian. In the process of the experiment, it can accurately eliminate the useless noise and strip the useful nonnoise signal for signal acquisition. Therefore, it is used as a signal analysis method of advanced statistics. Compared with the principal component analysis method, it is more accurate and more widely used. These problems not only bring troubles to patients' daily life, study, and interpersonal relationships but also affect the patients' family life. The onset of depression can be as short as two weeks or more and as long as several years, and most cases have a tendency to recur. It will inevitably bring many problems to the family and society, so timely intervention and treatment of depression are particularly important.

2.2. Resting Function Connection Method. The resting state originally refers to the BOLD signal (fMRI) of people being awake, blindfolded, and relaxed, used to detect abnormalities in brain structure or brain activity. Initially, researchers believed that EEG signals at rest were relatively random and subject to interference. Therefore, in the study of work situations, researchers use the brain activity of participants when they are not working as the basis for the study.

EEG equipment is used to record and amplify changes in the biopotential information inside the brain on the surface

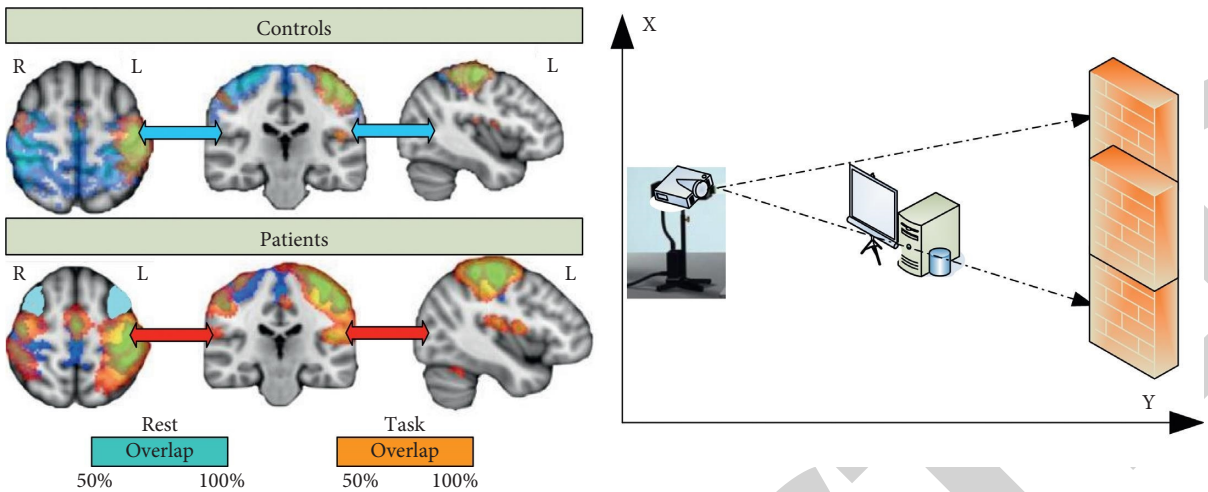

Figure 1: Sample image of monitoring using fMRI.

of the scalp, reflecting the activity status of different areas of the brain [29]. EEG signal acquisition is a convenient and effective noninvasive way to explore brain activity. The potential changes it reflects are the result of the joint action of many nerve cells in the brain.

The functional connectivity analysis of the resting state EEG mainly consists of three steps as follows: (1) The calculation of the connectivity between different regions of the brain, (2) according to the results of the connectivity, the functional network of the brain and the analysis of related attributes are constructed through the minimum spanning tree, and (3) hierarchical clustering of the minimum spanning tree is different. In this study, the coherence of all 72 electrode EEG signals at each single frequency was calculated by using amplitude squared coherence (MSC). Each element in the coherence matrix represents an estimate of the coherence between the corresponding two electrodes, which indicates the degree of interdependence of different brain regions throughout the brain. Then, a minimum spanning tree (MST) is constructed based on the EEG coherence matrix, and the edges are selected according to the coherence in the process of constructing the minimum spanning tree. Figure 2 is a process analysis diagram. At present, some studies have explored the relationship between the course of the disease, age, and cognitive impairment in patients with depression, and some studies have explored the influence of factors such as whether to take medication, the degree of depression, and whether it is the first episode. However, related studies mostly use single-factor analysis methods, lacking systematic comprehensive analysis, and the results obtained may be biased.

Alzheimer's disease (AD) is a progressive neurodegenerative disease with insidious onset. Clinically, it is characterized by general dementia such as memory impairment, aphasia, apraxia, agnosia, visual and spatial skills impairment, executive dysfunction, and personality and behavior changes. The etiology is still unknown. Those who have the disease after 65 years old are called Alzheimer's disease.

2.3. Introduction to Brain Function Connection. Correlation is the most commonly used linear synchronization method and is defined as follows. Two discrete time series measured at the same time are considered, and then, the cross-correlation function is defined as follows:

$$C_{xy}(\tau) = \frac{1}{N-t}\sum_{n=1}^{N-\tau}\left(x_n - \frac{\overline{x}}{\sigma_x}\right)\left(y_{n+t} - \frac{\overline{y}}{\sigma_y}\right). \quad (1)$$

However, due to the limited size of the collected EEG data signals, in order to accurately estimate the true frequency spectrum, researchers widely use smoothing techniques (Welch's method), so the MSC formula can be expressed as

$$\gamma_{xy}(f) = \frac{\left|S_{xy}(f)\right|^2}{\left|\{S_{xx}(f)\}\right|\left|S_{yy}(f)\right|}. \quad (2)$$

In an undirected network, the aggregation coefficient C can be used to express the aggregation coefficient of $v2$:

$$C_{v2} = \frac{n}{C_k^2} = \frac{2n}{k(k-1)}, \quad (3)$$

where k represents the number of all adjacent nodes of node $v2$, that is, the number of neighbors of node $v2$, and n represents the number of edges connected to each other between all adjacent nodes of node v2.

The average aggregation rate of all nodes in the network can be expressed as

$$C = \langle C_i \rangle. \quad (4)$$

When each end of the network has its own weight, the average shortest path length L is used to describe the average of the shortest path length between two nodes in the network.

$$L = \frac{1}{N(N-1)}\sum_{i,j\in V, i\neq j} l_{ij}. \quad (5)$$

d is defined as the similarity of any two nodes (any two rows in C), using Spearman distance calculation.

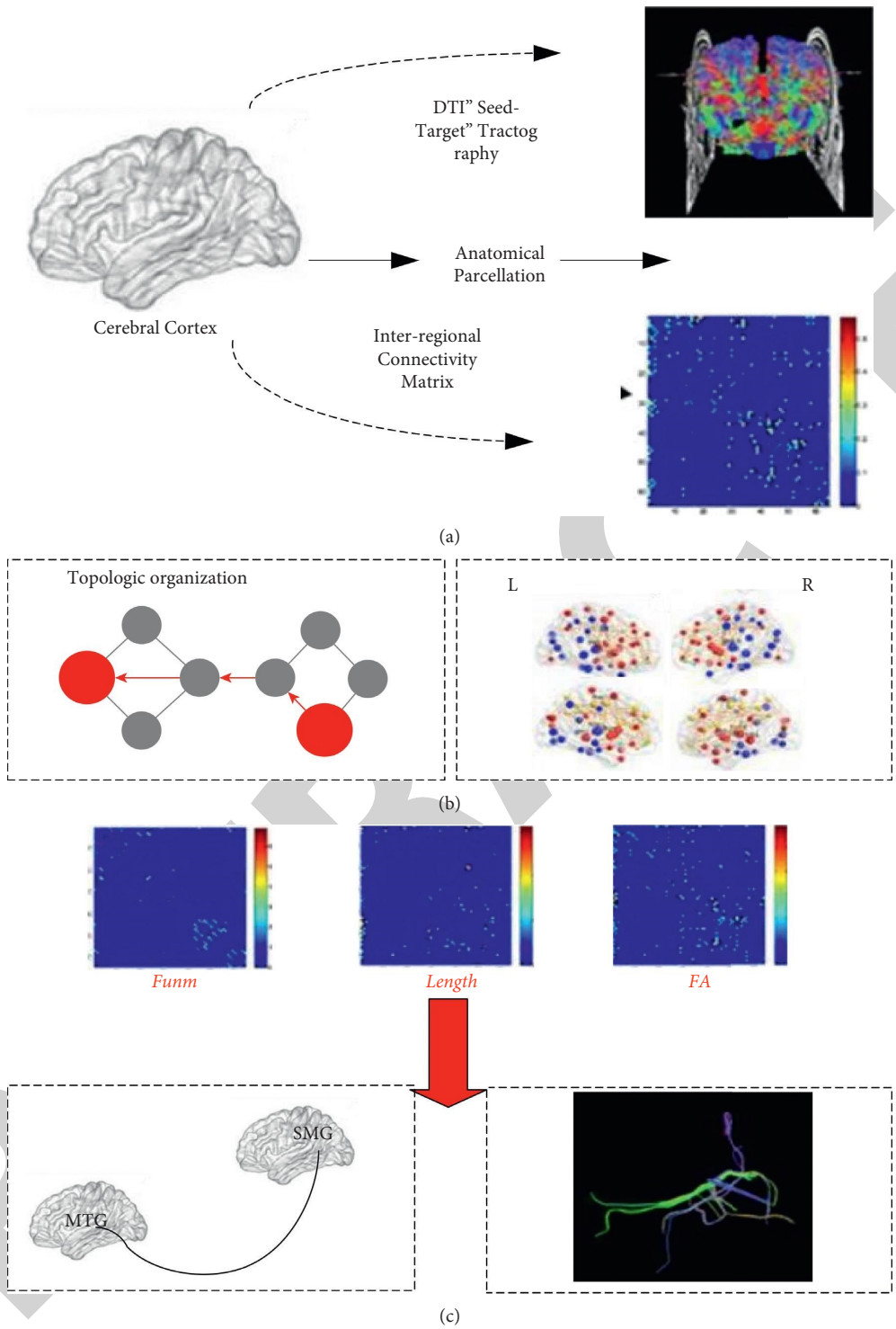

Figure 2: Process analysis. (a) Connectome mapping: using DTI data to build a whole-brain structure network. (b) Topological analysis: comparing the differences in the topological properties of the whole brain through the whole-brain structure network. (c) Fiber tracts analysis: distinguishing the types of fiber damage through the differences in the properties of the three white matter fibers.

$$\rho = 1 - \frac{6\sum d_i^2}{n^3 - n}. \tag{6}$$

When using statistical analysis methods to study multivariate topics, too many variables will increase the complexity of the topic. People naturally hope that fewer variables will get more information. In many cases, there is a certain correlation between variables. When there is a certain correlation between two variables, it can be explained that the two variables that reflect the information of this

subject have a certain overlap. The principal component analysis is to delete the redundant variables (closely related variables) for all the variables originally proposed and establish as few new variables as possible so that these new variables are pairwise unrelated, and these new variables are reflecting keep the original information as much as possible in the information aspect of the subject.

This method of solving problems by adding conditions or restricting requirements is the normalization method. Currently, sLORETA is used more frequently. Through the Monte Carlo comparison and analysis with the MWN and SLF algorithms, it is found that sLORETA has the best effect under different noise intensities and different stimulation depths, and the placement error is the lowest. The calculation process of sLORETA is as follows:

$$\begin{aligned} \Phi &= KJ, \\ F &= \|\Phi - KJ\|^2 + \alpha\|J\|^2, \\ J &= \mathrm{T}\Phi, \\ T &= K^T\left[KK^T + \alpha H\right]^+. \end{aligned} \tag{7}$$

Estimating the standardization of J requires estimating its variance.

In this process, the actual source variance can be seen as

$$S_j = I, \quad I \in R^{(3Nv)\times(3Nv)}. \tag{8}$$

In addition, from a Bayesian point of view, the potential difference is due to noise measurement.

$$S_\Phi^{\text{noise}} = \alpha H. \tag{9}$$

Considering the independence of the actual source activity and the measurement noise, then the potential variance is as follows:

$$S_j = TS_\varphi T^T = T\left(KK^T + \alpha H\right)T^T = K^T\left[KK^T + \alpha H\right]^+ K. \tag{10}$$

You can get

$$j = TKJ = K^T\left[KK^T + \alpha H\right]^+ KJ = RJ = S_J J, \tag{11}$$

in

$$S_j = R = K^T\left[KK^T + \alpha H\right]^+ K. \tag{12}$$

When the forecast of each time series is added to the past value of another time series, Granger causality analysis is performed. The specific bivariate autoregressive model is expanded as follows:

$$Y_t = \sum_{i=1}^{p} A_i X_{(t-i)} + \sum_{i=1}^{p} B_i Y(t-i) + CZ_t + \varepsilon_t, \tag{13}$$

$$X_t = \sum_{i=1}^{p} A_i' Y_{(t-i)} + \sum_{i=1}^{p} B_i' X_{t-i} + C' Z_t + \varepsilon_t'. \tag{14}$$

Gamma distribution is given by

$$f(r) = \text{const} \times r^{(1-3b)/b} \exp\left(-\frac{r}{ab}\right). \tag{15}$$

In summary, the introduction of the algorithm is complete, and the experiment is ready to begin.

3. Experiments and Analysis of the Mechanism of Depression through Brain Function Imaging Analysis of Depression Patients and Normal People

3.1. Preparation before the Experiment. Several patients with major depression were recruited through outpatient clinics. The subjects of the study were all adults (18–60 years old), which matched the individual gender and education level of the normal population in the previous PPI study. They were diagnosed with major depression by an experienced doctor through interviews and using the fourth edition of the Clinical Diagnosis and Statistics Manual of Visceral Diseases. In order to study the relatively stable depression pattern, the following criteria are used to eliminate confounding factors: (1) are you currently receiving or are receiving any antidepressant therapy (antidepressants, psychotherapy, etc.); (2) consolidation or mental illness I; (3) anxiety history of mania and hypomania; (4) under treatment or with neurological diseases; (5) history of head injury and/or drug abuse; and (6) contraindications of magnetic resonance imaging. The severity of depression is assessed by the 17-item Hamilton Depression Inventory (17-HDR) and the second edition of the Beck Depression Inventory (BDI-II). This study strictly followed the "Declaration of Helsinki" and was approved by the Review Committee of the Institute of Ethics of the First Affiliated Hospital of Xinxiang Medical College. In order to protect the rights and interests of the subjects, each person signed and confirmed a written consent form after knowing it. The population data and clinical symptom scores of the subjects are shown in Table 1.

Cognition is a kind of human mental activity. It refers to the mental process of an individual to recognize and understand things. Cognitive function is composed of multiple cognitive domains, including attention, inhibition, mental operation ability, concept formation and conversion ability, and memory and many other aspects. Cognitive impairment refers to the abnormality of the brain's advanced intelligent processing related to the above-mentioned attention, inhibition, and mental operation abilities, which leads to the damage of attention, inhibition, and mental operation abilities.

Hamilton Depression Scale (HAMD) was compiled by Hamilton in 1960. It is the most commonly used scale in the clinical evaluation of depression. There are 3 versions of this scale, including 17 items, 21 items, and 24 items. This scale is performed by two trained raters to perform a HAMD joint examination on the patient. Generally, speaking and observation are used. After the examination, the two raters separately score independently; scores before and after treatment can evaluate the severity of the disease. Table 1 selects the return on investment previously shown in healthy individual studies and finds the coordinates of the area of

Table 1: Participant population data and clinical symptom score.

	Depression group	Normal control group	P value
Gender (male/female)	7/13	7/13	0.754
Age	41.8 (14.2)	41.6 (13.6)	0.931
Years of education	11.3 (2.6)	10.3 (3.0)	0.305
PANSS			
Positive score	12.9 (5.6)		
Negative score	18.0 (7.0)	—	—
General symptom score	27.8 (5.3)		
Total score	58.7 (12.5)		
HAMD-24		5.3 (1.3)	

interest in the MNI standard. The brain network marker threshold for the independent component analysis is set to $z > 2.3$, and then, all markers for the brain structure of the area of interest and the resting network coordinates of the ICA are recorded, as shown in Table 2.

Although timely intervention can effectively control the disease, most of the patients have repeated attacks, leading to the decline of social function and even suicide in patients with depression. Fifty percent of patients will relapse again within a two-year recovery period, and more than 80% of depression patients will experience more than one stage of depression in their lifetime. The distribution of the region of interest is shown in Figure 3.

On the other hand, this study found that there is a certain correlation between the right fusiform gyrus of the temporal lobe and the speed of information processing in cognitive function. There is a correlation between the left cerebellum and FAST's cognitive function dimension and total anxiety score. The medial frontal gyrus on the left is correlated with changes in cognitive function dimensions. Two ROIs are defined through a priori theory. These two points represent a brain network that has been fully verified in previous studies. PPI analysis determines the adjustment area of the connectivity between the selected area of interest and the second area of interest and determines the interaction based on the increase or decrease of statistics. For each PPI analysis, we defined two regions of interest (ROI), and each network found this item in the ICA analysis scoreboard. Therefore, PPI analysis will find that the brain area is based on the activity of other brain area networks and the regulation connection of another brain area. This analysis will help you understand the dynamic changes in the brain network connections. The functional connection map of the dorsal, ventral, and posterior insula subregions of the insula is shown in Figure 4.

The overall t-test is to test whether the difference between the average of two samples and the population represented by each is significant. The two-population t-test is divided into two situations, one is the independent sample t-test (there is no correlation between the experimental treatment groups, that is, the independent sample), and the other test is used to test the two groups of unrelated sample subjects obtained difference of the data; the first is the paired sample t-test, which is used to test the data obtained by two groups of matched subjects or the difference of the data obtained by the same group of subjects under different conditions. These two situations constitute a sample that is

Table 2: Settings and coordinates of interest.

Network name		Brain area	Mini coordinates		
			X	Y	Z
Default network	19	PCC	3	−52	26
		MPFC			
Executive network on the left	17	LSFG	3	58	6
		LSPL	−33	22	52
Execution network on the right	9	RSFG	−50	−51	50
		RSPL	27	28	52
Highlight the network	13	LIFG	36	−66	48
		LIFG	−48	19	−5
Dorsal attention network	5	RIFG	48	16	−5
		LIPL	−45	−42	56
Auditory network	7	RIPL	48	−39	55
		LSTG	−62	−1	9
Lateral striatum network	20	RSTG	62	−26	16
		LMTG	−50	−65	10
Sports network	1	RMTG	45	−76	10
		LPCG	−48	−7	54
		RPCG	48	−13	54

the relevant sample. The key brain areas of the core network are shown in Table 3.

3.2. ALFF Results. Recent studies have shown that the acquisition of brain function is both network and local, and the organic combination of the two makes the brain's rich functions. In order to define the local activity of a specific brain area, people put forward the hypothesis that specific signals have local consistency. Based on this, a large number of researchers have used functional magnetic resonance imaging technology to study the brain function activity in the resting state and developed a variety of related characterization methods, such as local consistency ReHo (regional homogeneity). The general information of the three groups of subjects is shown in Table 4.

It can be seen from Table 4 that the three groups have no significant differences in age and gender composition ($P > 0.05$); there is a significant difference in the number of training years between the depression patient group and the depression-susceptible group ($P < 0.01$). There was no significant difference between the depression sensitivity control group and the normal control group ($P > 0.05$). The fMRI comparison of several groups is shown in Figure 5, and there is no significant difference between the two in the main motor

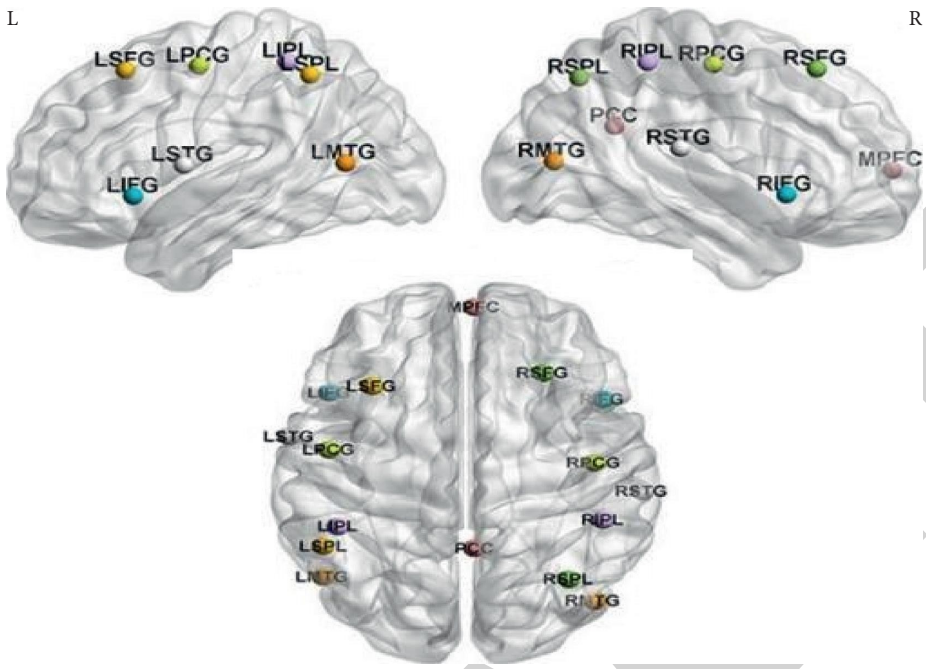

Figure 3: Distribution of regions of interest.

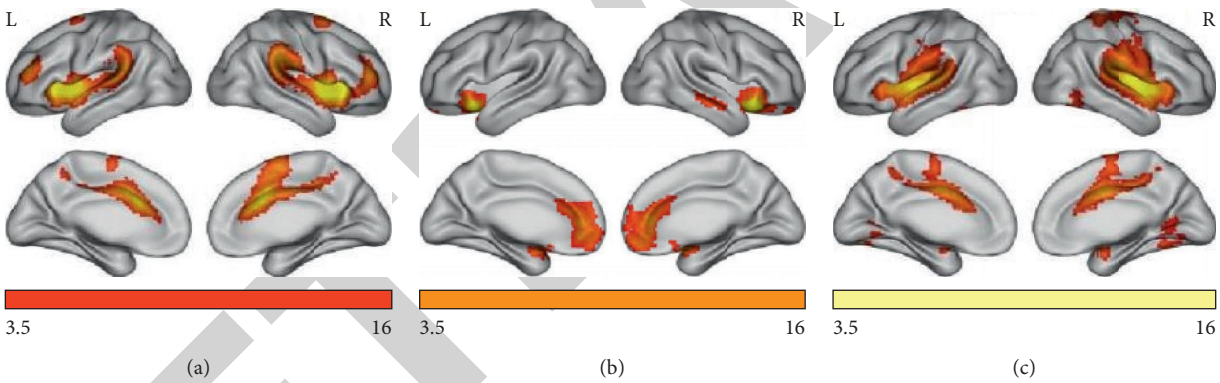

Figure 4: The functional connection map of the dorsal, ventral, and posterior insula subregions of the insula.

Table 3: Key brain areas of the core network.

Seed point	Brain area	Left and right	Mini coordinates			T value
			x	y	z	
Dorsal forebrain insula (to highlight the network)	Ventrolateral prefrontal cortex	Right	33	12	21	12.77
		Left	−36	42	21	10.43
	Temporoparietal junction	Right	63	−33	21	13.87
		Left	−60	−39	21	11.35
	Top leaflet	Right	6	18	30	16.82
		Left	33	−57	39	7.47
Dorsolateral prefrontal cortex (central executive network) posterior cingulate (default network)	Inferior temporal gyrus	Right	−36	−54	36	6.72
		Left	54	−6	−24	7.64
	Angular gyrus	Right	−57	−9	−24	7.82
		Left	51	−51	24	9.61
	Middle back	Right	−42	−75	27	9.9
		Left	24	33	36	9.33
	Medial prefrontal cortex	Right	−27	30	39	7.92
		Left	−3	63	0	8.06
	Para hippocampus	Right	30	−36	−18	6.23
		Left	−33	−42	−18	7.24
	Posterior cerebellum	Left	−9	−60	−48	9.24

Table 4: The general information of the three groups of subjects.

	Depression group	Depression-susceptible group	Normal control group	P
Age	30.65	31.31	29.33	0.776
Gender	14/9	17/9	8/7	0.748
Education (years)	12.26	16.54	14.53	
HAMD score	29.09	2.27	1.27	

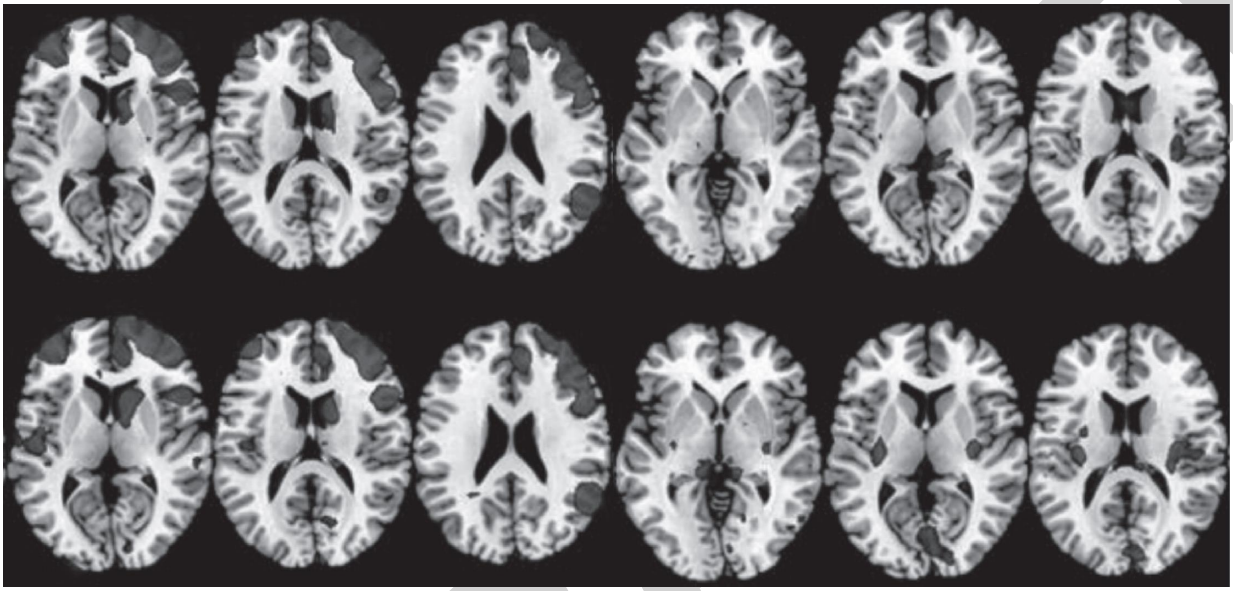

Figure 5: Comparison of several groups of fMRI.

cortex area. But outside the motor cortex, the brain motor function projection network in the normal control group was significantly higher in the lateral insular area than in depression patients ($P < 0.001$). However, some areas of the orbital frontal lobe in depression patients were significantly higher than those in the normal control group ($P < 0.001$).

The correlation between the ReHo value of abnormal brain areas and clinical variables in the depression group is shown in Table 5.

The severity of depression in the depression group was negatively correlated with the ReHo value of the posterior left cerebellum ($P = 0.010$). The sense of despair was negatively correlated with the ReHo value of the back of the right cerebellum ($P = 0.013$). The diurnal variation is related to the ReHo value of the left ring. It was negatively correlated ($P = 0.014$), and positively correlated with the ReHo value of the left ventricle ($P = 0.048$).

A sample of subjects with a CUMS stimulating depression phenotype was randomly divided into two groups: a depression group receiving 10 mg/kg fluoxetine solution, once a day, for 21 consecutive days; a depression group and an empty control group receiving the same dose of saline, once a day. Conduct assessment was performed 21 days after the drugs were administered. Fluoxetine should be ready for immediate use. Weight change is shown in Figure 6.

The open-air test is shown in Figure 7.

Figure 7 shows that in the open-air environment, after eight weeks of drug use, it can be found that the subjects moved closer and the degree of depression was deeper. The day experiment in the article is to facilitate the distinction and reduce the content of toxic substances.

Sucrose preference is shown in Figure 8.

It can be seen from Figure 8 that after eight weeks, under the action of the fluoxetine solution, the subjects not only increased their weight significantly but also increased their preference for sucrose, and the degree of depression was higher than that of the normal group.

The correlation analysis between CPT task indicators and related factors is shown in Figure 9.

According to Figure 9, it can be seen that there is a correlation between the low reporting rate of CPT and the score of the scale ($P < 0.01$), and the course of the disease, whether it is the first episode of these two items and medication, gender, age, and education level. There is a significant correlation ($P > 0.05$). The false-positive rate was related to the time of CPT report, and there was no significant correlation between whether the first episode of the disease occurred and whether the drug was used, gender, gender, age, and education level ($P > 0.05$).

4. Discussion of the Mechanism of Depression through Brain Function Imaging of Patients with Depression and Normal People

Current research believes that depression is a mental disorder that involves multiple areas and multiple systems of the brain. At present, a large number of studies using

Table 5: Correlation between the ReHo value of abnormal brain area and clinical variables in the depression group.

Clinical variables	Brain area	x	y	z	Correlation coefficient (r)	P
HAMD	Left posterior cerebellum	−3	−75	−30	−0.7597	0.010
Despair	Right posterior cerebellum	3	−81	−30	−0.7655	0.013
Day and night changes	Left cingulate back	−18	−33	30	−0.6106	0.048
Day and night changes	Left thalamus	−3	−9	6	0.7768	0.014

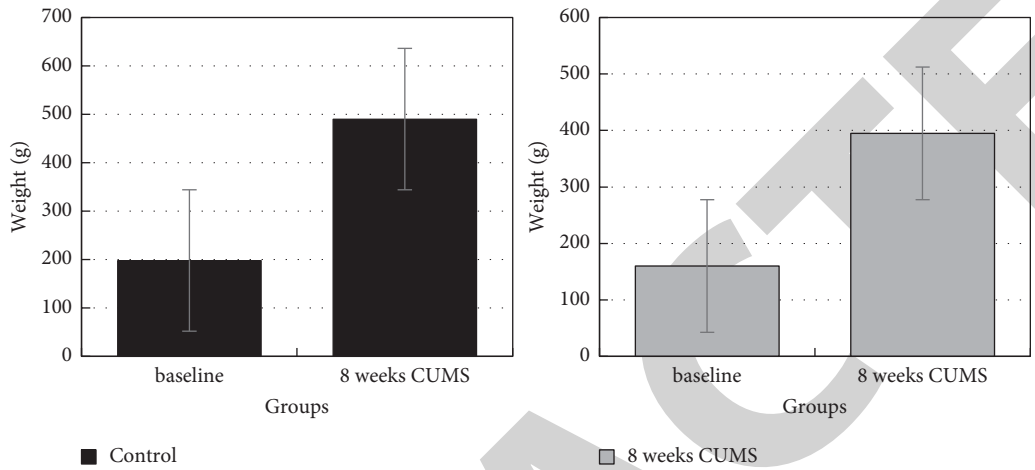

Figure 6: Body weight change.

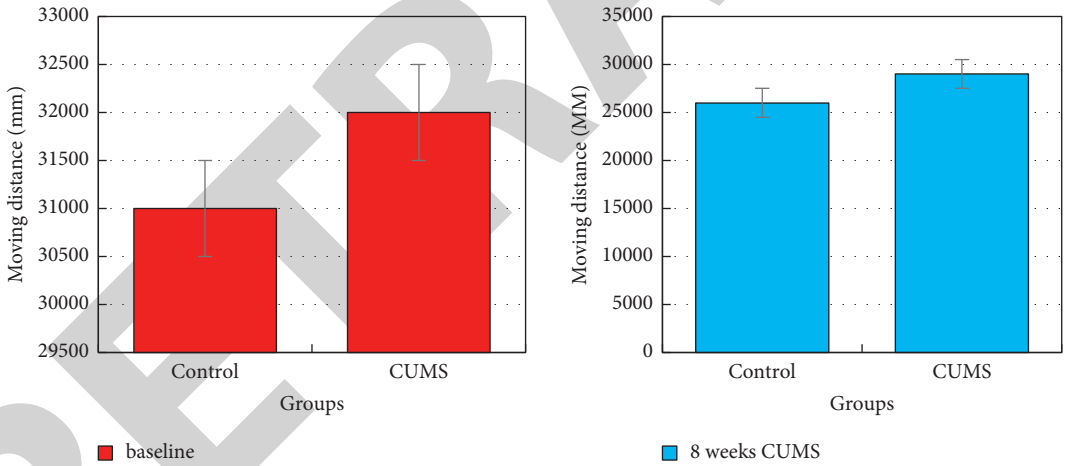

Figure 7: Open-air test.

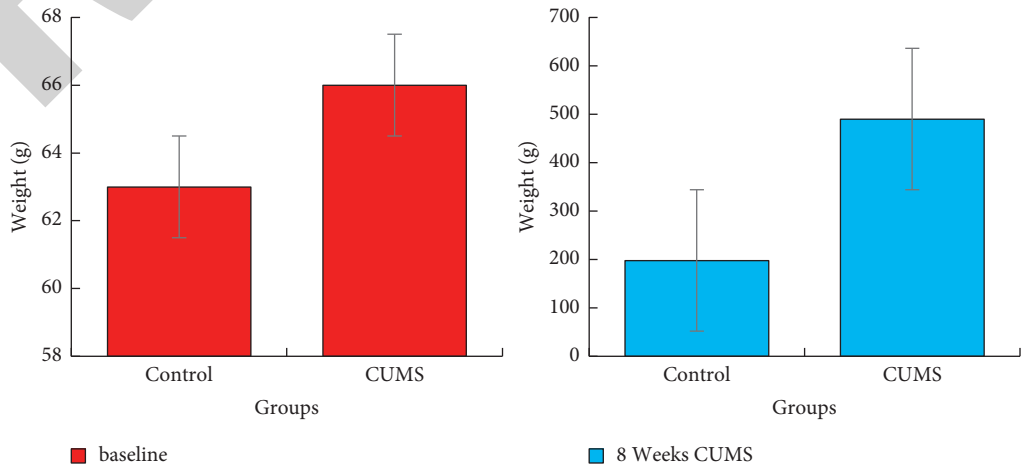

Figure 8: Sucrose preference.

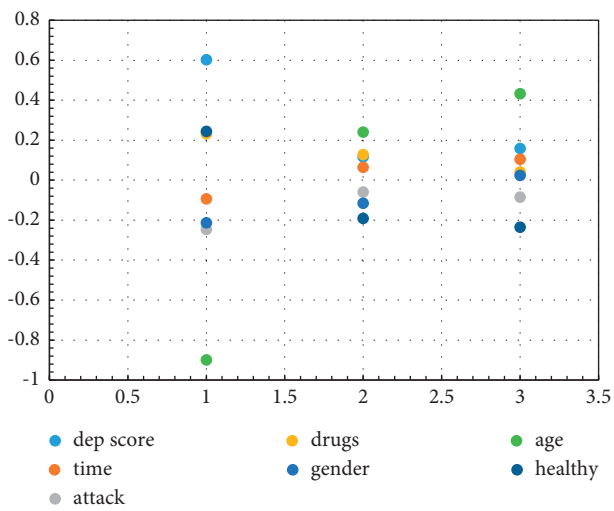

Figure 9: Correlation analysis of CPT task indicators and related factors.

Diffusion Dilation Imaging (DTI) provide a structural basis for the abnormal functional connection of MDD. Compared with the normal control group, the functional connectivity between the DMN and the frontal ventricular blind network in depression patients is reduced. In the cortical border network, the anisotropy score (FA) between the sgACC and the amygdala of adolescent depression patients is reduced. In addition, when depressed patients face terrible faces, the structural activity of the dorsal prefrontal cortex (DLPFC) decreases. All these results indicate that MDD will change in the structural topology of the network.

The functional network of MDD patients has been extensively explored and studied. And a lot of achievements have been made. However, due to the differences in environment, research objects, and analysis methods in the process of experiment and data analysis, different or even opposite results have been found in the research of MDD brain function network. Some research groups have found an increase in brain functional connections in patients with MDD, but some studies have found a decrease in brain functional connections. When building functional connections, most studies usually use thresholds to convert coherence into edges. The choice of threshold has a strong subjective bias, which is also a reason for inconsistent conclusions in different studies that cannot be ignored. In this article, the study uses unbiased methods to build the functional connections of the brain. This method has been used in the research of a variety of mental disorders.

This research uses the method of functional topology analysis to study the connection between the brain and the functional network. It is verified that the brain function topology obtained has the same pattern as the resting state function network. According to the spatial pattern of the resting brain functional projection network, the functional projection network of the brain was used to compare the topological structure of the functional projection network of the depression group, the depression-susceptible group, and the normal control group and found that there were significant differences in the brain function of the right forehead among the three groups. In some areas of the leaf, the brain function connection of depression-susceptible people is significantly reduced. The motor projection network is also abnormal in the pretreatment depression group, but the abnormal area is located in the lateral insula rather than the main functional area of the motor network. The spatial multivariate regression algorithm is used to map the selected functional network to each thalamus voxel, and the connection distribution of the thalamus voxel and each functional projection network is obtained. Finally, the connection value of the thalamus and each function projection network was compared among the depression group, depression-susceptible people, and the normal control group. The results showed that the connection between the anterior region of the right brain of depression patients and the right subnetwork of CEN was significantly lower than that of the normal control group. It was further found that the functional connection between the entire right thalamus and the right subnetwork of CEN in patients with depression was also significantly lower than that of the right subnetwork of CEN. In the normal control group, the functional connection between the right thalamus and the right subnetwork of CEN was partially restored after treatment, and there was no significant difference from the normal control group. Without correction for multiple comparisons, the connection between the lower part of the brain and the motor network of the depression patients before treatment was significantly lower than that of the normal control group, but there was no significant difference in the connection between the left and right brains and the motor network as a whole.

5. Conclusions

The experimental results show that the research on the mechanism of depression through brain function imaging analysis of depression patients and normal humans proposed in this article is more intelligent and scientific in monitoring than other methods of studying the mechanism of depression. Monitoring the cause is also more timely. The article conducted an analysis of depression based on the resting state. The article selected the return on investment previously shown in the study of healthy individuals and found the coordinates of the region of interest in the MNI standard. The author defined two ROIs through a priori theory and performed an fMRI comparative analysis of normal and depressed human brains, and the research on the whole-brain structure network of depression has also been roughly completed. The data showed that the severity of depression in the depression group was negatively correlated with the ReHo value of the left posterior cerebellum, and the sense of despair was negatively correlated with the ReHo value of the right posterior cerebellum. Outside the motor cortex, the brain motor function projection network of the normal control group is significantly higher than that of depression patients in the lateral insular area. The area of the orbital frontal lobe of depression patients was significantly higher than that of the normal control group. The

shortcomings of this article are as follows: (1) the data collected by the sample is relatively limited, and the experimental samples can be expanded in future research to obtain the credibility of the research results and (2) the research method in this article only performed fMRI imaging analysis on the human brain but did not control other variables, such as the living habits of the two groups, growth experience, and other variables. This article may be slightly inadequate in rigor. In future research, we can focus on supplementing this piece of content to make the experiment more scientific.

Data Availability

No data were used to support this study.

Conflicts of Interest

The authors declare that there are no conflicts of interest with any financial organizations regarding the material reported in this manuscript.

Acknowledgments

Science and Technology Key Project of Henan, Nos. 212102310836 and 212102310242; Science and Technology Project of Xinxiang No. GG2019002; Key Scientific Research Projects of Colleges and Universities in Henan No. 22A890007; National Scientific Research Project Cultivation Fund of Henan Normal University, No. 2020PL11; and the Henan Province Youth Talent Lift Project of China, No. 2021HYTP042.

References

[1] J. Xu, K. He, K. Zhang et al., "Low-dose copper exposure exacerbates depression-like behavior in ApoE4 transgenic mice," *Oxidative Medicine and Cellular Longevity*, vol. 2021, no. 159, pp. 1–20, Article ID 6634181, 2021.

[2] C. Y. Xia, Z. Z. Wang, T. Yamakuni, and N. H Chen, "A novel mechanism of depression: role for connexins," *European Neuropsychopharmacology: The Journal of the European College of Neuropsychopharmacology*, vol. 28, no. 4, pp. 483–498, 2018.

[3] K. J. Manish, A. Minhajuddin, B. S. Gadad et al., "Can C-reactive protein inform antidepressant medication selection in depressed outpatients? Findings from the CO-MED trial," *Psychoneuroendocrinology*, vol. 78, no. 9, pp. 105–113, 2017.

[4] M. D. Hu, Y. Zhong, S. X. Xie, H. B. Lv, and Z. H. Lv, "Fuzzy system based medical image processing for brain disease prediction," *Frontiers in Neuroscience*, vol. 15, p. 965, 2021.

[5] K. Hoorel Be Ke and E. Koster, "Internet-delivered cognitive control training as a preventive intervention for remitted depressed patients: evidence from a double-blind randomized controlled trial study," *Journal of Consulting and Clinical Psychology*, vol. 85, no. 2, p. 135, 2016.

[6] Y. Liu, F. Xu, S. Liu et al., "Significance of gastrointestinal tract in the therapeutic mechanisms of exercise in depression: synchronism between brain and intestine through GBA," *Progress in neuro-psychopharmacology & biological psychiatry*, vol. 103, no. 2, Article ID 109971, 2020.

[7] X. Han, Y. Gao, X. Yin et al., "The mechanism of electro-acupuncture for depression on basic research: a systematic review," *Chinese Medicine*, vol. 16, no. 1, pp. 4–6, 2021.

[8] M. Shalini and P. Sanchita, "Classification of depression patients and normal subjects based on electroencephalogram (EEG) signal using alpha power and theta asymmetry," *Journal of Medical Systems*, vol. 44, no. 1, pp. 28–31, 2019.

[9] U. Anusri, G. Dhatchayani, Y. P. Angelinal, and S. Kamalraj, "An early prediction of Parkinson's disease using facial emotional recognition," *Journal of Physics: Conference Series*, vol. 37, no. 1, pp. 012–058, 2021.

[10] B. Stetka, "In search of the optimal brain diet," *Scientific American Mind*, vol. 27, no. 2, pp. 26–33, 2016.

[11] J. M. Perelman et al., "The impact OF patients' cooperativeness and depression ON the asthma control Achievement," *Respirology*, vol. 21, no. 1, pp. 163-164, 2016.

[12] S. Atluri, W. Wong, D. M. Blumberger, Z. J. Daskalakis, and F. Farzan, "Insights from EEG microstate analysis on the pathophysiology of depression and mechanisms of seizure therapy," *Biological Psychiatry*, vol. 81, no. 10, pp. 216–218, 2017.

[13] Y. Lou, P. Huang, D. Li et al., "Altered brain network centrality in depressed Parkinson's disease patients," *Movement Disorders*, vol. 30, no. 13, pp. 1777–1784, 2016.

[14] M. A. Camkurt, Ş. Acar, S. Coşkun et al., "Corrigendum to "Comparison of plasma MicroRNA levels in drug naive, first episode depressed patients and healthy controls,"Psychiatr. Res. 69 (2015) 67–71]," *Journal of Psychiatric Research*, vol. 75, no. 6, p. 23, 2016.

[15] X. Li, Y. Wang, and G. Liu, "Structured medical pathology data hiding information association mining algorithm based on optimized convolutional neural network," *IEEE ACCESS*, vol. 8, no. 1, pp. 1443–1452, 2020.

[16] V. S. Fang, B. J. Tricou, A. Robertson, and H. Y. Meltzer, "Plasma ACTH and cortisol levels in depressed patients: relation to dexamethasone suppression test," *Life Sciences*, vol. 29, no. 9, pp. 931–938, 2016.

[17] P. D. Gargoloff, R. Corral, L. Herbst, M. Marquez, G. Martinotti, and P. R. Gargoloff, "Effectiveness of agomelatine on anhedonia in depressed patients: an outpatient, open-label, real-world study," *Human Psychopharmacology: Clinical and Experimental*, vol. 31, no. 6, pp. 412–418, 2016.

[18] P. L. Jacobsen, G. G. Nomikos, W. Zhong, A. J. Cutler, J. Affinito, and A. Clayton, "Clinical implications of directly switching antidepressants in well-treated depressed patients with treatment-emergent sexual dysfunction: a comparison between vortioxetine and escitalopram," *CNS Spectrums*, vol. 25, no. 1, pp. 50–63, 2020.

[19] S. K. Biswas, D. Devi, and M. Chakraborty, "A hybrid case based reasoning model for classification in internet of things (iot) environment," *Journal of Organizational and End User Computing*, vol. 30, no. 4, pp. 104–122, 2018.

[20] N. Sarubin, T. Baghai, J. Lima-Ojeda et al., "Translocator protein (TSPO) expression in platelets of depressed patients decreases during antidepressant therapy," *Pharmacopsychiatry*, vol. 49, no. 05, pp. 204–209, 2016.

[21] C. M. Pariante, "Why are depressed patients inflamed? A reflection on 20 years of research on depression, glucocorticoid resistance and inflammation," *European Neuropsychopharmacology*, vol. 27, no. 6, pp. 554–559, 2017.

[22] V. De Carlo, R. Calati, and A. Serretti, "Socio-demographic and clinical predictors of non-response/non-remission in treatment resistant depressed patients: a systematic review," *Psychiatry Research*, vol. 240, no. 8, pp. 421–430, 2016.

Hindawi
Journal of Healthcare Engineering
Volume 2023, Article ID 9785980, 1 page
https://doi.org/10.1155/2023/9785980

Retraction

Retracted: To Analyze the Influencing Factors of Senile Coronary Heart Disease Patients Complicated with Frailty Syndrome

Journal of Healthcare Engineering

Received 26 September 2023; Accepted 26 September 2023; Published 27 September 2023

This article has been retracted by Hindawi following an investigation undertaken by the publisher [1]. This investigation has uncovered evidence of one or more of the following indicators of systematic manipulation of the publication process:

(1) Discrepancies in scope
(2) Discrepancies in the description of the research reported
(3) Discrepancies between the availability of data and the research described
(4) Inappropriate citations
(5) Incoherent, meaningless and/or irrelevant content included in the article
(6) Peer-review manipulation

The presence of these indicators undermines our confidence in the integrity of the article's content and we cannot, therefore, vouch for its reliability. Please note that this notice is intended solely to alert readers that the content of this article is unreliable. We have not investigated whether authors were aware of or involved in the systematic manipulation of the publication process.

Wiley and Hindawi regrets that the usual quality checks did not identify these issues before publication and have since put additional measures in place to safeguard research integrity.

We wish to credit our own Research Integrity and Research Publishing teams and anonymous and named external researchers and research integrity experts for contributing to this investigation.

The corresponding author, as the representative of all authors, has been given the opportunity to register their agreement or disagreement to this retraction. We have kept a record of any response received.

References

[1] T. Qin, W. Sheng, and G. Hu, "To Analyze the Influencing Factors of Senile Coronary Heart Disease Patients Complicated with Frailty Syndrome," *Journal of Healthcare Engineering*, vol. 2022, Article ID 7619438, 6 pages, 2022.

Hindawi
Journal of Healthcare Engineering
Volume 2022, Article ID 7619438, 6 pages
https://doi.org/10.1155/2022/7619438

Research Article

To Analyze the Influencing Factors of Senile Coronary Heart Disease Patients Complicated with Frailty Syndrome

Tian Qin,[1,2] Wang Sheng,[3] and Guoheng Hu[3]

[1]*Hunan University of Chinese Medicine, Changsha 410000, China*
[2]*The Second Hospital of Hunan University of Chinese Medicine, Changsha 410000, China*
[3]*The First Hospital of Hunan University of Chinese Medicine, Changsha 410000, China*

Correspondence should be addressed to Guoheng Hu; 1816160322@e.gzhu.edu.cn

Received 27 November 2021; Revised 18 December 2021; Accepted 21 December 2021; Published 7 January 2022

Academic Editor: Gu Xiaoqing

To analyze the influencing factors of senile coronary heart disease patients complicated with frailty syndrome. A total of 80 elderly patients with coronary heart disease admitted to our hospital from March 2020 to March 2021 were selected as the research subjects. The Fried Frailty Symptom Scale was used to evaluate whether the 80 patients were complicated with frailty syndrome. According to the evaluation results, the patients were divided into a nonfrailty syndrome group (52 cases in total) and frailty syndrome group (28 cases in total). Clinical data of two groups of patients were collected, and multivariate logistic regression was used to analyze the influencing factors of senile coronary heart disease patients complicated with frailty syndrome. Among 80 patients, the incidence of frailty syndrome was 35.00% (28/80), including 18 cases in early frailty and 10 cases in frailty stage. Univariate analysis showed that age, body mass (BMI), diabetes mellitus, congestive heart failure, chronic renal insufficiency, chronic obstructive pulmonary disease (COPD), tumor, high uric acid hematic disease, arrhythmia, interleukin-6 (IL-6), c-reactive protein (CRP), fibrinogen (FIB), brain natriuretic peptide (BNP), uric acid (UA), serum creatinine (Scr), serum protein (ALB), white blood cell count (WBC), and neutrophil count were the possible risk factors for senile coronary heart disease complicated with frailty syndrome ($P < 0.05$). Multivariate logistic regression analysis showed that combined COPD, combined tumor, IL-6, BNP, UA, SCR, ALB, and neutrophil count were independent risk factors for senile CHD complicated with frailty syndrome ($P < 0.05$). Combined with COPD, combined with tumor, IL-6, BNP, UA, SCR, ALB, and neutron cell count are the influencing factors for senile coronary heart disease patients complicated with frailty syndrome. These factors can be used as the basis for the diagnosis of frailty syndrome and guide the clinical development of targeted diagnosis and treatment plan.

1. Introduction

Coronary heart disease mainly refers to the abnormal lipid metabolism. The lipids in the blood deposit on the smooth arterial intima. The accumulation of atheroma-like lipids in the arterial intima leads to the formation of white plaques. As the plaques gradually increase, it can cause arterial stenosis, block blood flow, and heart ischemia and induce angina pectoris [1–3]. In recent years, with the increasing aging of our society, the clinical incidence of coronary heart disease is getting higher and higher, and it has become a major disease threatening the health of the elderly [4]. For patients with coronary heart disease, their functional status will have a great impact on treatment and prognosis, and frailty syndrome is the main manifestation of reduced functional status. Frailty syndrome is a nonspecific state in which the physiological reserve of the elderly decreases, increases the vulnerability of the body, and weakens the body's ability to resist stress [5, 6]. In recent years, studies have gradually begun to explore the relevant influencing factors of elderly coronary heart disease complicated by frailty syndrome and to predict the patient's condition in a timely manner. In view of this, this study selected 80 elderly patients with coronary heart disease admitted in our hospital

from March 2020 to March 2021 as the research objects, aiming to analyze the influencing factors of elderly coronary heart disease patients with debilitating syndrome.

2. Materials and Methods

2.1. General Information. We selected 80 elderly patients with coronary heart disease accepted by our hospital from March 2020 to March 2021 as the subjects of this study. The Fried Debilitating Symptom Scale was used to assess whether the 80 patients were associated with debilitating syndromes, and the patients were classified as noncombined patients based on the evaluation results.

2.1.1. Inclusion Criteria

(a) Coronary angiography showed that one or more coronary arteries had stenosis ≥50%

(b) Age ≥60 years

(c) Complete clinical data

(d) Patients and their family members were aware of the study and had already signed the informed consent form

2.1.2. Exclusion Criteria

(a) Patients with malignant tumors.

(b) Patients with hematological diseases or systemic infectious diseases.

(c) Patients who refuse to cooperate with debilitating examinations.

(d) Patients with history of mental illness or cognitive dysfunction. The study has been approved by the ethics committee of the hospital.

2.2. Methods. The "Fried Debilitating Symptom Scale" was used to evaluate the debilitating condition of 80 patients. The evaluation content included fatigue, decreased BMI, weakness, decreased walking speed, and decreased physical activity. If none of the above exists, it is a nondebilitating period, with 1-2 items in the predebility period and 3 items and above in the debility period. According to the evaluation results, 80 patients were divided into a nondebilitating syndrome group and debilitating syndrome group (including predebility and debilitating period).

The clinical data of 80 patients were collected, and the "general information questionnaire" designed by our hospital was used for investigation, which included the patient's name, gender, age, body mass (BMI), smoking history (previous smoking for six months or more) and drinking history (previous drinking for half a year or more), and combined diseases (hypertension, diabetes, congestive heart failure, chronic renal insufficiency, chronic obstructive pulmonary disease (COPD), tumor, hyperuricemia, arrhythmia, and cerebrovascular disease).

80 patients were tested for laboratory indicators: 5 mL of fasting venous blood was collected from the patients in the morning, and the blood samples were tested by the inspectors of the laboratory of our hospital. The measurement indicators mainly include interleukin-6 (IL-6), procalcitonin (PCT), C-reactive protein (CRP), D-dimer (DD), fibrinogen (FIB), brain natriuretic peptide (BNP), uric acid (UA), serum creatinine (Scr), serum albumin (ALB), total cholesterol (TC), triacylglycerol (TG), low-density lipoprotein cholesterol (LDL-C), high-density lipoprotein cholesterol (HDL-C), hemoglobin (Hb), white blood cell count (WBC), and neutrophil count.

2.3. Statistical Methods. SPSS 22.0 statistical software was used for data analysis. Measurement data conforming to the normal distribution were expressed as mean ± standard deviation ($\overline{x} \pm s$). The comparison between the two groups was performed by the t-test. Those who did not conform to the normal distribution were converted to normal distribution and then counted. Scientific analysis: counting data were expressed by rate, and comparison between groups was performed by the $\chi 2$ test; multivariate analysis was conducted by logistic regression analysis; $P < 0.05$ was considered as the statistically significant difference.

3. Results

After evaluation, it was found that 80 patients had 28 cases of debilitating syndrome, with an incidence rate of 35.00%, of which 18 were in the predebilitating stage and 10 were in the debilitating stage. As shown in Table 1, there was no significant difference between the two groups in terms of gender, smoking history, drinking history, hypertension, and cerebrovascular disease ($P > 0.05$); in terms of age, BMI, diabetes, congestive heart failure, chronic renal insufficiency, COPD, tumor, hyperuricemia, and arrhythmia, the difference between the two groups was statistically significant ($P < 0.05$). Table 1 shows the comparison of general information between the nondebilitating syndrome group and the debilitating syndrome group.

The levels of PCT, DD, TC, TG, LDL-C, HDL-C, and Hb in the two groups were similar, and the difference was not statistically significant ($P > 0.05$); IL-6, CRP, FIB, BNP, UA, Scr, WBC, and neutrophil count levels in the frailty syndrome group were higher than those in the nondebilitating syndrome group, and their ALB levels were lower than those in the nondebilitating syndrome group ($P < 0.05$). Table 2 is the comparison of laboratory indicators between the two groups. Figure 1 is the comparison of IL-6, Scr, and ALB levels between the two groups. Figure 2 illustrates the comparison of CPR, FIB, WBC, and NC levels between the two groups. Figure 3 shows the comparison of BNP and UA levels between the two groups.

Multivariate logistic regression analysis was carried out according to single-factor analysis in Tables 2 and 3. The results showed that the combined COPD, combined tumor, IL-6, BNP, UA, Scr, ALB, and neutrophil count are the combination of elderly patients with coronary heart disease combined with frailty independent risk factors for symptoms ($P < 0.05$). Table 3 is the multivariate logistic regression analysis.

Table 1: Comparison of general information between the nondebilitating syndrome group and the debilitating syndrome group (n, %).

Project		Nondebilitating syndrome group ($n = 52$)	Frailty syndrome group ($n = 28$)	χ^2	P
Gender	Male	27 (51.92)	17 (60.71)	0.568	0.451
	Female	25 (48.08)	11 (39.29)		
Age (years)	60–70	40 (76.92)	10 (35.71)	13.187	0.000
	> 70	12 (23.08)	18 (64.29)		
BMI (kg/m^2)	≤24.5	37 (71.15)	8 (28.57)	13.410	0.000
	> 24.5	15 (28.85)	20 (71.43)		
History of smoking	Yes	30 (57.69)	17 (60.71)	0.069	0.793
	No	22 (42.31)	11 (39.29)		
History of drinking	Yes	31 (59.62)	18 (64.29)	0.167	0.683
	No	21 (40.38)	10 (35.71)		
Comorbidity	Hypertension	26 (50.00)	15 (53.57)	0.093	0.761
	Diabetes	18 (34.62)	17 (60.71)	5.038	0.025
	Congestive heart failure	18 (34.62)	18 (64.29)	6.474	0.011
	Chronic renal insufficiency	15 (28.85)	16 (57.14)	6.140	0.013
	COPD	13 (25.00)	20 (71.43)	16.189	0.000
	Tumor	5 (9.62)	15 (53.57)	18.755	0.000
	Hyperuricemia	3 (5.77)	14 (50.00)	21.277	0.000
	Arrhythmia	5 (9.62)	17 (60.71)	23.835	0.000
	Cerebrovascular disease	10 (19.23)	6 (21.43)	0.055	0.815

Table 2: Comparison of laboratory indicators between the two groups ($\overline{x} \pm s$).

Index	Nondebilitating syndrome group ($n = 52$)	Frailty syndrome group ($n = 28$)	t value	P value
IL-6 (ng/L)	10.28 ± 2.54	24.35 ± 3.19	17.252	0.000
PCT (μg/L)	2.04 ± 0.15	2.12 ± 0.18	1.707	0.257
CRP (mg/L)	4.58 ± 0.85	6.84 ± 1.02	8.511	0.000
D-D (ng/mL)	235.68 ± 25.47	241.35 ± 26.77	0.767	0.485
FIB (g/L)	4.05 ± 0.56	5.02 ± 0.58	6.016	0.000
BNP (ng/L)	782.36 ± 50.19	2054.39 ± 103.42	55.327	0.000
UA (μmol/L)	301.54 ± 23.28	336.75 ± 25.16	5.136	0.000
Scr (μmol/L)	78.94 ± 6.84	92.33 ± 7.51	6.591	0.000
ALB (g/L)	37.05 ± 4.06	30.14 ± 3.51	6.438	0.000
TC (mmol/L)	3.85 ± 0.84	4.01 ± 0.89	0.654	0.517
TG (mmol/L)	1.72 ± 0.34	1.68 ± 0.31	0.435	0.559
LDL-C (mmol/L)	2.51 ± 0.76	2.65 ± 0.79	0.639	0.508
HDL-C (mmol/L)	1.20 ± 0.28	1.10 ± 0.25	1.332	0.236
Hb (g/L)	132.19 ± 15.42	130.18 ± 14.63	0.473	0.523
WBC (×109/L)	7.15 ± 0.63	8.45 ± 0.73	6.741	0.000
NC (×109/L)	4.51 ± 0.48	7.11 ± 0.61	16.748	0.000

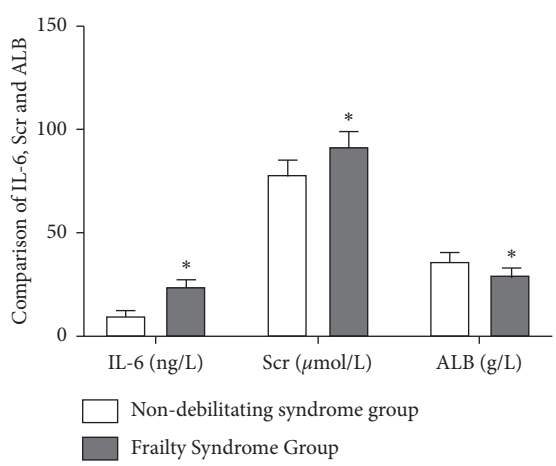

Figure 1: Comparison of IL-6, Scr, and ALB levels between the two groups. *Note*. Compared with the nondebilitating syndrome group, $^*P < 0.05$.

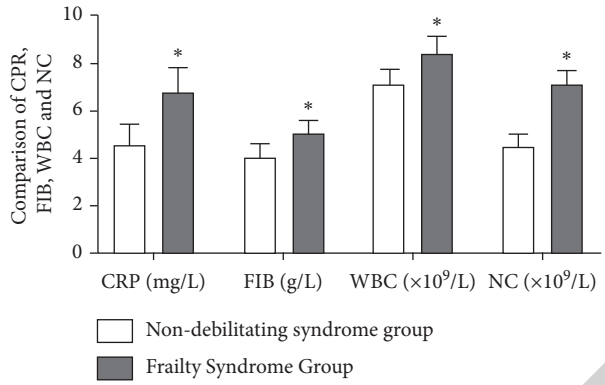

Figure 2: Comparison of CPR, FIB, WBC, and NC levels between the two groups. *Note*. Compared with the nondebilitating syndrome group, $^{*}P < 0.05$.

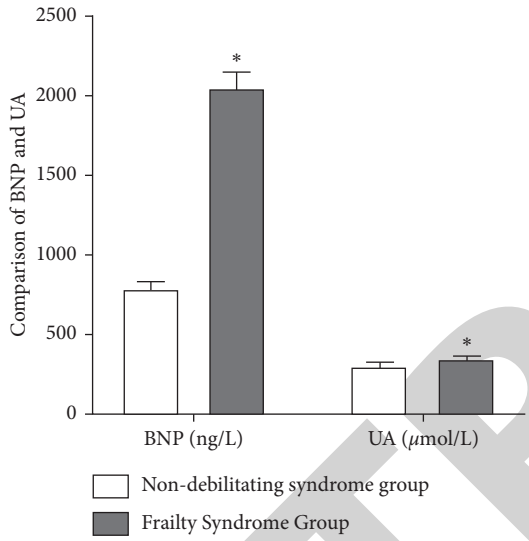

Figure 3: Comparison of BNP and UA levels between the two groups. *Note*. Compared with the nondebilitating syndrome group, $^{*}P < 0.05$.

4. Discussion

Coronary heart disease is a common disease in the elderly. According to relevant statistics, the number of patients suffering from cardiovascular disease in our country is 290 million, of which 11 million are coronary heart disease, and the incidence of this disease is still on the rise in recent years [7]. In the elderly population, weakening of physical function is very common, and the decline of physical function is the main factor that causes weakness, and the occurrence of weakness is an important factor in predicting the poor prognosis of cardiovascular disease. According to relevant statistics, the incidence of frailty syndrome in elderly patients with coronary heart disease is as high as 48.5%–79.0% [8]. Therefore, the influencing factors of elderly coronary heart disease with frailty syndrome have become a hot spot in clinical research at this stage.

In this study, it was found that a total of 28 cases of frailty syndrome occurred in 80 patients, with an incidence rate of 35.00%. Frailty syndrome is more common in elderly patients with coronary heart disease. In terms of influencing factors, multivariate logistic regression analysis showed that combined COPD, combined tumor, IL-6, BNP, UA, Scr, ALB, and neutrophil count are independent risk factors for elderly coronary heart disease patients with frailty syndrome ($P < 0.05$). The specific analysis is as follows: The first is the combination of COPD and tumor: COPD is a lung disease characterized by airflow limitation. This disease will severely reduce the patient's lung function and weaken the physical function [9, 10]. The presence of tumors will seriously affect the various body functions of the patient, and it is also a major factor leading to the decline of body functions. In clinical practice, the combination of one of the abovementioned diseases will increase the risk of debilitating elderly patients with coronary heart disease [11]. Chatterjee et al. [12] believe that, for elderly patients with coronary heart disease, clinicians need to understand the status of their combined diseases in order to do a good job in the early screening of elderly patients with coronary heart disease and improve the prognosis of patients as much as possible. The second is laboratory indicators: this study found that IL-6, BNP, UA, Scr, ALB, and neutrophil count are one of the influencing factors of elderly coronary heart disease with frailty syndrome, so these indicators can be used as a clinical assessment of patient frailty-related laboratory indicators. The reason is that the subclinical and comorbidities of elderly patients with coronary heart disease will reduce their systemic physiological reserves, reduce body balance, and cause significant changes in the abovementioned laboratory indicators [13–15]. However, in the study of Stewart et al. [16], the univariate analysis believed that BNP and Scr were possible influencing factors in elderly patients with coronary heart disease, but multivariate logistic regression analysis showed that BNP and Scr could not be influencing factors. There is a certain difference between this result and the results of this study, which may be related to factors such as individual differences in patients and differences in the sample size of the study. In short, for elderly patients with coronary heart disease, the overall reserve function status of the patient can be assessed based on the abovementioned related influencing factors, so as to accurately screen the occurrence of debilitating syndrome early and improve the patient's prognosis [17]. The related research on elderly patients with coronary heart disease complicated by frailty syndrome is still in the preliminary stage, and the

Table 3: Multivariate logistic regression analysis.

Factors	B value	SE value	Wx^2	*P* value	OR value	95% CI
Age	−0.55	0.61	0.45	0.51	0.62	0.28–2.67
BMI	−0.71	0.78	0.59	0.63	0.74	0.31–2.89
Diabetes	−0.40	0.58	0.41	0.48	0.57	0.21–2.34
Congestive heart failure	−0.48	0.60	0.43	0.49	0.60	0.25–2.42
Chronic renal insufficiency	−0.65	0.71	0.54	0.60	0.71	0.28–2.75
COPD	2.15	0.96	0.43	0.02	1.23	1.05–5.63
Tumor	1.56	0.83	0.45	0.01	1.15	1.02–5.43
Hyperuricemia	−0.61	0.68	0.52	0.55	0.64	0.30–2.57
Arrhythmia	−0.53	0.60	0.42	0.48	0.59	0.24–2.51
IL-6	2.62	0.99	0.48	0.02	2.05	1.86–6.34
CRP	1.69	0.95	0.51	0.02	2.31	2.05–7.14
FIB	−1.05	0.86	0.63	0.69	0.71	0.35–2.64
BNP	2.05	0.87	0.63	0.01	2.45	2.16–7.33
UA	−0.92	0.75	0.69	0.77	0.68	0.41–2.93
Scr	2.16	0.88	0.71	0.01	3.52	2.57–7.84
ALB	2.28	0.95	0.76	0.01	3.61	2.67–7.95
WBC	−0.86	0.70	0.63	0.83	0.78	0.40–2.86
Number of neutral cells	1.84	0.91	0.82	0.02	2.89	1.76–6.48

lack of large-scale epidemiological investigations has led to the lack of frailty scores or diagnostic models. After this study, the related factors of frailty can be further clarified, which is of great significance for constructing frailty scores or diagnostic models [18, 19].

5. Conclusions

In conclusion, combined COPD, combined tumor, IL-6, BNP, UA, Scr, ALB, and neutrophil count are the influencing factors of elderly patients with coronary heart disease combined with frailty syndrome, and these factors can be used as the basis for the diagnosis of frailty syndrome and to guide the clinical development of targeted diagnosis and treatment plans.

Data Availability

The simulation experiment data used to support the findings of this study are available from the corresponding author upon request.

Conflicts of Interest

The authors declare no conflicts of interest regarding the publication of this paper.

References

[1] K. Pafili, P. Steiropoulos, and N. Papanas, "The relationship between obstructive sleep apnoea and coronary heart disease," *Current Opinion in Cardiology*, vol. 30, no. 4, pp. 439–446, 2015.

[2] N. Doba, Y. Tokuda, N. E. Goldstein, T. Kushiro, and S. Hinohara, "A pilot trial to predict frailty syndrome: the Japanese Health Research Volunteer Study," *Experimental Gerontology*, vol. 47, no. 8, pp. 638–643, 2012.

[3] H. Pajukoski, J. H. Meurman, P. Halonen, and R. Sulkava, "Prevalence of subjective dry mouth and burning mouth in hospitalized elderly patients and outpatients in relation to saliva, medication, and systemic diseases," *Oral Surgery, Oral Medicine, Oral Pathology, Oral Radiology & Endodontics*, vol. 92, no. 6, pp. 641–649, 2001.

[4] W. J. Paulus and C. Tschöpe, "A novel paradigm for heart failure with preserved ejection fraction," *Journal of the American College of Cardiology*, vol. 62, no. 4, pp. 263–271, 2013.

[5] A. A. Damluji, G. Gerstenblith, and J. B. Segal, "Frailty measurement using administrative data in older patients with cardiovascular disease," *JAMA Cardiology*, vol. 5, no. 8, pp. 967-968, 2020.

[6] B. Joseph and F. S. Jehan, "The mobility and impact of frailty in the intensive care unit," *Surgical Clinics of North America*, vol. 97, no. 6, pp. 1199–1213, 2017.

[7] F. Grodstein, J. E. Manson, and M. J. Stampfer, "Hormone therapy and coronary heart disease: the role of time since menopause and age at hormone initiation," *Journal of Women's Health*, vol. 15, no. 1, pp. 35–44, 2006.

[8] B. Fuhrman, "The urokinase system in the pathogenesis of atherosclerosis," *Atherosclerosis*, vol. 222, no. 1, pp. 8–14, 2012.

[9] C. G. Musso, J. R. Jauregui, and J. F. Macías Núñez, "Frailty phenotype and chronic kidney disease: a review of the literature," *International Urology and Nephrology*, vol. 47, no. 11, pp. 1801–1807, 2015.

[10] M. T. Vidán, V. Blaya-Novakova, E. Sánchez, J. Ortiz, J. A. Serra-Rexach, and H. Bueno, "Prevalence and prognostic impact of frailty and its components in non-dependent elderly patients with heart failure," *European Journal of Heart Failure*, vol. 18, no. 7, pp. 869–875, 2016.

[11] P. P. Vitaliano, J. M. Scanlan, J. Zhang, M. V. Savage, I. B. Hirsch, and I. C. Siegler, "A path model of chronic stress, the metabolic syndrome, and coronary heart disease," *Psychosomatic Medicine*, vol. 64, no. 3, pp. 418–435, 2002.

[12] K. Chatterjee, H. J. C. Swan, W. W. Parmley, H. Sustaita, H. S. Marcus, and J. Matloff, "Influence of direct myocardial revascularization on left ventricular asynergy and function in patients with coronary heart disease," *Circulation*, vol. 47, no. 2, pp. 276–286, 1973.

[13] R. Hamonangan, I. P. Wijaya, S. Setiati, and K. Harimurti, "Impact of frailty on the first 30 days of major cardiac events in elderly patients with coronary artery disease undergoing elective percutaneous coronary intervention," *Acta medica Indonesiana*, vol. 48, no. 2, pp. 91–98, 2016.

Hindawi
Journal of Healthcare Engineering
Volume 2023, Article ID 9826214, 1 page
https://doi.org/10.1155/2023/9826214

Retraction

Retracted: Controlled Hypotension Combined with Femoral Nerve Block for Knee Replacement without Tourniquet

Journal of Healthcare Engineering

Received 10 November 2022; Accepted 10 November 2022; Published 18 January 2023

Journal of Healthcare Engineering has retracted the article titled "Controlled Hypotension Combined with Femoral Nerve Block for Knee Replacement without Tourniquet" [1] due to concerns that the peer review process has been compromised.

Following an investigation conducted by the Hindawi Research Integrity team [2], significant concerns were identified with the peer reviewers assigned to this article; the investigation has concluded that the peer review process was compromised. We therefore can no longer trust the peer review process, and the article is being retracted with the agreement of the Chief Editor.

References

[1] L. Wang, Y. Zheng, X. Zhang, and Q. Ke, "Controlled Hypotension Combined with Femoral Nerve Block for Knee Replacement without Tourniquet," *Journal of Healthcare Engineering*, vol. 2021, Article ID 3219337, 8 pages, 2021.

[2] L. Ferguson, "Advancing Research Integrity Collaboratively and with Vigour," 2022, https://www.hindawi.com/post/advancing-research-integrity-collaboratively-and-vigour/.

Hindawi
Journal of Healthcare Engineering
Volume 2021, Article ID 3219337, 8 pages
https://doi.org/10.1155/2021/3219337

Research Article

Controlled Hypotension Combined with Femoral Nerve Block for Knee Replacement without Tourniquet

Liangming Wang, Yiqiang Zheng, Xiaolu Zhang, and Qingfeng Ke

Department of Joint and Trauma Surgery, The Second Affiliated Hospital of Fujian Medical University, Quanzhou, China

Correspondence should be addressed to Qingfeng Ke; kqf@fjmu.edu.cn

Received 12 September 2021; Revised 27 September 2021; Accepted 19 October 2021; Published 9 December 2021

Academic Editor: Gu Xiaoqing

In the process of knee replacement surgery, the use of tourniquet technology for hemostasis is the most common method. But the adverse reactions of tourniquets in knee replacement surgery have become more prominent in recent years. More and more scholars have begun to advocate the optimization of the use of tourniquet technology, thereby controlling the use of tourniquet technology. In this study, 125 patient cases were randomly divided into four experimental groups for comparative analysis. The two sets of variables are whether to use tourniquet during surgery and use intravenous analgesia or nerve block analgesia. Studies have shown that when using a tourniquet for knee replacement surgery, the chance of hidden blood loss increases after use. The tourniquet was not used during the operation, the patient's thighs were swollen, and postoperative pain was reduced. Compared with intravenous analgesia, knee joint replacement with uncontrolled tourniquet combined with femoral nerve block has a better analgesic effect and can effectively relieve pain after knee replacement. Therefore, under the method of controlled hypotension combined with femoral nerve block, TKA surgery without using tourniquet technology is more conducive to early health recovery and pain relief after TKA surgery, as well as functional exercise and knee joint recovery during postoperative recovery.

1. Introduction

TKA has widely been used in medical clinical treatment in recent decades. TKA surgery isveryeffective for the advanced management of knee arthritis, and it is arelativelymature and complete surgical method[1]. With the maturity of surgical operation technology and the development of the prosthetic material industry in recent years, patients with knee arthritis will generally choose knee replacement surgery to cure inflammation in the late stage of arthritis[2]. The tourniquet is a common method of hemostasis in clinical research,andit isveryeffective in reducing bleeding during surgery. The tourniquet not only reduces the amount of bleeding during surgery, but also has a good effect in providing a clean and clear surgical field of view;however, in recent years, with the theoretical point of view on the restrictive use of tourniquets[3], more and more scholars have begun to call for optimization and upgrading of tourniquet use methods.

Reducing the amount of bleeding is an important indicator during the operation of TKA. At this time, the use of tourniquet can not only reduce the amount of bleeding, but also provide a clear vision and reduce the bleeding of the bone surface. The use of tourniquets during surgery allows the bone cement component of knee surgery to penetrate better into loose bones and thus can fit the bone surface more firmly [4]. In addition, the tourniquet can reduce the amount of bleeding during the operation, thereby providing the operator with a clear surgical field of vision, cleaner bone cement, and a better bone interface. Therefore, it is widely used in clinical applications of TKA. However, it is currently controversial whether the use of tourniquets can really reduce the total blood loss during the perioperative period of TKA and improve the effect of recovering from the healing period after surgery [5]. The use of tourniquets during surgery may increase the chance of postoperative complications [6]. The application of the tourniquet technique in the TKA process will reduce the pain and swelling of patients

during postoperative recovery, speed up postoperative recovery time, and affect the changes in total operation time and total blood loss. In recent years, these claims have been increasing in TKA surgery research. Is the length of tourniquet used related to the occurrence of various complications after surgery [7]? The application methods of tourniquets in replacement surgery have been roughly divided into three categories in recent years. Compared with the frequency of using tourniquets during surgery, they are divided into three situations: the tourniquet is used throughout the procedure, some tourniquets are used, and no tourniquets are used. There are great disputes among experts and scholars on the three types of application methods [8]. Experts and scholars who adhere to the concept of rapid rehabilitation believe that if the use of tourniquets is reduced or not used during TKA surgery [9], it may reduce ischemia-reperfusion injury and thrombosis during surgery [10]. This study proposes a new method of use: combining controlled hypotension with femoral nerve block and using tourniquet only when using bone cement [11].

Although the tourniquet brings some convenience, it also causes some postoperative complications, such as site damage caused by ischemia-reperfusion, local swelling, paralysis, and pain in the tourniquet work area [12]. Therefore, TKA surgery also has disadvantages such as greater trauma and more perioperative blood loss. How to apply tourniquet in the surgical process to maximize the benefits of the tourniquet application during surgery has become a hot research in recent years. Therefore, this study proposes a new method of use: the application of tourniquet under controlled hypotension combined with femoral nerve block [13]. By comparing the impact of the rehabilitation efficiency of different hemostatic methods, the best solution for using a tourniquet in knee replacement surgery is sought. The research team believes that if the reduction or restriction of the use of tourniquets during TKA surgery may reduce the damage caused by the use of tourniquets during and after surgery. The use of a balloon tourniquet during surgery is a routine operation for joint surgeons at home and abroad [14]. It can provide a clear surgical field of view, shorten the operation time, reduce the amount of bleeding during the operation, and provide a good bone cement interface. However, at the same time, the use of tourniquets during surgery can cause discomfort and may even cause pain, venous thrombosis, and muscle and nerve damage [15]. Whether the tourniquet is used during TKA surgery has many different opinions in the medical community [16]. This article uses a systematic review method to analyze the randomized control parameters of tourniquet used in TKA surgery to explore the effect of controlled blood pressure combined with femoral nerve block tourniquet on TKA clinical practice [17].

2. Research Methods

2.1. Patients' Information. After the approval of the relevant departments of the hospital and the consent of the patient and his family, the research project includes patients with unilateral TKA unilateral limbs who were seen in the hospital from March 2018 to January 2020, regardless of gender, age from 50–80 years, ASA I–III, and NYHA I–III. Some cases that could not be studied were screened, and some cases that had serious complications after TKA surgery or could not be completed due to other reasons and could not complete the data standards required for this surgical study were screened and excluded. We exclude patients with a history of allergy to related surgical drugs, mental illness, cognitive dysfunction, or cardiovascular and cerebrovascular diseases, and other factors that affect the patient's medical experience and safety. Using random allocation, the software automatically divides the selected patients into four groups: the first group's surgical method is TKA surgery using tourniquet combined with vein-controlled analgesia; the second group used tourniquet technique before TKA operation and analgesia with femoral nerve block after operation; the third group used TKA operation without using tourniquet technology and cooperates with intravenous analgesia to reduce postoperative pain; and the fourth group's surgical method is TKA surgery without using tourniquet technology combined with femoral nerve block technology to relieve pain after surgery [18].

2.2. Tools. All patients followed the routine fasting and fasting requirements before surgery and routinely monitored HR, SpO_2, invasive arterial pressure, and depth of EEG consciousness after entering the operating room. In the first and second experimental types, patients with TKA surgery use tourniquet technique on the affected limb, and the pressure of the tourniquet will increase the contraction pressure of the affected limb by 100 mmHg. In the second and fourth groups of surgical experiments, the femoral nerve block was used for anesthesia induction during TKA surgery, and the third and fourth patients underwent TKA surgery without using tourniquet technique. Anesthesia induction was performed in the third and fourth groups of surgery: propofol 1.5 mg/kg, sufentanil 0.5 μg/kg, midazolam 0.5 mg/kg, and rocuronium 0.8 mg/kg. After the induction is completed, the following doses should be maintained during the operation: propofol 3 $mg \cdot kg^{-1} \cdot h^{-1}$, remifentanil 0.2 $\mu g \cdot kg^{-1} \cdot min^{-1}$ continuous intravenous pump input, and continuing to inhale 1% sevoflurane and rocuronium 15 mg to maintain muscle relaxation by intermittent intravenous bolus injection. About thirty minutes right before the operation, the muscle relaxant injection was stopped. At the same time, in order to suppress postoperative vomiting, parecoxabine 50 mg analgesia and tropisetron 3 mg were administered, and the suture operation was started after the use of sedative drugs was stopped. After the operation of the first group of patients, continuous intravenous self-controlled analgesia was performed in order to alleviate the suffering of the patients. This method is referred to as patient controlled intravenous analgesia (PCIA). Its formula is tramadol 10 mg/ml, flurbiprofen axetil 1.25 mg/ml, total volume 80m, background dose 1 ml/h, single injection dose 1.5 ml; lock-in time: 15 min. The second group performed the operation of self-controlled analgesia of the femoral nerve block after

operation. This method is referred to as patient controlled nerve block analgesia (PCNA). Its formula is concentration of ropivacaine is 0.125%, the total volume is 300 ml, flurbiprofen axetil is 1.25 mg/ml, total volume is 80m, background dose is 5 ml/h, and single injection dose is 5 ml; lock-in time: 45 min. The PCIA method was used for analgesia in the third group after the operation, and the content of the PCIA formula was the same as that of the first group. The PCNA method was used for analgesia in the fourth group after the operation, and the content of the PCNA formula was the same as that of the second group. The time and blood loss of the patients in the TKA operation were used as observation indicators for statistical analysis The total blood loss data Hb(g/L) on the day before the operation and the day after the operation are calculated as follows:

$$\text{total blood loss} = (\text{Hb before surgery} - \text{Hb after surgery}) \times \text{body weight (kg)} \times 7.5. \tag{1}$$

The circumference of the upper third of the patient's thigh was measured on the day before the start of the TKA operation and one, two, and three days after the end of the operation. Peripheral venous blood of the affected limb was collected to determine the WBC count, NEUT%, and CRP concentration data. The patient's affected knee joint activity (AROM) was evaluated one day before the operation, and one, two, three, and seven days, and three months after the operation. One day before surgery, and one, two, three, and seven days, and three months after surgery, using the VAS, pain during rest and activities was measured [19], and the scoring standard was set as follows: 0 points, painless; and 10 points, unbearable pain [20]. This study used the MoCA scale to evaluate cognitive function [21], and continuous data monitoring and statistical analysis were performed on the day before the operation, the first day after the operation, the second day after the operation, and the third day after the operation. In the MoCA scale, a total of eight data display performances such as visual space, executive function, naming, and memory can be listed.

2.3. Analysis Method. Using the statistical analysis method of this study [22], the collected data information is analyzed and processed statistically by using SPSS 19.0 statistical software. If the measurement data after analyzing the data conform to the normal distribution law, then the data are expressed in the form of mean and standard deviation ($x \pm s$). Two-way ANOVA was used as the standard to compare the analysis methods between the two groups of data. The SNK-q test standard was used as the method standard for the comparison between the two sets of data [23]. We use the SNK-q test standard as the method standard for pairwise comparison between the two sets of data. We use the LSD-t method to test the data and compare the values at different time points in the data set. The LSD-t method was used to test the data, and the numerical values at different time points in the dataset were compared. The counting data were tested by χ^2. When $P < 0.05$, it was indicated that the statistical standard was met, and the data standard had statistical significance.

3. Results

Among the clinical cases of surgery that covered 128 patients with knee arthritis, only 125 were effective cases in this study. A total of 3 patients in the 128-patient case suffered from other serious complications after surgery and were transferred to the respiratory medicine department and excluded from the screening criteria. A total of 125 TKA patients participated in the completion of this study, and there was no statistical difference between patients' characteristics, such as age, gender, occupation, and education level. Within the period of postoperative recovery in the hospital where the operation was performed, there was no statistical difference between the four groups of patients. The difference in the time spent during the TKA operation was not much different in the data analysis of the groups of patients studied, so it was not statistically significant. During the TKA operation, the bleeding volume in the first and second groups was significantly lower than that in the third and fourth groups ($P < 0.05$). However, the total blood loss of the first and second groups was higher than that of the third and fourth groups ($P < 0.05$), as shown in Figure 1.

On the 1st, 2nd, and 3rd days after the operation, the thigh circumference of the first and second groups increased more than that of the third and fourth groups ($P < 0.05$). Since the data difference between the first and second groups is not statistically significant at different points in time, and the data difference between the third and fourth groups is not statistically significant, this difference can be ignored, not counted, and therefore not considered to be the parameters of this study, as shown in Figure 2.

Compared with the day before the TKA operation, the WBC data and NEUT% values of each group of patients on the first day after the operation had a significant increase ($P < 0.05$). At the same time, the data between the groups is not very different, so there is no statistical significance. On the first day, the second day, and the third day after the TKA operation, the CRP concentration in the first and second groups was lower than that in the third and fourth groups ($P < 0.05$). The CRP concentration data between the first group and the second group were not different at different time points, and the CRP concentration data between the third group and the fourth group were not different at different time points, so the data were not statistically significant, as shown in Table 1.

According to the statistical analysis of the data on first and second days after the TKA operation, the AROM of the second and fourth groups is greater than that of the first and third groups ($P < 0.05$). At three and seven days and three months after the operation, there was not much difference between the four groups, so there was no statistical significance. Because at different time points, the difference in AROM values between the first and third groups and between the second and fourth groups is not statistically significant, it is ignored and not considered the object, as shown in Figure 3.

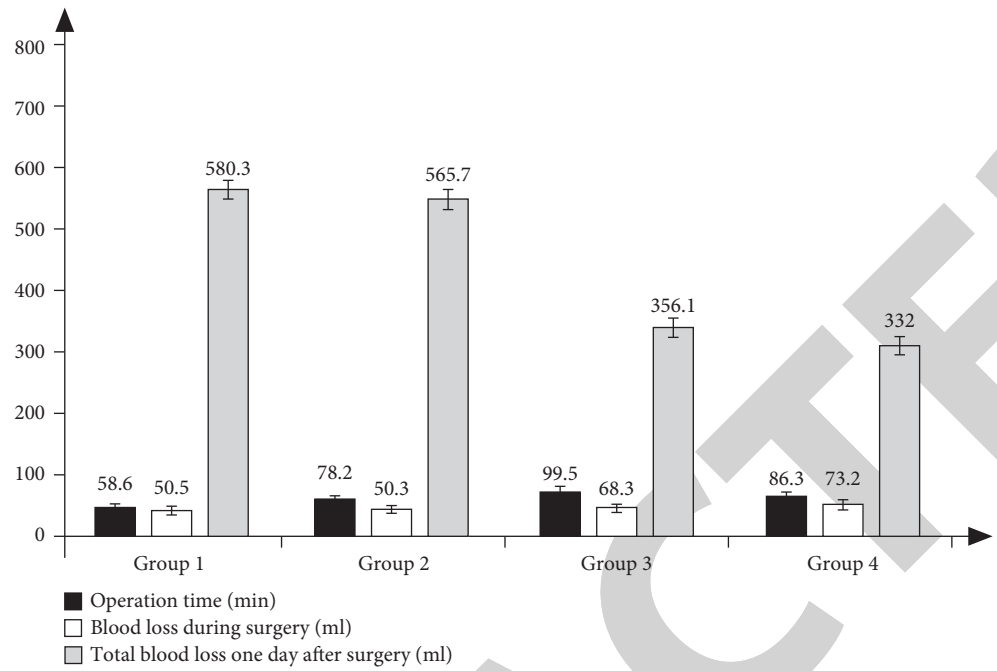

Figure 1: Comparison of operation time and bleeding volume of four groups of patients.

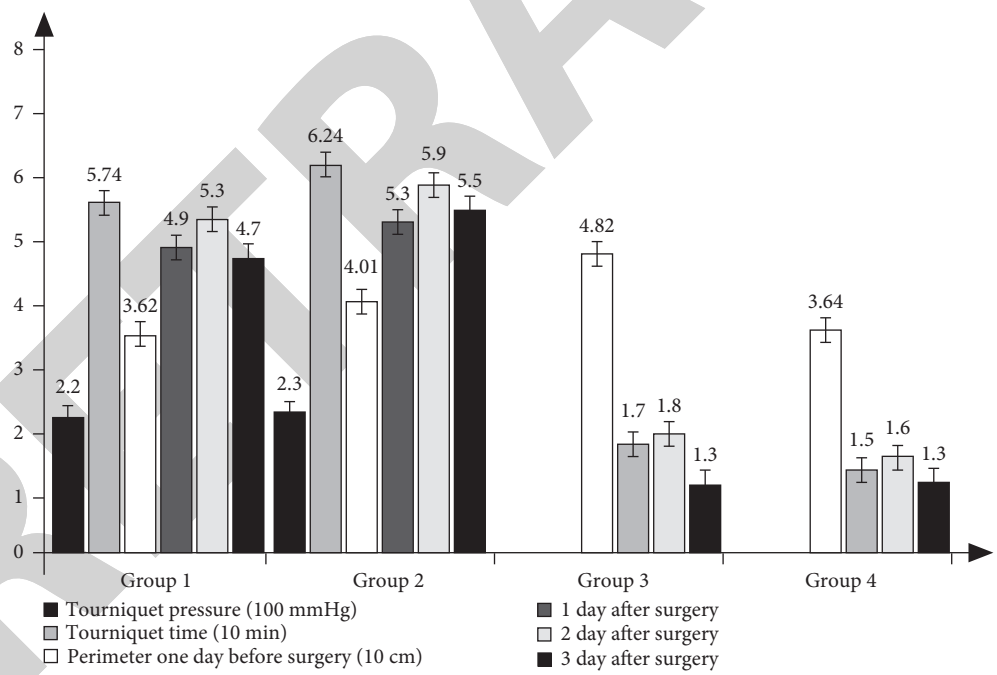

Figure 2: Thigh swelling in the four groups of patients: comparison of thigh circumference.

On the first day and second day after surgery, the VAS scores of the first group were higher than those of the second, third, and fourth groups ($P < 0.05$). The VAS scores of patients at rest in the second group, the third group, and the third group were not statistically different, so they were ignored and not considered the study object. The VAS score data of the third group of clinical cases were higher than those of the second and fourth groups ($P < 0.05$). The difference between the first group and the second group is not statistically significant, so it is ignored, and three days and seven days, and three months after the completion of the operation, the VAS scores were not significantly different between the four groups during the rest and activities through different surgical protocols, so there was no statistical significance, as shown in Table 2.

Compared with before surgery, the MoCA scores of the third and fourth groups were significantly lower on the first day after surgery ($P < 0.05$). The MoCA scores of the first

Table 1: Comparison of AROM of knee joints in the four groups at different time points.

Index	Group	Number of cases	The day before surgery	1 day after surgery	2 days after operation	3 days after surgery
WBC (10^9)	1	28	5.5 ± 1.1	10.5 ± 2.4	6.7 ± 1.9	6.1 ± 1.7
	2	30	6.0 ± 1.3	9.8 ± 2.1	6.1 ± 1.5	6.3 ± 1.4
	3	28	5.3 ± 1.4	13.1 ± 2.9	5.2 ± 1.4	5.1 ± 1.6
	4	39	5.8 ± 2.1	13.2 ± 3.4	5.9 ± 2.3	5.7 ± 2.2
NEUT (%)	1	28	55.9 ± 8.4	86.1 ± 11.1	73.1 ± 18.1	66.6 ± 11.1
	2	30	59.6 ± 9.4	81.9 ± 12.4	73.1 ± 17.2	64.3 ± 10.2
	3	28	59.7 ± 7.5	86.9 ± 11.8	69.9 ± 16.6	62.3 ± 11.4
	4	39	68.2 ± 8.8	88.6 ± 15.4	68.9 ± 17.9	66.1 ± 10.9
CRP (mg/L)	1	28	2.9 ± 0.4	18.2 ± 9.1	58.9 ± 11.9	36.3 ± 5.4
	2	30	5.3 ± 1.6	39.1 ± 10.5	59.2 ± 14.1	42.3 ± 9.1
	3	28	4.5 ± 1.5	49.1 ± 9.4	58.5 ± 13.6	56.3 ± 10.4
	4	39	4.5 ± 0.5	53.1 ± 12.8	89.6 ± 16.4	66.7 ± 11.1

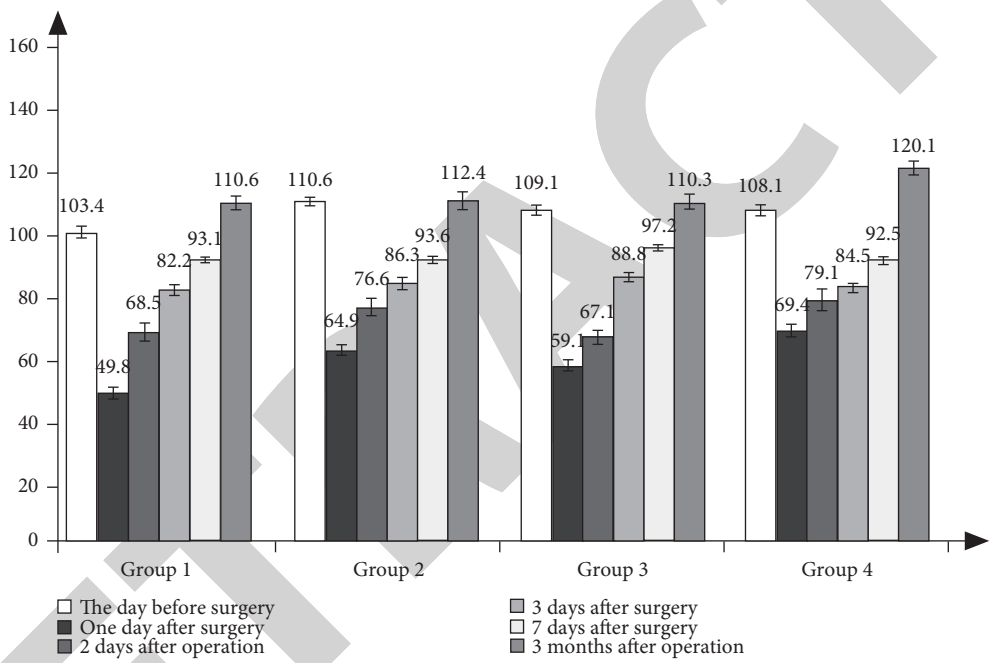

Figure 3: Comparison of AROM of knee joints in four groups at different time points.

Table 2: Comparison of VAS scores of four groups of patients at rest and at different time points.

Status	Group	Number of cases	The day before surgery	1 day after surgery	2 days after surgery	3 days after surgery	7 days after surgery	3 months after surgery
At rest	1	28	1.1 ± 0.2	4.5 ± 1.5	3.8 ± 0.8	2.4 ± 0.1	1.4 ± 0.3	0.7 ± 0.3
	2	30	1.2 ± 0.1	2.3 ± 0.2	22 ± 0.5	2.5 ± 0.1	1.3 ± 0.4	0.5 ± 0.4
	3	28	1.4 ± 0.2	2.5 ± 0.2	2.4 ± 0.5	2.6 ± 0.2	1.4 ± 0.4	0.3 ± 0.2
	4	39	1.5 ± 0.2	2.5 ± 0.5	2.6 ± 0.2	2.3 ± 0.5	1.8 ± 0.2	0.8 ± 0.2
When active	1	28	1.7 ± 0.4	4.3 ± 1.5	4.5 ± 1.2	3.0 ± 0.1	1.3 ± 0.3	0.4 ± 0.2
	2	30	1.8 ± 0.3	3.4 ± 1.4	3.1 ± 1.0	2.9 ± 0.5	1.7 ± 0.5	0.9 ± 0.3
	3	28	2.1 ± 0.4	4.8 ± 1.1	4.2 ± 0.5	2.8 ± 0.8	1.9 ± 0.5	1.0 ± 0.3
	4	39	2.0 ± 0.3	3.1 ± 1.4	2.0 ± 0.8	2.6 ± 0.5	1.2 ± 0.8	0.7 ± 0.1

and second groups were significantly lower than those of the third and fourth groups, which is obvious ($P < 0.05$). There is no statistical difference between the first and second groups and between the third and fourth groups, so it is ignored. On the second and third days after the operation, there was no statistical difference in the MoCA scores between the four groups of patients, so they were ignored and not considered the subjects of this study. Within three days after surgery, the total incidence of cognitive impairment in the first and second groups was significantly lower than that in the third group, and the difference was even more significant in the fourth group ($P < 0.05$). The data study found that within

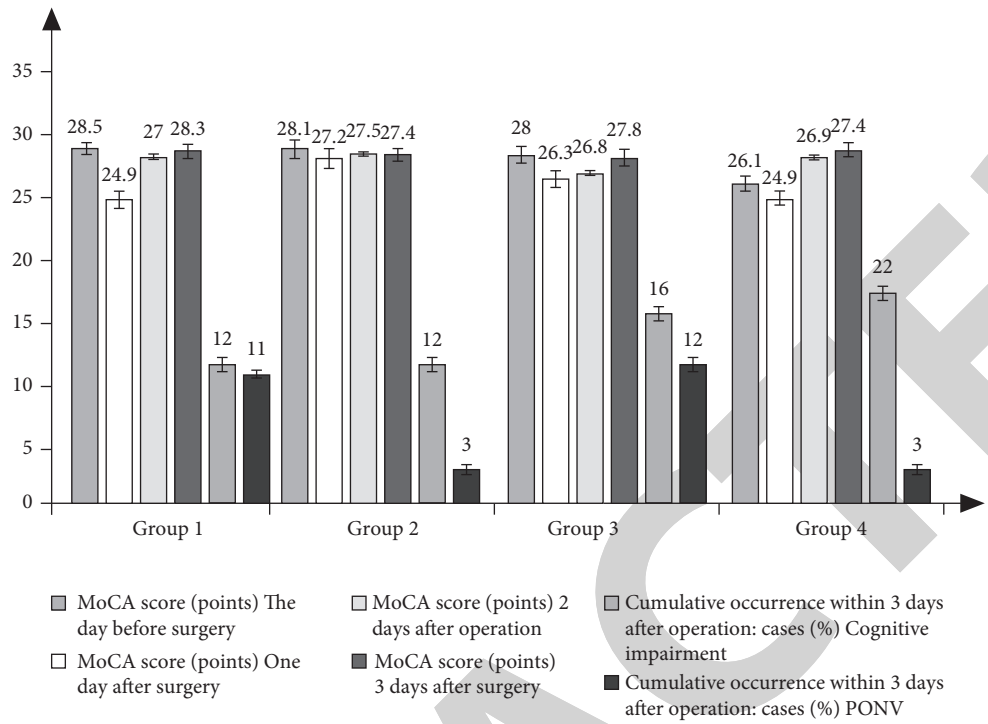

Figure 4: Comparison of MoCA scores of four groups of patients at different time points, cognitive impairment, and PONV occurrence within 3 days after surgery.

three days after TKA surgery, the total incidence of PONV in the first and third groups was lower than that in the second and fourth groups ($P < 0.05$), as shown in Figure 4.

4. Discussion

In order to reduce the amount of bleeding during the operation during the TKA operation, the tourniquet technique is often used. The use of the tourniquet technique can provide conditions for the hardening of bone cement. Although there will be a small amount of bleeding and the surgery area is slightly blurred, it will not hinder the operation. Therefore, when performing TKA surgery without tourniquet, the clarity of the surgical field of vision does not affect the surgery. In the above study, it was found that the amount of bleeding in the operation after the use of the tourniquet during the TKA operation was significantly reduced, but the total blood loss within one day after the operation of the patient after one day would be greater than that during the operation without the tourniquet of patients. The causes of complications such as ischemia, nerve damage, and swelling of the lower limbs have little to do with the use of tourniquets, and the use of tourniquets during surgery may affect postoperative recovery. The data of this study showed that, under the control of the tourniquet pressure and time, the lower limb limbs will swell for more than three days after guarding. Similarly, when using a tourniquet to stop bleeding, it will cause muscle strain, increase muscle fiber cross section, structural abnormalities and reduced function, and other symptoms for several months. Whether it will affect the recovery after TKA surgery in the future is uncertain. The results of the joint mobility values of the patients who were followed up for three months showed that there was no statistical significance for the use of tourniquet. The surgical method without the tourniquet technique in TKA surgery was performed on the patients for one year after TKA. The data in the tracking search show that there is not much difference between the long-term recovery efficiency of patients who do not use tourniquet technology and those who use tourniquet in TKA surgery. In contrast, the use of tourniquets during surgery is more conducive to the early recovery of surgical patients, and there is no significant difference in long-term effects. After the operation of total knee replacement surgery, because of the growth and recovery of a new tissue after the replacement of the knee joint, the affected patient's limb usually suffers from swelling and severe pain. When the tourniquet is used for surgery, it will aggravate severe pain, which will affect the patient's physical recovery after surgery and affect the exercise and recovery of the knee joint. In order to alleviate the severe pain after the operation in total knee replacement surgery, it is recommended that the tourniquet should not be used or the use of tourniquet should be restricted during the postoperative procedure. And the postoperative analgesia program can choose controlled hypotension combined with femoral nerve block technology for analgesia, so as to alleviate the strong pain and discomfort caused by TKA surgery to the patient. The degree/amplitude of blood pressure reduction should be comprehensively measured with reference to many indicators such as electrocardiogram, heart rate, pulse pressure

difference, and central venous pressure. For ordinary patients, reducing the original blood pressure by 30% can reduce bleeding, reduce bleeding, and promote surgery without causing serious complications.

This study points out that the use of controlled blood pressure reduction combined with femoral nerve block without tourniquet technique in TKA surgery is more conducive to pain relief at rest after surgery. Patients using tourniquets had poor analgesic effects in the early stage of surgery, and patients using PCNA had significantly lower VAS scores than PCIA in two days. It shows that the analgesic effect is good and it is beneficial to the recovery of the affected limb after operation. Because after the PCNA analgesia operation, the patient's pain is lighter, so the PCNA analgesia technology is more effective than the PCIA two analgesia methods. Therefore, the analgesic method of using PCNA during TKA surgery is more conducive to the early recovery of patients after TKA surgery. In the course of this study, the WBC and NEUT% values both increased and basically returned to normal after two days. This study shows that the change in the NEUT% value is not related to whether the tourniquet technique is used, and is associated with postoperative limb pain not much related to postoperative recovery. This study shows that, within a few days after the end of TKA surgery, the patient's CRP index continues to increase and is above average. And the data detected within three days after the operation showed that the CRP index is still slightly higher than the average level. Persistent inflammation is one of the causes of postoperative cognitive impairment, and it mostly occurs in the first three days after the operation and the data show that the outbreak rate is higher on the first day after the operation. The high incidence of cognitive function may be related to inflammation, but the specific reasons need to be investigated.

5. Conclusion

In summary, when the controlled blood pressure reduction combined with femoral nerve block technique is used without a tourniquet in TKA, the degree of swelling and pain of the thighs after surgery was lower than that of patients using tourniquet technique. The analgesic effect of the tourniquet-free method under continuous femoral nerve block is far more effective than intravenous analgesia and can significantly relieve the pain after knee replacement surgery. Therefore, under the method of controlled blood pressure lowering combined with femoral nerve block, surgery without tourniquet is more conducive to the early rehabilitation of patients and pain relief after TKA surgery. At the same time, it also has a significant effect on the functional exercise during the recovery period and the recovery of the knee joint activity after the operation.

Data Availability

The datasets and codes of this article are available from the corresponding author upon request.

Conflicts of Interest

The authors declare that they have no conflicts of interest.

References

[1] A. M. Weinstein, B. N. Rome, W. M. Reichmann et al., "Estimating the burden of total knee replacement in the United States," *The Journal of Bone and Joint Surgery*, vol. 95A, no. 5, pp. 385–392, 2013.

[2] E. Losina, T. Plerhoples, A. H. Fossel et al., "Offering patients the opportunity to choose their hospital for total knee replacement: impact on satisfaction with the surgery," *Arthritis & Rheumatism*, vol. 53, no. 5, pp. 646–652, 2005.

[3] T. W. Tai, C. W. Chang, K. A. Lai, C. J. Lin, and C. Y. Yang, "Effects of tourniquet use on blood loss and soft-tissue damage in total knee arthroplasty," *Journal of Bone and Joint Surgery American Volume*, vol. 94, no. 24, pp. 2209–2215, 2012.

[4] M. Girardis, S. Milesi, S. Donato et al., "The hemodynamic and metabolic effects of tourniquet application during knee surgery," *Anesthesia & Analgesia*, vol. 91, no. 3, pp. 727–731, 2000.

[5] A. Fowler, M. Stechman, and D. Mitchell, "A randomised controlled trial of the effect of esmarch tourniquet use on blood loss, bruising and quality of life in elective varicose vein surgery," *Phlebology*, vol. 17, no. 1, pp. 10–12, 2002.

[6] S. Röhl and B. Schücking, "Does tourniquet time in primary total knee arthroplasty influence clinical recovery," *Journal of Knee Surgery*, vol. 28, no. 4, pp. 335–342, 2015.

[7] B. Lynne, I. U. Shridhar, and S. Anand, "Tourniquet failure during total knee replacement due to arterial calcification: case report and review of the literature," *Journal of Perioperative Practice*, vol. 20, no. 2, pp. 55–58, 2010.

[8] S. Katsumata, M. Nagashima, K. Kato et al., "Changes in coagulation-fibrinolysis marker and neutrophil elastase following the use of tourniquet during total knee arthroplasty and the influence of neutrophil elastase on thromboembolism," *Acta Anaesthesiologica Scandinavica*, vol. 49, no. 4, pp. 510–516, 2005.

[9] Y. Fan, J. Jin, Z. Sun et al., "The limited use of a tourniquet during total knee arthroplasty: a randomized controlled trial," *The Knee*, vol. 21, no. 6, pp. 1263–1268, 2014.

[10] J. A. G. Gutiérrez, M. S. Pérez, R. A. V. García, C. A. M. Salas, and V. M. G. Cisneros, "Cemented total knee replacement: comparative study between the use or not of tourniquet on the inmediate results," *Acta Ortopedica Mexicana*, vol. 30, no. 1, p. 7, 2016.

[11] V. T. Domingo, S. Selfa, F. Martínez et al., "Ultrasound guidance for lateral midfemoral sciatic nerve block: a prospective, comparative, randomized study," *Anesthesia & Analgesia*, vol. 104, no. 5, pp. 1270–1274, 2007.

[12] G. Konrad, M. Markmiller, A. Lenich, E. Mayr, and A. R??ter, "Tourniquets may increase postoperative swelling and pain after internal fixation of ankle fractures," *Clinical Orthopaedics and Related Research*, vol. 433, no. 433, pp. 189–194, 2005.

[13] A. Atim, A. Ergin, E. Kurt, Y. Ozdemiroglu, and E. Guzeldemir, "211The comparison of combined sciatic psoas and sciatic femoral 3-in-1 block for knee arthroscopy," *Regional Anesthesia and Pain Medicine*, vol. 31, no. 5, p. 75, 2006.

[14] F. A. Shah, K. Mahmood, and S. U. Din, "A survey of tourniquet use in limbs surgery among the orthopaedic

Hindawi
Journal of Healthcare Engineering
Volume 2023, Article ID 9862937, 1 page
https://doi.org/10.1155/2023/9862937

Retraction

Retracted: A Study of Cloud-Based Remote Clinical Care Technology

Journal of Healthcare Engineering

Received 10 October 2023; Accepted 10 October 2023; Published 11 October 2023

This article has been retracted by Hindawi following an investigation undertaken by the publisher [1]. This investigation has uncovered evidence of one or more of the following indicators of systematic manipulation of the publication process:

(1) Discrepancies in scope
(2) Discrepancies in the description of the research reported
(3) Discrepancies between the availability of data and the research described
(4) Inappropriate citations
(5) Incoherent, meaningless and/or irrelevant content included in the article
(6) Peer-review manipulation

The presence of these indicators undermines our confidence in the integrity of the article's content and we cannot, therefore, vouch for its reliability. Please note that this notice is intended solely to alert readers that the content of this article is unreliable. We have not investigated whether authors were aware of or involved in the systematic manipulation of the publication process.

In addition, our investigation has also shown that one or more of the following human-subject reporting requirements has not been met in this article: ethical approval by an Institutional Review Board (IRB) committee or equivalent, patient/participant consent to participate, and/or agreement to publish patient/participant details (where relevant).

Wiley and Hindawi regrets that the usual quality checks did not identify these issues before publication and have since put additional measures in place to safeguard research integrity.

We wish to credit our own Research Integrity and Research Publishing teams and anonymous and named external researchers and research integrity experts for contributing to this investigation.

The corresponding author, as the representative of all authors, has been given the opportunity to register their agreement or disagreement to this retraction. We have kept a record of any response received.

References

[1] B. Lin and W. Huang, "A Study of Cloud-Based Remote Clinical Care Technology," *Journal of Healthcare Engineering*, vol. 2021, Article ID 8024091, 12 pages, 2021.

Hindawi
Journal of Healthcare Engineering
Volume 2021, Article ID 8024091, 12 pages
https://doi.org/10.1155/2021/8024091

Research Article

A Study of Cloud-Based Remote Clinical Care Technology

Bo Lin[1] and Wei Huang[2]

[1]*Department of Fundamental Nursing, West Anhui Health Vocational College, Lu'an, Anhui Province 237005, China*
[2]*Intensive Care Unit, Affiliated Hospital of West Anhui Health Vocational College, Lu'an, Anhui Province 237005, China*

Correspondence should be addressed to Wei Huang; huangwei140102@163.com

Received 6 October 2021; Revised 26 October 2021; Accepted 27 October 2021; Published 6 December 2021

Academic Editor: Gu Xiaoqing

This paper uses cloud computing to build and design remote clinical care technology, and the study refines the evaluation approach for the elements and builds an evaluation prototype for the strategy, uses service design theory to improve the design of the service part of the assistive system, summarizes the list of requirements based on system design and service design, and designs a service design prototype. Through design practice, the detailed design of the software interaction interface and the auxiliary product of the care assistance system based on the prototype are investigated. Based on the user perspective, the strategy of meeting user expectations and improving user information literacy is proposed; based on the social network perspective, the strategy of establishing a long-term mechanism for smart medical operation and improving the information interaction network environment is proposed; and based on the system service perspective, the strategy of optimizing the system function design and innovating the service model is proposed. Compared with the traditional written patient handover, the application of MNIS under cloud computing can significantly shorten the handover time of surgical patients, improve the standardized rate of surgical safety verification execution and the qualified rate of nursing documents, while the rate of standardized application of prophylactic antibiotics is also significantly higher than that of the control group. The questionnaire survey of nursing staff in the operating room showed that clinical nursing staff was generally satisfied with the clinical application of MNIS under cloud computing, with an average satisfaction score of 64.5 to 11.3, and an average score of 3.58 to 0.54 for each item. Among them, pre-application training of MNIS, departmental support for MNIS, and its ease of verification in surgical patients were the three main factors favoring the clinical application of MNIS in the operating room with cloud computing, while barriers to wireless network connectivity, inconvenient PDA input, and small screen size were the three main drawbacks affecting its application. The determined clinical evaluation index system of MNIS in the operating room is innovative, which not only includes clinical care indicators but also covers general hardware and software indicators, which can effectively reflect the practical application capability of mobile terminal clinical and user experience feelings, and the evaluation index system is comprehensive.

1. Introduction

Nursing information competency is a combination of knowledge, skills, and attitudes that match the prescribed level of nursing practice and are demonstrated in various nursing information activities, and nursing information competency mainly covers nursing information competency and nursing information practice competency [1]. Nursing staff must have sufficient information competence to actively participate in and lead the development of hospital information technology. With the continuous development of remote nursing, mobile nursing, and intelligent nursing, the role of NIS no longer was limited to transcription, transmission, and transcription of medical orders, and the function of NIS has changed from traditional disease-care-centered to nursing support and health care, which requires nurses' computer application ability, computer software management ability, nursing information awareness, and management ability increasingly [2]. Therefore, innovative practice behaviors in nursing information systems require nurses to have the above information competencies. Innovative competencies of nurses are the ability of clinical nurses to proactively seek and develop new methods, techniques, and appliances for health promotion, pre-

squared diseases, and improved quality of patient care, and to apply innovations to their work through teamwork and reasonable channels of support. The innovative behavior of nurses is the external manifestation of innovative ability, and the innovative behavior of nurses includes idea generation, idea support, and idea realization, and in different stages of innovative behavior, the innovative behavior of nurses is related to individual traits and collective atmosphere, where the innovative use behavior of NIS is related to individual traits of innovative consciousness, willingness to innovate, IT knowledge, and skills [3]. Eliminate the uncertainty of the information recipient's understanding of things. Traditional information transmission methods mainly include sensory transmission, written transmission, and telecommunications transmission. The speed of sensory transmission is faster, but the information is more difficult to store. In summary, nurses' innovative use behavior of NIS should be based on information competence and innovation ability, and nurses should have the courage and methods to reform the existing functions of the system, identify problems from nursing practice, and use IT to solve clinical problems to truly promote the change of their innovative use behavior, i.e., nurses' innovative use behavior of NIS needs both nursing information competence and innovation ability [4].

The behavior of nurses in the process of using information systems is measured by problem and strategy formulation, participation in innovative behaviors, and continuously improving information system module functions and developing new system functions or ways of using the system by giving feedback on problems and collaborating with relevant departments to propose improvement strategies [5]. However, the implementation of the current HIS is based on the operation of computer terminals in fixed places, so medical and nursing staff sometimes cannot give timely diagnosis and treatment advice when making rounds or operating at the patient's bedside; nursing staff needs to fill in relevant data and information in writing during the "three checks and seven pairs" at the bedside; in addition, some patient health information also needs to be collected clinically by medical and nursing staff and then input into the computer terminal [6]. In addition, some patient health information needs to be clinically collected by medical staff and then input into the computer terminal. Even in domestic tertiary hospitals where information technology construction is relatively advanced, medical and nursing staff still need to complete a considerable number of written medical documents manually, which not only wastes medical costs and human resources but also easily leads to errors when repeatedly transcribing data entered into patient information, resulting in errors in relevant medical information, which not only affects the consistency of data and information but also easily induces unnecessary medical disputes in the current medical environment.

MNIS under cloud computing platform can be free from the current hardware constraints on medical care information processing system and can call relevant data resources at any time in medical care, including the patient's complete medical history resources dating several years ago, or when encountering rare problems in medical care that are difficult to explain or solve, the relevant database information can be called for comparison and identification. The MNIS under the cloud computing platform enables nursing staff to process patient-related information in a more timely and efficient manner, while spending more time on patient care, truly realizing the "patient-centered" requirement. The medical staff can enter health information, check medical prescriptions and medication records, charge billing, as well as the patient's current complaints and signs into the mobile terminal at the patient's bedside and save them in the information system, thus avoiding repeated transcriptions and assisting the medical staff to execute the relevant important points of diagnosis and care operations on time, thus reducing the occurrence of medical errors. The operating room, as a relatively centralized department for medical care operations, is a multidisciplinary and multi-departmental centralized platform with more stringent care requirements. As an important platform department of the hospital, the operating room is a decisive core department to ensure the safety of patient surgery and provide quality perioperative care to patients, and it can be said that the safety and quality of nursing care in the operating room is one of the fundamental conditions for the quality of hospital operation. Community influence refers to the extent to which the interpersonal relationships and social structure around users affect their use of information systems or technologies; convenience conditions refer to the extent to which factors such as economic level, institutional policies, innovative technologies, and application environments support users' use of information systems or technologies. In the current era of big data, digital management has become the development direction of modern operating room construction, as well as an important part of digital hospital construction. According to the national diagnosis and treatment technical specifications and surgical safety target requirements, safe care involves not only the management of the surgical process, but it also involves all aspects of the perioperative period, so the comprehensive control and fine management of all these contents need a lot of information and data support.

2. Current Status of Research

Since the concept of cloud computing has only been proposed for about 10 years, and the health cloud is still being explored, the impact of the existing private clouds on healthcare management has not yet been highlighted, and its impact on nursing management is still not reported in detail. The current research on nursing information technology is more focused on MNIS application research, which is only an important part of the cloud computing platform [7]. The operating room is a multidisciplinary and multi-specialist platform for performing surgery or resuscitation of patients with acute and critical illnesses, and its safe and effective operation is crucial to the overall operational efficiency of the hospital. In the current healthcare environment, one of the important cores of surgical nursing is nursing safety [8]. Nursing safety requires that nursing staff at all levels to

follow strict systems and standard practices, ensure that medical orders are carried out accurately, and develop and implement individualized and appropriate care plans so that patients can fully benefit from their treatment and recovery. Information technology in surgical care theoretically helps to improve the quality and efficiency of care and enhances nursing safety [9]. At present, due to security and privacy concerns, public health clouds are not fully developed but more often limited to private clouds within individual organizations, i.e., hospital cloud computing platforms, which serve as support platforms for internal hospital operations and are not open to the public [10]. For example, Taiwan Taichung Renmin Hospital's network application cloud image data center (CIDC) platform; patients can visit any hospital in the cloud, image data can be uploaded by Taichung Renmin General Hospital physicians to give consultation and diagnosis, thereby shortening patient consultation time, and improving the quality of medical care [11]. It has effectively improved the speed, efficiency, and quality of medical services.

Some scholars, on the other hand, suggest the establishment of specialized hybrid clouds, such as the establishment of an advanced 3D analysis master-slave system integrated with cloud computing for cardiovascular image database, which helps clinicians to evaluate the surgical outcome during endoluminal aortic valve replacement [12]. The establishment of a cloud computing platform also helps medical diagnosis, such as for lung nodules, by storing huge amounts of relevant medical data in the cloud platform, so that clinicians can quickly and accurately make a diagnosis by comparing and referring to existing databases through cloud computing. It is considered that the core content of smart medical includes the intelligent perception of medical objects, standardized disposition of medical processes, and integration of medical objects and medical processes through interconnection technology, and based on intelligent management of people, objects, and equipment, the medical IoT application model is studied from the medical service application model, medicine management application model, and medical device management application model, and the internal hospital medical [13]. The process of the digital collection, processing, storage, transmission, and sharing of medical information, equipment information, drug information, personnel information, and management information within the hospital is designed. After sorting out the status of research on smart medical systems, it was found that there is a lack of empirical research on the impact of smart medical system applications on patient satisfaction with medical care in China; so the mechanism of the impact of smart medical system applications on patient satisfaction with medical care was explored, and it was concluded that self-efficacy and perceived usefulness can positively affect patient satisfaction with medical care [14].

This MNIS architecture uses a combination of a data flow style and a warehouse style. Each node in the data flow style has its input and output pathway, and the data flow input is processed internally and then the corresponding data flow results are output. This process enriches the data by adding information step-by-step, which makes the software well hidden, highly cohesive, and low coupled, and facilitates the statistical analysis of the system. And, the warehouse style is a data-centric system that is practical for data storage, analysis, maintenance, and application.

3. Analysis of Remote Clinical Care Technologies for Cloud Computing

3.1. Analysis of Remote Clinical Care Cloud Computing Methods. It is a streamlined scheduling model, which is prototyped for distributed programming and efficient data scheduling tasks, in information systems, to facilitate the characteristics of computer parallelism, and it is necessary to constitute a common model as if the use of multi-threaded, multi-process processing, cloud computing technology is an important basis for the development of cloud computing, so as to focus on efficient programming models, in the case of large-scale data programming [15]. The parallelism of processes is major when it comes to large-scale data programming, as it can demonstrate efficient scheduling capabilities and can handle huge-scale data sets. Accurately meeting the diverse and multi-level health needs of patients is a nursing service model with development potential. In-hospital care focuses on optimizing the nursing process online. For example, the use of PDA enables nursing staff to identify patients, record the nursing process, collect physical data, query drug usage, and enter consumables charges. When the command is executed, the data area is divided and then the result of data processing is summarized to finalize the program, so that the programmer focuses more on the process of writing the program and does not pay attention to how the background is running; if the platform of cloud computing can be played, this will be the intuitive feedback of the performance of the whole cloud platform. The distributed system can store a large amount of data, guarantee data security, provide reliable storage, test IO throughput capacity, and expand its indicators. The number of users of the cloud computing system is mostly to improve its ability to handle data and the ability of computing; it must have safe data processing capacity and storage capacity. Traditional computer technology takes the form of direct-connected storage, network access storage. Traditional information processing is difficult to manage in terms of maintenance and management, with dedicated hardware in the branch office in-network access servers. Cloud computing data storage room can be extended into a distributed file system, using a simple storage device model. After meeting the daily security requirements, in many of the client distribution systems, you can achieve storage performance.

$$Q_N(w) = \sum_{i,j}\left(1 + P_{ij}\right)^3 + \left(m_i - m_j\right). \tag{1}$$

When mass data calculation is carried out on a large scale, data in the process of analysis, cloud computing data for processing, must have a powerful function of processing data. In data management, massive data are very necessary,

as this is the future development, and the management of data must be effective. Data management system in data optimization and fault tolerance is the most important way of data management. Class data management is mainly to improve the operation of the system. One can take a series of data cache, indexing, partitioning, and other data centralized management, the server processing the data process, to improve the operational characteristics of data, the use of centralized data management, and take information technology construction to improve the system. Data analysis capability and information technology construction are taken to centralized data management. The system's function is more scientific. Cloud computing must rely on distributed management model. Data are distributed in each node. Each node are processed, and the data processing capability is improved, reducing the corresponding time, as shown in Figure 1.

Information transfer refers to the movement of information in a physical location, i.e., the sender of the information transmits it to the person who needs it, clearing the uncertainty of the information receiver's knowledge of things. Traditional information transmission methods mainly include sensory transmission, written transmission, and telecommunication transmission. Sensory transmission is faster, but the information is more difficult to store; the written transmission can avoid information distortion, but it takes too long; telecommunication transmission can ensure the integrity of information, but the release process is more cumbersome [16]. Invite experts to familiarize themselves with the content of the meeting in advance, to think and prepare for the meeting outline and key issues that need to be discussed. After the meeting begins, the researchers will report on the research background, the status quo of the department, and the progress of the implementation of this research. With the continuous development of science and technology, the Internet of Things has become an emerging medium of information dissemination in recent years.

The core and foundation of the Internet of Things information transmission is still the Internet while using intelligent perception, identification technology, and pervasive computing and other communication perception technologies for automatic acquisition and release of the text, image, sound, and other information, to achieve personalized, fast, and efficient transmission of information.

$$a_G D_t^v f(t) = \lim_{h \longrightarrow 0} \frac{1}{h^v} \sum_{n=0}^{\left[\frac{t-a}{h}\right]} (-1)n \frac{\Gamma(v-1)}{n!\Gamma(v-n+1)} f(t+nh),$$
$$m_i(g) \leq \frac{fit_i - worst(g)}{best(g) + worst(g)}. \tag{2}$$

The integrated technology acceptance and use theory contains four core dimensions, namely, performance expectations, effort expectations, community influence, and facilitation, and identifies four control variables that significantly influence these core dimensions, namely, gender, age, experience, and voluntary use. Performance expectation refers to the user's perception that using the information system or technology will help him/her to be more efficient; effort expectation refers to the user's perceived ease of operation when using the information system or technology; community influence refers to the extent to which the interpersonal and social structures around the user influence his/her use of the information system or technology; convenience refers to the economic level, institutional policies, innovative technologies, application environment, and other factors that help; and facilitation refers to the extent to which factors such as economic level, institutional policies, innovative technologies, and application environment support and help users to use information systems or technologies. At present, research based on UTAUT theory is becoming increasingly mature and has been widely used in many research fields, and its application has long gone beyond the scope of IT adoption to cover service models, marketing, new media forms, information behavior, etc. Research in the empirical field also shows that UTAUT has stronger explanatory power for adoption practices than the original adoption model, as shown in Figure 2.

Nursing care is not only an important part of medical work but also one of the benchmarks for measuring the quality of medical services. In the context of intelligent medical care, patient-centered, safe, and orderly care is the direction pursued by the nursing industry. Smart nursing consists of in-hospital nursing and out-of-hospital nursing, which interact with each other and are conducive to expanding the supply of nursing services and precisely matching the diverse and multi-level health needs of patients, and is a nursing service model with development potential. In-hospital care is based on online optimization of nursing processes, such as the use of PDA to realize the functions of nursing staff to identify patients, record the nursing process, collect sign data, query drug dosage, and enter consumables charges; out-of-hospital care, on the other hand, monitors sign data of discharged patients through mobile nursing devices, reminds patients to take medication on time and in the right amount, reasonably matches diet, controls exercise intensity, and alerts blood sugar alarms [17]. The out-of-hospital nursing service provides home nursing service for patients with limited mobility through the "online appointment, offline service" model of online appointment nurse. Multiple users conduct

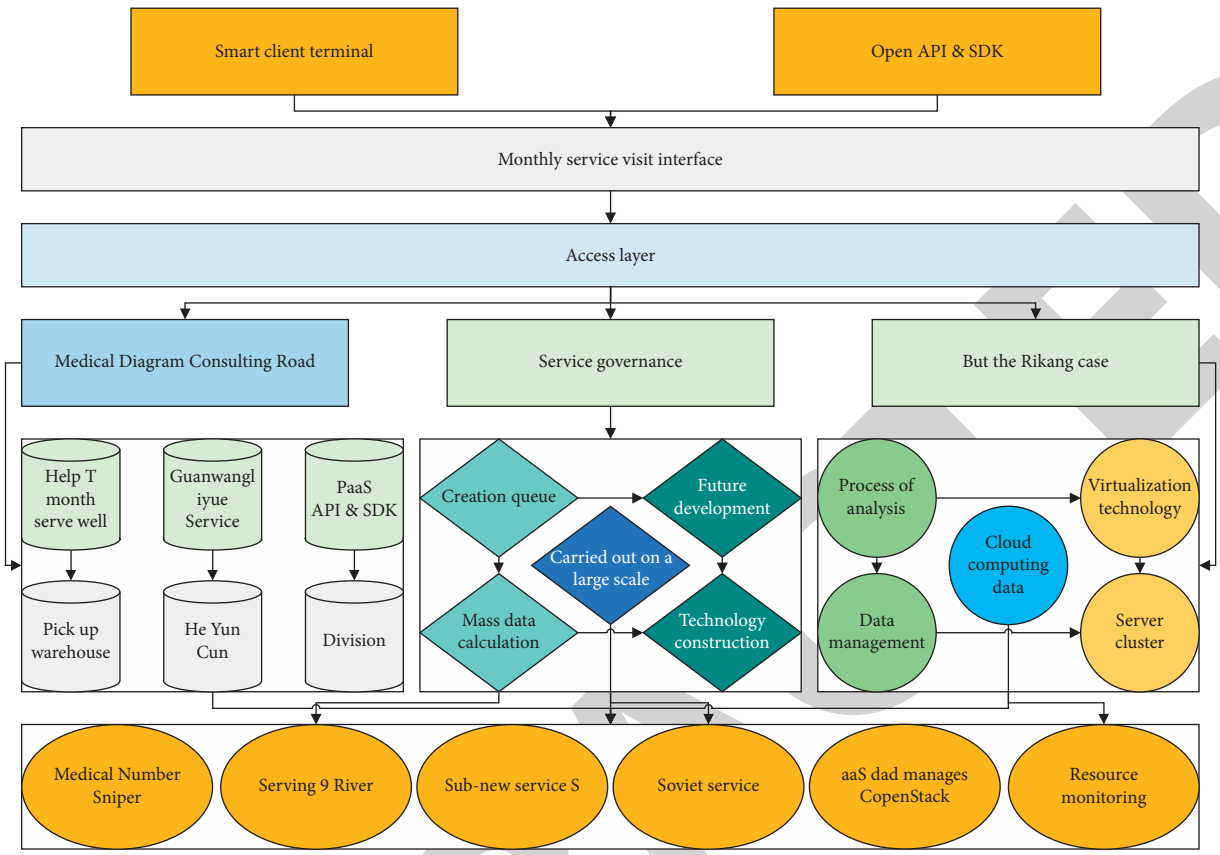

Figure 1: Architecture model of nursing cloud computing platform.

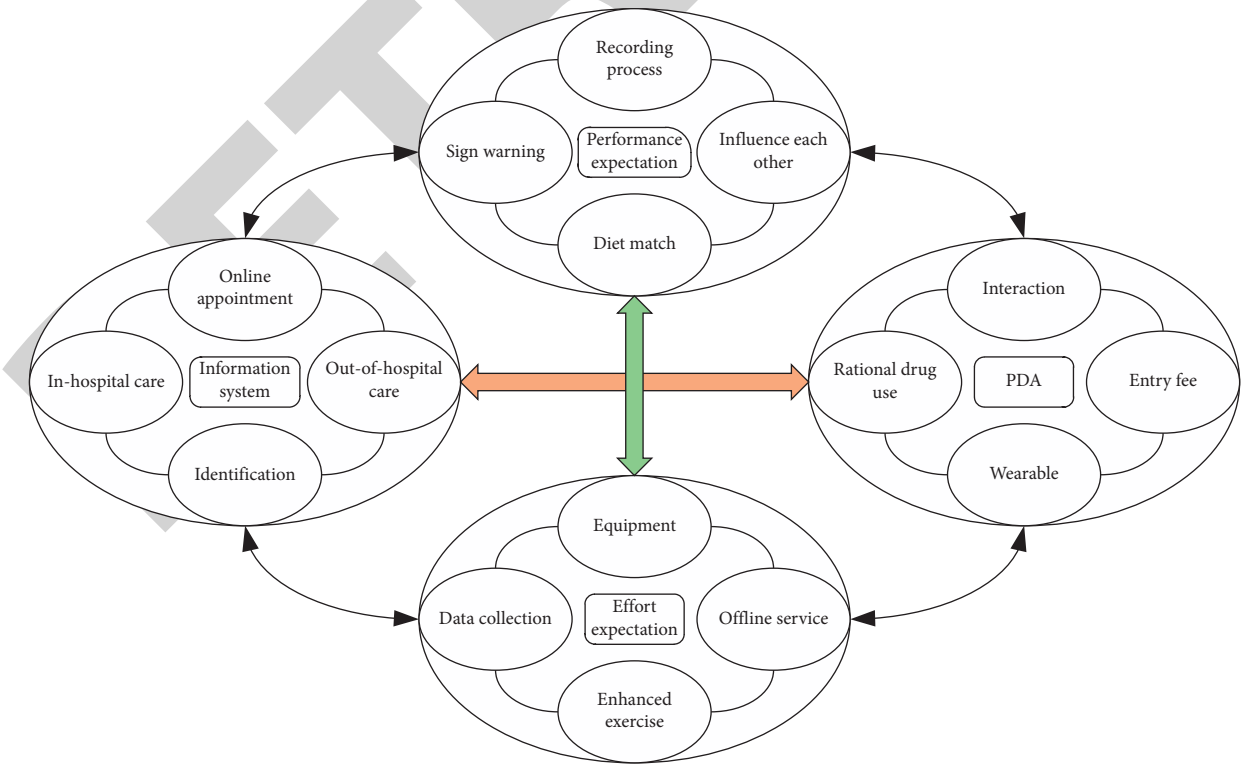

Figure 2: Smart care information interaction process.

in-depth discussions on a certain medical topic, and express their opinions in combination with professional experience, past medical records, scientific research conclusions, academic research, etc. During this process, disputes and doubts will arise, and the goal is to arrive at the best treatment plan that has certain practical value.

Smart follow-up effectively combines the existing medical system with the traditional forms of telephone follow-up, receiving consultation, face-to-face follow-up, and written contact to form a new form of follow-up that allows patients to feel the quality of hospital services that helps purposeful interaction between nurses and patients and even family members, enhances patient satisfaction, and improves the quality of life of patients. The smart follow-up system usually connects the Internet to various hospital information systems and supports the import of patient information such as case number, disease diagnosis, attending physician, procedure mode, and discharge date, and the recording of follow-up information such as discharge summary, examination results, nursing assessment, and return status. Doctors can determine the time and type of follow-up visits according to patients' conditions, and the system pushes appointment reminders to patients according to the type of follow-up visits. Patients make appointment consultations through cloud communication, and follow-up personnel retrieve patients' medical records through the hospital information system and provide follow-up interaction, medication tips, rehabilitation guidance, health records, and follow-up reminders to patients.

3.2. Cloud Computing Tele-Clinical Care Validation Analysis. To increase the scientific tenor of the model construction and improve the professionalism of the model structure and content, this study adopted the expert meeting method and invited experts in the fields of gastroenterology medicine, nursing management, clinical nursing, chronic disease management, and information engineering to discuss the operation process and main service content of the cloud-based total patient management model, the functional settings of the total patient management cloud platform, and to solicit expert opinions. The preliminary draft of the model was revised, supplemented, and improved accordingly. One week before the meeting, the researcher sent the draft of the operation process and main service contents of the cloud-based patient management model, the preliminary design of the framework structure, functional modules of the cloud-based patient management platform, and the meeting theme and discussion outline to all participating experts, inviting them to familiarize themselves with the content of the meeting in advance, and to reflect on and prepare for the outline and key issues to be discussed [18]. The meeting started with the researcher reporting the background of the study, the status of the department, and the progress of the implementation of this study; introducing the purpose of the meeting, the content, and focus of the discussion; inviting the experts to discuss; and taking audio recordings and field notes on the content of the meeting.

$$H_{\sum(m,n)} = \sum_{j=2}^{j\leq m} H(m,n). \tag{3}$$

The user login module is mainly on how users can log in, how users with different permissions can enter the service system belonging to their permissions. The main role of the background is to judge the background users, first of all, through the account password to log in. Through the background processing, connecting the database, the foreground incoming data and the background data are compared, respectively. If the account number, password, and database storage are consistent, you can enter the corresponding page; if the password, account, and permissions are inconsistent, you can enter the corresponding page; if the password, account, and permissions are inconsistent, respectively, you can enter the corresponding page; if the password, account and permissions are inconsistent, respectively, you can enter the corresponding page, as shown in Figure 3.

In this platform system, the new user login password system is the same as the initial password of the work number. The password is set by the platform system administrator. When the new user uses, the system does not actively prompt the user to change the password, but for security, it is recommended that the user first change the password when using. The opinion and appraisal of the software by the clinical practical application personnel is the final requirement for the program design. At the same time, to ensure the user's safety and prevent data leakage, it is best to change the password regularly. To change the password, you need to enter the old password first, that is, the original password consistent with the work number; then enter the new password and then confirm the new password; the new password has to be entered twice before the password can be changed successfully. In this platform system, we use a graphical interface to display all hospital beds with 5 beads per row [19].

This provides a very intuitive view of the patient-bed match and allows you to see briefly which hospital has an empty bed. For beds that are already occupied, the bed icon displays the patient's name, admission number, time of admission, diagnosis, and the names of the responsible doctor and nurse. The management of beds in the system is for newly admitted patients.

$$\begin{aligned} \frac{CI}{RI} &= \frac{\lambda_{\max}+n}{n+1}\times\frac{3}{RI}, \\ \frac{\partial L}{\partial a} &= \sum_{i=1}^{n}\left[y_i + \frac{\exp\left(a+\sum_{j=1}^{m} x_{ij}\beta_j\right)}{1-\exp\left(a+\sum_{j=1}^{m} x_{ij}\beta_j\right)}\right] = 0. \end{aligned} \tag{4}$$

The software interface specifically includes the design of the appearance, the composition of the components, and the development and application of the program to meet the communication needs of health care professionals and patients. The software interface has the following characteristics to better realize the information interaction between healthcare professionals, patients, and medical systems. In

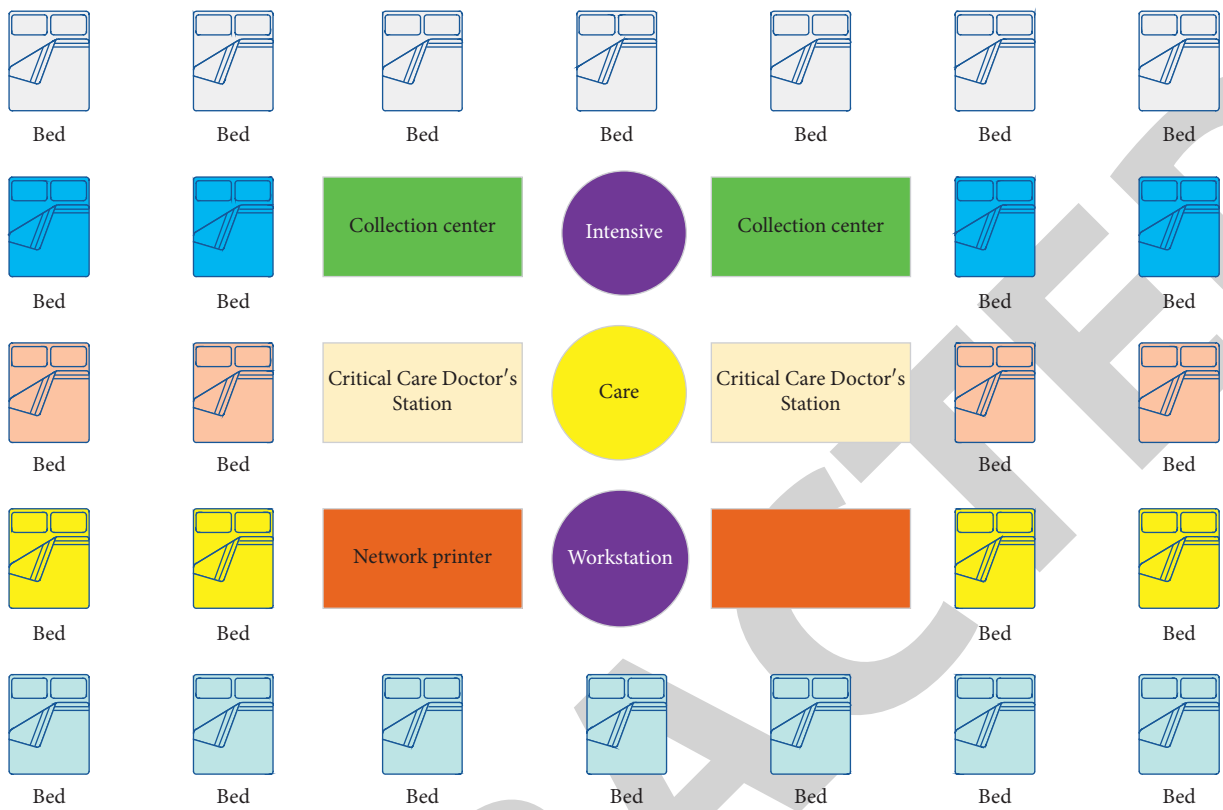

Figure 3: Overall structure of telecare.

the application process of the medical system, the operation steps should be simplified, and the optimization and modification based on the interface must ensure that the users can quickly understand the functions and roles of the system and circumvent the complex processes. Wrong medical advice transmission, execution, feedback, and tracking will directly threaten the health status and even the safety of smart medical users, and the risk is generally blocked by multimodal information emergency processing mechanisms supplemented by offline symbolic interaction. For the design of the software interface, its aesthetics should not only contain the aesthetics of the art form but also meet the needs of medical service practice. The interface should not only bring aesthetic pleasure experience for patients but also make patients relieve anxiety and tension through this aesthetic experience, that is, to achieve a balance of aesthetic value and practical value, as shown in Figure 4.

The human-human interaction mode in the context of smart health includes question and answer, discussion, and transmission. At the same time, the caregivers' work time is approaching 24 hours, which brings considerable physical and psychological pressure to the caregiver. The interaction process of Q&A mode is: the questioner asks questions according to his or her own needs, and the answerer makes corresponding answers based on his or her own knowledge and professional experience, and in the subsequent communication process, the questioner and the answerer communicate and interact in depth for some contents until the questioner obtains satisfactory answers; the interaction process of discussion mode is: multiple users conduct in-

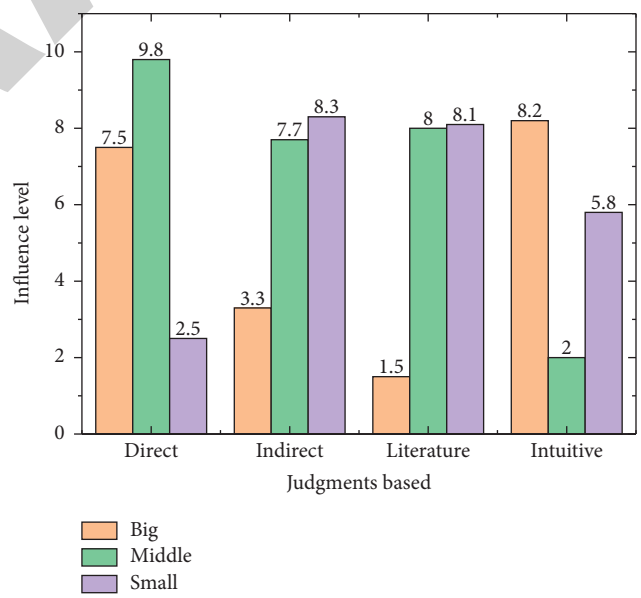

Figure 4: Quantification of the basis of judgment and the degree of impact.

depth discussions on a medical topic [20]. The interaction process of the discussion mode is: multiple users conduct in-depth discussions on a medical topic, combining their professional experience, past medical records, scientific findings, academic research, etc., and in this process, arguments and questions will arise, with the ultimate goal of arriving at the best treatment plan, which has certain

practical value; the interaction process of the teaching mode is: experts and teachers in the medical field use new media to conduct online lectures, and when students have questions about the course or homework, they can ask questions on the message board, and the teacher will answer them after class, so as to improve the quality of medical knowledge dissemination. In this way, the quality of medical knowledge dissemination is improved.

Software testing is an essential step before the formal operation of the software; software design team's high-intensity software testing can find error messages and defects, improve the stability and reliability of software operation, and ensure the reliability of clinical applications. Before testing the software, it is necessary to install the execution files on the designated hospital server and configure the corresponding operating conditions. In addition, it is necessary to provide technical training and operational guidance to clinical application nursing staff, and the opinions and comments of clinical application staff on the software are the final requirements for the program design. Before formally debugging and testing the functional modules of MNIS under cloud computing, the software developer should first input the basic testing data for the tested modules for the corresponding functional testing and record them. According to the defects detected and the opinions of the actual clinical application personnel, the feasibility and correctness should be discussed and analyzed article by article at the same time, and the final practical modification opinions should be formed by the clinical experts of the operating room and the technical experts of the information section, and submitted to the software designers for repair, to ensure the feasibility and accuracy of the software.

4. Analysis of Results

4.1. Remote Clinical Care Cloud Performance Results. Improve the perceived usefulness and ease of use of the model by patients and health care managers. The purpose of building a cloud-based IBD patient management model is to maintain patients' long-term disease stability and improve their quality of life through scientific and efficient disease management, which requires patients' active cooperation and participation in the management process, so patients' attitudes and behaviors toward the model are crucial. According to the technology acceptance model, the perceived usefulness and perceived ease of use of new technology affect the user's attitude, which in turn affects the user's intention to use and ultimately determines the user's actual user behavior. Therefore, when building a cloud-based IBD patient management model, we should consider the actual needs of patients and improve the relevance and quality of the service content, to improve the perceived usefulness of the model for patients. In addition, the user experience of patients and healthcare managers should be fully considered, and simple and convenient operation methods should be provided as much as possible to reduce the workload, to improve the perceived ease of use of the model by patients and healthcare managers. The so-called standard means that the surgeon, anesthesiologist, and operating room nurse complete all verification items and sign them within the specified time. If one or more items are omitted, it will be regarded as irregular.

In the cloud-based IBD patient management model, the patient terminal of the cloud platform provides service contents such as disease symptom monitoring and self-assessment, and the results generated by patient self-monitoring and assessment can be automatically uploaded to the cloud platform, which will analyze and store them, determine whether the relevant indexes are abnormal, and when there is no abnormality or the index value is within the controllable range, the cloud platform gives feedback to the patient directly, sends health education materials, and gives information support and automatically generates management records, as shown in Figure 5.

Institutional care is divided into two main lines of conduct: life care and medical care. There is a clear spacing and rhythm to the tasks of living care, where a single caregiver's tasks can be replaced by other caregivers, and where caregivers are given breaks in between. The design of home care support systems interrupts the original timeline of companionship as much as possible to give the home caregiver enough free time to relieve stress. Because of the lack of professional medical facilities and equipment in the home care environment and the lack of professional medical caregivers, the design of assistive systems needs to improve the facilities and equipment that are lacking in the medical environment.

The members of the cloud platform design and development team first discussed and reorganized the operation process and specific scheme of the proposed IBD patient management model, and clarified the functions that the cloud platform needed to have; members from various disciplines in the team collaborated in the design and development of the cloud platform, and the specific division of labor among the members was as follows: the care management experts were mainly responsible for the coordination and coordination work, and provided suggestions and guidance on the beautification of the platform interface and optimization of the operation process. Nursing information ability mainly covers nursing information ability and nursing information practice ability. Nursing staff must have enough information ability to actively participate in and lead the development of hospital informatization. With the continuous development of remote care, mobile care, and smart care, nursing management experts are mainly responsible for coordinating and coordinating work, and providing suggestions and guidance in terms of platform interface beautification and operation process optimization. Medical experts and clinical nursing experts are responsible for reviewing and evaluating the health education materials, assessment scales, follow-up management forms, and other materials configured after the development of the cloud platform, and providing suggestions for modification and improvement from the perspective of clinical diagnosis and nursing practice. The nursing graduate students are responsible for organizing and importing the professional information needed for the IBD total management cloud

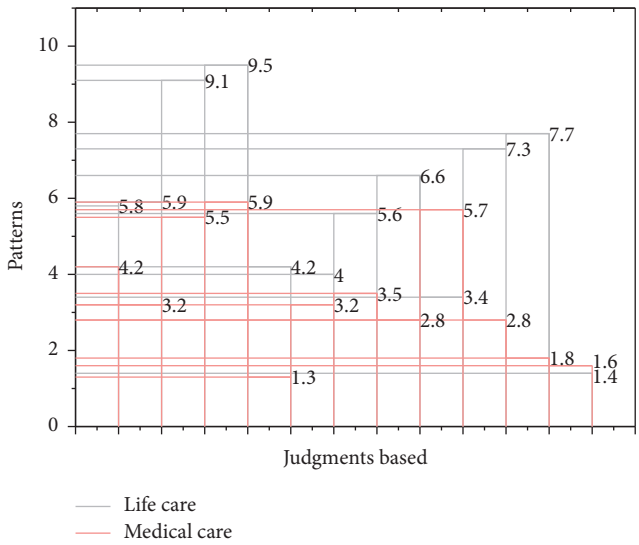

Figure 5: Patterns of institutional caregiving behavior.

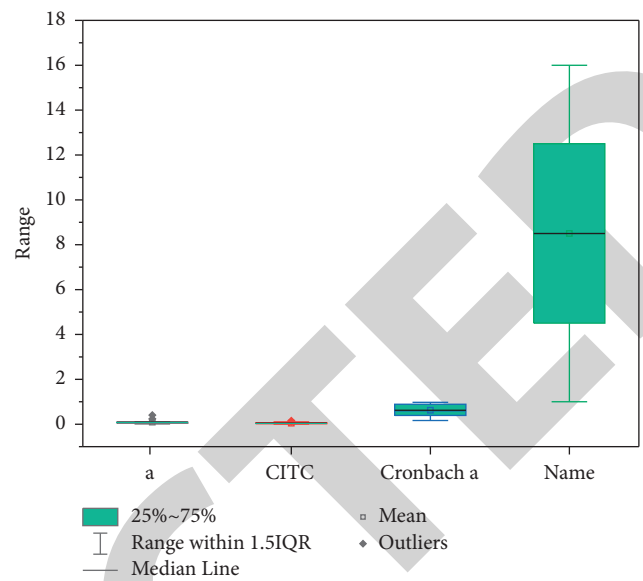

Figure 6: Confidence analysis of results.

platform, modifying and improving it according to the experts' suggestions, coordinating and communicating with the software engineers, jointly testing the platform functions, optimizing the operation process and the cloud platform interface, etc. The software engineer is responsible for specific matters of platform design and development, providing cloud platform information exchange technology, clarifying the cloud platform system architecture, improving the functions of the IBD total management cloud platform together with the nursing graduate student, and maintaining and optimizing the cloud platform from the information technology level, as shown in Figure 6.

Based on data analysis and follow-up opinion survey, the system has good overall quality and interface quality, the information quality needs further improvement, the improvement method is to improve the display of information, improve the organization of information, and the system prompts when there is error; secondly, the fault tolerance for the system error needs to be redesigned, otherwise the user produces great antipathy after falling into the error; the system is relatively friendly for people with high education but less friendly for people with low learning; this makes it difficult to use, and so the level has to be increased or reduced to guide the user. Nursing staff need to fill in relevant data and information in writing when they are at the bedside "three checks and seven pairs"; in addition, some patient health information also needs to be collected by medical staff before entering the computer terminal. The interface design of the service prototype was carried out using system design strategy. The entire service interface contains the hardware products and interface products used for in-home care for the disabled elderly. This chapter first identifies the boundaries of the service interface design by identifying the operations that must be performed by the caregiver to accomplish the goal through the GOMS model and the task input-output method, and the assistance of these operations is accomplished through hardware and software assistance, which also serves as the basis for their design.

4.2. Remote Clinical Care Validation Results. Data were increasingly concentrated in the system's server, in telecommunications, social networks, software, etc., affecting all aspects of life. With the development of business, the system bears increased load, the performance of the system and the enterprise has a very direct relationship. With the development of the enterprise, there is an increase in the number of users, the server load also increased, and the security of the system is considered the most by users. The security of the system is the most important issue for the users and is also a big issue for the development of the enterprise. Therefore, before the system is put in place, each business should be tested to ensure that the system is diagnosed and optimized. System administrators, network engineers, and programmers are required to assist in diagnosis and optimization, and testing is a complex and challenging task. In-depth testing is carried out mainly for performance testing and product characteristics, and simulation can be tested in a way that ensures the correctness of the software and whether it meets the customer's needs. The system administrator, as well as the software testing team, determines the maximum number of users supported by the system, the system's stability habit, and the system's probable habits. The testers can have control over the entire performance of the software because the research and development crew is more concerned with the rationality of the software. The testers are the gatekeepers of software quality since the research and development team is more focused on whether the memory is used appropriately, whether the system is stable, probable bottlenecks, the formation of anomalies, and whether there is unreasonable competition as R & D workers.

Realize the requirement of "patient-centered." Medical staff can enter health information, check medical advice and medication records, pricing, and charges, and enter the patient's current main complaint and physical signs into the mobile terminal at the bedside of the patient, and save it

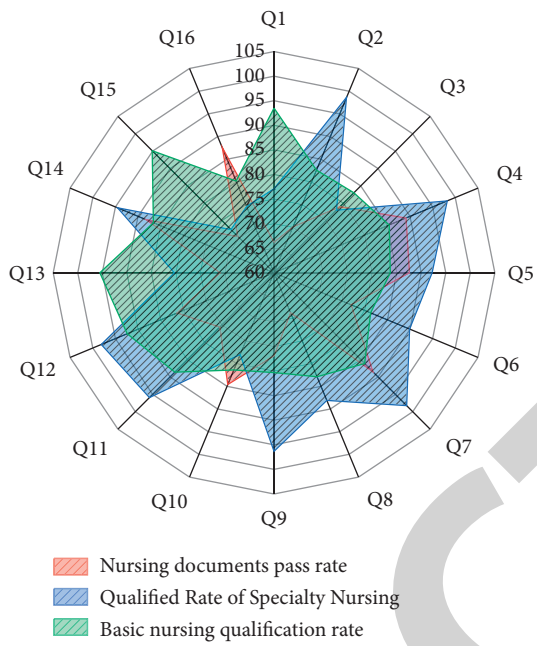

Figure 7: Comparison of quality-of-care indicators.

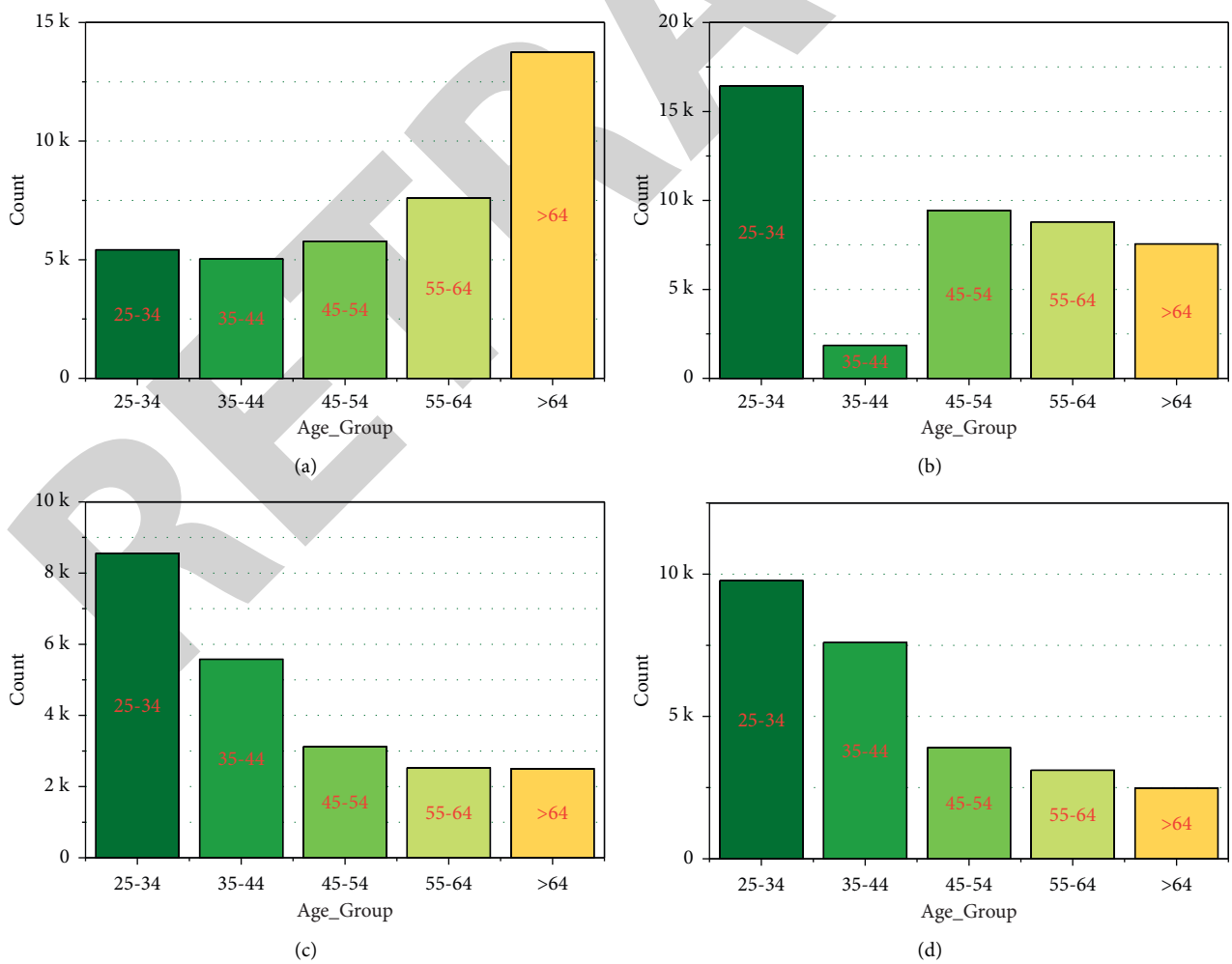

Figure 8: Impact of mobile workstations on surgical safety care indicators with cloud computing.

in the information system, thereby avoiding repeated copying. Testers use testing tools to analyze the system structure, data structure, and internal control structure of the source code, generate function call relationship diagrams, module flow diagrams, and internal file call relationship diagrams to get a clear understanding of the entire software's composition and structure methods, internal relationship diagrams, and call diagrams to get a clear understanding of the entire software's structure. The tester traverses the program by traversing the logical structure. Symbolic testing method: allows the program to change more than just specific values; the symbols can be basic symbols or symbolic variable expressions. Path coverage method: the loop mechanism is simplified; paths are reduced and coverage of all paths becomes possible. Program variation testing method: is an error-driven test that verifies various errors, as shown in Figure 7.

Average nurse time spent on nursing care per day. Total time spent per nurse completing nursing care and the number of days monitored. The histogram shows that with the use of the platform system, the time spent by nursing staff on nursing order writing has decreased, reducing this workload. The time spent on direct patient care, the time spent on health promotion to patients and their families, the time spent on observing their condition, and the time spent on responding to changes in their condition promptly to care for patients has increased. Through thorough testing of the system, all test entries have been passed, basic requirements have been achieved, and the system is operational. After the testing, the main approach taken by this group is the black box testing, which has tested the functionality comprehensively and can follow the steps and can query all the information required, and the software needs to be logged in again after closing to ensure the security of the data. It can embody efficient scheduling ability and can handle huge-scale data sets. When executing commands, it divides the data area, then summarizes the results of data processing, and finally completes the development of the program, so that programmers pay more attention to the process of writing the program.

The surgical turnaround time is defined as the interval between the end of the previous surgery when the patient leaves the operating room and the next surgery when the patient enters the same operating room. The rate of standardized execution of surgical safety verification is the percentage of the number of surgical procedures in which the medical and nursing staff performed safety verification in a standardized manner and the total number of procedures were checked. By standardized, we mean that the surgeon, anesthesiologist, and operating room nurse completed and signed all the verification items within the specified time, and any omission of one or more items was counted as irregular. The correct rate of surgical pathology application form is the percentage of surgical specimen delivery application form that was not rejected by the pathology department because of incomplete or irregular information filling to the total samples sent. The surgical nursing document writing pass rate is the percentage of the number of qualified surgical nursing documents to the total number of nursing documents checked, and any nursing document with missing information that leads to the final file return from the medical case office is a failed nursing document. The statistics were all obtained from the electronic file results of the nursing quality inspection form in the hospital cloud nursing management repository, as shown in Figure 8.

With the application of digital information systems in MNIS under cloud computing, verification of surgical patient information by wristband scanning is more accurate and efficient, which effectively reduces the verification time. The results of our retrospective analysis suggest that applying MNIS can reduce the patient handover time from an average of 6.78 minutes to 3.52 minutes, and significantly reduce the basic information verification time of surgical patients throughout the perioperative period, thus reducing the operating room turnaround time (32.16 clay 8.23 vs 46.22 clay 13.61). In the cumbersome surgical item count, the application of MNIS by scroll bar selection can lead to a significant reduction in item count time as well. Thus, the application of mobile workstations under cloud computing can increase the efficiency of nursing staff and improve the utilization of the operating room.

5. Conclusion

The remote clinical care information system under cloud computing is the same as the traditional nursing information recording system, which contains patient information with high accuracy and can avoid errors in repeated transcription. Although theoretically, it is helpful to improve the quality of safety of nursing care in the operating room under cloud computing, there is still a lack of scientific and effective evaluation of its role and effectiveness in clinical care because it has only entered clinical application recently. Overall, there is still a positive endorsement of MNIS in the operating room. Data optimization and fault tolerance in the data management system are the most important methods of data management. Class data management is mainly to improve the operating capacity of the system. A series of centralized data management methods such as data caching, indexing, and partitioning can be adopted. The top three items that were most favorable were pre-application training, departmental support, and the ease of PDA for surgical patient identification. The three lowest scoring items were that network connectivity was sometimes a barrier, inconvenient PDA input, and small screen size. The most prominent was the wireless network issue with a score of only 2.1740.74, with 35.7% of nursing staff citing poor wireless network signal as the biggest influencing factor in clinical application. Due to the lack of wireless network routers lined up in the original operating room and the special structure of the operating room itself, especially in some protected operating rooms, some MNIS may not receive the signal, resulting in the actual work being affected because of the network connection barrier not being able to

Hindawi
Journal of Healthcare Engineering
Volume 2021, Article ID 7799793, 10 pages
https://doi.org/10.1155/2021/7799793

Research Article

A Novel Fatigue Driving State Recognition and Warning Method Based on EEG and EOG Signals

Li Liu, Yunfeng Ji, Yun Gao, Zhenyu Ping, Liang Kuang, Tao Li, and Wei Xu

Jiangsu Vocational College of Information Technology, Wuxi, Jiangsu 214153, China

Correspondence should be addressed to Li Liu; 101074@jsit.edu.cn

Received 16 October 2021; Revised 29 October 2021; Accepted 5 November 2021; Published 22 November 2021

Academic Editor: Shengrong Gong

Traffic accidents are easily caused by tired driving. If the fatigue state of the driver can be identified in time and a corresponding early warning can be provided, then the occurrence of traffic accidents could be avoided to a large extent. At present, the recognition of fatigue driving states is mostly based on recognition accuracy. Fatigue state is currently recognized by combining different features, such as facial expressions, electroencephalogram (EEG) signals, yawning, and the percentage of eyelid closure over the pupil over time (PERCLoS). The combination of these features increases the recognition time and lacks real-time performance. In addition, some features will increase error in the recognition result, such as yawning frequently with the onset of a cold or frequent blinking with dry eyes. On the premise of ensuring the recognition accuracy and improving the realistic feasibility and real-time recognition performance of fatigue driving states, a fast support vector machine (FSVM) algorithm based on EEGs and electrooculograms (EOGs) is proposed to recognize fatigue driving states. First, the collected EEG and EOG modal data are preprocessed. Second, multiple features are extracted from the preprocessed EEGs and EOGs. Finally, FSVM is used to classify and recognize the data features to obtain the recognition result of the fatigue state. Based on the recognition results, this paper designs a fatigue driving early warning system based on Internet of Things (IoT) technology. When the driver shows symptoms of fatigue, the system not only sends a warning signal to the driver but also informs other nearby vehicles using this system through IoT technology and manages the operation background.

1. Introduction

Fatigue is a very complex physical and psychological state that can be divided into mental fatigue and physical fatigue. In most cases, mental fatigue and physical fatigue are intertwined and appear at the same time. Mental fatigue is often caused by long-term cognitive activity in the brain. Under brain fatigue, people's cognitive function is limited, and their alertness is reduced. Drivers are prone to both mental and physical fatigue during long-term driving, but mental fatigue is the main problem. Fatigue driving is one of the major hidden dangers of road traffic safety. Research on fatigue driving recognition and early warning technology can reduce the frequency of traffic accidents [1]. Fatigue driving status recognition is a prerequisite for early warning, so fatigue driving status recognition is very important. At present, research on fatigue driving identification methods mainly focuses on three aspects: (1) identification based on driver behavior characteristics: the driver's fatigue state is judged by the recognition of the driver's behavior, such as the movement of the eyelids, the closed state of the eyes [2], and facial expressions [3]. The identification method is simple and easy to implement, but the scoring standard is easily affected by conditions such as personal behavior, light, and image acquisition angle. The collection of various modal data will inevitably be noisy, causing the recognition result to fail to correctly identify the driver's fatigue state. (2) Detection based on vehicle parameters: through the detection of vehicle parameters such as vehicle speed, vehicle position, and steering wheel rotation angle during driving, the driver's operating indicators are obtained, and then the degree of fatigue is judged. Since vehicle parameters are closely related

to the actual driving quality of the driver, this method is closer to the actual driving situation. However, vehicle parameters need to be measured during actual operation, which increases the cost of the vehicle. (3) Recognition based on the physiological parameters of the driver: the driver's fatigue state can be judged by identifying the driver's physiological characteristics, such as with electrocardiograms [4], electroencephalograms [5, 6], electrooculograms [7], and electromyography [8, 9].

Since the EEG signal directly reflects the driver's brain activity and the price of EEG signal acquisition devices are declining, they are therefore convenient to use. Therefore, identifying driving fatigue states based on the EEG signals is considered to be one of the most objective and accurate analysis methods. Reference [5] proposed a new real-time fatigue driving detection method based on EEG signals. The study combines two characteristics of power spectral density (PSD) and sample entropy (SampEn) to judge mental fatigue. The results show that the method is effective for fatigue detection because the prediction results of fatigue are consistent with the phenomena recorded in the simulated driving process. This is considered an objective measure of behavior. Reference [10] proposed a recurrent network-based convolutional neural network (RN-CNN) method to detect fatigue driving. The data used in the experiment are the EEG signals collected during driving simulation. This method can achieve an average recognition accuracy of 92.95%. Reference [11] proposed the detection of the fatigue driving state based on the feature data of sample entropy, approximate entropy, and complexity, which can well identify four different mental fatigue states. Reference [12] uses five different entropies, the relative energy of the alpha wave, and $(\theta + \alpha)/\beta$ as indicators for judging fatigue. The experimental results show that this fusion method can accurately judge the fatigue degree of the driver. Reference [13] uses the fast Fourier transform to extract four rhythm $\alpha, \theta, \beta, \delta$ features. By analyzing the trend and mutual relationship of these four features, it is found that using $(\theta + \alpha)/\beta$ as the feature to assess the mental state is the most effective. Reference [14] studied sample entropy, fuzzy entropy, approximate entropy, and spectral entropy as the inputs of a decision tree. Experiments have shown that this method has an accuracy of 94% for the identification of fatigue driving, and it can identify fatigue driving more accurately. Typical EEG signal characteristic analysis methods are mainly divided into the time domain [15], frequency domain [16], and time-frequency domain analysis methods [17]. The EEG signal in the frequency domain has obvious characteristics and strong distinguishability. It is of great significance to the analysis of EEG signals. EEG signals in different frequency bands can effectively reflect people's mental state and excitement [18]. Reference [19] uses a convolutional neural network (CNN) to realize emotion recognition based on the time-frequency diagram of EEG signals obtained by a wavelet transform. However, the time-frequency diagram cannot effectively reflect the correlation of EEG signals between different electrodes. The above studies have shown that fatigue driving recognition based on EEGs is the most objective and accurate fatigue recognition method and is known as the "gold standard" of fatigue detection.

Fatigue driving state recognition based on EOGs mainly separates the horizontal and vertical EOG signals from the electrode signals of the forehead and extracts a series of features, such as gaze, blinking, and saccade, for driver fatigue state recognition. Reference [20] found that as driver fatigue increases, it will be accompanied by long-term blinking, which reflects the relationship between slow eye movement and driver fatigue. By extracting the eye movement features in the EOG signal, machine learning algorithms are used to identify the driver's fatigue state. Reference [21] detected fatigue driving by extracting the fatigue characteristics of blinking, slow eye movement, amplitude, and periodicity in the EOG signal, and the experimental results showed that the detection effect was effective. In summary, driver fatigue detection based on EOG signal characteristics is also feasible.

At present, most studies mainly focus on the fusion of multiple features and the application of integrated classifiers. The purpose of these studies is to maximize the accuracy of fatigue recognition. However, most studies ignore the real-time performance of fatigue driving recognition and early warning. In a real-life environment, the timely identification and early warning of fatigue driving are more meaningful. With the rapid development of modern industry, collection methods of EEG and EOG signals are becoming more advanced. The volume of collection equipment is becoming increasingly miniaturized and portable, their collection accuracy is increasing, and their production cost is decreasing. With the development of Internet of Things (IoT) technology in recent years, it is no longer difficult to collect driver EEG signals without interference. Based on the above background, this paper proposes a fast identification method of fatigue driving based on EEG and EOG. This method can collect the driver's EEG and EOG signals in a real environment and complete rapid identification and timely warning. The contents of this study can be divided as follows:

(1) More objective EEG and EOG signal data are used as the identification data of the fatigue driving state. For EEG data, its PSD and differential entropy are extracted as feature data. For EOG, EOG features extracted based on independent component analysis (features_table_ica), EOG features extracted based on subtraction rules (features_table_minus), and EOG features extracted using both subtraction rules and principal component analysis (features_table_icav_minh) are used as feature data. The multifeature data of the two modalities can represent more comprehensive sample information.

(2) A fast SVM algorithm based on sample geometric features is proposed. For the case of nonlinear separability, the support vector in the high-dimensional space should also be on the edge of the positive and negative classes. Measured by distance, the support vector is composed of those sample points with larger distances of the same kind and smaller distances of different kinds. The key is to

find such sample points. FSVM can greatly reduce the number of training samples and reduce the number of support vectors, resulting in a reduction in the training time of the model, and at the same time, the impact on sample classification accuracy is minimal.

(3) Based on the results of fatigue driving status recognition and IoT technology, this paper designs an early warning system. The system can realize data collection, identification, and early warning. When a driver is detected to be fatigued, the system not only sends a warning signal to the driver but also informs other nearby vehicles using this system through the Internet of Things technology and manages the operation background.

2. Related Information

2.1. EEG Multifeature Extraction Method

2.1.1. Differential Entropy Feature Extraction. The differential entropy feature is expanded on the basis of Shannon entropy. In 2013, differential entropy was used for the first time to characterize EEG characteristics. Compared with the traditional PSD, it shows superior performance [22]. The original definition of calculating differential entropy is as follows:

$$h(x_n) = -\int_X f(x)\log(f(x))\mathrm{d}x. \tag{1}$$

When a random variable follows the Gaussian distribution $N(u, \sigma^2)$, the differential entropy can be simply calculated by the following formula:

$$h(X) = -\int_{-\infty}^{+\infty} f(x)\log(f(x))\mathrm{d}x = \frac{1}{2}\log 2\pi e\sigma^2, \tag{2}$$

where $f(x) = 1/\sqrt{2\pi\sigma^2}\exp(x-\mu)^2/2\sigma^2$.

2.1.2. PSD Feature Extraction. PSD is used to characterize the change in signal power with changes in frequency. In practical applications, the average value of the signal value in a certain frequency band is generally regarded as the PSD of the frequency band, and the calculation formula is

$$p(x_n) = \frac{1}{N}X(x_n)X^*(x_n), \tag{3}$$

where $X(x_n)$ is the discrete Fourier change value of segment n and $X^*(x_n)$ is the conjugate function of $X(x_n)$.

2.2. Typical Classification Model. Table 1 gives the relevant introduction of each commonly used classification model. At present, the classification model of fatigue driving state recognition can be divided into machine learning [23, 24] and deep learning [25, 26]. The mathematical model of the machine learning algorithm is simple, and the algorithm time complexity is relatively low, but the recognition accuracy is not as good as that of the deep learning algorithm. The model of the deep learning algorithm is complex, there are many parameters that need to be adjusted, and the time complexity of the algorithm is high, but the recognition rate of the algorithm is high. In summary, the two types of classification models have their own characteristics and applicable scenarios. Since the scenarios used in this article do not belong to the category of large samples and fatigue driving recognition and early warning have high real-time requirements, the machine learning algorithm can fully meet the requirements. Therefore, the classic SVM in machine learning is used as the basic algorithm to classify datasets.

2.3. Labeling of Fatigue Signal Labels. The key to fatigue identification based on EOG is calculating the PERCLOS value. The PERCLOS value indicates the degree of closure of the eyelids per unit time. The calculation formula is as follows:

$$\text{PERCLOS} = \frac{\text{eye\_closing\_time}}{\text{total\_time}}. \tag{4}$$

PERCLOS is marked as P, and the threshold of P is set to determine whether it is fatigued. When $P < 0.35$, it indicates that the driver is awake. When $P > 0.35$, it indicates that the driver is tired. According to different P values, two different states can be obtained. This type of research can be described as a binary classification task. The awake state is recorded as 0, and the fatigue state is recorded as 1. Table 2 shows the specific labeling method.

2.4. ZigBee Wireless Technology. The ZigBee standard is a wireless ad hoc network standard suitable for wireless sensor networks proposed by the ZigBee Alliance in 2004. ZigBee chips usually integrate basebands, microcontrollers, and memory, and ZigBee can work in the frequency bands of 868 MHz, 915 MHz, and 2.4. The data transmission rate of the ZigBee network ranges from 20 to 900 kpbs. Each ZigBee network contains a coordinator, and the task of the coordinator allows the router to expand the communication range of the network. Since ZigBee nodes can wake up from sleep in 30 ms, which makes ZigBee's response delay far lower than other types of wireless technologies, ZigBee is very suitable for small data volume burst data transmission. The system designed in this paper will not only alert drivers of fatigue but also transmit alerts to other vehicles. This requires the establishment of a suitable wireless network connection between the vehicles. Since the driver is not always in a state of fatigue, the exchange of data between vehicles will be intermittent, and there will be no continuous data exchange. Moreover, the amount of data carried by each fatigue alert is very small. Based on the above analysis, this article selects a ZigBee network suitable for sudden small data transmission. As a typical protocol for wireless sensor networks, ZigBee is suitable for the transmission of such data. Therefore, this article selects ZigBee as the wireless network standard between vehicles.

Table 1: Typical classification model.

Model	Main idea	Advantages and disadvantages
Artificial neural network (ANN)	There are three types of processing units in the network: input unit, output unit, and hidden unit. The input unit receives signals and data from the outside world. The output unit realizes the output of system processing results. A hidden unit is a unit that lies between an input and output unit and cannot be viewed from outside the system. ANN is a kind of nonprogrammed, adaptive, and brain-style information processing mode, whose essence is to obtain a parallel and distributed information processing function through network transformation and dynamic behavior.	Advantages: ① it is a simple application; ② it has more accurate classification results; and ③ it has the ability to quickly search for optimization. Disadvantages: ① it easily enters the local optimum.
SVM	The algorithm finds a dividing hyperplane that can correctly separate the two types of data on both sides to achieve the effect of data classification and prediction. This hyperplane is determined by the support vectors.	Advantages: ① the "curse of dimensionality" can be avoided; ② it has a known effective algorithm that can be used to find the global minimum of the objective function; ③ the generalization ability of the algorithm is good. Disadvantages: ① it is difficult to implement large-scale training samples; ② it has difficulty solving the multicategory problem; ③ it is sensitive to parameter and kernel function selection.
Random Forest (RF)	The forest is composed of many trees, so the result of RF depends on the decision result of multiple trees. This is an integrated learning idea. For example, there is a new animal in the forest, and the forest holds a forest meeting to determine what kind of animal it is. Every tree must express its opinions. The result with the most votes will be the final result.	Advantages: ① it can handle very high-dimensional (many features) data, and there is no need to perform feature selection; ② the training speed is fast, and it is easy to make a parallel method; ③ the implementation is relatively simple. Disadvantages: ① it is prone to overfitting; ② for data with attributes with different values, the attribute weights produced by RF on such data are unreliable.
AdaBoost	The algorithm trains several individual learners with a certain combination strategy so that a strong learner can finally be formed to achieve the goal of more people and more power.	Advantage: ① under the framework of AdaBoost, various classification models can be used to build weak learners, which is very flexible; ② given its high precision, it can be applied to most classifiers without the need to adjust parameters. Disadvantages: ① unbalanced data leads to a decrease in classification accuracy; ② training is time-consuming.
CNN	A method consisting of the following layered form: input layer: data entry Convolutional layer: for feature extraction Pooling layer: used to extract features again Hidden layer: the layer in the middle Fully connected layer: after vectorizing the extracted feature matrix, classify its features.	Advantages: it has a high classification accuracy rate. Disadvantages: ① parameters need to be adjusted; ② it needs large amount of data; ③ it requires a large amount of calculation.

Table 2: Fatigue marking status.

P value range	State	Label
$P < 0.35$	Wide awake	0
$P > 0.35$	Fatigue	1

3. Fatigue Driving Status Recognition and Early Warning System

3.1. System Framework. In this study, a rapid fatigue state recognition and early warning system was designed. The architecture of the system is shown in Figure 1. The hardware system of the whole system mainly includes a Bluetooth headset and a vehicle-mounted terminal. The Bluetooth headset is mainly responsible for collecting EEG and EOG signals. Through the Bluetooth communication protocol, the data are transmitted to the vehicle terminal for storage, processing, and analysis. The fatigue state recognition module in the vehicle terminal is responsible for classifying the received EEG and EOG signals to determine whether the driver is tired. When the result of the identification is fatigue, a warning message will be issued to the driver, operation manager, and surrounding vehicles. A set of equipment can be installed on each vehicle, and the system includes a sending end and a receiving end.

3.2. Recognition Model. This study uses a fast SVM model to classify feature data. For nonlinearly separable data, the support vector in the high-dimensional space should also be on the edge of the positive and negative classes. Measured by distance, the support vector is composed of those sample

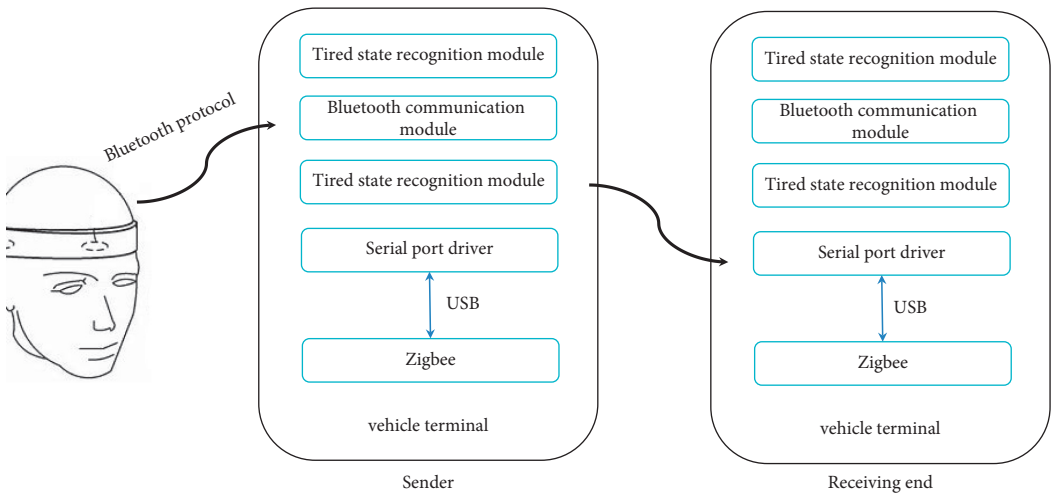

Figure 1: System structure diagram.

points with a larger distance from the same class and a smaller distance from the heterogeneous group. The key is to find such sample points. First, the distance between any two points is described. The following mapping formula is used:

$$\phi\colon x \in R^P \longrightarrow \phi(x) \in R^m, m > p, \quad \forall x_i, x_j, x_j \in R^P. \tag{5}$$

The distance between any two points is defined in space R^m:

$$\begin{aligned} d\big(\phi(x_i), \phi(x_j)\big) &= \big\|\phi(x_i) - \phi(x_j)\big\|, \\ &= \sqrt{\big(\phi(x_i) - \phi(x_j)\big) \cdot \big(\phi(x_i) - \phi(x_j)\big)} \\ &= \sqrt{\phi(x_i) \cdot \phi(x_i) - 2\phi(x_i) \cdot \phi(x_j) + \phi(x_j) \cdot \phi(x_j)} \\ &= \sqrt{K(x_i, x_i) - 2K(x_i, x_j) + K(x_j, x_j)} \\ &= \sqrt{2 - 2K(x_i, x_j)}. \end{aligned} \tag{6}$$

Assume sample point $z_k \in G^+$; for any $k \in I^+$, it corresponds to point $\phi(z_k)$ in the high-dimensional space.

A pair of distance values (d_k^+, d_k^-) is assigned to point $\phi(z_k)$,

$$\begin{cases} d_k^+ = \dfrac{1}{l^+} \displaystyle\sum_{i \in I^+} d(\phi(z_k), \phi(x_i)), \\ d_k^- = \dfrac{1}{l^-} \displaystyle\sum_{i \in I^+} d\big(\phi(z_k), \phi(x_j)\big). \end{cases} \tag{7}$$

The parameter r represents the proportion of possible support vectors in the training sample set. There are critical values c1 and c2 such that $P\{d_k^+ > c_1\} = r$ and $P\{d_k^- < c_2\} = r$. That is, we find those points $\phi(z_k)$ with a larger average distance from the positive point and a smaller average distance from the negative point. The support vector is the point z_k that satisfies the condition $\{\phi(z_k) | d_k^+ > c_1, d_k^- < c_2, k \in I^+\}$. As shown in Figure 2, the points in set $T_1^+ = \{\phi(z_k) | d_k^+ > c_1, k \in I^+\}$ correspond to the points in the shape of ① in the figure. The point in $T_2^+ = \{\phi(z_k) | d_k^- < c_2, k \in I^+\}$ corresponds to point ② in the figure. Then, point $\phi(z_k) \in T^+, T_1^+ \cap T_2^+$. In the same way, for $z_k \in G^-$ and any $k \in I^-$, set T^- can be found. Then, the set formed by the support vector is $T^{BD} = T^+ \cup T^-$.

The FSVM algorithm follows a certain principle of the distance between samples to extract support vectors, which are used as training samples for the SVM, and then the SVM is used for training. The implementation steps of the algorithm are 5 in total, and details of each step are shown below:

Step 1. Set the scale parameter $r\,(0 < r < 1)$.

Step 2. In the high-dimensional space, calculate the distance matrix $D = (d_{ij})_{l \times l} \begin{bmatrix} D_{11} & D_{12} \\ D_{21} & D_{22} \end{bmatrix}$, where $d_{ij} = d(\phi(x_i), \phi(x_j)) = \sqrt{2 - 2K(x_i, x_j)}$. $D_{11}\,(D_{22})$ represents the block matrix formed by the distance between any two points in the positive and negative sets. $D_{12}\,(D_{21})$ represents the block matrix formed by the distance between each point of the positive and negative clusters.

Step 3. Calculate the average matrix $V = \begin{bmatrix} V_{11} & V_{12} \\ V_{21} & V_{22} \end{bmatrix}_{(l^+ + l^-) \times 2}$. Set $I_{l^+} = 1/l^+ e_{l^+ \times 1}$, $I_{l^-} = 1/l^- e_{l^- \times 1}$; then $V_{11} = D_{11} I_{l^+}$, $V_{12} = D_{12} I_{l^-}$, $V_{21} = D_{21} I_{l^+}$, and $V_{22} = D_{22} I_{l^-}$.

Step 4. Extract the support vector set according to the given ratio r. Sort the components in V_{11} and V_{22} in descending order. Sort the components in V_{12} and V_{21} in ascending order. Extract the top $l^+ \cdot r$ and $l^- \cdot r$ samples after sorting to form a new training set $T^{BD}\,(|T^{BD}| < l \cdot r)$.

Step 5. The SVM algorithm is trained on T^{BD} to obtain the final model.

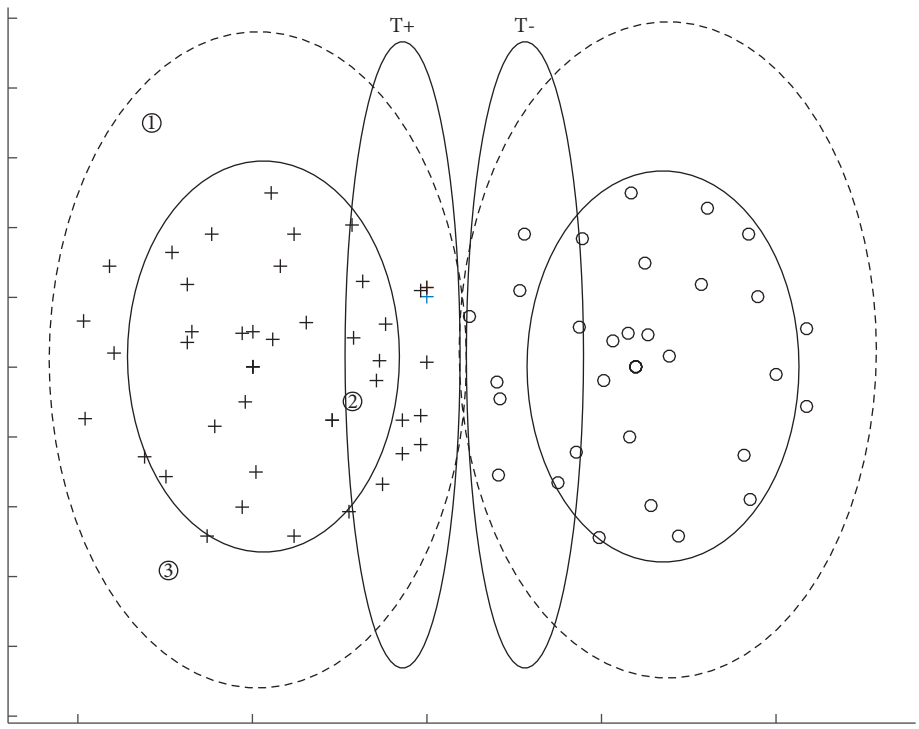

Figure 2: Distribution of sample points based on distance analysis.

4. Experiment

4.1. Introduction to Simulation Data. The SEED-VIG [27] dataset was used for experimental simulation, which is mainly composed of EEG and EOG signals. To collect the dataset in the real scene, the data collector used the Neuroscan system to collect the relevant signals of the driver in the simulated driving environment. The sampling frequency is 1 kHz, and 21 channels of data are collected in total. The electrode position during EOG acquisition is shown in Figure 3(a), and there are 4 channel electrodes in total. The electrodes set for the EEG signal are 6 channels in the temporal brain area and 11 channels in the back brain area. The specific electrode positions are shown in Figure 3(b). The placement of these positions meets the international 10–20 electrode distribution requirements.

The collected initial EEG signal contains problems such as noise, which requires preprocessing, feature extraction, and smoothing operations on signals from different brain regions. The different brain areas mainly include the temporal lobe brain area, T area; the occipital brain area, P area; the prefrontal EEG, F area; and the brain area signal leads, bandwidth, and characteristic dimensions, which are shown in Table 3. First, the forehead EEG is separated from the forehead electrode signals, and the EEG signals of each brain area are divided into 5-band EEG signals. The features of EEG and EOG data are extracted, as shown in Table 4.

4.2. Experimental Setup. During the experiment, the main contrastive algorithms used are BP [28], RF [29], SVM [30], and CNN [31]. Both SVM and FSVM use a radial basis kernel function, and the kernel function parameter is set to 0.001. The parameters of the other comparison algorithms are the same as those in the reference. The evaluation index of the model used is the recognition accuracy rate, and its calculation formula is as follows:

$$\mathrm{Acc} = \frac{TP + TN}{TP + TN + FP + FN}. \tag{8}$$

The computer configuration information used in the experiment is 32 G of memory, an i7-11700F CPU, a Win10 operating system, and the MATLAB 2020a programming tool.

4.3. Experimental Results and Analysis

4.3.1. Fatigue Recognition Accuracy Rate Experiment. The dataset is randomly divided into a training set and a test set at a ratio of 7 : 3. First, the EEG feature and EOG feature are classified separately using the classifier and then the two features are combined for classification. The experimental data are the mean value after running the algorithm 10 times. The experimental results are shown in Tables 5–7.

The data in Table 5 show that, for most classification algorithms, the recognition rate based on DE features is slightly better than that based on PSD features. This shows that the evaluation effect based on the DE feature is better than that based on the PSD feature. Regarding the recognition accuracy index, regardless of whether it is based on PSD or DE features, the recognition rate of the CNN deep learning algorithm is significantly ahead of that of the machine learning algorithm. This shows that, in terms of recognition accuracy, the performance of deep learning algorithms is significantly better than that of machine

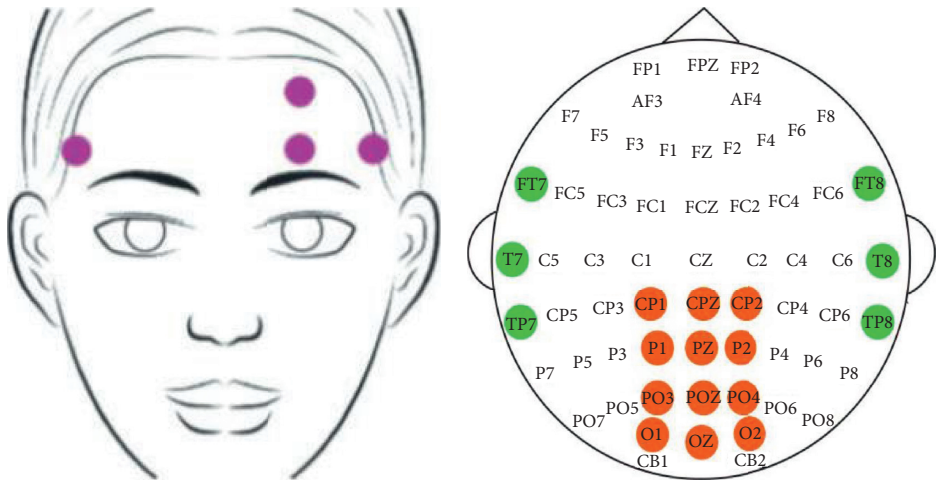

(a) (b)

Figure 3: Electrode position during EOG and EEG acquisition.

Table 3: Signal distribution and characteristic dimensions of brain regions.

Brain area	Signal lead	Characteristic frequency band	Feature dimension
P	11	$\delta, \theta, \alpha, \beta, \gamma$	55
T	6	$\delta, \theta, \alpha, \beta, \gamma$	30
F	4	$\delta, \theta, \alpha, \beta, \gamma$	20

Table 4: EEG and EOG characteristics.

Signal	Feature extraction method	Feature
EEG	Short-time Fourier transform	Power spectral density linear dynamic system smoothing characteristics (PSD). Smoothing characteristics of differential entropy linear dynamic system (DE).
EOG	Wavelet transform peak detection method	Electroocular features extracted based on independent component analysis (features_table_ica). Eye electrical features extracted based on subtraction rules (features_table_minus). Electrooculogram features extracted by fusion of subtraction rules and principal component analysis (features_table_icav_minh).

Table 5: Recognition accuracy based on EEG features.

Brain area	Feature	BP	RF	SVM	CNN	FSVM
P	PSD	0.8892	0.8791	0.9146	0.9287	0.9128
	DE	0.8957	0.8880	0.9245	0.9420	0.9215
T	PSD	0.8921	0.8687	0.9112	0.9117	0.9126
	DE	0.8985	0.8763	0.9197	0.9421	0.9204
F	PSD	0.8864	0.8725	0.9020	0.9223	0.9043
	DE	0.8903	0.8804	0.9189	0.9468	0.9180
Mean	PSD	0.8892	0.8734	0.9093	0.9209	0.9099
	DE	0.8948	0.8816	0.9210	0.9436	0.9200

learning algorithms. Among the machine learning algorithms, the SVM algorithm has the best recognition rate. This is also the reason why SVM is chosen as the basic algorithm. The recognition accuracy of FSVM is comparable to that of classic SVM.

The data in Table 6 show that, for different classification algorithms, the recognition rate based on the features_table_icav_minh feature is the best. This shows that the classification information carried by the EOG features extracted by both subtraction rules and principal component analysis is more abundant. Among the different classification algorithms, CNN has the highest recognition rate, which shows that the recognition effect of deep learning algorithms is indeed very good. The recognition rates of SVM and FSVM are similar, and the recognition rate of FSVM is slightly higher.

To explore the influence of multimodal data on the recognition accuracy, EEG and EOG signals were fused for experimental analysis. EEG uses differential entropy feature data, using the average of the three brain regions P, T, and F as the final experimental data. EOG uses the features_table_icav_minh feature with the best recognition effect as the input feature data. The recognition results of the fusion features of each algorithm are shown in Table 7.

The experimental data shown in Table 7 show that, in addition to the BP algorithm, the recognition accuracy of other algorithms based on fusion features is better than the recognition accuracy of a single feature. This shows that the fusion feature can effectively improve the fatigue recognition

Table 6: Recognition accuracy based on EOG features.

Algorithm	features_table_ica	features_table_minus	features_table_icav_minh
BP	0.9032	0.9104	0.9131
RF	0.9153	0.9086	0.9178
SVM	0.9343	0.9357	0.9406
CNN	0.9481	0.9396	0.9484
FSVM	0.9391	0.9325	0.9412

Table 7: Recognition accuracy rate of fusion features.

Algorithm	EEG	EOG	EEG + EOG
BP	0.8948	0.9131	0.9124
RF	0.8816	0.9178	0.9209
SVM	0.9210	0.9406	0.9478
CNN	0.9436	0.9484	0.9517
FSVM	0.9200	0.9412	0.9511

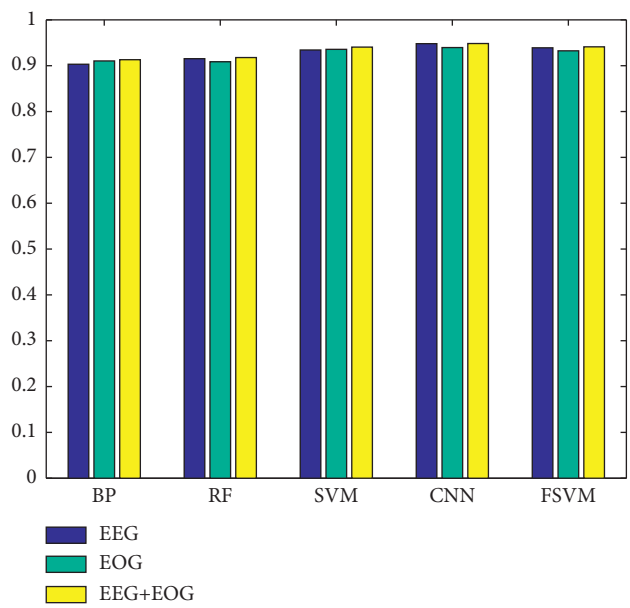

Figure 4: Recognition accuracy of each algorithm based on different features.

accuracy. The changes in the recognition accuracy of each algorithm based on different features are shown in Figure 4. It can be clearly seen from the figure that the recognition rate of CNN and FSVM based on fusion features has the largest increase, followed by SVM, and RF has the smallest increase. The recognition accuracy of the BP algorithm has declined to a certain extent. In summary, the use of fusion features has advantages in the recognition rate.

4.3.2. Fatigue Recognition Model Training Time Consumption Experiment. The recognition model is trained based on the fusion features, and the time taken to train the model 10 times is averaged. The training time consumption details of each model are shown in Table 8. The data in Table 8 show that the time spent on machine learning algorithms is lower than the time spent on deep learning algorithms. For scenarios that require a quick response time, machine learning algorithms are more suitable. Among the many machine learning algorithms, the training time required for the FSVM model mentioned in this article is greatly reduced. Compared with the classic SVM model, the training time is reduced by 33.95%. Compared with the CNN, the training time of the FSVM model is only a quarter of it. In summary, the model proposed in this paper can not only ensure a better recognition rate but also reduce the training time for the model. Therefore, it can fully meet the task of real-time fatigue identification and has good practical value.

Table 8: Training time.

Model	BP	RF	SVM	CNN	FSVM
Time (s)	286	225	217	639	162

5. Conclusion

The rapid identification and early warning of the fatigue driving state are the key to reducing traffic accidents. Quick and accurate fatigue identification is a prerequisite for effective early warning. This study is based on two-modal data of EEGs and EOGs to identify the fatigue driving state and extracts multiple features of the two-modal data for experimental analysis. Experimental data show that the fatigue state recognition accuracy of multimodal data fusion is higher. In the selection of classification models, deep learning algorithms have a leading advantage, and the recognition accuracy is higher than that of machine learning algorithms. However, considering the real-time requirements of fatigue state recognition tasks, this study proposes an FSVM algorithm that can quickly provide model training. The FSVM algorithm greatly improves the training speed of the model without reducing the recognition accuracy and achieves the expected effect. On the other hand, based on fast and accurate recognition results, this article designed a set of early warning systems based on IoT technology to extend the early warning information from a single vehicle to the Internet of Vehicles. When the driver is in a fatigue state, the

system can not only send a warning signal to the driver but also notify other nearby vehicles using this system and manage the operation background through IoT technology. Regarding the identification of fatigue status, the next step of this research will be to improve the accuracy of identification, and more modal data can be introduced for comprehensive decision-making. In an early warning system, when the vehicle speed is too high and the distance is too large, the signal between the vehicle and other vehicles is likely to be weak, and it is impossible to guarantee the successful warning of other vehicles. LoRa has the characteristics of long communication distance, low power consumption, and low cost, which may be able to solve the above problems. This is also the content of this study, which needs further research in the future.

Data Availability

The labeled dataset used to support the findings of this study is available from the corresponding author upon request.

Conflicts of Interest

The authors declare no conflicts of interest.

Acknowledgments

This work was supported by the Jiangsu Province Higher Vocational Education High-level Professional Group Construction Project under Grant Su Jiao Han [2021] no. 1, Jiangsu Province Higher Vocational Education Industry-Education Integration Platform Construction Plan Project under Grant Su Jiao Han [2019] no. 26, Natural Science Research Foundation of Higher Education in Jiangsu Province under Grant no. 18KJD510011, Jiangsu Provincial High-Level Backbone Specialty Construction Project under Grant Su Jiao Gao [2017] no. 17, and Projects for Research on Educational Reform of Higher Education in Jiangsu Province under Grant no. 2017JSJG077.

References

[1] A. P. Smith, "A UK survey of driving behaviour, fatigue, risk taking and road traffic accidents," *BMJ open*, vol. 6, no. 8, Article ID e011461, 2016.

[2] L. L. D. Stasi, M. B. Mccamy, A. Catena, S. L. Macknik, J. J. CanAs, and S. Martinez-Conde, "Microsaccade and drift dynamics reflect menta fatigue," *European Journal of Neuroscience*, vol. 38, no. 3, pp. 2389–2398, 2013.

[3] R. George, Y. Goletsis, and P. Bougia, "Towards driver's state recognition on real driving conditions," *International Journal of Vehicular Technology*, vol. 201114 pages, Article ID 617210, 2011.

[4] F. Wang, H. Wang, and R. Fu, "Real-time ECG-based detection of fatigue driving using sample entropy," *Entropy*, vol. 20, no. 3, p. 196, 2018.

[5] H. Wang, A. Dragomir, N. I. Abbasi, J. Li, N. V. Thakor, and A. Bezerianos, "A novel real-time driving fatigue detection system based on wireless dry EEG," *Cognitive Neurodynamics*, vol. 12, no. 4, pp. 365–376, 2018.

[6] F. Gharagozlou, G. Nasl Saraji, A. Mazloumi et al., "Detecting driver mental fatigue based on EEG alpha power changes during simulated driving," *Iranian Journal of Public Health (English ed.)*, vol. 44, no. 12, pp. 1693–1700, 2015.

[7] Y. Wang and J. Ma, "Automation detection of driver fatigue using visual behavior variables," *Archives of Civil Engineering*, vol. 64, no. 2, pp. 175–185, 2018.

[8] R. Fu and H. Wang, "Detection OF driving fatigue BY using noncontact emg and ecg signals measurement system," *International Journal of Neural Systems*, vol. 24, no. 3, Article ID 1450006, 2014.

[9] M. Patel, S. K. L. Lal, D. Kavanagh, and P. Rossiter, "Applying neural network analysis on heart rate variability data to assess driver fatigue," *Expert Systems with Applications*, vol. 38, no. 6, pp. 7235–7242, 2011.

[10] Z.-K. Gao, Y.-L. Li, Y.-X. Yang, and C. Ma, "A recurrence network-based convolutional neural network for fatigue driving detection from EEG," *Chaos: An Interdisciplinary Journal of Nonlinear Science*, vol. 29, no. 11, Article ID 113126, 2019.

[11] C. Zhang, H. Wang, and R. Fu, "Automated detection of driver fatigue based on entropy and complexity measures," *IEEE Transactions on Intelligent Transportation Systems*, vol. 15, no. 1, pp. 168–177, 2014.

[12] S. Kar, M. Bhagat, and A. Routray, "EEG signal analysis for the assessment and quantification of driver's fatigue," *Transportation Research Part F: Traffic Psychology and Behaviour*, vol. 13, no. 5, pp. 297–306, 2010.

[13] B. T. Jap, S. Lal, P. Fischer, and E. Bekiaris, "Using EEG spectral components to assess algorithms for detecting fatigue," *Expert Systems with Applications*, vol. 36, no. 2, pp. 2352–2359, 2009.

[14] J. Hu and J. Min, "Automated detection of driver fatigue based on EEG signals using gradient boosting decision tree model," *Cognitive Neurodynamics*, vol. 12, no. 4, pp. 431–440, 2018.

[15] H. Wang, "Optimizing spatial filters for single-trial EEG classification via a discriminant extension to CSP: the Fisher criterion," *Medical, & Biological Engineering & Computing*, vol. 49, no. 9, pp. 997–1001, 2011.

[16] C.-H. Chuang, L.-W. Ko, Y.-P. Lin, T.-P. Jung, and C.-T. Lin, "Independent component ensemble of EEG for brain-computer interface," *IEEE Transactions on Neural Systems and Rehabilitation Engineering*, vol. 22, no. 2, pp. 230–238, 2014.

[17] M. Li, W. Chen, and T. Zhang, "Classification of epilepsy EEG signals using DWT-based envelope analysis and neural network ensemble," *Biomedical Signal Processing and Control*, vol. 31, no. 1, pp. 357–365, 2017.

[18] W. L. Wei-Long Zheng and B. L. Bao-Liang Lu, "Investigating critical frequency bands and channels for EEG-based emotion recognition with deep neural networks," *IEEE Transactions on Autonomous Mental Development*, vol. 7, no. 3, pp. 162–175, 2015.

[19] B. Zhang, H. Jiang, and L. Dong, "Classification of EEG signal by WT-CNN model in emotion recognition system," in *Proceedings of the The 2017 IEEE 16th International Conference on Cognitive Informatics & Cognitive Computing (ICCI CC)*, pp. 109–114, Oxford, UK, July 2017.

[20] Y. Jiao and B. L. Lu, "Detecting slow eye movement for recognizing driver's sleep onset period with EEG features," in *Proceedings of the 38th Annual International Conference of the IEEE Engineering in Medicine and Biology Society (EMBC)*, pp. 4658–4661, Orlando, FL, USA, August 2016.

[21] A. Némcova, O. Janousek, M. Vitek, and I. Provazník, "Testing of features for fatigue detection in EOG,"

Bio-Medical Materials and Engineering, vol. 28, no. 4, pp. 379–392, 2017.

[22] A. H. Mooij, B. Frauscher, M. Amiri, W. M. Otte, and J. Gotman, "Differentiating epileptic from non-epileptic high frequency intracerebral EEG signals with measures of wavelet entropy," *Clinical Neurophysiology*, vol. 127, no. 12, pp. 3529–3536, 2016.

[23] Y. Jiang, K. Zhao, K. Xia et al., "A novel distributed multitask fuzzy clustering algorithm for automatic MR brain image segmentation," *Journal of Medical Systems*, vol. 43, no. 5, pp. 118–1189, 2019.

[24] Y. Jiang, Y. Zhang, C. Lin, D. Wu, and C.-T. Lin, "EEG-based driver drowsiness estimation using an online multi-view and transfer TSK fuzzy system," *IEEE Transactions on Intelligent Transportation Systems*, vol. 22, no. 3, pp. 1752–1764, 2021.

[25] Z. Jiao, X. Gao, Y. Wang, J. Li, and H. Xu, "Deep Convolutional Neural Networks for mental load classification based on EEG data," *Pattern Recognition*, vol. 76, no. 1, pp. 582–595, 2018.

[26] S. Chaudhary, S. Taran, V. Bajaj, and A. Sengur, "Convolutional neural network based approach towards motor imagery tasks EEG signals classification," *IEEE Sensors Journal*, vol. 19, no. 12, pp. 4494–4500, 2019.

[27] W.-L. Zheng and B.-L. Lu, "A multimodal approach to estimating vigilance using EEG and forehead EOG," *Journal of Neural Engineering*, vol. 14, no. 2, 14 pages, Article ID 026017, 2017.

[28] G. Li, "Research on sports simulation and fatigue characteristics of athletes based on machine learning," *Journal of Intelligent and Fuzzy Systems*, vol. 40, no. 4, pp. 7531–7542, 2021.

[29] Q. Chang, W. Yang, J. Liu, H. Gao, and M. Yao, "A research on fatigue crack growth monitoring based on multi-sensor and data fusion," *Structural Health Monitoring*, vol. 20, no. 3, pp. 848–860, 2019.

[30] D. Sun, Y. Huang, M. Zhao, D. Chen, and W. Han, "Recognition of fatigue driving based on steering operation using wearable smart watch," *Green, Smart and Connected Transportation Systems*, vol. 617, pp. 235–248, 2020.

[31] W. Lu, H. Hu, J. Wang, L. Wang, and Y. Deng, "Tractor driver fatigue detection based on convolution neural network and facial image recognition," *Nongye Gongcheng Xuebao/Transactions of the Chinese Society of Agricultural Engineering*, vol. 34, no. 7, pp. 192–199, 2018.

Hindawi
Journal of Healthcare Engineering
Volume 2023, Article ID 9835083, 1 page
https://doi.org/10.1155/2023/9835083

Retraction

Retracted: A Novel Method of Clinical Nursing under the Medical Internet of Things Technology

Journal of Healthcare Engineering

Received 26 September 2023; Accepted 26 September 2023; Published 27 September 2023

This article has been retracted by Hindawi following an investigation undertaken by the publisher [1]. This investigation has uncovered evidence of one or more of the following indicators of systematic manipulation of the publication process:

(1) Discrepancies in scope
(2) Discrepancies in the description of the research reported
(3) Discrepancies between the availability of data and the research described
(4) Inappropriate citations
(5) Incoherent, meaningless and/or irrelevant content included in the article
(6) Peer-review manipulation

The presence of these indicators undermines our confidence in the integrity of the article's content and we cannot, therefore, vouch for its reliability. Please note that this notice is intended solely to alert readers that the content of this article is unreliable. We have not investigated whether authors were aware of or involved in the systematic manipulation of the publication process.

In addition, our investigation has also shown that one or more of the following human-subject reporting requirements has not been met in this article: ethical approval by an Institutional Review Board (IRB) committee or equivalent, patient/participant consent to participate, and/or agreement to publish patient/participant details (where relevant).

Wiley and Hindawi regrets that the usual quality checks did not identify these issues before publication and have since put additional measures in place to safeguard research integrity.

We wish to credit our own Research Integrity and Research Publishing teams and anonymous and named external researchers and research integrity experts for contributing to this investigation.

The corresponding author, as the representative of all authors, has been given the opportunity to register their agreement or disagreement to this retraction. We have kept a record of any response received.

References

[1] T. Ou, X. Cai, M. Wang, F. Guo, and B. Wu, "A Novel Method of Clinical Nursing under the Medical Internet of Things Technology," *Journal of Healthcare Engineering*, vol. 2021, Article ID 2234457, 10 pages, 2021.

Hindawi
Journal of Healthcare Engineering
Volume 2021, Article ID 2234457, 10 pages
https://doi.org/10.1155/2021/2234457

Research Article

A Novel Method of Clinical Nursing under the Medical Internet of Things Technology

Tingting Ou,[1] Xuehua Cai,[2] Meichun Wang,[3] Feirong Guo,[1] and Biyu Wu[3]

[1]*Vascular Channel Nursing Specialist Clinic, Quanzhou First Hospital, Quanzhou 362000, China*
[2]*Outpatient Department, Quanzhou First Hospital, Quanzhou 362000, China*
[3]*Nursing Department, Quanzhou First Hospital, Quanzhou 362000, China*

Correspondence should be addressed to Biyu Wu; qyhlbwby@126.com

Received 23 September 2021; Revised 11 October 2021; Accepted 12 October 2021; Published 9 November 2021

Academic Editor: Gu Xiaoqing

Internet of things technology began to spread to all industries of our lives; the application of medical internet of things in many hospitals highlighted its advantages and brought a lot of convenience to patients and medical staff. With the continuous progress of China's medical reform and the continuous improvement of patients' requirements for medical service quality, this paper discusses the application of medical internet of things in clinical nursing in ward, and the basic information collection, infusion, and mobile nursing were discussed and studied. Through the parallel control study of the laboratory itself, this paper evaluates whether the two different clinical measurement methods of medical internet of things technology and traditional technology are consistent in body temperature, pulse, respiration, and blood oxygen saturation. At the same time, it also deeply studies the value and advantages of internet of things technology in the application of other monitoring indicators in clinical nursing and analyses the problems in its application. The experimental data show that the two measurement methods with different principles can be completely replaced in clinical application, and the time efficiency of the new clinical nursing method under the medical internet of things technology in mapping body temperature, pulse, and respiration has been improved by 76.20% and 72.02%, respectively, surpassing the traditional information technology and realizing the intelligent, automatic, and standardized data acquisition method. It ensures the authenticity of data and the real-time of information flow and meets the needs of resource sharing and medical regional interconnection.

1. Introduction

Due to the complexity and breadth of clinical nursing work, the collection of transactional nursing information occupies a lot of manpower, material resources, and time; the computer processing process of nursing information has high requirements for information processing methods and technologies. Nursing information has different attributes and different processing methods. Highly subjective information must be collected and recorded on site by nurses with professional knowledge and stored on paper carriers or mobile devices [1]. The objective information is collected one by one by the nursing staff carrying measuring instruments to the patient's bedside and then recorded manually. After completing the information collection, it is returned to the nursing station for classification and processing, and part of it is input into the computer nursing information database for storage, analysis, and re-extraction so as to realize nursing information management [2]. The other part is kept in the form of paper materials, and the nursing management personnel carry out quality control afterwards. On the one hand, nurses must participate in many links of data processing in the whole process; on the other hand, they must complete complicated manual operation and nursing tasks such as treatment, observation, and feedback at the same time. Its high labour intensity, low efficiency, high error rate, and low value embodiment making nurses in a high-tension working state for a long time, resulting in high work pressure and serious job burnout [3]. From the perspective of patients, clinical

diagnosis, and treatment, nursing data from collection, analysis, cleaning, and storage to the final service application have obvious periodicity and lag, which cannot provide necessary dynamic data for clinical nursing diagnosis and treatment and affect the accuracy of clinical nursing diagnosis and treatment decision-making and effect [4]. From the perspective of information equipment, restricted by the advanced degree and the relatively fixed mobile range of equipment, the efficiency of medical treatment will be affected to varying degrees in the process of information processing, which will complicate the workflow, and there is a situation that the information process and the medical care process are seemingly inseparable [5]. The above phenomena truly reflect the current situation and level of clinical nursing information management and are also the doubts and difficulties that must be faced and solved in the in-depth application of the nursing information management system [6].

The organic integration of internet of things and nursing activities is one of the important characteristics of nursing development in the 21st century. The advantage of the application of the internet of things in clinical nursing lies in that the information receiver with sensors replaces people to "perceive" the information of human body, facilities, and environment and is not limited by time and space [7]. It can automatically collect, transmit, and process real-time information comprehensively, efficiently, dynamically, continuously, and conveniently and synchronously realize the functions of real-time analysis and decision support [8]. This has become an opportunity for the innovative development of clinical nursing. Due to the characteristics of thorough perception, comprehensive interconnection, and intelligent insight of the internet of things, it can realize the tracking and supervision of the whole process of medical and nursing affairs and clinical nursing business, expand the coverage of clinical nursing business, management, and service, and comprehensively systematize intelligent medical treatment, precision nursing, and quality service [9]. The goal of clinical nursing work is made more efficient and convenient; complete, true, and reliable judicial evidence is provided for handling medical disputes or accidents; it also provides an objective basis for scientific evaluation to improve nursing value and highlight nursing quality level and management benefit [10]. Based on this research background, the innovative development and value of internet of things technology to clinical nursing are further thought. How to achieve the timely, accurate, efficient, and standardized collection of clinical nursing information, particularly after integration with the nursing information management system, and the degree of high integration and sharing, directly affect the level of nursing quality [11].

This paper aims at the current situation that the traditional methods have high labor intensity, low efficiency, high error rate, and low value embodiment, which makes the nurses in a high-tension working state for a long time, thus affecting the accuracy of clinical nursing diagnosis and treatment decision-making and effect, discusses the application of medical internet of things in clinical nursing in ward, and discusses and studies the basic information collection, infusion, and mobile nursing. Through the parallel control study of the laboratory itself, this paper evaluates whether the two different clinical measurement methods of medical internet of things technology and traditional technology are consistent in body temperature, pulse, respiration, and blood oxygen saturation. At the same time, it also deeply studies the value and advantages of internet of things technology in the application of other monitoring indicators in clinical nursing and analyses the problems in its application. The experimental data show that the two measurement methods with different principles can be completely replaced in clinical application, and the mapping efficiency of the new clinical nursing method under the medical internet of things technology exceeds the traditional information technology, realizes the intelligent automation and standardized data acquisition method, and ensures the authenticity of data and the real-time of information flow; it meets the needs of resource sharing and medical regional interconnection.

The chapters of this paper are arranged as follows. Section 1 summarizes the research background and significance of this paper. Section 2 introduces the internet of things-related technologies. Section 3 analyses the implementation ways of new methods for the application of medical internet of things technology in clinical nursing. Section 4 carries out experimental analysis, and Section 5 summarizes the full text.

2. Relevant Technologies of Internet of Things

2.1. Overall Structure. With the development of technology and application, the connotation and extension of the concept of internet of things are also expanding. Its overall framework includes the following five parts, namely, community architecture, technological know-how system, preferred system, associated enterprise device, and useful resource system. The terminal sensing layer consists of sensing terminal devices, such as RF readers, electronic tags, cameras global positioning system, and various sensors, and other sensing terminals collect data information [12]. The sensing terminal is equivalent to the peripheral nerve in the human structure, such as the human facial features. It is the terminal source for the internet of things to identify objects and collect information [13]. The community transmission processing layer, additionally acknowledged as the community layer, transmits the records and statistics amassed by way of the grasp layer to the vacation spot safely, rapidly, and reliably through the internet, conversation community, and community cloud platform. The network transport layer is equivalent to the command centre in the human structure, such as the central nerve and brain, which is responsible for the transmission and processing of information collected by the sensing terminal. Intelligent application layer: it is a bridge connecting the internet of things and users [14]. Users can be people, other systems, and organizations. It is used to analyse and process the information obtained by the sensing terminal and realize the intelligent application of the internet of things in combination with the needs of the industry, as shown in Figure 1.

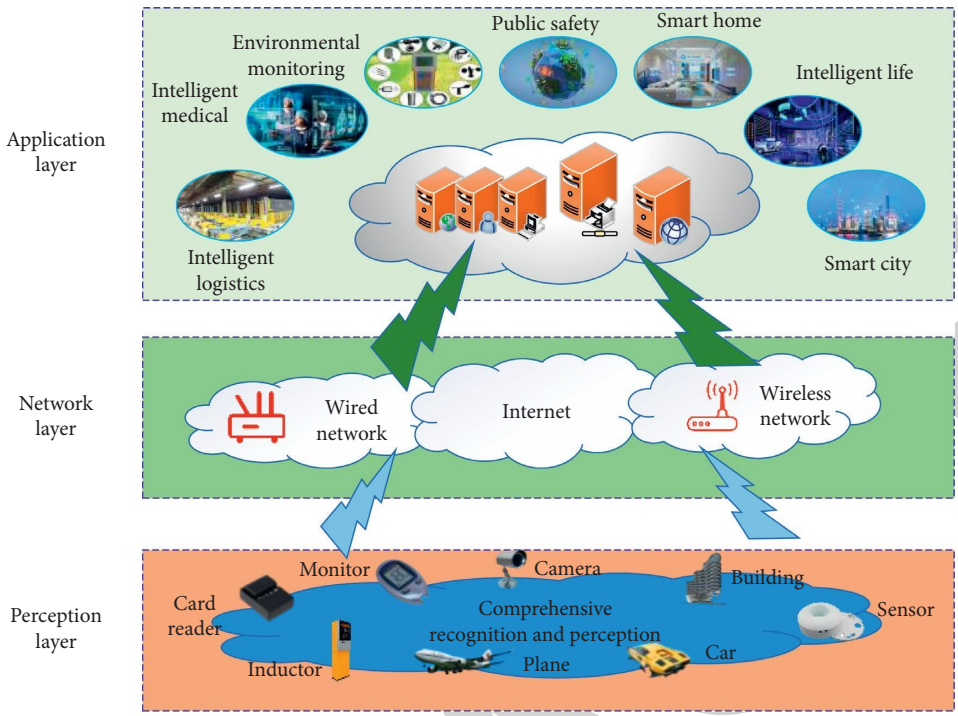

Figure 1: Architecture of internet of things.

2.2. Significance of Internet of Things in Clinical Nursing. The application of internet of things technology in the hospital nursing information system is of great significance and value. First, internet of things technology can quickly evaluate patients and accurately grade patients. Based on the internet of things technology, the preinspection system is set at the same time. The preinspection system can effectively, quickly, and accurately obtain patient information and conduct triage according to the severity of patients' diseases [15]. In addition, the patient information can be transmitted to doctors in real-time through the internet of things system, which can improve the efficiency of patients' treatment. In addition, the application of internet of things technology in the nursing information system can timely transmit patient information to rescue nurses; nurses can get information in time and implement rescue in time. Second, internet of things technology is conducive to improve nurses' work efficiency [16]. At the same time, the application of internet of things in the nursing information system can significantly reduce the incidence of errors. On the basis of internet of things technology, smart wristbands can be used to wear smart wristbands for newly admitted patients without bedside cards. Patients can be identified through wristbands, which not only facilitate nurses but also save time and improve work efficiency. By using smart watches for patients in the hospital, it can ensure that nurses work orderly and can be busy without disorder [17]. In addition, shrewd identification via the web of matters can radically decrease medicinal drug errors, keep away from patients' blunders in executing clinical orders, and extensively enhance the pleasant of work [18]. Third, the internet of things provides transparent data through the communication layer, obtains the physiological information of patients through the perception layer, and can reflect the information to nurses through the network layer. Nurses do not need to use traditional instruments to monitor the vital signs of patients and do not need to arrive at the patient's bed every hour or 30 minutes to collect information. Nurses solely accumulate the patient's existence signs and symptoms and situation modifications via the screen and wise show screen and transmit the patient's atypical facts to doctors, so as to facilitate analysis and treatment, improve the patient's cure probability, and effectively protect the patient's life and health [19].

2.3. Specific Application of Medical Internet of Things. Combined with the previous design, the internet of things network based on Wi-Fi and RFID technology is designed to realize specific applications. In this project, the medical internet of things is selected as the final technical landing point. The application environment and conditions of medical internet of things are as follows: Wi-Fi signal coverage has been realized in the ward environment, and the nurse workstation has network access to the hospital LAN. The hospital has its own database system; according to the environment and requirements, the overall structure of the designed medical internet of things network is shown in Figure 2.

In this system, the sphygmomanometer, as a sensor node, has RFID read-write function and Wi-Fi communication function. In use, the sphygmomanometer first collects the patient's personal information in the label, then measures the patient's blood pressure data by the Coriolis auscultation method, and then connects the Wi-Fi network through the wireless access point to bind the patient

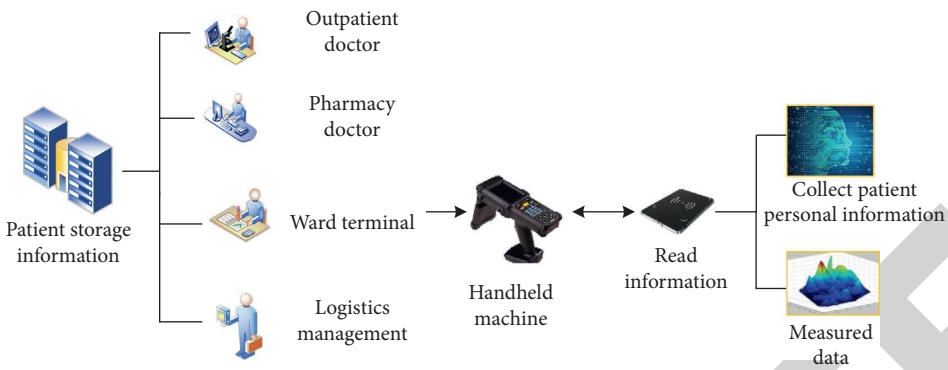

Figure 2: Frame diagram of mobile nursing structure.

information and blood pressure data and send them to the nurse station PC; the PC runs the application software to further save the data to the hospital database system [20]. Through the analysis of the system, the main contents of the work are in two aspects: the design of sphygmomanometer terminal and the preparation of nurse workstation application software. The application software has been written by other students, so the focus of the work is mainly on the design of sphygmomanometer terminal.

3. A New Method for the Application of Medical Internet of Things Technology in Clinical Nursing

3.1. System Design. According to the needs of clinical nursing and the application environment of the system, the following problems must be solved in the system design. (1) *Portable Device.* The sensor is concentrated in a portable device with high reliability, which meets the requirements of small volume and convenient use and has the performance of high measurement accuracy. (2) *Low-Power Consumption*. Due to the frequent use of sensing terminal equipment, but the amount of data collected is small and no high transmission rate is required, low-power consumption can ensure a long service time of the equipment without frequent charging [21]. (3) *Automatic Networking*. Each ward has at least 40 beds, so at least 40 sets of sensing terminal equipment shall be allocated. These 40 sets of equipment shall automatically form a network and send vital signs parameters to the server through wireless mode. (4) *Expansibility*. The environment of the ward is complex, there are many interference factors, and the environment and area of each ward are different. Therefore, it is necessary to ensure that the sensing terminal equipment can be used in different environments and has high expansion performance. Through the investigation of existing communication technology in the early stage and combined with the characteristics of the current hospital information system, the system structure developed is shown in Figure 3. The ward intelligent nursing system mainly includes: electronic thermometer with wireless communication function and two-parameter measuring instrument of pulse and blood pressure. Through the physiological signal acquisition equipment in the hands of patients and the wireless gateway deployed in the ward corridor, the physiological parameter information is transmitted to the hospital information system to realize the intelligent acquisition of physiological parameters in the ward [22].

In terms of technical implementation, the research and development of nRF905 low-power RF communication module with 433 MHz communication frequency band are focused. Combined with low-power MCU and physiological signal sensing equipment, it collects, analyses, and processes three key parameters that must be measured every day in the general ward: blood pressure, body temperature, and pulse. Accordingly, wireless electronic thermometer and wireless blood pressure pulse meter are developed in the sensing layer. The network realizes the conversion of RF communication into Wi-Fi communication and enhances the functions of temporary storage and automatic networking. In the application layer, the key physiological signal nursing system based on PDA and the real-time acquisition and control system based on PC are made.

3.2. Design of Sensor Layer. The body temperature sensor is mainly composed of temperature measurement circuit, main control chip, wireless transmission module, and power management module. The temperature measurement circuit is mainly composed of chip and thermistor. The main control chip of TI company and the wireless transmission module is nRF905 module [23, 24]. The temperature measurement chip converts the temperature into an electrical signal. The main control chip reads the electrical signal by interrupting and calculates the pulse data of the OEB pin of chip to read the temperature data. The main control chip judges whether the temperature is the maximum temperature by interrupt counting and saves it when it is the maximum temperature. When the main control chip gets the stable maximum temperature, it starts to configure the wireless transmission module to reduce the power consumption of the system and prolong the service time of the battery. When designing the temperature sensor, the following points must be considered: (1) it must meet the requirements of medical temperature measurement, and the measurement error is less than 0.1°C; (2) it has simple operation, anyone can use the thermometer quickly; (3) the

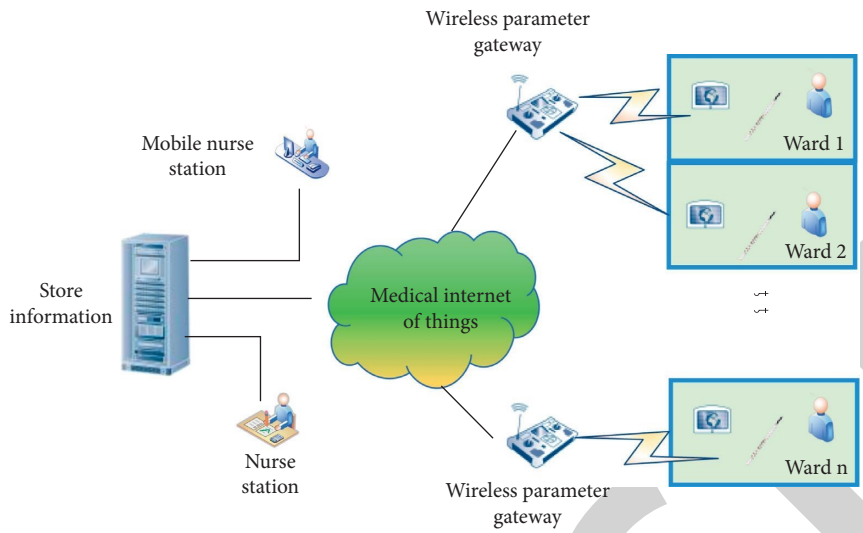

Figure 3: Intelligent monitoring system for ward.

shell is sealed, and the surface is smooth and has the functions of bacteriostasis and antidisinfection; (4) data transmission and control do not need manual participation and interference; (5) the measurement error compensation function is designed to solve the problem of temperature drift caused by thermistor aging; and (6) it has low-power consumption and extended battery life [25].

The sphygmomanometer adopts a high-performance sound pressure sensor to judge the blood pressure value by extracting the Coriolis sound signal of auscultation. This method can eliminate the individual difference of the oscillography electronic sphygmomanometer and improve the accuracy of blood pressure measurement. In the design process, the Coriolis tone delay time technology is developed to further accurately determine the systolic and diastolic blood pressure and ensure the accuracy of individual measurement. High precision pressure sensor and customized Coriolis sound sensor are used to extract blood pressure related signals, and the overall performance of the system is improved through linear deflation and automatic pressure zeroing. The appearance of the mercury manometer is simulated by liquid crystal, with high scale resolution [26, 27]. It can accurately display the cuff pressure and observe the pulsation signal of the cuff. The functions of automatic data storage, playback, and analysis are realized. It has RF wireless transmission interface to realize the interconnection of Internet of things. The principle of pulse and sphygmomanometer is shown in Figure 4.

3.3. Design of Application Layer Service Software. The main functions of application layer service software are maintenance, display, collection, writing, viewing, and alarm of life parameter information. The maintenance function is mainly used for database maintenance, including adding, deleting, and updating records. The man-machine interface of the system is written based on C++ language, and the development tool is MFC application program based on VC++ 6.0 dialog box class [28]. The basic process is to discharge the basic information of patients in the ward from the hospital HIS, including patients' ID numbers, bed numbers, room numbers, diagnostic information, and attending doctors; nurses and doctors can intuitively see the patient's information [29]. When the life parameters are transmitted to the PC or server, they can be displayed to the interface in real-time. After receiving, the doctor or nurse can click the save button to save the parameter data to the server. The received data are displayed in the column corresponding to the patient [30]. When saving, it is also saved according to the patient's information. There will be no dislocation between the patient and vital signs parameters. The man-machine interface can also modify the number of the sensing terminal equipment. When the patient's equipment is damaged, the equipment can be replaced for the patient in time [31, 32]. The database adopts the link mode to connect the application software to the Oracle database in the background of the hospital and then executes the corresponding database programming statements to complete the reading and saving of the database and realize the operation of the fields in the corresponding table.

4. Experiment and Analysis

Under the condition of overcoming individual differences, the experimental research design scheme of self parallel control is adopted. With the help of traditional measurement tools and medical internet of things, the control group and experimental group are set. The same person collects four vital sign parameters, body temperature, pulse, respiration, and blood oxygen saturation at 7 different time points in a day. This experiment is aimed at healthy groups to verify the feasibility and accuracy of the new technology in clinical nursing application. For the above data management work, the personnel in charge of nursing division or above shall be invited to guide and participate in data quality control, supervision, and management. Because the data collected by

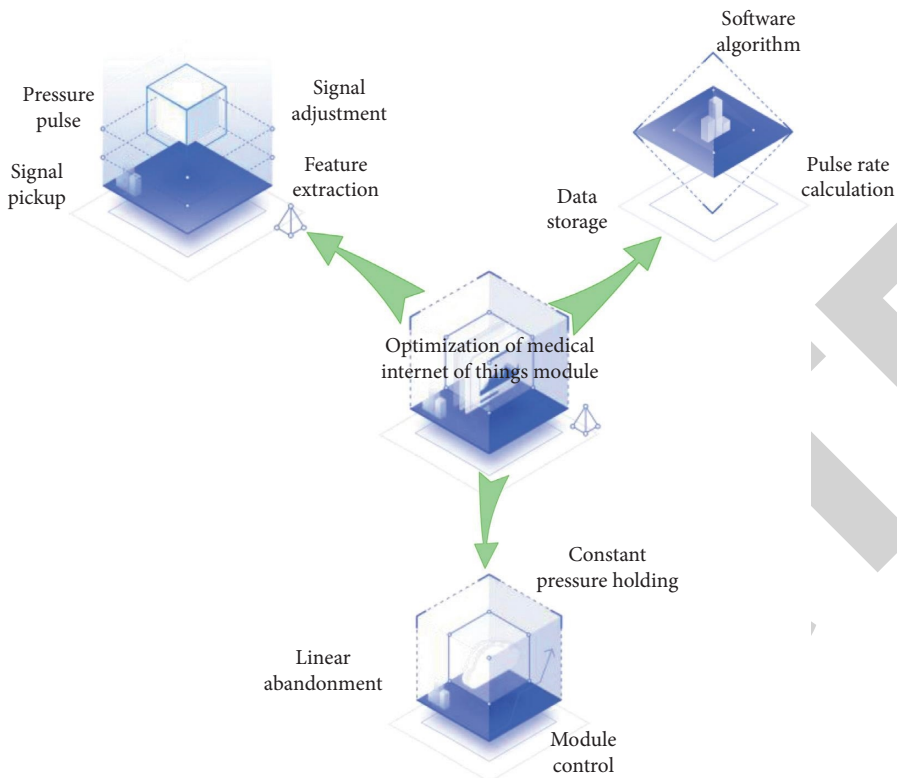

Figure 4: Realize the medical internet of things interconnection of clinical nursing.

the two methods of comparison have the characteristics of point and surface differences, the latter is processed by the mean method and then compared. SPSS 22.0 statistical software was used to analyse the continuous repeated measurement data collected in the experiment by analysis of variance, paired t test, correlation coefficient, and Bland Altman method.

After the experiment, the data stored in the medical IoT system were transferred, and the tables were counted after counting. Finally, the recorder shall fill in the comparison form uniformly and the supervisor shall check it. The experiment is started after completing the pre-experiment. First, the data are entered into excel by the double entry method and then imported into SPSS 22.0 software for statistical analysis and description. The analysis of variance is used to understand the difference between the two groups of data, and the degree of difference is statistically described by paired t test, and then the correlation test is carried out for the two groups of data samples to understand the degree of correlation and bias. The above analysis of variance shows that the data of two different principal measurement methods of R are completely consistent, and there is no statistical difference, while the data of temperature, pulse, respiration, and blood oxygen saturation are not completely consistent, and there are statistical differences. With the help of the plot's submenu, the mean change trend diagram of the indicators measured repeatedly for 7 times is made, and the linear correlation regression equation of temperature and pulse is calculated, as shown in Figure 5. The temperature and pulse data meet the linear correlation analysis conditions, there is no obvious abnormal value, and the correlation coefficient is statistically significant.

$F = 8.504$, $P = 0.005 \leq 0.005$, there is no linear correlation, and the control data of the two groups are different. The blood oxygen saturation results of control group (ECG) and experimental group (medical internet of things) were 98.00 ± 0.52 and 98.63 ± 0.81. Due to the difference in precision between the two different methods, it is necessary to further analyse the data in combination with clinical application standards. Therefore, the Bland Altman analysis method is used to evaluate the consistency of the two different measurement methods, and the calculated results are shown in Figure 6.

The difference between the measurement results of the two different methods is described by paired t test, as shown in Figure 7. Although the results of the two measurement methods are not completely consistent, there is always a certain deviation difference that the consistency of medical internet of things values is often greater than that of the control group, and there is a linear correlation between the two groups of data, indicating that the linear relationship between the two-control data is close and consistent. Through the analysis of the above statistical methods, the measurement results of the two measurement methods in the control group and the experimental group (medical internet of things) on the four parameters of temperature, pulse, respiration, and blood oxygen saturation are consistent; that is, the two methods can replace each other.

Through data analysis and clinical consistency evaluation, it is concluded that these two different measurement

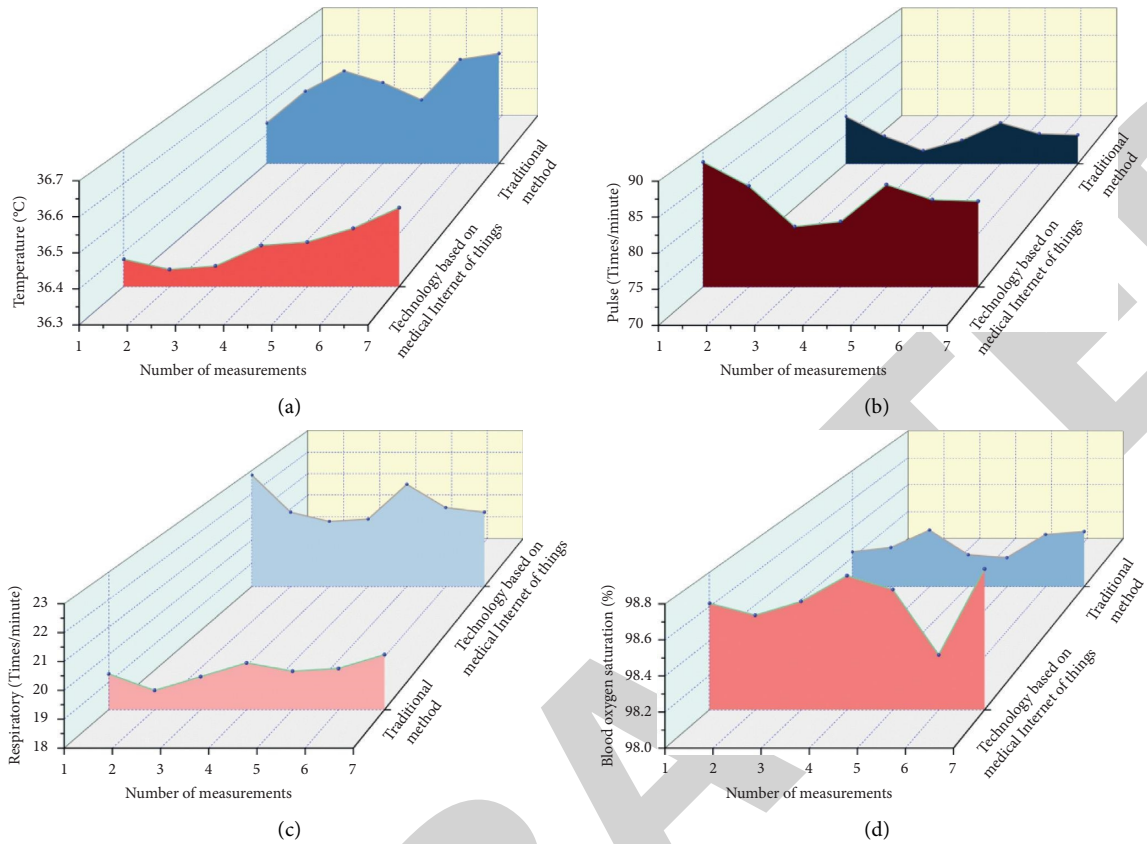

Figure 5: Correlation analysis of body temperature, pulse, respiration and blood oxygen saturation: (a) measured value of temperature; (b) measured value of pulse; (c) respiratory measurements; (d) monitoring value of blood oxygen saturation.

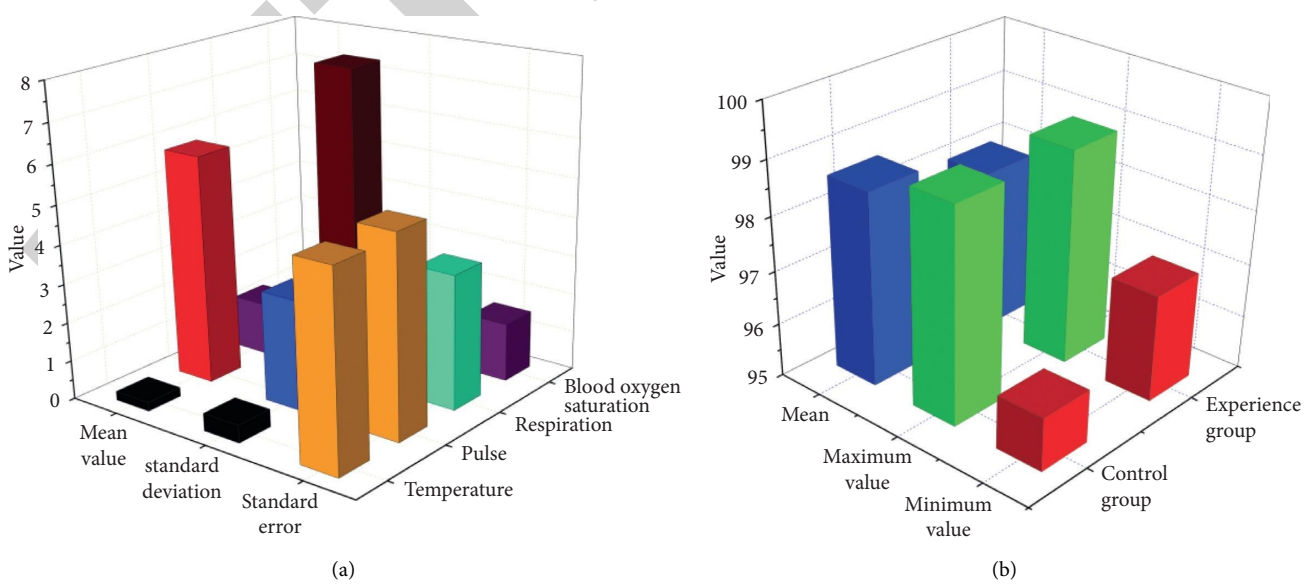

Figure 6: Comparison table of consistency evaluation: (a) evaluation of consistency; (b) comparison of limit value data.

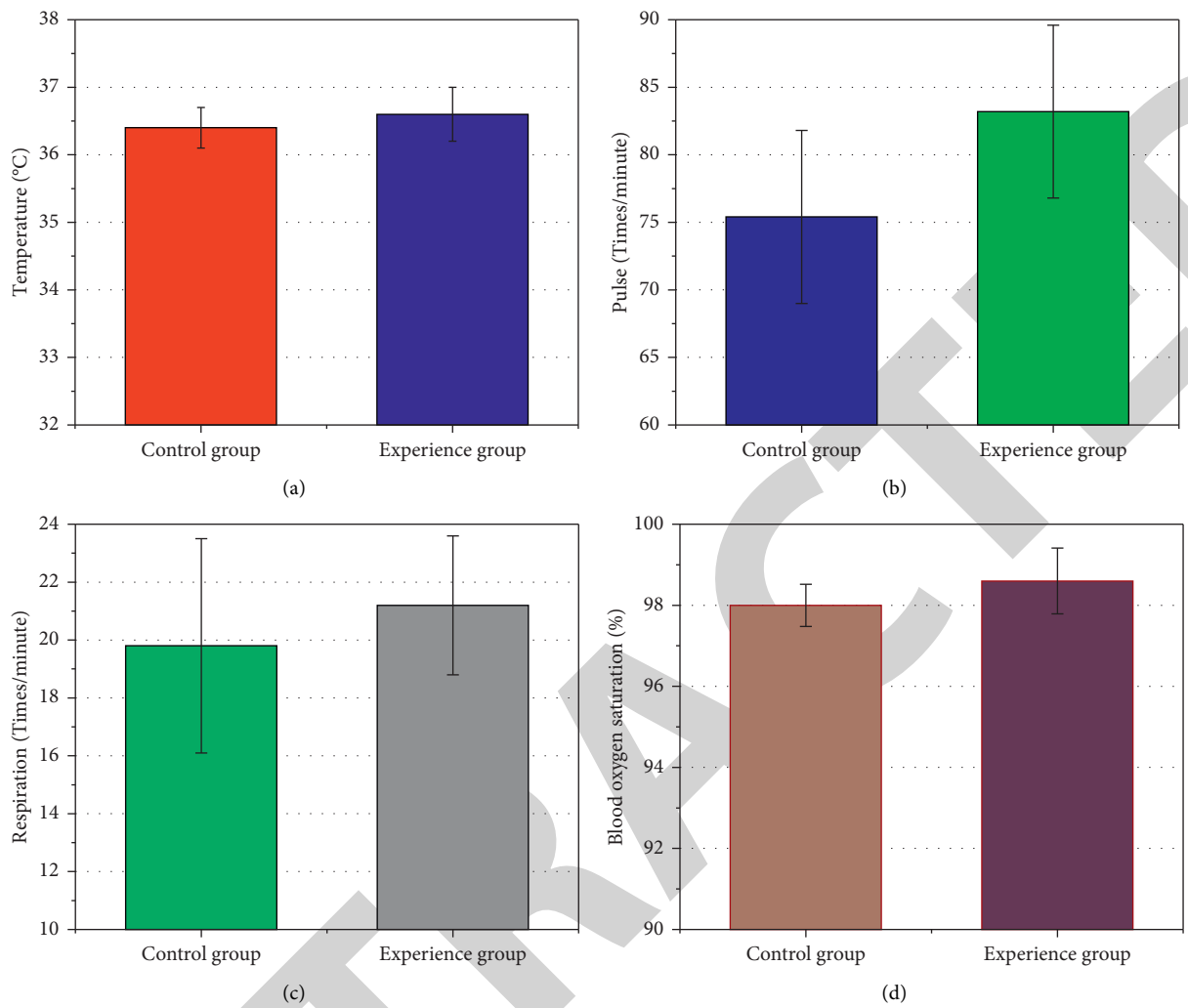

Figure 7: Comparison of measurement results by different methods: (a) comparison of temperature; (b) comparison of pulse; (c) comparison of respiration; (d) comparison of blood oxygen saturation.

methods can completely replace each other in the accuracy of temperature, pulse, respiration, and blood oxygen saturation measurement, and the accuracy and sensitivity of medical internet of things are higher. The medical internet of things is fully used, highly operable, highly accepted by patients, and has strong clinical practicability and popularization. Under the internet of things technology, the integration of temperature, pulse, respiration surveying, and mapping in the three nursing test sheets has improved the time efficiency by 76.20% and 72.02%, respectively, compared with the traditional surveying and mapping methods 1 and 2. Time comparison of different surveying and mapping methods is shown in Figure 8.

Intelligent automation and standard dynamic data collection are realized in information collection, highlighting the advantages of standard collection, unified access, and transmission, data sharing, and unified service. It shortens the operation time of nurses' manual measurement of temperature, pulse, and respiration, reduces the error rate of data input system, and reduces the process links of vital signs measurement and drawing. In terms of monitoring human physiological parameters, it is more widely used and more powerful, convenient, and practical than the current ECG monitor. For example, the increased fall index, sleep index, and other more than a dozen indicators, including the noninvasive blood glucose and blood pressure monitoring channel to be opened soon, to comprehensively monitor the health status of patients, undoubtedly extend the nurse workstation to the patients and directly point the nursing safety management and nursing quality monitoring to the target of real-time dynamic management. It laid a solid foundation for realizing nursing scientific management and intelligent decision-making.

The medical internet of things system in this test is seamlessly connected with NIS. Taking only one routine nursing work "mapping temperature, pulse, and respiration" as an example, the mapping efficiency of internet of things is about 76.2% and 72.02% higher than that of traditional methods (manual and semiautomatic). This result shows that the application of the new technology directly reduces the indirect nursing time. While improving the work efficiency and reducing the labour intensity, it also

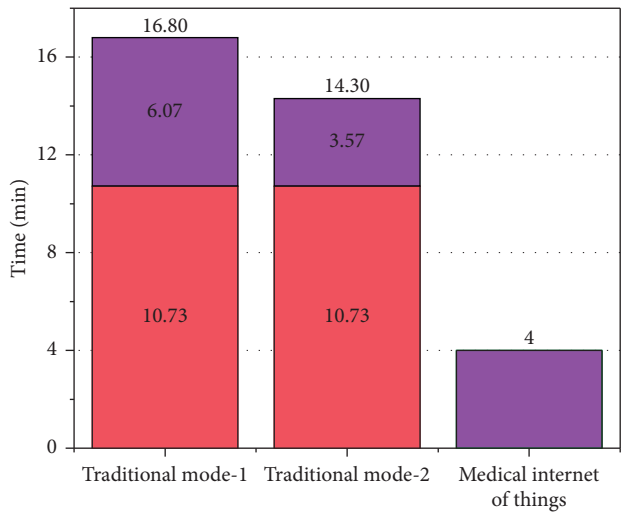

Figure 8: Time comparison of different surveying and mapping methods.

correspondingly reduces the office consumables. Especially, when a large number of patients are treated in the ward and temperature, pulse, and respiration surveyed, nurses will have a deeper experience in artificial intelligence mapping, which provides technical support for the transformation of the nursing workflow of collecting vital signs. In addition, compared with the traditional working mode, it highlights its strong artificial intelligence characteristics in the standardization, authenticity, correctness, timeliness, and sharing of data collection, which lays a solid foundation and rich resources for enriching the clinical nursing database system, and provides a scientific and safe guarantee for patient condition monitoring management, safety management, and high-quality service.

5. Conclusion

The use of medical internet of things in the ward can greatly improve the work efficiency of medical staff and reduce work errors. At the same time, it can also make the doctor-patient relationship more harmonious and improve the patient's nursing satisfaction. Medical internet of things can concentrate all information on the same platform so that resources can be used effectively; this paper designs and implements a new clinical nursing method based on medical internet of things. Based on the design principle of improving the automatic management level of hospital ward, reducing the work intensity of medical staff, reducing cost investment, and reducing patient bed accompanying, communication technology, photoelectric detection technology, microcomputer technology, computer network technology, and relational database technology are successfully applied to the ward intelligent monitoring system based on internet of things. The use of the system provides convenience for nurses' nursing work, provides a reliable safety guarantee for patients' daily treatment, and has high application value. The trial in several clinical wards shows that the system has high accuracy, stability, and consistency in the measurement of blood pressure, pulse, and body temperature. At the same time, both the sensor end and the application end can output reliable alarm signals when the data are abnormal or reach the warning value. Finally, the system is divided into multiple functional modules in a reasonable way, which can be customized and tailored to meet the application of different levels of hospitals or wards.

Data Availability

The data used to support the findings of this study are included within the article.

Conflicts of Interest

The authors declare that there are no conflicts of interest.

References

[1] X. F. Huan, L. Li, and Q. Guo, "Research on the effect of goal management theory in clinical nursing management," *China Health Industry*, vol. 16, no. 8, pp. 1–7, 2019.

[2] W.-F. Cheng, T.-Y. Zhao, and Y. Guo, "Research progress on narrative education in clinical nursing education," *Chinese Nursing Research*, vol. 3, no. 4, pp. 151–153, 2016.

[3] X. Xu, X. Li, L. Wang, Y. Ma, and J. Liu, "Research on training of nursing students' comprehensive quality and clinical nursing ability," *China Continuing Medical Education*, vol. 9, no. 6, pp. 34–36, 2017.

[4] R. Sierakowski, I. Azumi, A. M. Rahman et al., "The internet of things for basic nursing care—a scoping review," *International Journal of Nursing Studies*, vol. 6, no. 9, pp. 78–90, 2017.

[5] S. O'Connor and T. Andrews, "Mobile technology and its use in clinical nursing education: a literature review," *Journal of Nursing Education*, vol. 54, no. 3, pp. 137–144, 2015.

[6] H. Mostafa, T. Kerstin, and S. Regina, "Wearable devices in medical internet of things: scientific research and commercially available devices," *Healthcare Informatics Research*, vol. 23, no. 1, pp. 4–15, 2017.

[7] A. Hao and L. Wang, "Medical device integration model based on the internet of things," *The Open Biomedical Engineering Journal*, vol. 9, no. 1, pp. 256–261, 2015.

[8] Y. Xia and Y. Fan, "Security analysis of sports injury medical system based on internet of health things technology," *IEEE Access*, vol. 8, no. 3, pp. 211–213, 2020.

[9] Y. Shu, Y. Qi, and S. Bo, "The key technology study on cloud computing platform for ECG monitoring based on regional internet of things," *Chinese Journal of Medical Instrumentation*, vol. 40, no. 5, pp. 341–343, 2016.

[10] A. Apsel, "A Simple guide to low-power wireless technologies: balancing the tradeoffs for the internet of things and medical applications," *IEEE Solid-State Circuits Magazine*, vol. 10, no. 4, pp. 16–23, 2018.

[11] M. Elayah, K. A. Ezzat, H. E Nashar, and L. N Omran, "Cybersecurity architecture for the internet of medical things and connected devices using blockchain," *Biomedical Engineering Applications Basis and Communications*, vol. 33, no. 2, pp. 215–220, 2021.

[12] X. Wang, "The architecture design of the wearable health monitoring system based on internet of things technology," *International Journal of Grid and Utility Computing*, vol. 6, no. 4, pp. 207–209, 2015.

Hindawi
Journal of Healthcare Engineering
Volume 2023, Article ID 9781731, 1 page
https://doi.org/10.1155/2023/9781731

Retraction

Retracted: Applied Research on the Combination of Weighted Network and Supervised Learning in Acupoints Compatibility

Journal of Healthcare Engineering

Received 10 October 2023; Accepted 10 October 2023; Published 11 October 2023

This article has been retracted by Hindawi following an investigation undertaken by the publisher [1]. This investigation has uncovered evidence of one or more of the following indicators of systematic manipulation of the publication process:

(1) Discrepancies in scope
(2) Discrepancies in the description of the research reported
(3) Discrepancies between the availability of data and the research described
(4) Inappropriate citations
(5) Incoherent, meaningless and/or irrelevant content included in the article
(6) Peer-review manipulation

The presence of these indicators undermines our confidence in the integrity of the article's content and we cannot, therefore, vouch for its reliability. Please note that this notice is intended solely to alert readers that the content of this article is unreliable. We have not investigated whether authors were aware of or involved in the systematic manipulation of the publication process.

Wiley and Hindawi regrets that the usual quality checks did not identify these issues before publication and have since put additional measures in place to safeguard research integrity.

We wish to credit our own Research Integrity and Research Publishing teams and anonymous and named external researchers and research integrity experts for contributing to this investigation.

The corresponding author, as the representative of all authors, has been given the opportunity to register their agreement or disagreement to this retraction. We have kept a record of any response received.

References

[1] X. Qiu, X. Zhong, and H. Zhang, "Applied Research on the Combination of Weighted Network and Supervised Learning in Acupoints Compatibility," *Journal of Healthcare Engineering*, vol. 2021, Article ID 4699420, 8 pages, 2021.

Hindawi
Journal of Healthcare Engineering
Volume 2021, Article ID 4699420, 8 pages
https://doi.org/10.1155/2021/4699420

Research Article

Applied Research on the Combination of Weighted Network and Supervised Learning in Acupoints Compatibility

Xia Qiu, Xiaoying Zhong, and Honglai Zhang

College of Medical Information Engineering, Guangzhou University of Chinese Medicine, Guangzhou 510006, China

Correspondence should be addressed to Honglai Zhang; zhanghl@gzucm.edu.cn

Received 23 September 2021; Revised 13 October 2021; Accepted 20 October 2021; Published 29 October 2021

Academic Editor: Gu Xiaoqing

To enhance the depth of excavation and promote the intelligence of acupoint compatibility, a method of constructing weighted network, which combines the attributes of acupoints and supervised learning, is proposed for link prediction. Medical cases of cervical spondylosis with acupuncture treatment are standardized, and a weighted network is constructed according to acupoint attributes. Multiple similarity features are extracted from the network and input into a supervised learning model for prediction. And, the performance of the algorithm is evaluated through evaluation indicators. The experiment finally screened 67 eligible medical cases, and the network model involved 141 acupoint nodes with 1048 edge. Except for the Preferential Attachment similarity index and the Decision Tree model, all other similarity indexes performed well in the model, among which the combination of PI index and Multilayer Perception model had the best prediction effect with an AUC value of 0.9351, confirming the feasibility of weighted networks combined with supervised learning for link prediction, also as a strong support for clinical point selection.

1. Introduction

Acupoint compatibility is the application of two or more acupoints under the principle of selecting acupoints, through which the synergy between the acupoints is strengthened and medical efficacy is achieved [1]. Acupuncture prescription, which has high clinical value, is the combination of clinical practice and TCM theories, including principle, method, prescription, and acupoint. Among them, the compatibility of acupoints is the basic element of acupuncture prescription, so most studies use acupuncture prescriptions as the basis for exploring the laws of acupoint compatibility. Acupoint compatibility is not a simple "1 + 1" in a mathematical equation, the number of acupoints is not directly proportional to the quality of the combination, and there are various methods of acupoint compatibility, such as distant and near acupuncture points, following the meridian and identifying the evidence, which makes the factors affecting the efficacy of acupoint compatibility unclear. How to effectively analyse the pattern of acupoint compatibility to enhance clinical efficacy has made acupoint compatibility a hot research topic.

The selection of acupoints for clinical treatment is mainly dependent on medical records and the clinical experience of the practitioner and is subjective and limited. With the development of information technology, the research of acupoint compatibility has made progress with the help of data mining technology, especially complex network technology that expresses the nonlinear and complex relationships between nodes by constructing network models. Zhen et al. [2] used quantitative indicators such as network topology and structural parameters to objectify and assess the collocation relationships between acupoints. Wen et al. [3] used the angle and direction of needling to construct a network model to explore the characteristics of moxibustion. Jiang et al. [4] constructed an acupuncture point network model and showed that the distal and proximal point allocation method is often applied in acupoints compatibility for hiccups. In reality, the acupoint network is not a single network: it is a reflection of the theory of TCM diagnosis and treatment, and most studies combining acupoint compatibility with complex networks have limitations such as a single model of the acupoint network, the degree of connection between acupoints is not quantified, and only the

frequency of cooccurrence is used to show the pattern of acupoint coordination.

Link prediction is one of the cores of complex network research and can reveal the implicit connection rules of nodes in the graph. The research ideas and methods are derived from Markov chains and machine learning. Nowadays, it is widely used in many fields of research, such as disease networks [5], drugs networks [6], and social networks [7]. With the rapid development of machine learning, a large number of researches on the combination of supervised learning and link prediction have been conducted [6, 8–11]. Although link prediction has not been seen applied to acupuncture point networks in studies combining acupoint compatibility with complex networks, link prediction can effectively transform the problem of measuring the degree of relationship between nodes in a network into a problem of the likelihood of establishing links between nodes, which provides a new perspective on acupoint compatibility. To solve the problems above, this research is designed to construct a weighted complex network in order to abstract the actual acupuncture prescriptions for cervical spondylosis with the consideration of acupoints attributes. Based on weight, multiple types of features are extracted. In order to improve the depth of mining and explore the law of acupoint compatibility, the features are input into the supervised learning model for training and prediction, and the effects of features and models on forecasting performance are compared. The research is the preliminary exploration of intelligent acupoint selection and compatibility in TCM.

2. Weighted Network

2.1. Data Collection and Processing. From the platform of modern medical records cloud (http://www.yiankb.com/), the prescriptions of acupuncture and moxibustion used in cervical spondylosis were collected. To ensure the effectiveness of the network construction, it is necessary to collect the medical records of the patients who are diagnosed with cervical spondylosis. In the selection, the prescription should be clear, the treatment should be conducted mainly by acupuncture, and the condition of patient should be improved obviously. Finally, 67 medical records were collected, involving 115 acupoints and 1048 groups of acupoint combinations. The names of the acupoints were represented by the international code, and the extra points without international code were represented by Chinese Pinyin. Through *Python*, the medical records were revised with standardized names.

2.2. Network Construction. In the study, the acupoints extracted from the prescriptions of acupuncture treatment for cervical spondylosis were used to construct a weighted acupoint network. The weighted acupoint network was expressed as $G = (V, E, W)$, where V, E, and W were the set of nodes in the network, the set of edge relations, and the set of weights, respectively. The process of constructing a weighted acupoint network model could be mainly divided into three steps. (1) Extract all the acupoints in the prescription to form a set of nodes (V). (2) Each two acupoints in a prescription were connected as an edge to form the edge subset. And as such, the total set of the relations was built (E). (3) The similarity between all acupoint nodes was calculated and was used as the weight to build the weight set (W). Finally, V, E, W were combined to construct a weighted network. As shown in Figure 1, the network was visualized through Gephi.

The weight was determined by the similarity between the acupoints. Based on the attributes of nodes, the similarity was shown in a numerical form. It is believed that [12] the meridians, body surface location, and deep structure of acupoints are the inherent attributes, and the indication is the functional attributes. And the understanding of the attributes could improve the syndrome differentiation and acupoint compatibility in clinical acupuncture and moxibustion treatment. In the research, the attributes of meridian, location, and indication were used to calculate the similarity. Refering to the textbook Acupuncture and Moxibustion, the attributes of acupoints in the prescription for the treatment of cervical spondylosis were summarized, including 15 types of meridians (14 meridians and extra acupoints), 63 locations, and 670 indications, as shown in Table 1. Combining the acupoints in the prescription for the treatment of cervical spondylosis, the vectorized acupoint attributes were calculated by the cosine similarity. And then, the similarity of the acupoint group was obtained. The calculation formula is shown in

$$\cos(x, y) = \frac{x \cdot y}{\|x\| \cdot \|y\|}. \quad (1)$$

3. Link Prediction

Link prediction was mainly divided into four types of methods, including node attributes, network topology, machine learning, and maximum likelihood. Comparing to the difficulty of obtaining the information of node attributes, the method of link prediction, which is based on the network topology, can judge the possibility of establishing a connection between nodes clearly through the network structure [13]. Based on network topology, link prediction could also be divided into three research directions: local information, random walk, and path. In the link prediction of acupoint network, some features in the local information were selected. Although the link prediction was not based on node attributes, the essential information of attributes was not discarded. Instead, the information was converted into network weights, which was combined with network structure and machine learning in link prediction. In the weighted acupoint network that was constructed in the study, E was the set of all possible relationships between nodes, E_y was used to indicate that there existed edge in the network, and E_n was used to indicate that there did not exist edge in the network. The relationships of them were as follows: $E_y \cup E_n = E$, $E_y \cap E_n = \varnothing$. E_y was marked as a true positive sample, denoted by $y = 1$, and E_n was marked as a false negative sample, denoted by $y = 0$. And then, the compatibility of acupoints in clinical acupoint selection

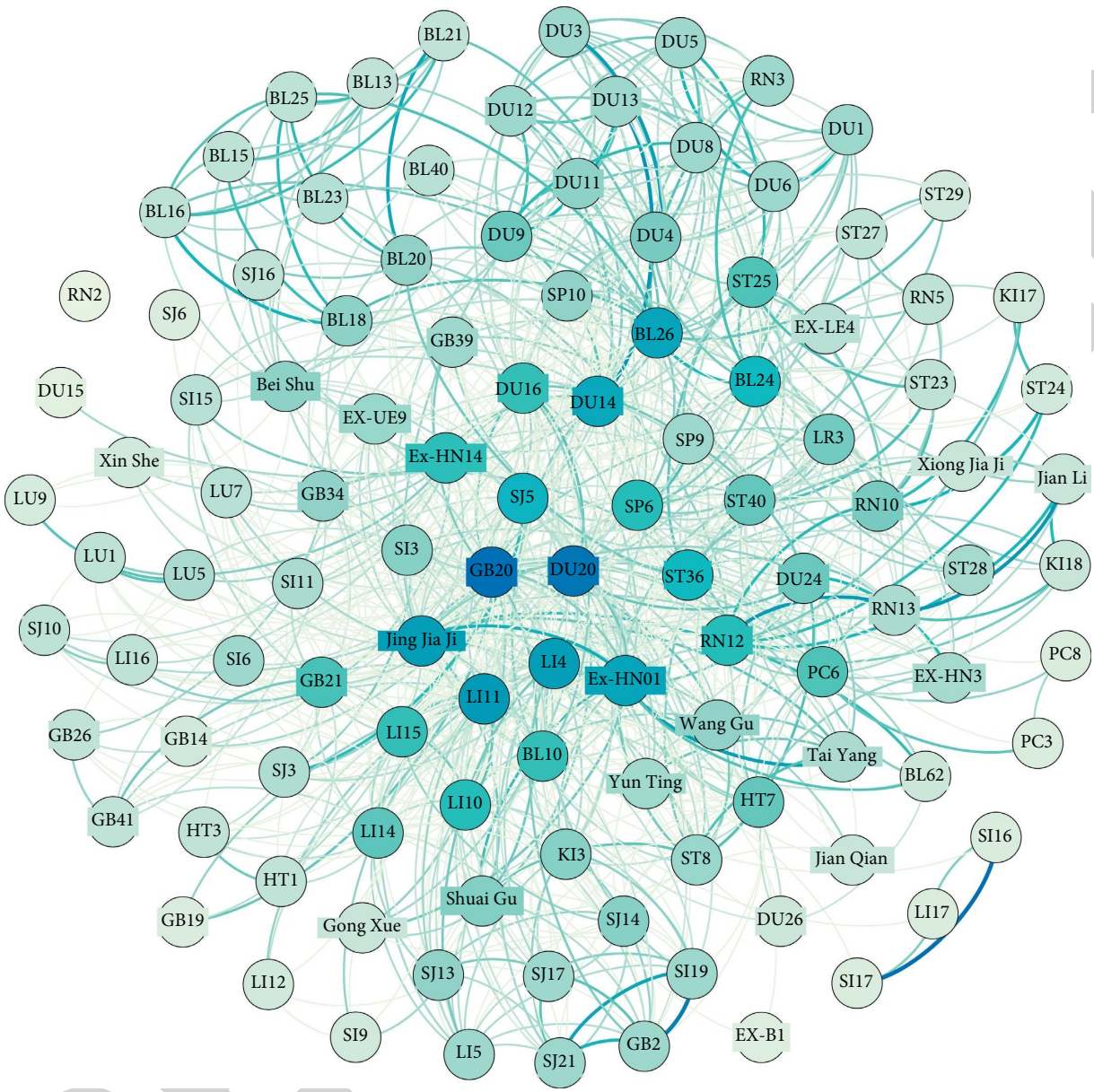

Figure 1: Network diagram of weighted acupoints.

Table 1: Attributes of acupoints.

Attributes	Number	Elements
Meridian	15	Large intestine meridian (LI), spleen meridian (SP), bladder meridian (BL), pericardium meridian (PC), stomach meridian (ST), conception vessel (CV), small intestine meridian (SI), kidney meridian (KI), lung meridian (LU), gallbladder meridian (GB), triple energizer meridian (TE), heart meridian (HT), liver meridian (LR), governor vessel (GV), extra point
Location	63	Region of oral cavity, toe, ear, knee, back of hand, ankle, sacrum, forearm, head, lateral abdomen, sole, lower abdomen, lateral neck, medial foot, lateral lower leg, medial lower leg, palm, posterior lower leg, anterior wrist, anterior femoral, chest, sternocleidomastoid muscle, inguinal, posterior elbow, umbilical cord, medial hand, anterior forearm, neck, waist, anterior arm, plantar, wrist, posterior arm, lateral thigh, upper lip, upper abdomen, anterior neck, posterior shoulder, forearm, buttocks, triangle muscle, abdomen, face, anterior knee, posterior wrist, palm, anterior shoulder
Indication	670	Contracture pain of leg and foot, pediatric acute wind, acute stomach pain, urinary incontinence, hiccup, elbow numbness, defecation, swelling and pain in the back of hand, lumbosacral pain, fatigue, gall, pain of elbow and arm, blurred vision, axillary swelling, dystocia, upper limb paralysis, arm soreness, pediatric umbilical wind, difficult urination, arm numbness, ulcers, skin itching, shoulder pain, insomnia, fever, palpitation, lower limb paralysis, lack of lactation, hemiplegia, belching, occipital neuralgia, eclipse, pulseless disease, crooked mouth, aphasia, biliary tract ascariasis, sores, addictive rash

was transformed. Link prediction in the network was transformed into a second kind problem in machine learning.

3.1. Similarity Index. Local similarity is widely used in link prediction studies for its simplicity, scalability, and competitive prediction accuracy. The link prediction algorithm based on local similarity indexes predicts the likelihood of future links between x and y by the degree of intersection of the common neighbors of network nodes x and y. Common Neighbor (CN), Adamic-Adar (AA), and Resource Allocation (RA) are three common neighbor-based similarity indexes and Preferential Attachment (PA) is a preference connection similarity index. In this paper, four weighted similarity indexes were extracted from the weighted acupoint network structure and the fused four weighted similarity indexes were defined as PI, PI = {WCN, WAA, WRA, WPA}.

3.2. Local Similarity

3.2.1. Weighted CN Index (WCN) [14]

$$s_{xy} = \sum_{z \in \Gamma(x) \cap \Gamma(y)} \frac{w_{xz} + w_{zy}}{2}, \tag{2}$$

where $\Gamma(x)$ and $\Gamma(y)$ indicated the set of neighbor nodes of x and y and w_{xz} indicated the weight between nodes of x and z; when all the weight values were 1, formula (2) was equivalent to the unweighted CN index.

3.2.2. Weighted AA Indicator (WAA) [14]

$$s_{xy} = \sum_{z \in \Gamma(x) \cap \Gamma(y)} \frac{w_{xz} + w_{zy}}{2 \log(1 + s_z)}, \tag{3}$$

where s_z was the strength of node z. The degree of common neighbor nodes was considered by WAA. The contribution of the common neighbor with low degree was greater than the common neighbor with high degree. For example, compared to the users who listened to popular songs, the users who listened to niche songs were more likely to establish connections in a music recommendation system.

3.2.3. Weighted RA Indicator (WRA) [15]

$$s_{xy} = \sum_{z \in \Gamma(x) \cap \Gamma(y)} \frac{w_{xz} + w_{zy}}{2 s_z}. \tag{4}$$

Nodes that were not directly connected in the network could transfer resources through common neighbors. In the process of transferring, the resources were allocated to neighbors equally according to the number of node neighbors. WRA was the number of resources finally received by the node.

3.3. Preference Connection Similarity. The weighted PA index (WPA) [16] indicated that the probability of establishing a connection between nodes was proportional to the product of the strength. And, the calculation formula is shown in

$$s_{xy} = \sum_{i \in \Gamma(x)} w_{ix} + \sum_{j \in \Gamma(y)} w_{jy} = s_x s_y. \tag{5}$$

3.4. Evaluation Index. Area under ROC Curve (AUC), precision, and ranking score (recall) were the three evaluation indicators that were often used to measure the accuracy of link prediction algorithms. In the research, multiple supervised learning models were combined to make link prediction. So that model was one of the main influencing factors of the results. Therefore, three types of evaluation indicators, including AUC, recall, and F1-score, were used in the article to make a comprehensive evaluation of the results.

3.4.1. AUC. In link prediction, an edge was randomly selected each time from the test set and the nonexistent edge set, and the fractional values of the two edges were compared. If the fractional value of edges in the test set is larger than that in the nonexistent edge set, 1 point will be added. If the fractional values are equal, 0.5 point will be added. The calculation formula is shown in formula (6), where n represented the number of independent comparisons, n' represented the number of times that the fractional value of edges in the test set was larger than that in nonexistent edge set, and n'' represented the number of times that the fractional values of the two sets were equal.

$$\text{AUC} = \frac{n' + 0.5n''}{n}. \tag{6}$$

3.4.2. Recall. Recall indicated the number of cases that True Positive (TP) samples were predicted to be TP. There existed the following two situations: TP samples were predicted to be TP, and TP samples were predicted to be False Negative (FN). The calculation formula is shown as

$$\text{recall} = \frac{TP}{TP + FN}. \tag{7}$$

3.4.3. F1-Score. F1-score was the harmonic average of precision and recall. The calculation formula is shown in formula (8). P represented precision and R represented recall. When $\alpha = 1$, the formula was used for the calculation of F1-score.

$$F = \frac{(\alpha^2 + 1)P * R}{\alpha^2 (P + R)}. \tag{8}$$

3.5. Supervised Learning. The main differences between supervised learning and unsupervised learning existed in data labels. Supervised learning, which is mainly used to solve regression and classification problems, predicts

unknown data with labeled data sets. The supervised learning algorithms that are commonly used are as follows: Support Vector Machine (SVM), Logistic Regression (LR), Multilayer Perception (MLP), k-Nearest Neighbor (KNN), Decision Tree (DT), and Adaptive Boosting (AdaBoost). Ying et al. [17] constructed three weighted disease networks derived from different medical data sets. The similarities were input as features into multiple supervised learning models to predict relationships of potential comorbidity. It was shown that the combination of global similarity features and supervised learning models could effectively improve the performance of the prediction algorithm. Zhao Sufen et al. [18] compared the application of 8 supervised learning algorithms on academic networks. The results showed that the performance of MLP was the best, and the performance of naive Bayes algorithm was the worst. The method of KNN was only better than naive Bayes. And the performance of other algorithms was almost the same. Considering the existed researches, four common algorithms were used in the study, including MLP, SVM, DT, and AdaBoost for link prediction of weighted acupoint networks. The steps of link prediction based on similarity features were divided into the following three steps.

The first step was data standardization. The similarity indexes extracted from the network were converted into a feature matrix. Due to the different dimensions of the matrix data, the matrix was standardized by Min-Max, and the data were linearly transformed. The data value was normalized from 0 to 1 to eliminate the impact of imbalance in proportion.

The second step was data balance. In the distribution of data categories, the ratio of TP to FN in the data set was 12 : 1. And there existed a typical data imbalance problem, which would cause the model prediction to be biased towards the side with a large sample size and would reduce the generalization ability of the model. So that the method of undersampling was adopted in the FN to achieve data balance in order to obtain 1 : 1 ratio of TP to FN.

The third step was model training. The data set was divided into training set and test set. Four supervised learning models were input in the training set for training. Finally, the test set was input to verify the results.

4. Results and Analysis

4.1. Experimental Setup. Based on the Jupyter notebook platform, Pandas and NumPy were used in the experiment to preprocess the data, NetworkX was used to build a weighted acupoint network. Four single similarity indexes and one fusion index were chosen as feature input to the supervised learning model, and the four models, MLP, SVM, DT, and AdaBoost, called by the scikit-learn (sklearn) package, were used to predict the similarity indexes and models in a two-by-two combination. RBF kernel function was selected and used in SVM model, and the parameters in the rest of the models were all default settings. The three evaluation indexes, AUC, recall, and F1-score, were chosen to evaluate the performance of the link prediction algorithm. In order to improve the accuracy of the results, ten-fold cross-validation was used to divide the data set, and the average value of ten times output was selected as the final result. And the three evaluation indicators were compared to evaluate the performance of the link prediction algorithm. The overall flow chart of the experiment is shown in Figure 2.

4.2. Experimental Results. The similarity indices were applied on the weighted acupoint network to evaluate the performance of various algorithms. The results are shown in Figures 3–5. AUC value was the standard for evaluating the predictive ability of the model. As shown in Figure 3, based on the similarity index, the AUC values predicted by each model were in the range from 0.5 to 1. The prediction accuracy of the model was better than random guessing and had predictive value. The top three values of AUC were 0.9351 (PI + MLP), 0.9312 (WRA + MLP), and 0.9306 (PI + AdaBoost). Compared to other models, the performance of MLP model was the best in the weighted acupoint network. Combined with PI indicators, the forecast accuracy was improved significantly. Recall was used to calculate the number of the correct predictions of TP samples. Compared with the accuracy rate, the weighted acupoint network research paid more attention to recall. That is, the fewer prediction errors, the better performance. As shown in Figure 4, the top three values of recall ranking were 0.9209 (WCN + AdaBoost), 0.9085 (WAA + SVM), and 0.8981 (WAA + MLP, PI + MLP). Combining the similarity indices, the performance of AdaBoost, SVM, and MLP was good. The combination of DT with WRA was relatively good. However, the performance of DT combined with other indicators was worse than other models. In particular, the recall value of combination of DT and WPA was the lowest, which reflected the fact that DT model was not suitable in the weighted acupoint network. F1-score was the harmonic average of precision and recall, which was the comprehensive manifestation of the two indicators. As shown in Figure 5, the top three F1-score values were as follows: 0.8757 (PI + MLP), 0.8731 (WRA + SVM), and 0.8713 (WRA + MLP). The combination of WRA index and the four models performed well, which reflected the fact that the stability of WRA index was relatively strong. The experimental results showed that there existed differences in the performance of different similarity indices applied to different models. From the similarity indices, rank of stability was as follows: WRA > WAA > PI > WCN > WPA; predictive performance: PI > WRA > WAA > WCN > WPA. Combining a single similarity index and a fusion similarity index, the prediction performance was not proportional to the number of fusion indices. And there existed a phenomenon that a single index had a negative effect on the fusion index. For example, in a weighted acupoint network, WPA affected the stability of PI. From the perspective of the supervised learning model, MLP, AdaBoost, and SVM showed good adaptability and stability in the weighted acupoint network, especially the combination of MLP and PI, which achieved the maximum value in AUC and F1-score. Combining the performance of similarity indices, PI was selected to combine with four models for the evaluation of performance. As shown in Figure 6, MLP performance was

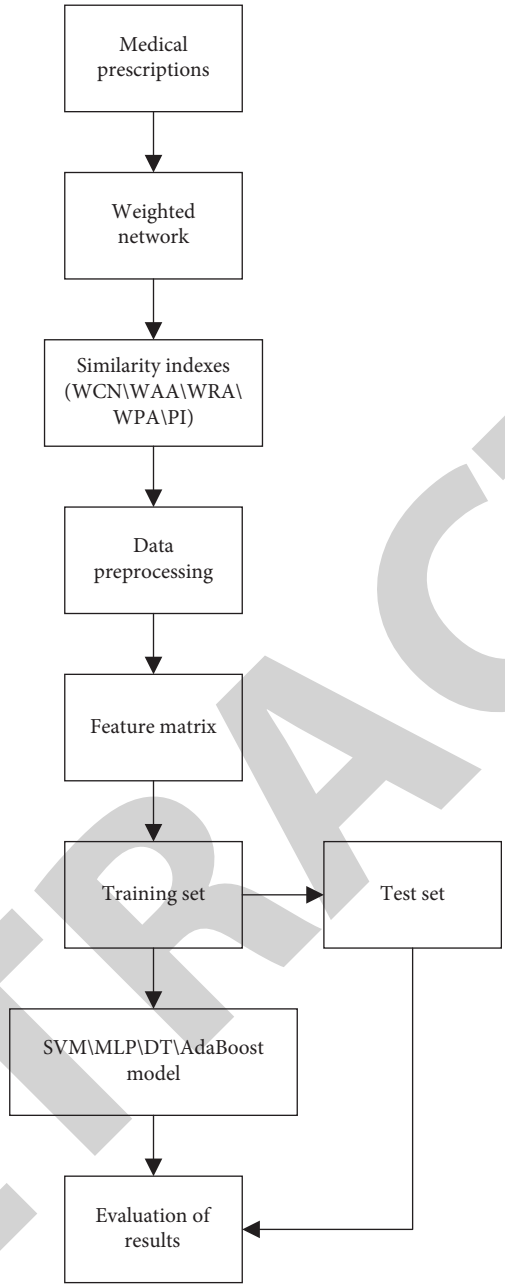

Figure 2: Experimental flowchart.

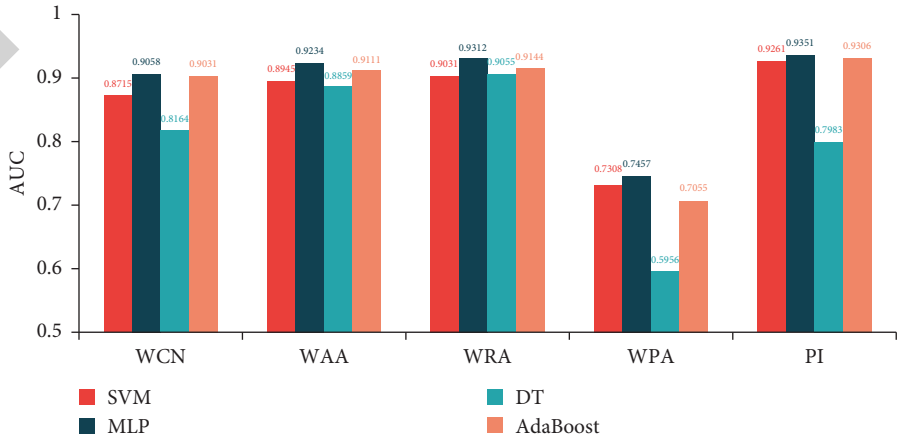

Figure 3: Forecasting performance of the combination of indicators and models (AUC).

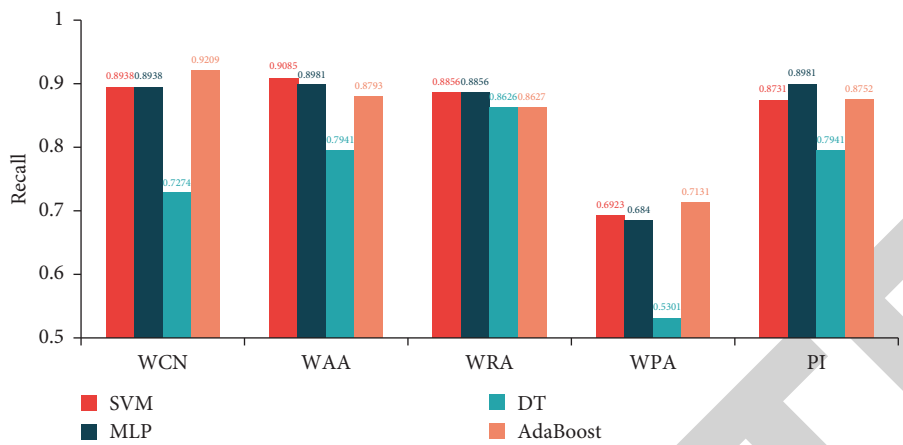

Figure 4: Forecasting performance of the combination of indicators and models (recall).

Figure 5: Forecasting performance of the combination of indicators and models (F1-score).

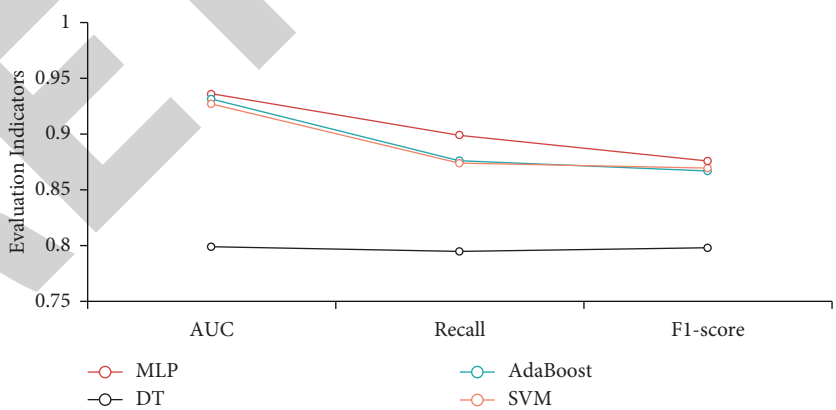

Figure 6: Forecasting performance based on PI indicators.

stable and was the best, AdaBoost and SVM were the second, and the indicators of DT were much lower than the other three models.

In summary, in the weighted acupoint network, it is a priority to select PI, WRA, and WAA indicators as similarity indices, and it is a priority to select MLP, AdaBoost, and SVM models as supervised learning models.

5. Conclusion

This paper proposes a weighted acupoint network construction method that incorporates the intrinsic and functional properties of acupoints and quantifies the closeness of the links between acupoints through the weight values. The link prediction experiments involved 481 combinations of

Hindawi
Journal of Healthcare Engineering
Volume 2023, Article ID 9825735, 1 page
https://doi.org/10.1155/2023/9825735

Retraction

Retracted: Self-Attention-Guided Recurrent Neural Network and Motion Perception for Intelligent Prediction of Chronic Diseases

Journal of Healthcare Engineering

Received 10 October 2023; Accepted 10 October 2023; Published 11 October 2023

This article has been retracted by Hindawi following an investigation undertaken by the publisher [1]. This investigation has uncovered evidence of one or more of the following indicators of systematic manipulation of the publication process:

(1) Discrepancies in scope
(2) Discrepancies in the description of the research reported
(3) Discrepancies between the availability of data and the research described
(4) Inappropriate citations
(5) Incoherent, meaningless and/or irrelevant content included in the article
(6) Peer-review manipulation

The presence of these indicators undermines our confidence in the integrity of the article's content and we cannot, therefore, vouch for its reliability. Please note that this notice is intended solely to alert readers that the content of this article is unreliable. We have not investigated whether authors were aware of or involved in the systematic manipulation of the publication process.

In addition, our investigation has also shown that one or more of the following human-subject reporting requirements has not been met in this article: ethical approval by an Institutional Review Board (IRB) committee or equivalent, patient/participant consent to participate, and/or agreement to publish patient/participant details (where relevant).

Wiley and Hindawi regrets that the usual quality checks did not identify these issues before publication and have since put additional measures in place to safeguard research integrity.

We wish to credit our own Research Integrity and Research Publishing teams and anonymous and named external researchers and research integrity experts for contributing to this investigation.

The corresponding author, as the representative of all authors, has been given the opportunity to register their agreement or disagreement to this retraction. We have kept a record of any response received.

References

[1] B. Ma, F. Zhang, and B. Ma, "Self-Attention-Guided Recurrent Neural Network and Motion Perception for Intelligent Prediction of Chronic Diseases," *Journal of Healthcare Engineering*, vol. 2021, Article ID 6382619, 7 pages, 2021.

Hindawi
Journal of Healthcare Engineering
Volume 2021, Article ID 6382619, 7 pages
https://doi.org/10.1155/2021/6382619

Research Article

Self-Attention-Guided Recurrent Neural Network and Motion Perception for Intelligent Prediction of Chronic Diseases

Baojuan Ma,[1] Fengyan Zhang,[1] and Baoling Ma[2]

[1]*Physical Education Department, Shijiazhuang Information Engineering Vocational College, Shijiazhuang 05000, Hebei, China*
[2]*Physical Education and Health College, Hebei Normal University of Science and Technology, Qinhuangdao 066004, Hebei, China*

Correspondence should be addressed to Fengyan Zhang; zhangfengyan202103@126.com

Received 28 August 2021; Revised 14 September 2021; Accepted 16 September 2021; Published 27 October 2021

Academic Editor: Gu Xiaoqing

Parkinson's disease is a common chronic disease that affects a large number of people. In the real world, however, Parkinson's disease can result in a loss of physical performance, which is classified as a movement disorder by clinicians. Parkinson's disease is currently diagnosed primarily through clinical symptoms, which are highly dependent on clinician experience. As a result, there is a need for effective early detection methods. Traditional machine learning algorithms filter out many inherently relevant features in the process of dimensionality reduction and feature classification, lowering the classification model's performance. To solve this problem and ensure high correlation between features while reducing dimensionality to achieve the goal of improving classification performance, this paper proposes a recurrent neural network classification model based on self attention and motion perception. Using a combination of self-attention mechanism and recurrent neural network, as well as wearable inertial sensors, the model classifies and trains the five brain area features extracted from MRI and DTI images (cerebral gray matter, white matter, cerebrospinal fluid density, and so on). Clinical and exercise data can be combined to produce characteristic parameters that can be used to describe movement sluggishness. The experimental results show that the model proposed in this paper improves the recognition performance of Parkinson's disease, which is better than the compared methods by 2.45% to 12.07%.

1. Introduction

Parkinson's disease (PD) [1, 2] is the second most common chronic central nervous system disease in the elderly population [3–5]. The loss of neuronal function is the most noticeable feature, and it has a significant impact on a person's motor function. In practice, this symptom affects a higher percentage of the elderly, and those over the age of 60 are more susceptible to the disease, with the proportion of patients under the age of 40 being relatively low. The treatment cycle of this disease is very long, and there is still a lack of very effective treatment methods [6]. Therefore, it will bring serious negative effects to the patient's family harmony and the stable operation of the society. Therefore, in order to better solve this problem, the initial auxiliary diagnosis [7, 8] of patients has very important practical significance.

There is currently no reliable method for detecting early-stage Parkinson's disease [9]. Most patients do not seek medical help in a timely manner and are unaware of the disease's existence due to a lack of comprehensive knowledge about Parkinson's disease. The symptoms of Parkinson's disease are frequently misdiagnosed as signs of aging. Parkinson's disease has a 60 percent delayed treatment rate due to a lack of early intervention and treatment [10]. Parkinson's disease is currently diagnosed primarily through clinical symptoms, which are highly dependent on clinician experience. As a result, there is a need for effective early detection methods.

Neuroimaging technology [11–14] is frequently used to quantify the loss of neurons in different areas of the brain to achieve the goal of detecting PD in order to better diagnose early PD. Magnetic resonance imaging (MRI) [15–18], functional magnetic resonance imaging (fMRI), and

positron emission computed tomography (PET) [19] are some of the most commonly used neuroimaging technologies. PET has the disadvantages of low spatial resolution and high cost, while the other two imaging technologies are radioactive while in use. As a result, doctors will need a noninvasive, high-resolution method to track the progression, progression, and treatment of neurodegenerative diseases. According to current research, MRI has the advantages of high spatial resolution, noninvasiveness, low cost, and wide availability and can be used for the diagnosis of PD.

The application of artificial intelligence [20–22] in many fields has been confirmed with the development of machine learning [23–25]. More research [26–28] is currently focusing on proposing advanced machine learning technologies to solve practical applications [29]. Artificial intelligence also has a large market and potential in the medical field. Medical image recognition, for example, can assist doctors in reading patient images more quickly and accurately. Medical services such as clinical diagnosis assistant systems, for example, are used in early screening and diagnosis, rehabilitation, and surgery risk assessment scenarios, among other things. Therefore, the use of MRI images and machine learning algorithms to detect early PD is very promising. Recently, domestic and foreign scholars have proposed a method of combining brain images and machine learning to achieve the purpose of automatically predicting and evaluating the pathological stage, and there are many studies on PD. However, most of these algorithms only classify PD and normal control group. There are not many auxiliary diagnosis algorithms for early PD, and the accuracy of the classification algorithm for early PD and normal control group has room for improvement at this stage. Therefore, the research of efficient and accurate PD early feature selection and classification algorithms is of great significance to realize the early diagnosis of PD.

Furthermore, a common Parkinson's disease dyskinesia symptom is bradykinesia, and it is important symptom for determining the disease's diagnosis. Bradykinesia is a symptom of Parkinson's disease that affects nearly all patients and interferes with their daily activities, and it is drug-sensitive. The most common clinical manifestations are slow movement, difficulty moving, and loss of active movement ability. Motor retardation in the upper limbs can make it difficult to control fine daily activities such as typing, writing, and buttoning buttons with the hands. In the lower extremities, slow motion usually causes the foot to drag on the ground. In severe cases, it can lead to a panic and freezing gait (freezing is manifested as a sudden and short-term inability to move). The freezing gait is the most common cause of falls and increases significantly. It increases the risk of hip fracture. Other symptoms of motor retardation include decreased spontaneous movement, dysphagia, salivation, speech disorders, decreased facial expressions, decreased blinking, and decreased arm swing when walking. The evaluation of bradykinesia usually involves the patient performing repetitive, rapid, and alternating movements. Commonly used movements include finger tapping, hand clenching, hand pronation-supination, and heel up. This article is based on the wearable inertial measurement unit to carry out an objective quantitative assessment of the symptoms of bradykinesia, which can assist doctors in diagnosing Parkinson's disease and help reduce the medical costs of patients, thereby reducing the burden on patients and their families.

The main contributions of this article are as follows:

(1) This paper proposes a novel intelligent predictive analysis model for chronic diseases based on self-attention-guided recurrent neural networks and motion perception, which is crucial for achieving early diagnosis of Parkinson's disease.

(2) To classify and train the five brain region features extracted from MRI and DTI images, the proposed model employs a combination of self-attention mechanisms and recurrent neural networks. At the same time, it collects clinical data and motion data using wearable inertial sensors that can be worn on the body. The data are used to extract the characteristic parameters that can be used to characterize slow motion.

The following is how the rest of the paper is organized. Section 2 examines some related work. In Section 3, some details about the proposed algorithm's principles and related submodules are presented. The experimental results are detailed in Section 4. In Section 5, the study's conclusion is presented.

2. Background

With the increasing incidence of Parkinson's disease, the problem of early PD detection has gradually become a new research hotspot that has attracted much attention in recent years. It belongs to the category of human activity recognition and is closely related to disciplines such as engineering, sports mechanics, and neuroscience. Some scholars have carried out a series of work on the extraction of physiological characteristics, motion characteristics, and the design of detection algorithms. In terms of feature extraction, the motion characteristics of PD patients have the following characteristics: (1) the stride length gradually decreases; (2) the joint range of the hip, knee, and ankle joints is greatly reduced; (3) the disordered time of the gait cycle control; (4) high-frequency alternating trembling leg movements.

Although there have been some studies using motion sensors to detect PD, the research work of many scholars is mainly focused on feature extraction and algorithm design. There are few studies on how to achieve the most effective system design, that is, to select the optimal sensor type, number, and deployment location. Considering the cost of deployment, a trade-off must be made between installing the least number of sensors and collecting the most information. Most studies use a single three-axis accelerometer, or combine it with a gyroscope, or combine it with a magnetometer to detect PD. Regarding the position where the patient wears the sensor, most studies use only one position. The tibia and waist are the most common placement

locations for sensors. The rest include feet, knees, thighs, wrists, forearms, pants pockets, belly button, chest, and scalp. In addition, although many scholars have used machine learning algorithms to automatically identify PD, they have not discussed some important parameters that affect model performance and efficiency, such as the ratio of frozen gait to normal gait sample size in the training set and the size of the time window. Since frozen gait is difficult to collect sample size compared to normal gait, how to balance the ratio of the two to obtain the best classifier becomes a research focus of this article.

In addition, in the clinical setting, MRI diagnoses PD by evaluating structural and functional abnormalities. In order to achieve high-precision diagnosis, people try to design a computer-aided decision support system to realize automatic analysis of medical images. Extracting clinically relevant features from these images and helping to distinguish different disease categories is the key to achieving high classification accuracy. With the development of machine learning and data-driven analysis, the application of artificial intelligence in many fields has been affirmed. In the medical field, artificial intelligence also has huge potential and market. For example, medical image recognition helps doctors read patient images faster and more accurately and is effectively used in early screening, diagnosis, and surgical risk assessment. Recently, scholars at home and abroad have proposed a large number of studies using brain images and machine learning to automatically predict and evaluate pathological stages.

Recognizing healthy people or PD patients from subject images is a binary classification problem, which is very suitable for the implementation of machine learning (ML) technology. Medical data sets contain incomplete, inaccurate, and sparse information, so for the classification of these data, machine learning plays a vital role. With the rise of big data and artificial intelligence, neuroimaging classification methods increasingly use machine learning-related algorithms. These technologies can automatically extract a lot of information from the image set without preassuming the location of the information in the image. Many studies have evaluated the diagnostic value of these technologies, such as the diagnosis of Alzheimer's disease and mild cognitive impairment and have shown good research results. There is currently a study using supervised machine learning to perform individual differential diagnosis of PD and PSP on MRI, which is based on the combination of PCA and SVM with feature extraction technology. The current machine learning algorithms used for PD diagnosis mainly include principal component analysis, linear discriminant analysis, and nonnegative matrix factorization. Usually, these features are input into algorithms based on supervised learning, such as support vector machines (SVM) for feature classification.

3. Methodology

3.1. Feature Extraction. Generally speaking, brain image data have the characteristics of high dimension and relatively limited sample, which leads to the decline of the performance of decision model. Therefore, dimensionality reduction is needed for feature data. Dimension reduction is a preprocessing method for high-dimensional feature data, which preserves some important features of high-dimensional data and removes noise and unimportant features, so as to achieve the purpose of enhancing data processing efficiency. PCA and LDA are the most commonly used dimensionality reduction methods in Parkinson's disease classification algorithms. The feature of PCA is that the extracted features can accurately represent the sample information, so that the loss of information is very small. The feature of LDA is the feature after feature extraction. The accuracy of classification results should be high, which cannot be lower than that of the original feature classification. According to the characteristics of brain images, this study only needs to extract the best feature matrix with high correlation to reduce the dimension, so the PCA feature extraction method is adopted in this study.

3.2. Motion Data Collection Based on Inertial Sensors. To obtain effective PD personnel slow motion sample data, it is necessary to design a detailed and complete experimental data collection plan prior to data collection in order to ensure the smooth progress of the experiment. The experiment plan includes the experimental task design, experimental site design, experimental collection equipment and wearing parts, and object screening, as well as sample object design and data collection.

3.2.1. Design of the Acquisition System. Fingers, wrists, waist, thighs, and ankles are the most common motion signals captured by the slow motion signal acquisition system. The signal collection system consists of a collection module with inertial sensors integrated. Velcro straps secure all collection modules to both hands' index and thumb fingers, wrists, thighs, ankles, and waist. The inertial sensors are worn in the positions as shown in Figure 1.

3.2.2. Wearable Device Design. The acquisition module is mainly used to acquire the three-dimensional motion information of the human body. This research selects two inertial sensors as the acquisition module according to the different wearing positions. The sampling frequency of all the acquisition modules is 100 Hz.

The LPMS-B2 sensor from Japan's LP-RESEARCH company is used in the body node. A three-axis acceleration sensor, a three-axis gyroscope, and a three-axis magnetometer are all integrated into the sensor, allowing it to calculate the sensor's attitude direction and linear acceleration in real time. The low-power Bluetooth 4.1 (BLE) wireless transmission is used, and the on-board memory is 32M. The measured motion signal can be recorded in real time.

3.3. Recurrent Neural Network. Recurrent neural network (RNN) refers to a structure that recurs over time. It is widely used in many fields such as natural language processing and speech and image. The biggest difference between the RNN network and other networks is that RNN can achieve a certain "memory function" and is the best choice for time

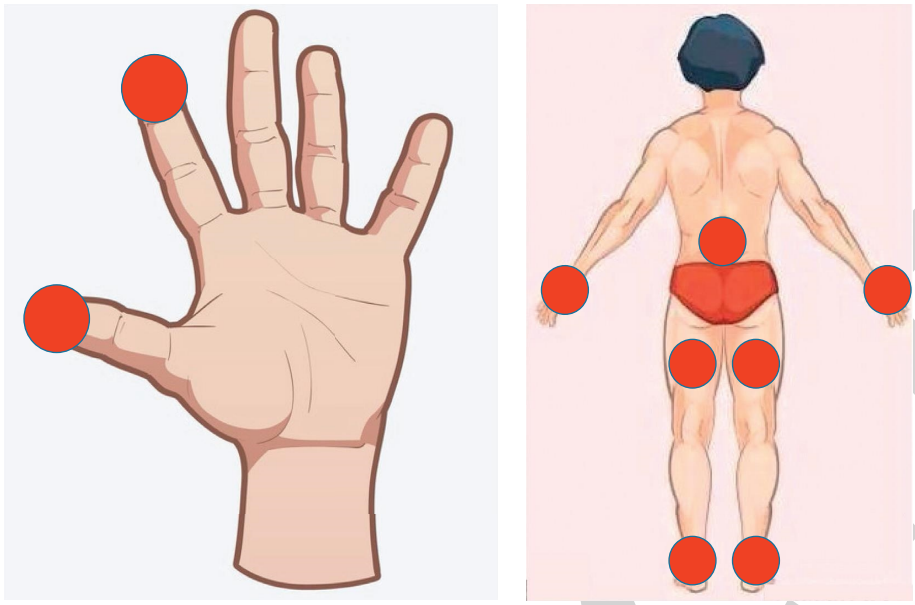

Figure 1: Schematic diagram of the inertial sensor wearing position.

series analysis, just as human beings can better understand the world with their own past memories. RNN also implements this mechanism similar to the human brain, which retains a certain amount of memory for processed information, unlike other types of neural networks that cannot retain memory for processed information.

We can see the parameters in the RNN network from Figure 2. Here, only the behavior and mathematical derivation of the network at time t are analyzed. At time t, the network ushered in an input x_t and the neuron state s_t of the network at this time is expressed by the following equation:

$$s_t = \varphi(Ux_t + Ws_{t-1}). \tag{1}$$

The network state s_t at time t is not only input to the network state at the next time $t+1$ but also the network output at that time. Of course, s_t cannot be output directly, and a coefficient V must be multiplied before output, and for the convenience of error back propagation, the output is usually normalized, that is, the output is softmaxed. Therefore, the output o_t equation of the network at time t is as follows:

$$o_t = \phi(Vs_t). \tag{2}$$

Then,

$$\begin{cases} s_t^* = Ux_t + Ws_{t-1} \longrightarrow s_t = \varphi(s_t^*), \\ o_t^* = Vs_t \longrightarrow o_t = \varphi(o_t^*). \end{cases} \tag{3}$$

The loss function of RNN selects cross entropy, and its calculation equation is as follows:

$$L = -\sum_{i=0}^{n} y_i \ln\ y_i^*, \tag{4}$$

where y_i is the true label value and y_i^* is the predicted value given by the model. Since the RNN model deals with the sequence problem, its model loss can not only be the loss of one moment but also should include the loss of all N moments. Therefore, the calculation equation of the loss function of the RNN model at time t is as follows:

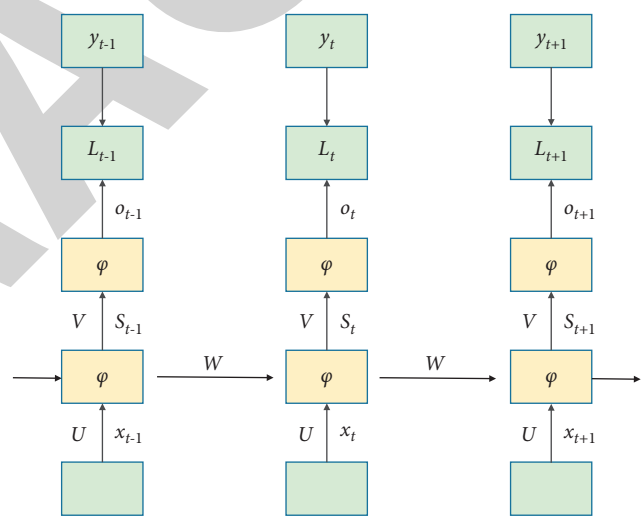

Figure 2: Schematic diagram of RNN structure.

$$L_{s_t} = -[y_t \ln(o_t) + (y_t - 1)\ln(1 - o_t)]. \tag{5}$$

Then, the calculation equation of the global loss for all N moments is as follows:

$$L = \sum_{t=1}^{N} L_{s_t} = -\sum_{t=1}^{N} [y_t \ln(o_t) + (y_t - 1)\ln(1 - o_t)]. \tag{6}$$

3.4. Self-Attention Mechanism. The attention mechanism is modeled after the internal process of the biological observational behavior, which aligns internal experience with

external sensation to increase the fineness of observation in some areas. Because it can quickly extract the important features of sparse data, the attention mechanism is widely used in natural language processing tasks, particularly in machine translation. The self-attention mechanism is an enhancement of the attention mechanism that reduces reliance on external information and improves the ability to capture the internal correlation between numbers and features.

As shown in Figure 3, the essence of the attention function can be described as a mapping from a query to a series of (key value) pairs. In general, a self-attention module has input n and output n. The self-attention mechanism allows the inputs to interact with each other and find areas where they should pay more attention. The output is the sum of these interactions and attention scores. The calculation equation of self attention is as follows:

$$A(Q, K, V) = \text{soft max}\left(\frac{QK^T}{\sqrt{d_k}}\right)V. \tag{7}$$

3.5. Proposed Prediction Model. As shown in Figure 4, this paper proposes a smart predictive analysis model for chronic diseases based on self-attention-guided recurrent neural networks and motion perception. The self-attention mechanism layer is added to the RNN in this study, which helps the classification algorithm pay more attention to the internal correlation of its own characteristics. Simultaneously, it collects clinical data and sports data using wearable inertial sensors, which can extract sports data to characterize sluggishness.

4. Experiments

4.1. Parameter Settings. All algorithm experiments are carried out on a computer with a single NVIDIA GTX1080 GPU (8 GB). The model was built using the TensorFlow deep learning library. Python 3.6.5 is the programming language we use, and 200 samples are processed in batches each time. In addition, the specific parameters are shown in Table 1.

4.2. Dataset. The data used in this article comes from Parkinson's Progression Markers Initiative (PPMI) database. PPMI is the first global collaborative project composed of researchers, funders, and research participants, dedicated to identifying biomarkers to improve the treatment of Parkinson's disease. They are committed to establishing standardized protocols for data acquisition and analysis to promote a comprehensive understanding of PD.

4.3. Evaluation Index. This article uses precision, accuracy (ACC), F1 value, recall, and AUC (area under curve) as the criteria for evaluating the pros and cons of the classification results. Their calculation equations are as follows:

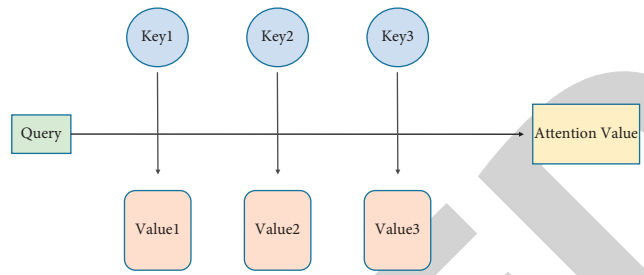

Figure 3: Schematic diagram of attention mechanism.

$$\begin{aligned} \text{precision} &= \frac{\text{TP}}{\text{TP} + \text{FP}}, \\ \text{recall} &= \frac{\text{TP}}{\text{TP} + \text{FN}}, \\ \text{ACC} &= \frac{\text{TP} + \text{TN}}{\text{TP} + \text{TN} + \text{FP} + \text{FN}}, \\ F1 &= \frac{2\text{TP}}{2\text{TP} + \text{FP} + \text{FN}}, \end{aligned} \tag{8}$$

where TP, TN, FP, and FN represent the positive samples with correct judgments, the negative samples with correct judgments, the positive samples with wrong judgments, and the negative samples with wrong judgments, respectively.

4.4. Experimental Results. Table 2 shows the PD identification prediction results. It can be seen from the table that the recall rate and F1 value of the proposed algorithm are 71.25% and 83.99%, respectively, which are superior to other algorithms in these indicators. The classification accuracy and specificity of CNN are both 89.23%, which is higher than the other three classifiers. As a result of ACC performance, we reached 93.55%. In this comparison, it is not difficult to find that the ACC of SVM, MPL, LR, and ELM is generally higher than that of CNN, but the F1 value is generally lower than these two deep learning algorithms. This may be caused by an unbalanced relationship in the PD data sample, so ACC cannot be considered unilaterally, and the F1 value should be combined as a measurement standard. Considering the F1 value, ACC, and other values comprehensively, it can be found that the proposed model is better than other methods in overall performance.

4.5. Ablation Experiment for Self Attention. In order to further prove the effectiveness of self-attention, we added the ablation experiment of self-attention. "No-self-attention" represents the absence of self-attention mechanism, and "self-attention" represents the use of self-attention mechanism. The ablation experiment results are shown in Table 3.

It can be seen from Table 3 that self-attention is better than no-self-attention in the four evaluation methods. This proves the effectiveness of the self-attention mechanism in the proposed algorithm.

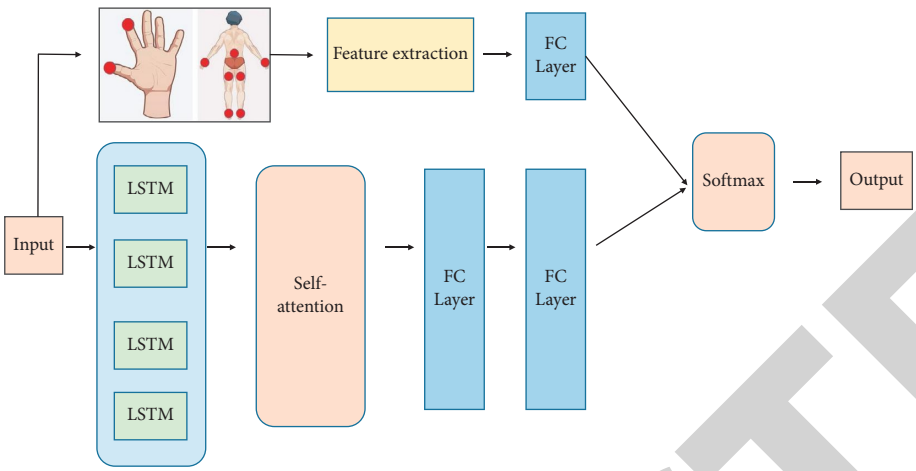

Figure 4: Schematic diagram of attention mechanism.

Table 1: Hyperparameter setting.

Type	Hyperparameter
Adam	lr = 0.0001 bata_1 = 0.99 bata_2 = 0.999 Epsilon = 1e-08 Decay = 3e-8

Table 2: Comparison of prediction results of different algorithms.

Methods	Precision	Recall	F1	ACC
SVM	49.36	52.36	51.23	89.12
MLP	61.21	62.35	69.33	91.25
ELM	45.58	52.36	58.78	90.23
CNN	89.23	69.26	81.25	82.25
Ours	92.36	71.25	83.99	93.55

Table 3: Results of self-attention ablation experiments.

Methods	Precision	Recall	F1	ACC
No-self-attention	91.11	70.87	79.58	92.58
Self-attention	92.36	71.25	83.99	93.55

5. Conclusion

In this paper, we propose a new type of recurrent neural network classification model based on self-attention mechanism and motion perception to improve the performance of Parkinson's chronic disease recognition and prediction. This model uses a self-attention mechanism and a cyclic neural network to categorize and train the five brain area features retrieved from MRI and DTI images (cerebral gray matter, white matter, cerebrospinal fluid density, and so on). It also uses wearable inertial sensors to gather clinical data, and the motion data can be used to identify characteristic properties that describe slow motion. The findings of the experiments suggest that the self-attention mechanism and the LSTM sequence module successfully improve Parkinson's disease recognition skills.

Data Availability

The data used to support the findings of this study are available from the corresponding author upon request.

Conflicts of Interest

All the authors do not have any possible conflicts of interest.

References

[1] C. Blauwendraat, M. A. Nalls, and A. B. Singleton, "The genetic architecture of parkinson's disease," *The Lancet Neurology*, vol. 19, no. 2, pp. 170–178, 2020.

[2] C. Raza, R. Anjum, and N. U Shakeel, "Parkinson's disease: mechanisms, translational models and management strategies," *Life Sciences*, vol. 226, pp. 77–90, 2019.

[3] M. Lemstra, C. Nwankwo, Y. Bird, and J. Moraros, "Primary nonadherence to chronic disease medications: a meta-analysis," *Patient Preference and Adherence*, vol. 12, pp. 721–731, 2018.

[4] R. Reynolds, S. Dennis, I. Hasan et al., "A systematic review of chronic disease management interventions in primary care," *BMC Family Practice*, vol. 19, no. 1, pp. 11–13, 2018.

[5] D. Jain and V. Singh, "Feature selection and classification systems for chronic disease prediction: a review," *Egyptian Informatics Journal*, vol. 19, no. 3, pp. 179–189, 2018.

[6] J. A. Lee, M. Choi, S. A. Lee, and N. Jiang, "Effective behavioral intervention strategies using mobile health applications for chronic disease management: a systematic review," *BMC Medical Informatics and Decision Making*, vol. 18, no. 1, pp. 12–18, 2018.

[7] D. Gao, X. Chen, H. Wu, H. Wei, and J. Wu, "The levels of serum pro-calcitonin and high-sensitivity C-reactive protein in the early diagnosis of chronic obstructive pulmonary disease during acute exacerbation," *Experimental and therapeutic medicine*, vol. 14, no. 1, pp. 193–198, 2017.

[8] P. T. Garcia, A. A. Dias, J. A. C. Souza, and W. K. T. Coltro, "Batch injection analysis towards auxiliary diagnosis of periodontal diseases based on indirect amperometric detection of salivary α-amylase on a cupric oxide electrode," *Analytica Chimica Acta*, vol. 1041, pp. 50–57, 2018.

[9] L. Parisi, N. RaviChandran, and M. L. Manaog, "Feature-driven machine learning to improve early diagnosis of

Hindawi
Journal of Healthcare Engineering
Volume 2023, Article ID 9845616, 1 page
https://doi.org/10.1155/2023/9845616

Retraction

Retracted: Heart Disease Prediction Based on the Embedded Feature Selection Method and Deep Neural Network

Journal of Healthcare Engineering

Received 5 December 2023; Accepted 5 December 2023; Published 6 December 2023

This article has been retracted by Hindawi, as publisher, following an investigation undertaken by the publisher [1]. This investigation has uncovered evidence of systematic manipulation of the publication and peer-review process. We cannot, therefore, vouch for the reliability or integrity of this article.

Please note that this notice is intended solely to alert readers that the peer-review process of this article has been compromised.

Wiley and Hindawi regret that the usual quality checks did not identify these issues before publication and have since put additional measures in place to safeguard research integrity.

We wish to credit our Research Integrity and Research Publishing teams and anonymous and named external researchers and research integrity experts for contributing to this investigation.

The corresponding author, as the representative of all authors, has been given the opportunity to register their agreement or disagreement to this retraction. We have kept a record of any response received.

References

[1] D. Zhang, Y. Chen, Y. Chen et al., "Heart Disease Prediction Based on the Embedded Feature Selection Method and Deep Neural Network," *Journal of Healthcare Engineering*, vol. 2021, Article ID 6260022, 9 pages, 2021.

Hindawi
Journal of Healthcare Engineering
Volume 2021, Article ID 6260022, 9 pages
https://doi.org/10.1155/2021/6260022

Research Article

Heart Disease Prediction Based on the Embedded Feature Selection Method and Deep Neural Network

Dengqing Zhang,[1,2] Yunyi Chen,[3] Yuxuan Chen,[3] Shengyi Ye,[1,2] Wenyu Cai,[1,2] Junxue Jiang,[1,2] Yechuan Xu,[1,2] Gongfeng Zheng,[1,2] and Ming Chen[1,4]

[1]*Jinjiang Hospital Affiliated to Fujian Medical University, Fujian, Jinjiang 362200, China*
[2]*Department of Cardiology, Jinjiang Hospital of Fujian Province, Fujian, Jinjiang 362200, China*
[3]*School of Informatics Xiamen University, Xiamen University, Fujian, Xiamen 361000, China*
[4]*Department of Public Health, Jinjiang Hospital of Fujian Province, Fujian, Jinjiang 362200, China*

Correspondence should be addressed to Ming Chen; 289975884@qq.com

Received 21 August 2021; Revised 7 September 2021; Accepted 16 September 2021; Published 29 September 2021

Academic Editor: Gu Xiaoqing

In recent decades, heart disease threatens people's health seriously because of its prevalence and high risk of death. Therefore, predicting heart disease through some simple physical indicators obtained from the regular physical examination at an early stage has become a valuable subject. Clinically, it is essential to be sensitive to these indicators related to heart disease to make predictions and provide a reliable basis for further diagnosis. However, the large amount of data makes manual analysis and prediction taxing and arduous. Our research aims to predict heart disease both accurately and quickly through various indicators of the body. In this paper, a novel heart disease prediction model is given. We propose a heart disease prediction algorithm that combines the embedded feature selection method and deep neural networks. This embedded feature selection method is based on the LinearSVC algorithm, using the L1 norm as a penalty item to choose a subset of features significantly associated with heart disease. These features are fed into the deep neural network we built. The weight of the network is initialized with the He initializer to prevent gradient varnishing or explosion so that the predictor can have a better performance. Our model is tested on the heart disease dataset obtained from Kaggle. Some indicators including accuracy, recall, precision, and F1-score are calculated to evaluate the predictor, and the results show that our model achieves 98.56%, 99.35%, 97.84%, and 0.983, respectively, and the average AUC score of the model reaches 0.983, confirming that the method we proposed is efficient and reliable for predicting heart disease.

1. Introduction

Heart disease is a common fatal disease and is currently the number one killer of the global population. According to the World Health Organization report [1], cardiovascular disease kills 17.9 million people every year, accounting for about 32% of the world's deaths. The report also stated that heart disease and stroke are the leading causes of cardiovascular diseases, accounting for approximately 85% of deaths. Like a circulatory system disease, cardiovascular disease is caused by many factors, such as high blood pressure, smoking, diabetes, and lack of exercise.

So far, methods to reduce deaths from heart diseases have always been the focus of research, and studies have shown that about 90% of heart diseases can be prevented [2]. In addition, heart disease has the characteristics of early detection, early treatment, and early recovery. Therefore, early detection of this illness is the key to treatment. To obtain the patient's cardiovascular status, the hospital needs to collect specific physical values, such as static blood pressure, blood sugar, cholesterol, maximum heart rate, chest pain type, and electrocardiogram. However, traditional manual analysis of huge heart disease-related data has the disadvantages of misdiagnosis and is time-consuming. Artificial intelligence is widely used in prediction to solve this problem, among which machine learning (ML) and deep learning (DL) are the majority. These prediction models analyze a large amount of medical data to determine whether

a patient has the disease and obtain more accurate prediction results than manual diagnosis.

This study combines machine learning with deep learning, applies LinearSVC and DNN technology, and proposes a new heart disease prediction model. The LinearSVC algorithm is applied to the feature selection module after data preprocessing. At the same time, we use Lasso as a penalty term to generate a sparse weight matrix, filter out a subset of features closely related to heart disease, and provide more reliable input for DNN. Furthermore, we compare several widely used weight initializers and finally choose the He initialization method since it can provide the best initial weight for the network. According to the results, the proposed model achieved accuracy, recall, and precision of 98.56%, 99.35%, and 97.84%.

The paper is structured as follows: Section 2 reviews the previous research on heart disease, Section 3 introduces the database we use and method analysis of our proposed model, followed by the detailed results of this research and the comparison with other algorithms in Section 4, and finally, Section 5 mentions a conclusion of this paper.

2. Literature Review

Researchers apply various data mining techniques to heart disease prediction methods. Amin et al. [3] used the UCI Cleveland database to confirm important features and mining techniques and finally used the UCI Statlog dataset for evaluation and verification. The research proposed 9 salient features from the 13 features of the original dataset and compared three data mining techniques: Vote, Naïve Bayes (NB), and Support Vector Machine (SVM). Among them, Vote has the best performance, and the accuracy is 87.41%. Similarly, Nalluri et al. [4] compared the performance of the XGBoost algorithm and the logistic regression (LR) method in predicting the value of Chronic Heart Disease (CHD). The results show that the accuracy of LR reaches 85.86%, which is better than XGBoost, which has an accuracy of 84.46%. Louridi et al. [5] used the UCI machine learning repository and compared three methods: SVM, k-Nearest Neighbor (kNN), and NB. Experiments show that the SVM with linear kernel has the best effect, with an accuracy of 86.8%. Shah et al. [6] used an existing dataset from the Cleveland database of the UCI Cardiology Patient Repository and considered 14 attributes. They compared four ML algorithms, namely, kNN, NB, DT, and random forest. The experimental results showed that kNN classification has the best effect (90.78%).

Decision tree (DT) also plays an essential role in the field of heart disease prediction. Kumar et al. [7] evaluated and analyzed three methods: NB, SVM, and DT, and the results showed that methods achieved 81.58%, 61.26%, and 90.79% accuracy. The effect of comparing DT is better than others. In a similar research, Pires et al. [8] compared a wealth of machine learning methods on neural networks, KNN, DT, SVM, combined nomenclature (CN2) rule inducer, and Stochastic Gradient Descent (SGD). The cross-validation results with different multiples show that DT and SVM have the best accuracy of 10-fold and 20-fold cross-validation (87.69%), and SGD has the best effect of 5-fold cross-validation (87.69%). There are also studies using mixed models to make predictions. Kavitha et al. [9] used random deep forest (RF), DT, and mixed model (RF; DT) on the UCI Cleveland dataset. The final result showed that the mixed model has the best effect, with an accuracy of 88.7%.

In addition, many new predictive models have also been proposed by researchers. Spencer et al. [10] combined feature selection technology with ML algorithm, and the created model combined chi-square feature selection and BayesNet algorithm to achieve an accuracy of 85%. Khan [11] proposed an improved deep convolutional neural network IoT framework. The framework is attached to a wearable detection device to detect the patient's blood pressure and electrocardiogram (ECG). Compared with the existing deep learning neural network and LR, this method has better performance (98.2%). Mohan et al. [12] combined RF with linear method (LM) and proposed a hybrid random forest (HRFLM) prediction model with a linear model. Experiments on the UCI Cleveland dataset showed that the accuracy of the classification model reached 88.7%, which is better than other classification methods. Magesh and Swarnalatha [13] adopted a cluster-based DT learning (CDTL) method. After feature processing, the CDTL-RF prediction accuracy can reach 89.30%, improving 12.60% compared to the non-CDTL method. Mehmood et al. [14] proposed a method called CardioHelp, which combines CNN with deep learning algorithms, involving the use of CNN for HF prediction and temporal model modeling at the earliest stage. Compared with other state-of-the-art methods, this method achieves the best performance, and its accuracy rate is 97%.

3. Materials and Methods

Data preprocessing, feature selection, and classification are the three most crucial parts of the heart disease prediction model. We carry out outlier processing and standardization on the dataset, ensuring all the data are well structured after the data preprocessing process. A feature selection process based on the LinearSVC algorithm is applied to choose valuable features. The selected feature subset is divided into the training set and test set at a ratio of 3 : 1; the former is fed into the deep neural network we built. Specifically, our deep neural network uses the he_normal initializer to construct the best initial weights to prevent gradients from exploding or vanishing and attain a better effect. Additionally, the effectiveness of the model is measured based on the test samples. The structure of our heart disease prediction model can be clearly seen in Figure 1.

3.1. Data Collection. There are many databases related to heart diseases, such as the Cleveland database and the heart disease database provided by the National Cardiovascular Disease Surveillance System. This paper uses a widely used heart disease dataset from Kaggle [15], composed of four databases: Cleveland, Hungary, Switzerland, and the VA Long Beach. The dataset has 14 attributes, and each attribute

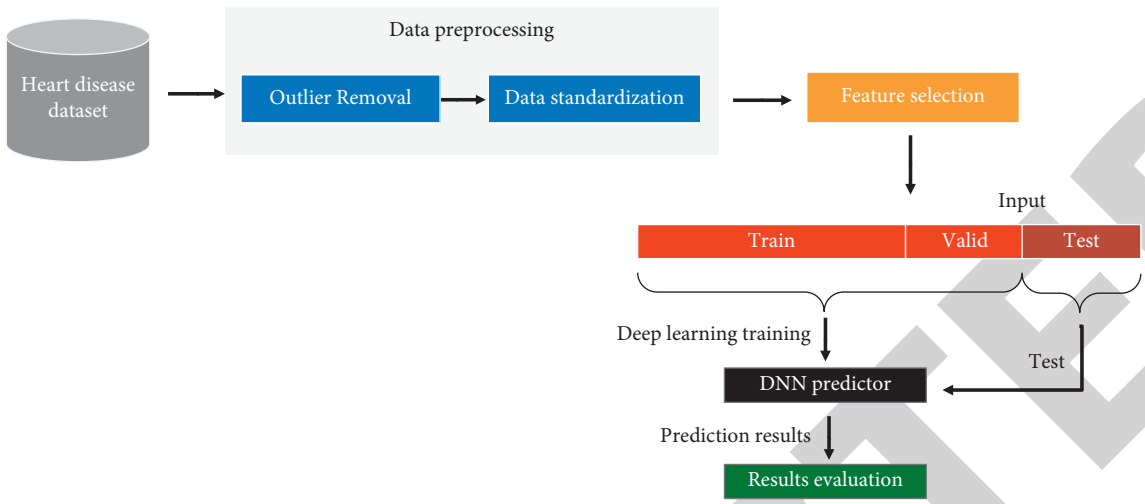

Figure 1: Proposed heart disease prediction system structure.

is set with a value. It contains 1025 patient records of different ages, of which 713 are male, and 312 are female. This dataset is a subset of [16]. The original dataset contains 76 attributes, but most scholars only use 14 of them, since other attributes have little effect on heart disease, such as time of exercise ECG reading and exercise protocol. The descriptions in this database are shown in Table 1.

3.2. Data Preprocessing. We choose the heart disease dataset publicly from Kaggle [15]. To ensure the stability and accuracy of the prediction model, it is essential to perform data analysis and preprocess before inputting them into the deep neural network. There are two main parts of data preprocessing: outlier removal and data standardization.

3.2.1. Outlier Removal Process. Well-processed and structured data determines the effectiveness of the model largely. The raw dataset contains a sort of unreasonable values commonly, whose attributes are inconsistent with the whole. These abnormal values are named outliers. We analyze the heart disease dataset and apply the interquartile range (IQR) method to detect and remove outliers. It is worth mentioning that the physical indicators of healthy people are usually in a similar range, and the abnormality of specific biological indicators may be a reflection of diseases.

Therefore, the heart disease prediction model needs to alert some outliers instead of removing all of them thoughtlessly. This paper applied the IQR method to deal with the outliers of chol and trestbps columns since these two columns are generally normally distributed, but the boxplot shows that they both have apparent abnormalities that deviate from the normal range. IQR is a technique used to help detect outliers in data. It defines the difference between the third quartile and the first quartile as IQR [17], and then the lower and upper boundaries can be calculated by the following equations:

$$\begin{aligned} \mathrm{IQR} &= Q_3 - Q_1, \\ B_l &= Q_1 - 1.5 * \mathrm{IQR}, \\ B_u &= Q_3 + 1.5 * \mathrm{IQR}. \end{aligned} \tag{1}$$

Now, the values outside the range of $B_l \sim B_u$ are recognized as outliers needed to be removed. After these outliers are filtered out, they can be abandoned from the dataset. Figure 2 shows the changes in the boxplot before and after the outlier processing.

3.2.2. Data Standardization Process. Data standardization aims to eliminate the differences between features so that subsequent models can learn weights wholeheartedly. Networks trained on standardized data usually produce better results [18]. Data standardization can convert the original data into normally distributed data without changing the initial data structure distribution. We use the StandardScaler method to standardize the data since all outliers are removed in the previous step and our data roughly obeys normal distribution. The conversion equation is as follows:

$$x^* = \frac{x - \mu}{\sigma}, \tag{2}$$

where u is the mean of the training samples or zero if *with_mean = False* and s is the standard deviation of the training samples or one if *with_std = False*.

Standardization calculates the mean and variance of the data and converts the data with them. The standardization process can transform the data into a standard normal distribution suitable for the network behind it.

3.3. Feature Selection Based on an Embedded Method. Irrelative features often affect the model's training process, and some noise features even make the model deviate from the correct track. Feature selection chooses a subset of variables that can effectively describe the input data and ensure good prediction results [19]. Some feature selection

Table 1: Description of features.

SN	Attribute	Description
1	age	Age in years
2	sex	1 = male; 0 = female
3	cp	Chest pain type
4	trestbps	Resting blood pressure (in mm Hg on admission to the hospital)
5	chol	Serum cholesterol in mg/dl
6	fbs	Fasting blood sugar >120 mg/dl (1 = true; 0 = false)
7	restecg	Resting electrocardiographic results
8	thalach	Maximum heart rate achieved
9	exang	Exercise-induced angina (1 = yes; 0 = no)
10	oldpeak	ST depression induced by exercise relative to rest
11	slope	The slope of the peak exercise ST segment
12	ca	Number of major vessels (0–3) colored by fluoroscopy
13	thal	1 = normal; 2 = fixed defect; 3 = reversible defect
14	target	1 = disease; 2 = no disease

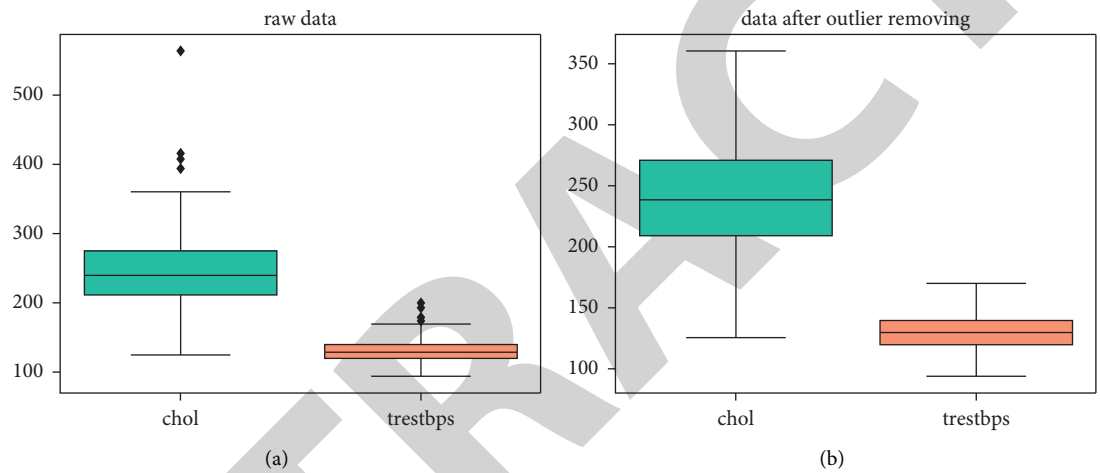

Figure 2: The changes of boxplot before and after the outlier removal using IQR. (a) Raw data. (b) Results of outlier removal.

methods are applied to reduce the influence of noise or irrelevant variables, roughly summarized into filter methods, wrapper methods, and embedded methods. However, the feature subset selected by the filter method has high redundancy, and the wrapper method has a high computational complexity because the evaluation of different feature subsets requires retraining and testing while the embedded method can efficiently select a subset with better performance. In this paper, the dataset we used has selected 14 attributes from 76 features in the original dataset. We use the penalty-based embedded feature selection method to verify these chosen features and try to pick the most related features based on them. Embedded feature selection integrates the feature selection process with the model training process. Instead of splitting the data into training and test sets, the two are completed in the same optimization process. The machine learning algorithm is used for training and obtains the weight coefficient of each feature, these weight coefficients often represent the importance of features to the model, and then the evaluation module selects the most contributing feature according to the value of the weight coefficient. The embedded feature selection method relies on model evaluation to complete feature selection.

Our embedded feature selection is based on the LinearSVC algorithm, which is applicable to this binary classification problem. We use L1 norm regularization [20] as a penalty term because it has good robustness and makes the coefficients sparse. The L1 regularization loss function is also called Lasso regression. It is expressed as follows:

$$\min_{w} \sum_{i=1}^{N} \left(w^T x_i - y_i\right)^2 + \lambda w_1, \tag{3}$$

where w represents the coefficient of the feature, x is the feature matrix, y is the target vector matrix, n is the number of samples, and λ represents the regularization strength.

The regularization can restrict the coefficient, and a sparse matrix can be obtained by using L1 regularization. The feature with a coefficient of 0 in the matrix can be regarded as inconsequential to the model, which will not affect the effectiveness of the model even if it is removed. Therefore, we can concentrate on the nonzero value features to achieve the purpose of feature selection. Through feature selection, we can reduce the number of features and select the most reliable feature subset.

3.4. Heart Disease Classification Using Deep Neural Networks

3.4.1. Deep Neural Networks. A deep neural network is a deep learning framework, usually a feedforward neural network. In addition, the deep neural network is a discriminative model, which can be trained through the backpropagation algorithm [21].

After continuous research, the network has been widely used in speech recognition, cancer detection, and other fields and has outstanding performance. This is because deep neural networks can use statistical learning methods to extract high-level features from the input data.

The basic structure of DNN can be divided into three layers, namely, the input layer, hidden layer, and output layer. Unlike perceptrons, deep neural network structures have at least one hidden layer. Therefore, deep neural networks are sometimes called Multilayer Perceptrons (MLP). This change increases the depth and complexity of the model, improves the model's capabilities, and can use multiple activation functions. Each hidden layer of the network has interconnected neurons. The process of the deep neural network is that after the hidden layer extracts the input features, the classification result is finally obtained in the output layer. Our DNN network structure diagram is shown in Figure 3. We input the 12 features selected in the feature selection module into the DNN network. This network has 7 hidden layers and finally gets 2 outputs, corresponding to the scores belonging to each category.

3.4.2. Loss and Activation Function. The heart disease prediction in this paper is essentially a binary classification problem. We use BinaryCrossentropy as a loss function to measure the quality of the model's prediction. BinaryCrossentropy is widely used in binary classification problems. To calculate the loss by BinaryCrossentropy, the following equation is used.

$$H_p(q) = -\frac{1}{N}\sum_{i=1}^{N} y_i \log(p(y_i)) + (1 - y_i)\log(1 - p(y_i)), \tag{4}$$

where y is a binary label, and p (y) is the probability of belonging to the y label.

BinaryCrossentropy can measure the quality of classification since the process of reducing the loss can make the sample whose label equals 1 obtained a larger predicted probability of p (y). In contrast, the probability of the sample with 0 labels becomes smaller. The accuracy of the model can be significantly improved with the process of reducing loss.

The input layer and hidden layer of our deep neural network use the ReLU activation function, while the Sigmoid activation function is used in the output layer to map the output to the range of [0, 1] to adapt to the BinaryCrossentropy loss function. In addition, choosing Sigmoid instead of ReLU makes the output easier to control. The ReLU and Sigmoid functions are as follows:

$$\begin{aligned} \mathrm{ReLu}(x) &= \max(0, x), \\ \mathrm{Sigmoid}(x) &= \frac{1}{1 + e^{-x}}. \end{aligned} \tag{5}$$

The output result obtained by Sigmoid can be regarded as the probability of belonging to the corresponding category. Therefore, we convert the data label into one-hot encoding. The one-hot encoding uses an N-bit status register to encode N states. The label is represented as a binary vector. In each code, only one bit is marked as 1, which represents a valid index, and the remaining bits are marked as 0. This encoding method converts the label into a convenient form for the network, which facilitates the calculation of the BinaryCrossentropy loss function.

3.4.3. Application of Initializers. Deep neural networks usually need to learn an extremely complex nonlinear model, and different initializers often lead to distinctive convergence speeds and effects. If the weights of each layer are all initialized to 0 or 1, the neural network cannot learn important features during the backpropagation process, and it is challenging to update parameters. In addition, an excessively large initial value will cause exploding gradient, while an initial value that is too small will cause the vanishing gradient; both lead to a decline in the learning ability of the network. To solve the problems mentioned above, it is necessary to find a suitable weight initialization method, which needs to meet the following demands:

(1) Avoid saturation of activation values of neurons in each layer

(2) Avoid the activation value of each layer which becomes zero

However, the prevalent random normal method for weight initialization may cause network optimization to a dilemma. Once the random distribution is not properly generated, it may encounter a situation where the output value of the deep network is close to 0, resulting in the vanishing gradient. The basic idea of Xavier [22] initialization is that the activation value of each layer and the variance of the gradient remain consistent during the propagation process, avoid all output values tending to 0, and make each layer get effective feedback during backpropagation. However, Xavier initialization has an advantage over Tanh but is ineffective with the ReLU activation function. He initialization [23] divides by two based on Xavier, which can keep the variance unchanged and make sure half of the neurons in each layer are activated. Equation (6) states the Xavier method, and equation (7) states He initialization method.

$$w_i \sim U\left(-\sqrt{\frac{6}{n_i + n_{i+1}}}, \sqrt{\frac{6}{n_i + n_{i+1}}}\right), \tag{6}$$

$$w_i \sim \frac{\left[U\left(-\sqrt{6/n_i + n_{i+1}}, \sqrt{6/n_i + n_{i+1}}\right)\right]}{2}. \tag{7}$$

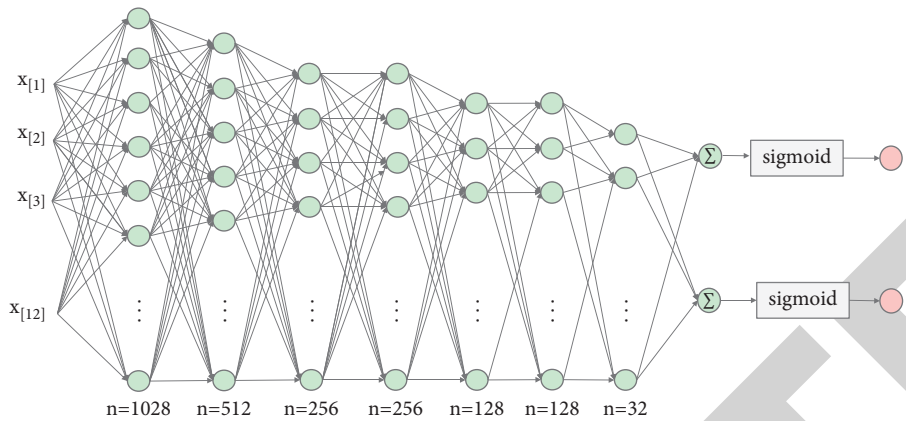

Figure 3: The structure of our deep neural network.

We compare some famous weight initialization methods, whose results are illustrated clearly in Section 4. Due to the advantages of the He initializer with the ReLU activation function, we employ this method in our network.

4. Results and Discussion

We employed the proposed method to predict heart disease and evaluated the results. The heart disease dataset was preprocessed through outlier removal and data standardization at the beginning, after which a feature selection module was applied, and the selected feature subset was fed into the deep neural network for training. We tried a wide range of network optimization algorithms to improve the effect and stability of the model.

We divided the data into a training and a test set at a ratio of 3 : 1, and 20% of the training data was partitioned for verification. The DNN network was trained and learned in the training set. We calculate the accuracy, recall, precision, and F1-score indicators to evaluate these results. Accuracy can describe the number of correct predictions over all of the predictions. Recall refers to the proportion of real positive cases that are correctly predicted positive, and precision denotes the proportion of predicted positive cases that are correctly real positives [24]; F1-score is a measure combining both precision and recall and can be regarded as the harmonic average of the two. The following equations present calculation of them:

$$\begin{aligned} \text{accuracy} &= \frac{\text{TP} + \text{TN}}{\text{TP} + \text{TN} + \text{FP} + \text{FN}}, \\ \text{recall} &= \frac{\text{TP}}{\text{TP} + \text{FN}}, \\ \text{precision} &= \frac{\text{TP}}{\text{TP} + \text{FP}}, \\ F1 - \text{score} &= \frac{2 * \text{precision} * \text{recall}}{\text{precision} + \text{recall}} \end{aligned} \tag{8}$$

where TP is the true positive, FP denotes the false positive, TN denotes the true negative, and FN is the false negative.

In our experiment, the Adam optimizer was selected, which is a stochastic gradient-based optimization. The Adam optimizer only needs first-order gradients and is computationally efficient with only little memory. This method calculates the individual adaptive learning rate of different parameters by estimating the first and second moments of the gradient, which has advantages compared with other optimization methods [25]. In this experiment, the learning rate is 0.0001, and the number of iterations is 150. To ensure the reliability of the results, all of the statistics we mentioned in this paper are average results of 10 experiments. It shows that our average accuracy is 98.56%, recall reaches 99.35%, precision is 97.84%, and F1-score achieves 0.983. Table 2 represents the detailed results and Figure 4 shows the confusion matrix of the predicted results of an experiment.

In addition, we use ROC and AUC to evaluate the performance of the model. Receiver operating characteristic curve (ROC) is a curve drawn based on a series of different boundary values with a true positive rate on the ordinate and a false positive rate on the abscissa [26]. AUC is the area under the ROC curve, which represents the probability of the calculated score of the positive sample higher than that of the negative sample when the samples are randomly selected, which can measure the pros and cons of the prediction model. Results show that the average AUC value of our model is 0.983 and the ROC curve of an experiment can be seen in Figure 5.

In the data preprocessing, we used the IQR method to remove the outliers of chol and trestbps and successfully normalized the dataset. In the feature selection module, we use an embedded feature selection method based on LinearSVC, using the L1 norm as a penalty term, and successfully picked 12 features that contribute to the model. The fbs feature with a score of 0 is removed in this module. See Table 3 for each feature score.

By using the He initialization method, our model obtained outstanding stability and accuracy as a consequence. We compare the neural network's performance using the He initialization method, RandomNormal method, and Xavier method. It is concluded that the He initialization shows superiority, the accuracy is 9.3% and 13.3% higher than the random and Xavier method, respectively, recall is 9.0% and

Table 2: Results of the proposed method.

	Class 0 (%)	Class 1 (%)
Accuracy	98.56	98.56
Recall	97.84	99.35
Precision	99.35	97.84

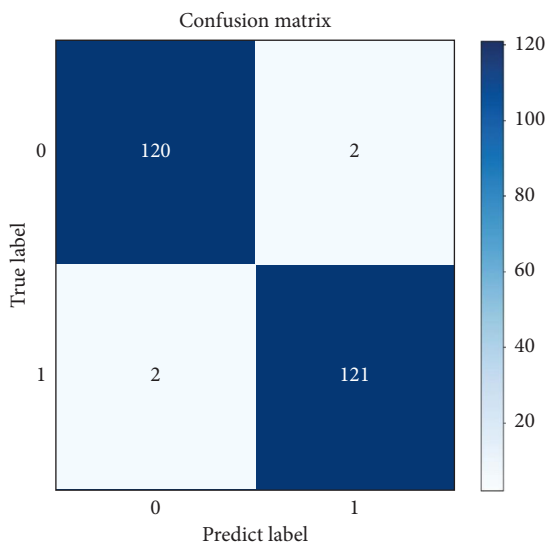

Figure 4: Confusion matrix on test data.

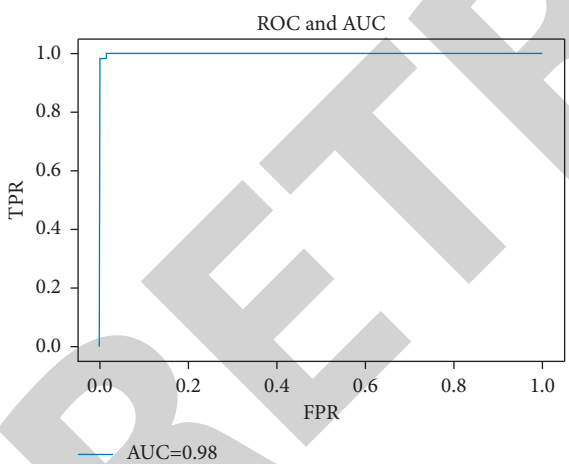

Figure 5: ROC curve and AUC of the proposed algorithms.

12.4% higher, respectively, precision is increased by 9.3% and 14.2%, and F1-score is increased in the number of 0.083 and 0.127. These results are demonstrated in detail in Figure 6.

Additionally, we found that batch normalization performed poorly in our model. We add batch normalization after the fully connected layer. The accuracy, recall, precision, and F1-score of the model change to 97.5%, 98.3%, 96.7%, and 0.98, respectively, which are decreased by 1.1%, 1.0%, 1.1%, and 0.003. Comparison results are illustrated in Figure 7. We conjecture this is because He initializer already gives the network good initial weights, so that each layer of

Table 3: Importance value of features.

SN	Attribute	Importance value
1	age	−0.00144
2	sex	−0.56535
3	cp	0.288000
4	trestbps	−0.005696
5	chol	−0.001637
6	fbs	0.0
7	restecg	0.1190487
8	thalach	0.0079078
9	exang	−0.332790
10	oldpeak	−0.199450
11	slope	0.1589541
12	ca	−0.252994
13	thal	−0.2927249

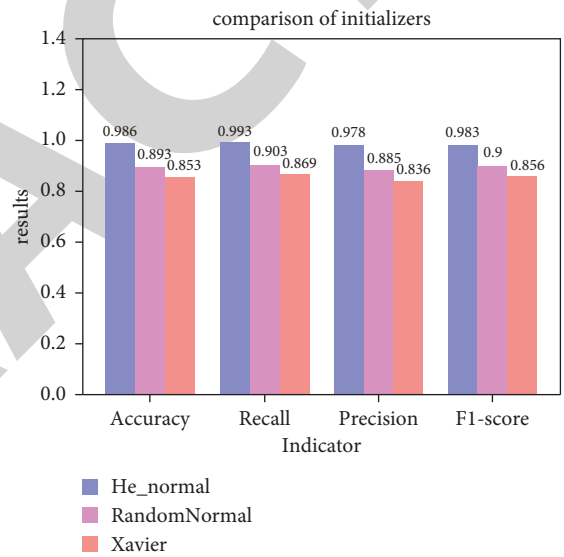

Figure 6: Results of different initializers.

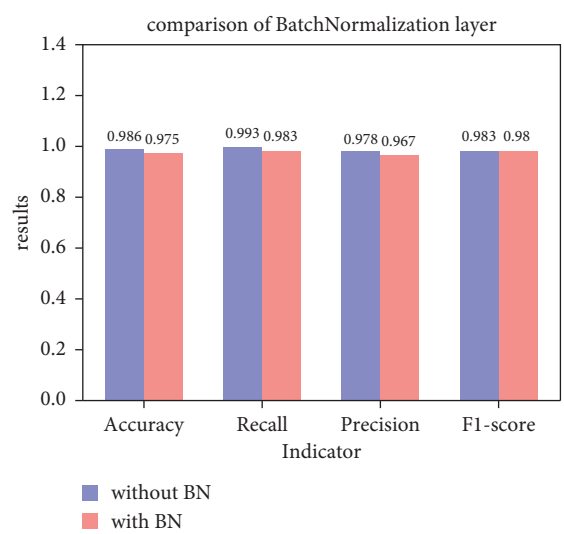

Figure 7: Comparison of results using batch normalization layer.

Table 4: Comparison of classification performance of the proposed method with others.

Authors	Methods	Accuracy (%)	Recall (%)	Precision (%)
Ramprakash et al. [27]	χ^2-DNN	94.0	93.00	—
Gao et al. [28]	Bagging ensemble method with decision tree	98.6	99.0	97.8
Gao et al. [28]	PCA + decision tree	99.0	97.0	98.0
Ali et al. [29]	MLP	97.95	98	98
Proposed	LinearSVC + DNN	**98.56**	**99.35**	**97.84**

the network has good input and output values, avoiding the vanishing and exploding gradients.

Furthermore, we compared our method with some published methods proposed by other scholars. For example, Ramprakash et al. [27] used the combination of the PCA feature extraction method and DNN to get a classification with high accuracy, but the recall only reached 97%. The specific comparison results are shown in Table 4.

5. Conclusions

In this paper, we propose a heart disease prediction algorithm based on DNN combined with LinearSVC embedded feature selection method. Through the IQR method, the outliers in the dataset are successfully removed and all data are standardized to obtain reliable input. In addition, the optimal feature subset is selected in the feature selection module based on the LinearSVC algorithm and L1 norm. A total of 12 most-relative features are selected and input into the subsequent DNN network. To enhance the network's performance, we compare three weight initialization methods including the He_normal, random_normal, and Xavier, concluding that He initialization method acquires the best results in this heart disease prediction model. Meanwhile, we find that the batch normalization layer is not suitable for this method, attaining lower scores in every indicator. In this two-classification problem, we choose BinaryCrossentropy as the loss function and Sigmoid as the activation function of the output layer to map the output to the range of [0, 1]. The experimental results show that a high-accuracy prediction model for heart disease is realized. The accuracy of our proposed method reaches 98.56%, recall is 99.35%, precision is 97.84%, and F1-score achieves 0.983, with an AUC score of 0.983, proving that this feature selection method and deep neural network are feasible and reliable in predicting heart disease. In the future, we will continue to adjust the depth and parameters of the DNN to enhance the stability of the model as well as research other deep learning optimization techniques to obtain better performance [30].

Data Availability

The heart disease dataset used to support the findings of this study is available at https://www.kaggle.com/johnsmith88/heart-disease-dataset.

Conflicts of Interest

The authors declare that there are no conflicts of interest regarding the publication of this study.

Authors' Contributions

Dengqing Zhang and Yunyi Chen contributed equally to this work.

References

[1] World Health Organization, https://www.who.int/health-topics/cardiovascular-diseases#tab=tab_1, 2021.

[2] H. C. McGill, C. A. McMahan, and S. S. Gidding, "Preventing heart disease in the 21st century," *Circulation*, vol. 117, no. 9, pp. 1216–1227, 2008.

[3] M. S. Amin, Y. K. Chiam, and K. D. Varathan, "Identification of significant features and data mining techniques in predicting heart disease," *Telematics and Informatics*, vol. 36, pp. 82–93, 2019.

[4] S. Nalluri, R. V. Saraswathi, S. Ramasubbareddy, K. Govinda, and E. Swetha, "Chronic heart disease prediction using data mining techniques, advances in intelligent systems and computing," in *Data Engineering and Communication Technology*, pp. 903–912, Springer, Singapore, 2020.

[5] N. Louridi, M. Amar, and B. E. Ouahidi, "Identification of cardiovascular diseases using machine learning," in *Proceedings of the 2019 7th Mediterranean Congress of Telecommunications (CMT)*, pp. 1–6, IEEE, Fez, Morocco, October 2019.

[6] D. Shah, S. Patel, and S. K. Bharti, "Heart disease prediction using machine learning techniques," *SN Computer Science*, vol. 1, no. 6, pp. 1–6, 2020.

[7] A. Kumar, P. Kumar, A. Srivastava, V. D. A. Kumar, K. Vengatesan, and A. Singhal, "Comparative analysis of data mining techniques to predict heart disease for diabetic patients," in *Proceedings of the International Conference on Advances in Computing and Data Sciences*, pp. 507–518, Springer, Valletta, Malta, April 2020.

[8] I. M. Pires, G. Marques, N. M. Garcia, and V. Ponciano, "Machine learning for the evaluation of the presence of heart disease," *Procedia Computer Science*, vol. 177, pp. 432–437, 2020.

[9] M. Kavitha, G. Gnaneswar, R. Dinesh, Y. R. Sai, and R. S. Suraj, "Heart disease prediction using hybrid machine learning model," in *Proceedings of the 2021 6th International Conference on Inventive Computation Technologies (ICICT)*, pp. 1329–1333, IEEE, Coimbatore, India, January 2021.

[10] R. Spencer, F. Thabtah, N. Abdelhamid et al., "Exploring feature selection and classification methods for predicting heart disease," *Digital health*, vol. 6, 2020.

[11] M. A. Khan, "An IoT framework for heart disease prediction based on MDCNN classifier," *IEEE Access*, vol. 8, Article ID 34717, 2020.

[12] S. Mohan, C. Thirumalai, and G. Srivastava, "Effective heart disease prediction using hybrid machine learning techniques," *IEEE access*, vol. 7, Article ID 81542, 2019.

[13] G. Magesh and P. Swarnalatha, "Optimal feature selection through a cluster-based DT learning (CDTL) in heart disease

Hindawi
Journal of Healthcare Engineering
Volume 2023, Article ID 9836413, 1 page
https://doi.org/10.1155/2023/9836413

Retraction

Retracted: An ECG Heartbeat Classification Method Based on Deep Convolutional Neural Network

Journal of Healthcare Engineering

Received 5 December 2023; Accepted 5 December 2023; Published 6 December 2023

This article has been retracted by Hindawi, as publisher, following an investigation undertaken by the publisher [1]. This investigation has uncovered evidence of systematic manipulation of the publication and peer-review process. We cannot, therefore, vouch for the reliability or integrity of this article.

Please note that this notice is intended solely to alert readers that the peer-review process of this article has been compromised.

Wiley and Hindawi regret that the usual quality checks did not identify these issues before publication and have since put additional measures in place to safeguard research integrity.

We wish to credit our Research Integrity and Research Publishing teams and anonymous and named external researchers and research integrity experts for contributing to this investigation.

The corresponding author, as the representative of all authors, has been given the opportunity to register their agreement or disagreement to this retraction. We have kept a record of any response received.

References

[1] D. Zhang, Y. Chen, Y. Chen, S. Ye, W. Cai, and M. Chen, "An ECG Heartbeat Classification Method Based on Deep Convolutional Neural Network," *Journal of Healthcare Engineering*, vol. 2021, Article ID 7167891, 9 pages, 2021.

Hindawi
Journal of Healthcare Engineering
Volume 2021, Article ID 7167891, 9 pages
https://doi.org/10.1155/2021/7167891

Research Article

An ECG Heartbeat Classification Method Based on Deep Convolutional Neural Network

Dengqing Zhang,[1] Yuxuan Chen,[2] Yunyi Chen,[2] Shengyi Ye,[1] Wenyu Cai,[1] and Ming Chen[3]

[1]*Department of Cardiology, Jinjiang Municipal Hospital, Fujian, Jinjiang 362200, China*
[2]*School of Informatics Xiamen University, Xiamen University, Fujian, Xiamen 361000, China*
[3]*Department of Public Health, Jinjiang Municipal Hospital, Fujian, Jinjiang 362200, China*

Correspondence should be addressed to Ming Chen; 289975884@qq.com

Received 5 August 2021; Revised 7 September 2021; Accepted 15 September 2021; Published 27 September 2021

Academic Editor: Gu Xiaoqing

The electrocardiogram (ECG) is one of the most powerful tools used in hospitals to analyze the cardiovascular status and check health, a standard for detecting and diagnosing abnormal heart rhythms. In recent years, cardiovascular health has attracted much attention. However, traditional doctors' consultations have disadvantages such as delayed diagnosis and high misdiagnosis rate, while cardiovascular diseases have the characteristics of early diagnosis, early treatment, and early recovery. Therefore, it is essential to reduce the misdiagnosis rate of heart disease. Our work is based on five different types of ECG arrhythmia classified according to the AAMI EC57 standard, namely, nonectopic, supraventricular ectopic, ventricular ectopic, fusion, and unknown beat. This paper proposed a high-accuracy ECG arrhythmia classification method based on convolutional neural network (CNN), which could accurately classify ECG signals. We evaluated the classification effect of this classification method on the supraventricular ectopic beat (SVEB) and ventricular ectopic beat (VEB) based on the MIT-BIH arrhythmia database. According to the results, the proposed method achieved 99.8% accuracy, 98.4% sensitivity, 99.9% specificity, and 98.5% positive prediction rate for detecting VEB. Detection of SVEB achieved 99.7% accuracy, 92.1% sensitivity, 99.9% specificity, and 96.8% positive prediction rate.

1. Introduction

According to the latest World Health Statistics 2019 [1] report, heart disease, the top killer of humanity, was the primary cause of death worldwide in the past two decades, accounting for 16% of all causes of death. Since this kind of disease severely contributes to a lower life expectancy, the detection and diagnosis of cardiovascular diseases perform an inestimable value for all human beings. At present, some diagnostic methods, including ECG, ultrasonic cardiogram (UGC), chest X-ray, and cardiac Magnetic Resonance Imaging (MRI), are extensively used to detect cardiovascular diseases. Specifically, the ECG plays a significant part among these measures due to its affordable and convenient superiority. ECG signals are the most popular way to monitor the health status of the cardiovascular system and identify diseases related to the cardiovascular system. The morphological changes of the electrocardiogram and the depolarization of the myocardium can be profitable to assist in the diagnosis of heart disease. However, the complex ECG data makes manual identification a challenge, which demands the rich experience of doctors. Considering this, many scholars have applied various algorithms to help detect these diseases, improving the classification model in accuracy, speed, and robustness. Many popular methods, such as decision trees, random forest, and SVM, are proposed in ECG data classification. Many scientists have researched popular machine learning algorithms and neural network algorithms, proving that the latter is effective for heart disease classification, with higher credibility and slighter

error. These neural networks can learn relationships and information that are difficult for people to discover from a large amount of complex data.

As manual analysis is time-consuming, laborious, and easy to misjudge, this paper refers to VGGNet [2], designing an ECG arrhythmia classification model based on CNN. We classify and learn ECG data thoroughly and aim to improve accuracy by building and optimizing neural networks. In our paper, the ECG dataset is divided into five categories to realize a rough assessment of the heart state, providing an essential and reliable reference for the doctor's further diagnosis. The proposed method is used to classify based on all datasets. The results show that our classifier achieved an average accuracy of 99.76%, an average sensitivity of 94.45%, an average specificity of 99.54%, and an average positive prediction rate of 97.40%. Moreover, to evaluate the proposed model, we compared the results of other deep learning algorithms to detect VEB and SVEB, and the proposed method obtained better results.

2. Literature Review

Many scientists have conducted related researches on the classification of ECG data. Houssein et al. [3] presented a new morphological features descriptor and proposed a method based on a metaheuristic algorithm termed Manta ray foraging optimization (MRFO) and SVM, obtaining 98.26% accuracy and 97.43% sensitivity. Mathunjwa et al. [4] converted 1D ECG signals into 2D segments, combined recurrence plot (RP) and CNN to make arrhythmia classification, and achieved the accuracy of 95.3% on ventricular fibrillation (VF) categories and 98.41% on the atrial fibrillation (AF), normal, premature AF, and premature VF categories. Pirova et al. [5] compared random forest, decision tree, and convolutional neural network algorithms, showing that the neural network is superior to other algorithms in ECG data classification, with an accuracy rate of 93.47%. Baloglu et al. [6] proposed an end-to-end deep learning model based on standard 12-lead ECG signals to diagnose myocardial infarction. They used a deep CNN model, which completed the ECG signal learning process at the end of a short period (10 epochs). Furthermore, manually extracting features from the original ECG data or using the features learned by other machine learning models is unnecessary with this method. Jun et al. [7] put forward a deep two-dimensional convolution method to classify ECG data and converted every ECG beat into a two-dimensional grey-scale image as the input data of the classifier. Their CNN-based ECG arrhythmia classification consists of two steps: ECG and data preprocessing. At the same time, they applied methods such as batch normalization, data enhancement, and Xavier initialization to optimize the CNN classifier, and the average accuracy rate was up to 97.85%. This result convinced that the use of ECG images and the CNN model to detect arrhythmia is effective.

Furthermore, various machine learning algorithms are widely used. Methods such as support vector machines (SVM) have been tested to classify ECG arrhythmia detection. Kohli et al. [8] compared three popular SVM algorithms, one-against-one, one-against-all, and fuzzy decision function, and finally concluded that the one-against-one method performs better results when distinguishing the cardiac arrhythmia and grouping them into the correct class. Considering that the artificial neural network (ANN) has the flaw of converging to a local minimum and is prone to overfitting, Walsh [9] used the support vector machine algorithm to classify the ECG data as it tends towards an optimal margin separation, as the search space constraints define a convex set. However, due to the imbalance of the data, the support vector machine macroaverage F1 score only reached 0.87.

In addition, as a commonly used classification algorithm, KNN is also applied to classify ECG data. Saini et al. [10] used it as a classifier to detect QRS waves of ECG signals. The detection rate of the CSE DS-3 MIT-BIH arrhythmia database is 99.89% and 99.81%, proving the effectiveness and reliability of KNN. The ECG signal was decomposed by wavelet transform to improve efficiency, and thirteen (including energy feature) statistical features were evaluated from these decomposed signals by Saini et al. [11]. The classification efficiency of the decomposed ECG signals was increased by 31.25% to 87.5%.

Besides, Kanani et al. [12] were concerned about the importance of data preprocessing, introducing a preprocessing technique used for ECG classification that significantly improves the accuracy and stability of the training models. Through data preprocessing, the system's accuracy can reach more than 99% without overfitting. Huang et al. [13] apply the cardiovascular disease electronic health framework based on IoT devices with wearable sensors, which can effectively and timely treat patients with cardiovascular disease.

3. Materials

3.1. ECG Database. In this paper, we apply the MIT-BIH arrhythmia dataset [14, 15], which is famous for assessing arrhythmias and applied for the fundamental analysis of cardiac dynamics. With the annotation of at least two cardiologists, this database contains excerpts from 48 and a half hour double-channel recordings. Gained by the BIH Arrhythmia Laboratory, these recordings were obtained from 47 testers from 1975 to 1979. Each contains two 11-bit resolution ECG lead signals in the 10 mv range, digitized at 360 samples per second. In compliance with the Association for the Advancement of Medical Instrumentation (AAMI) EC57 standard [16], these annotations were grouped into five different categories. To understand the mapping between different categories and descriptions and AAMI EC57 categories, refer to Table 1.

3.2. Convolutional Neural Network. The convolutional neural network is a feedforward neural network with a deep structure, and it is the most widely used algorithm for deep learning [17, 18]. It has the characteristics of multilevel network structure, no complicated preprocessing, partial connection, and shared weights. The three main

Table 1: Mapping between different categories and descriptions and AAMI EC57 categories.

Category	Descriptions	Annotations
N	Nonectopic beat	Normal (NOR) Left bundle branch block (LBBB) Right bundle branch block beat (RBBB) Atrial escape (AE) Nodal (junctional) escape (NE)
S	Supraventricular ectopic beat	Atrial premature (AP) Aberrated atrial premature (aAP) Nodal premature (NP) Supraventricular premature (SP)
V	Ventricular ectopic beat	Premature ventricular contraction (PVC) Ventricular escape (VE)
F	Fusion beat	Fusion of ventricular and normal (fVN)
Q	Unknown beat	Paced (P) Fusion of paced and normal (fPN) Unclassifiable (U)

convolutional neural network architecture layers are the convolutional, pooling, and fully connected layers.

The convolutional layer is the core layer of the neural network, composed by sliding the incompatible convolution kernel on the input matrix and running certain operations. A neuron in the convolutional layer is connected to only one neuron in the local window of the previous layer to form a local connection network. The convolution kernel only captures specific local features in the input data. Therefore, to extract multiple features, we need to use multiple different convolution kernels.

Pooling is a significant step in CNN, which is also called the subsampling layer. Max pooling divides the input data into several rectangular areas and outputs the maximum value for each subarea, reducing the number of neurons.

The fully connected layer plays a vital role in classifying the network, and each neuron is fully connected to all neurons in the upper layer. As shown in Figure 1, due to the effect of full connection, the parameters of the weight matrix will significantly increase. On the contrary, the convolution layer adopts a local connection. With the same color connection, the weight is the same, and the number of parameters of the final weight matrix will be significantly reduced.

4. Methodology

In this paper, we designed a CNN-based ECG arrhythmia classification method. The method has the following steps: ECG data preprocessing, model training, and model evaluation. We preprocessed the MIT-BIH arrhythmia database and divided the preprocessed five types of ECG data into mutually exclusive training sets and test sets for training and testing the CNN classifier. We used the training set to train the CNN classifier, and after getting the relevant training model, it is used to predict the classification of the 5 ECG types in the test set. The overall process of the method in this paper is shown in Figure 2.

4.1. Data Preprocessing. The dataset was preprocessed with a method proposed by Kachuee et al. [19], and we achieve good results by inputting the processed ECG data directly into the neural network we built. The process of data preprocessing proposed is as follows:

(1) *Normalization.* Select a specific 10 s window of ECG signal and normalize the amplitude to be in the range of 0 to 1.

(2) *Find the R-Peak Candidates of ECG Data.* Applying a threshold of 0 : 9, the R-peak candidate set is selected from the local maximum of normalized data.

(3) *Select the Signal.* For each r-peak, a signal with a length of 1.2 times the median of R-R time intervals is selected and paddled with zeros to satisfy a predefined fixed length.

After the original signal is processed, it is classified into five different ECG signals. After processing, we divide the data into the training and test sets, including the 87554 and 21892 test sets. Each data is part of the electrocardiogram, expressed as a vector of 187 values. Table 2 shows the distribution of datasets in different categories after preprocessing.

4.2. Apply Flattening to the Network. Because the output of the convolutional and pooling layers is two-dimensional, the data needs to be flattened. Then the result obtained by the convolutional layer is input to the fully connected layer. It follows that we use the fallen layer for transition between the convolutional layer and the fully connected layer, which converts the multidimensional results obtained by the convolutional layer to one dimension and inputs them into the fully connected layer. To summarize, the output of the convolutional layer is flattened to create a single long feature vector, as shown in Figure 3, and connected to the final classification model in the fully connected layer.

4.3. Apply the ELU Activation Function. The function of the activation function is to introduce nonlinear characteristics into the neural network model. In this paper, we mainly compare two nonlinear activation functions that are widely used in modern CNN models, including rectified linear unit

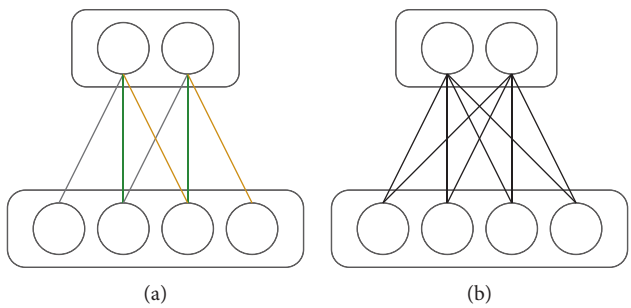

Figure 1: Schematic diagram of convolutional neural network: (a) convolutional layer and (b) fully connected layer.

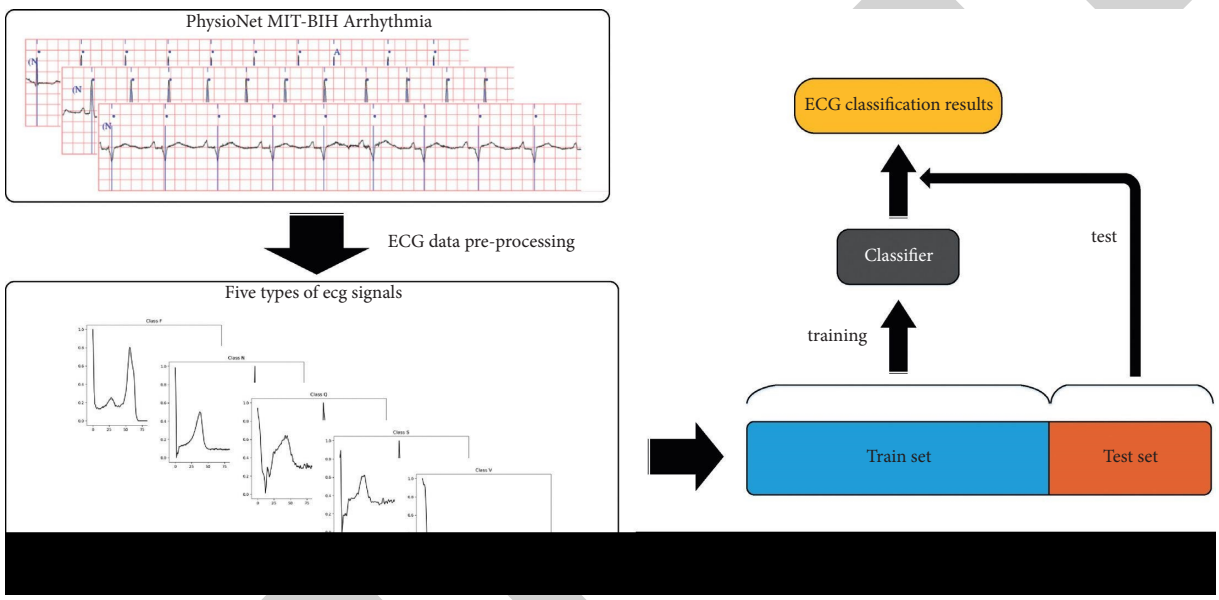

Figure 2: The proposed overall process of arrhythmia classification.

(ReLU) and exponential linear unit (ELU) [20]. ReLU is one of the most commonly used activation functions in CNN. When the input is positive, there will be no gradient saturation problem. Moreover, there is only a linear relationship, so the calculation speed is faster than sigmoid and tanh. However, it will convert the negative input to zero, which will cause some neurons to stop participating in changes in the neural network. ELU solves this dying ReLU problem and retains the advantages of ReLU. ELU is an exponential function when the input is negative, and its overall output value is around zero, which is more robust.

The functions of ReLU and ELU are as follows:

$$\mathrm{ReLU}(x) = \begin{cases} 0, & \text{if } (x \le 0), \\ x, & \text{if } (x > 0), \end{cases} \quad \mathrm{ELU}(x) = \begin{cases} \alpha(e^x - 1), & \text{if } (x < 0), \\ x, & \text{if } (x \ge 0), \end{cases} \tag{1}$$

where the value of the hyperparameter (α) is 1.0.

4.4. Optimized Classifier Architecture Similar to VGGNet. Given the above, we designed a CNN-based ECG arrhythmia classifier whose main structure is similar to VGGNet. Figure 4 shows a schematic of the proposed network. Table 3 describes the detailed architecture table of the proposed network. The proposed network contains 11 hidden layers, including nine one-dimensional convolutional layers and two fully connected layers. In this paper, kernel sizes of 3 and stride 2 are used in all convolutional layers, and all pooling layers use max pooling of size 2 and stride 2.

The mapping relationship between the heartbeat category and the heartbeat waveform is complicated [21], and we believe that single-layer convolution cannot complete the classification task well. Therefore, we use a coupled-convolution structure, two convolution layers, to get a better fitting effect. Furthermore, the use of deep convolution similar to the VGGNet framework can effectively improve the classification effect.

Most importantly, we used ELU as the activation function. We applied the TensorFlow open-source software library [22] to train and verify the model in the experiment. For network training, we used Adam optimizer [23] to optimize the parameters, where the learning rate is 0.001, beta-1 is 0.9, and beta-2 is 0.999, and used sparse categorical cross-entropy as the loss function.

Table 2: Distribution of datasets in different categories after preprocessing.

Category	*N*	*S*	*V*	*F*	*Q*	Total
Train data	72471	2223	5788	641	6431	87554
Test data	18118	556	1448	162	1608	21892
Total	90589	2779	7236	803	8039	109446

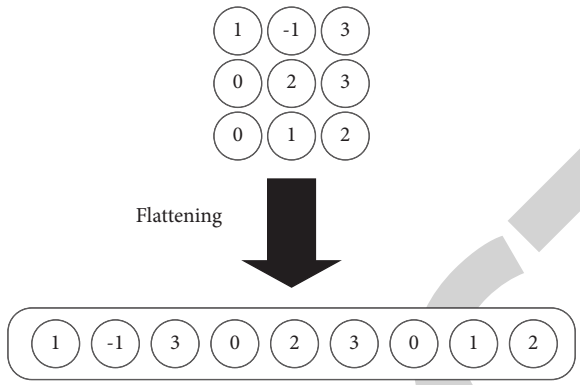

Figure 3: Schematic diagram of flattening layer.

In addition, to prevent overfitting of the model, we added Dropouts [24, 25] after the convolutional layers C2, C4, C6, and C9. Dropout randomly resets the weights of some neurons to 0 during each training process, reducing the number of parameters and avoiding overfitting.

4.5. Assessment Indicators. To evaluate the performance of the model, quantitative evaluation indicators are necessary. To this end, we applied four criteria to evaluate the classification effect of the CNN classifier proposed in this study, including accuracy (Acc), sensitivity (Sen), specificity (Spe), and positive prediction rate (Ppr).

The calculation formulas of the four indicators are as follows:

$$\begin{aligned} \mathrm{Acc} &= \frac{\mathrm{TP}+\mathrm{TN}}{\mathrm{TP}+\mathrm{TN}+\mathrm{FP}+\mathrm{FN}} \times 100, \\ \mathrm{Sen} &= \frac{\mathrm{TP}}{\mathrm{TP}+\mathrm{FN}} \times 100, \\ \mathrm{Spe} &= \frac{\mathrm{TP}}{\mathrm{TP}+\mathrm{FP}} \times 100, \\ \mathrm{Ppr} &= \frac{\mathrm{TP}}{\mathrm{TP}+\mathrm{FN}} \times 100, \end{aligned} \tag{2}$$

where TP denotes true positive, FP denotes false positive, TN denotes true negative, and FN denotes false negative.

5. Results and Discussion

Based on all samples, we used the proposed method to classify and evaluate the ECG arrhythmia classifier. Table 4 shows the confusion matrix of the classifier on all samples, and Table 5 shows the coefficients of the CNN method on all samples. Summarizing these data, we have less than 1% of ECG heartbeats misclassified in the experiment. Moreover, our proposed method achieved 99.76% average accuracy, 94.45% average sensitivity, 99.54% average specificity, and 97.40% average positive prediction rate based on all samples. Therefore, it is reasonable to believe that our proposed classifier can accurately predict and classify ECG arrhythmia signals.

Furthermore, we compare the proposed classifiers' performance with some other published methods based on evaluation indicators. Some studies only used part of the data from the MIT-BIH database, so it cannot be directly compared with the proposed method. For example, Jun et al. [7] excluded seven types of ECG arrhythmia from the MIY-BIH database, and only eight were classified.

Table 6 compares the VEB and SVEB classification performance of the proposed method with the other methods. The comparison experiments are based on the same dataset, which is intended to compare the classification performance of different classification methods. As it can be seen from this table, the proposed CNN classifier has excellent performance. The main reason behind this might be the fact that a network architecture similar to VGGNet is used. Research shows that network depth has an essential role in the classification effect [2]. All convolutional layers use smaller convolution kerVGGnels, which reduce the parameters and reduce the amount of calculation. It is worth mentioning that Shaker et al. [30] used Generative Adversarial Networks (GANs) equalization to process the dataset, making the model positive prediction rate slightly higher than the proposed model.

Additionally, by using a smaller convolution kernel to deepen the depth of the network and an activation function that accompanies each convolution layer, more activation functions can be added to have richer features and stronger dialectics. The classification accuracy of multiple small convolutions stacked is better than a single large

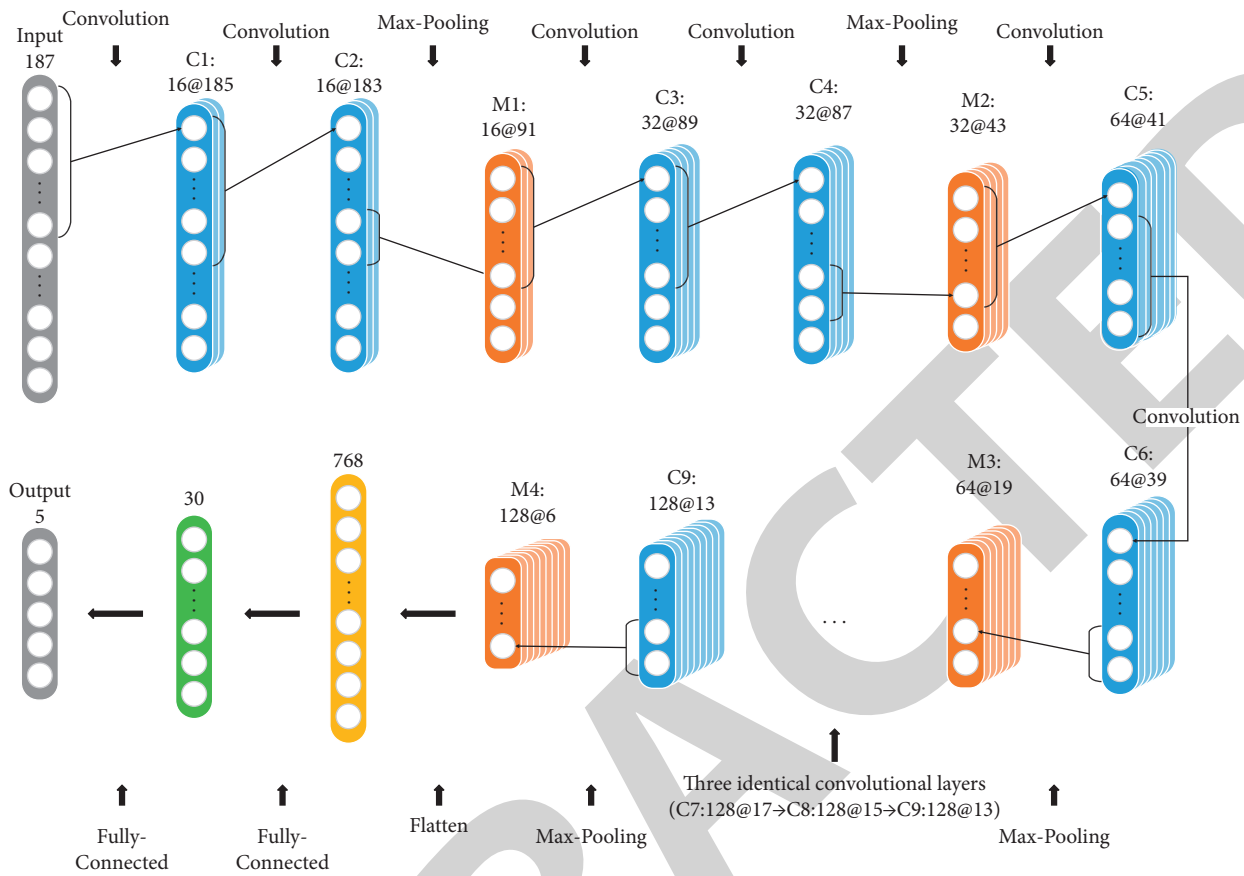

Figure 4: Architecture of the proposed CNN classifier.

Table 3: The structure of the proposed CNN classifier.

	Type	Biases	Kernel size	Stride	Output size
Layer 1	Convolution	16	3	1	(185, 16)
Layer 2	Convolution	16	3	1	(183, 16)
Layer 3	Max pooling	—	2	2	(91, 16)
Layer 4	Convolution	32	3	1	(89, 32)
Layer 5	Convolution	32	3	1	(87, 32)
Layer 6	Max pooling	—	2	2	(43, 32)
Layer 7	Convolution	64	3	1	(41, 64)
Layer 8	Convolution	64	3	1	(39, 64)
Layer 9	Max pooling	—	2	2	(19, 64)
Layer 10	Convolution	128	3	1	(17, 128)
Layer 11	Convolution	128	3	1	(15, 128)
Layer 12	Convolution	128	3	1	(13, 128)
Layer 13	Max pooling	—	2	2	(6, 128)
Layer 14	Flatten	—	—	—	(768)
Layer 15	Fully connected	30	—	—	(30)
Layer 16	Fully connected	5	—	—	(5)

convolution. In addition, we also selected ELU as the activation function, used the flattening layer to connect the convolutional layer and the fully connected layer, and used dropout to prevent overfitting. These works are also important reasons for obtaining good results.

During the experiment, we use dropout to prevent overfitting. Dropout is divided into a learning phase and a testing phase. In the learning phase, some hidden nodes will be temporarily ignored with a certain probability p, and the neural network will learn the local features in the data. In this way, feature learning in multiple simple networks can improve the generalization ability of the network. In the testing phase, the phases involved in learning and the hidden phase are summed with a certain probability p-weighted, and the network output is obtained by comprehensive calculation. Dropout can also be regarded as a kind of ensemble learning [31]. Figure 5 shows

Table 4: Confusion matrix of CNN method on all samples.

		Predicted				
		N	*S*	*V*	*F*	*Q*
Ground truth	*N*	90447	80	30	24	8
	S	199	2559	19	0	2
	V	74	3	7123	31	5
	F	83	1	58	661	0
	Q	33	0	3	0	8003

Table 5: Coefficients of the CNN classifier for classification of all samples.

Category	Acc (%)	Sen (%)	Spe (%)	Ppr (%)
N	99.51	99.84	97.94	99.57
S	99.72	92.08	99.92	96.82
V	99.80	98.44	99.89	98.48
F	99.82	82.32	99.95	92.32
Q	99.95	99.55	99.99	99.81
Average	99.76	94.45	99.54	97.40

Table 6: Comparison of VEB and SVEB classification performance of the proposed method with other methods.

Methods	Classifier	VEB				SVEB			
		Acc	Sen	Spe	Ppr	Acc	Sen	Spe	Ppr
Jiang et al. [26]	BBNN	98.8	94.3	99.4	95.8	97.5	74.9	98.8	78.8
Kiranyaz et al. [27]	1D-CNN	99.0	93.9	98.9	90.6	97.6	60.3	99.2	63.5
Acharya et al. [28]	DA + CNN	97.9	94.2	98.8	95.3	97.0	90.6	98.6	94.3
Zhai et al. [29]	2D-CNN	99.1	96.4	99.5	96.4	97.3	85.3	98.0	71.8
Shaker et al. [30]	GAN + CNN	99.5	94.5	99.7	98.6	99.1	91.2	99.3	97.7
Proposed	**1D-CNN**	**99.8**	**98.4**	**99.9**	**98.5**	**99.7**	**92.1**	**99.9**	**96.8**

BBNN: block-based neural networks, 1D: one-dimensional, 2D: two-dimensional, CNN: convolutional neural networks, DA: data augmentation, and GAN: generative adversarial networks.

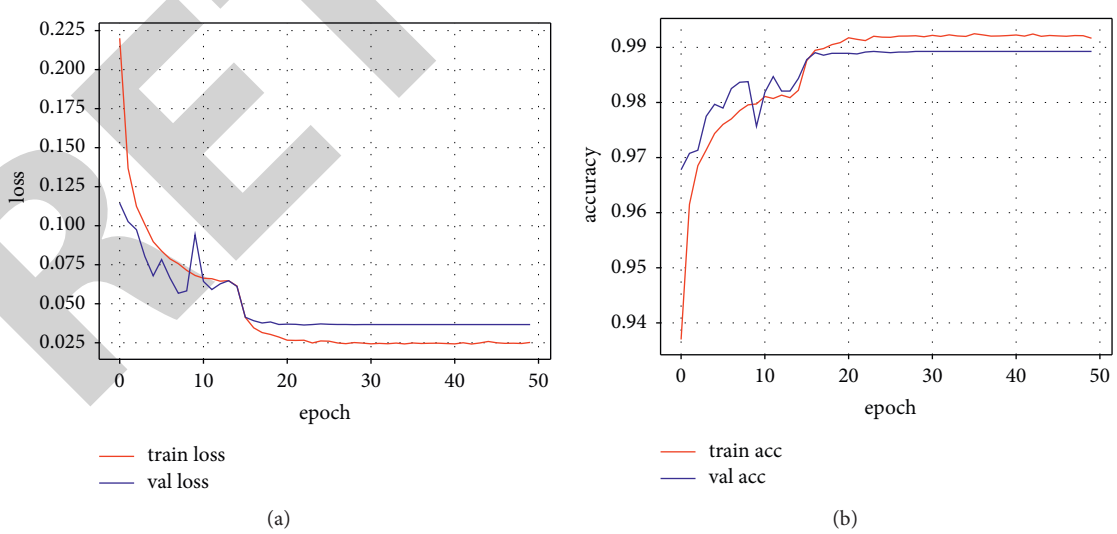

Figure 5: The (a) loss and (b) accuracy changes in training and verification steps.

the loss and accuracy changes of training and verification steps when the epoch is 50. It can be seen from Figure 5 that the loss and accuracy curves of the verification step show a trend close to the training curve, and there is no gradual upward trend. Therefore, it is reasonable to conclude that the proposed model is not overfitting.

6. Conclusion

In this paper, we proposed a CNN-based ECG arrhythmia classification method. The ECG records of the MIT-BIH arrhythmia database are preprocessed and used as model input data. Finally, the trained model classified the ECG signal into five beats: normal beat, supraventricular ectopic beat, ventricular ectopic beats, fusion beat, and unknown beat. The optimized CNN model is designed with a network architecture similar to VGGNet using ELU activation function, dropout, and other technologies. According to the results, our proposed method performs well in the four-finger VEB and SVEB classification, with an overall average accuracy rate of 99.76%, which could accurately classify ECG signals. In recent years, data enhancement has attracted attention in ECG arrhythmia classification. Our future work aims to use data enhancement technology and various deep learning optimization techniques to classify arrhythmia better.

Data Availability

The website for obtaining the MIT-BIH arrhythmia database is https://www.physionet.org/content/mitdb/1.0.0/, and the preprocessed ECG database is obtained from the website: https://www.kaggle.com/shayanfazeli/heartbeat.

Disclosure

Dengqing Zhang and Yuxuan Chen are the co-first authors.

Conflicts of Interest

The authors declare that there are no conflicts of interest regarding the publication of this paper.

Authors' Contributions

Dengqing Zhang and Yuxuan Chen contributed equally to this work.

References

[1] World Health Organization, *World Health Statistics 2019: Monitoring Health for the SDGs, Sustainable Development goals*, World Health Organization, Geneva, Switzerland, 2019.

[2] K. Simonyan and A. Zisserman, "Very deep convolutional networks for large-scale image recognition," 2014, https://arxiv.org/abs/1409.1556.

[3] E. H. Houssein, I. E. Ibrahim, N. Neggaz, M. Hassaballah, and Y. M. Wazery, "An efficient ECG arrhythmia classification method based on Manta ray foraging optimization," *Expert Systems with Applications*, vol. 181, Article ID 115131, 2021.

[4] B. M. Mathunjwa, Y.-T. Lin, C.-H. Lin, M. F. Abbod, and J.-S. Shieh, "ECG arrhythmia classification by using a recurrence plot and convolutional neural network," *Biomedical Signal Processing and Control*, vol. 64, Article ID 102262, 2021.

[5] D. Pirova, B. Zaberzhinsky, and A. Mashkov, "Detecting heart 2 disease symptoms using machine learning methods," in *Proceedings of the Information Technology and Nanotechnology (ITNT-2020)*, vol. 2667, pp. 260–263, Samara, Russia, 2020.

[6] U. B. Baloglu, M. Talo, O. Yildirim, R. S. Tan, and U. R. Acharya, "Classification of myocardial infarction with multi-lead ECG signals and deep CNN," *Pattern Recognition Letters*, vol. 122, pp. 23–30, 2019.

[7] T. J. Jun, H. M. Nguyen, D. Kang, D. Kim, D. Kim, and Y. Kim, "ECG arrhythmia classification using a 2-D convolutional neural network," 2018, https://arxiv.org/abs/1804.06812.

[8] N. Kohli, N. K. Verma, and A. Roy, "SVM based methods for arrhythmia classification in ECG," in *Proceedigs of the 2010 international conference on computer and communication technology (ICCCT)*, pp. 486–490, IEEE, Allahabad, India, September 2010.

[9] P. Walsh, *Support Vector Machine Learning for ECG Classification*, CERC, Delhi, India, 2019.

[10] I. Saini, D. Singh, and A. Khosla, "QRS detection using K-Nearest Neighbor algorithm (KNN) and evaluation on standard ECG databases," *Journal of Advanced Research*, vol. 4, no. 4, pp. 331–344, 2013.

[11] R. Saini, N. Bindal, and P. Bansal, "Classification of heart diseases from ECG signals using wavelet transform and kNN classifier," in *Proceedings of the International Conference on Computing, Communication & Automation. IEEE*, pp. 1208–1215, Greater Noida, India, May 2015.

[12] P. Kanani and M. Padole, "ECG heartbeat arrhythmia classification using time-series augmented signals and deep learning approach," *Procedia Computer Science*, vol. 171, pp. 524–531, 2020.

[13] C. Huang, Y. Zong, J. Chen, W. Liu, J. Lloret, and M. Mukherjee, "A deep segmentation network of stent s based on IoT for interventional cardiovascular diagnosis," *IEEE Wireless Communications*, vol. 28, no. 3, pp. 36–43, 2021.

[14] G. B. Moody and R. G. Mark, *MIT-BIH Arrhythmia Database Directory*, Massachusetts Institute of Technology, Cambridge, MA, USA, 1988.

[15] G. B. Moody and R. G. Mark, "The impact of the MIT-BIH arrhythmia database," *IEEE Engineering in Medicine and Biology Magazine*, vol. 20, no. 3, pp. 45–50, 2001.

[16] Association for the Advancement of Medical Instrumentation and others, *Testing and Reporting Performance Results Of Cardiac Rhythm And St Segment Measurement Algorithms*, ANSI/AAMI EC38, Washington, DC, USA, 1998.

[17] I. Goodfellow, Y. Bengio, and A. Courville, *Deep learning*, MIT press, Cambridge, MA, USA, 2016.

[18] J. Gu, Z. Wang, J. Kuen et al., "Recent advances in convolutional neural networks," *Pattern Recognition*, vol. 77, pp. 354–377, 2018.

[19] M. Kachuee, S. Fazeli, and M. Sarrafzadeh, "Ecg heartbeat classification: a deep transferable representation," in *Proceedings of the 2018 IEEE International Conference on Healthcare Informatics (ICHI)*, pp. 443-444, IEEE, New York, NY, USA, June 2018.

[20] D. A. Clevert, T. Unterthiner, and S. Hochreiter, "Fast and accurate deep network learning by exponential linear units (elus)," 2015, https://arxiv.org/abs/1511.07289.

[21] X. Xu and H. Liu, "ECG heartbeat classification using convolutional neural networks," *IEEE Access*, vol. 8, pp. 8614–8619, 2020.

[22] M. Abadi, A. Agarwal, P. Barham et al., "Tensorflow: large-scale machine learning on heterogeneous distributed systems," 2016, https://arxiv.org/abs/1603.04467.

[23] D. P. Kingma and J. Ba, "Adam: a method for stochastic optimization," 2014, https://arxiv.org/abs/1412.6980.

Hindawi
Journal of Healthcare Engineering
Volume 2023, Article ID 9875815, 1 page
https://doi.org/10.1155/2023/9875815

Retraction

Retracted: The Evaluation Model of College Students' Mental Health in the Environment of Independent Entrepreneurship Using Neural Network Technology

Journal of Healthcare Engineering

Received 10 October 2023; Accepted 10 October 2023; Published 11 October 2023

This article has been retracted by Hindawi following an investigation undertaken by the publisher [1]. This investigation has uncovered evidence of one or more of the following indicators of systematic manipulation of the publication process:

(1) Discrepancies in scope
(2) Discrepancies in the description of the research reported
(3) Discrepancies between the availability of data and the research described
(4) Inappropriate citations
(5) Incoherent, meaningless and/or irrelevant content included in the article
(6) Peer-review manipulation

The presence of these indicators undermines our confidence in the integrity of the article's content and we cannot, therefore, vouch for its reliability. Please note that this notice is intended solely to alert readers that the content of this article is unreliable. We have not investigated whether authors were aware of or involved in the systematic manipulation of the publication process.

In addition, our investigation has also shown that one or more of the following human-subject reporting requirements has not been met in this article: ethical approval by an Institutional Review Board (IRB) committee or equivalent, patient/participant consent to participate, and/or agreement to publish patient/participant details (where relevant).

Wiley and Hindawi regrets that the usual quality checks did not identify these issues before publication and have since put additional measures in place to safeguard research integrity.

We wish to credit our own Research Integrity and Research Publishing teams and anonymous and named external researchers and research integrity experts for contributing to this investigation.

The corresponding author, as the representative of all authors, has been given the opportunity to register their agreement or disagreement to this retraction. We have kept a record of any response received.

References

[1] X. Meng, J. Zhang, and G. Ren, "The Evaluation Model of College Students' Mental Health in the Environment of Independent Entrepreneurship Using Neural Network Technology," *Journal of Healthcare Engineering*, vol. 2021, Article ID 4379623, 9 pages, 2021.

Hindawi
Journal of Healthcare Engineering
Volume 2021, Article ID 4379623, 9 pages
https://doi.org/10.1155/2021/4379623

Research Article

The Evaluation Model of College Students' Mental Health in the Environment of Independent Entrepreneurship Using Neural Network Technology

Xiangmin Meng,[1,2] **Jie Zhang**,[1] **and Guoyan Ren**[2]

[1]*College of Economics and Management, Nanjing University of Aeronautics and Astronautics., 29 Jiangjun Avenue, Nanjing, Jiangsu 211100, China*
[2]*Zhejiang Wanli University, 8 Qianhu South Road, Ningbo, Zhejiang 315100, China*

Correspondence should be addressed to Xiangmin Meng; mengxiangmin@zwu.edu.cn

Received 2 September 2021; Revised 19 September 2021; Accepted 20 September 2021; Published 25 September 2021

Academic Editor: Shengrong Gong

In recent years, the employment of college students is becoming more and more prominent; no matter for the society, universities, college students themselves, and their families have formed a huge pressure, in the current situation, the success rate of college students to start their own business is not high; one of the important reasons is that college students generally have defects in entrepreneurial psychology. Therefore, effective evaluation of college students' mental health under the environment of independent entrepreneurship is conducive to comprehensively improving the quality of talent training in colleges and universities. In this paper, we propose a novel three-channel multifeature fusion network based on neural network technology to identify and predict college students' mental health problems in the self-entrepreneurship environment. Specifically, we first extract the behavior characteristics, visual characteristics, and social relations as a three-channel network input. Second, in view of the behavior characteristic, we use the length of the memory deep context dependent on network access. In view of visual features, we use the convolution neural network to face emotional characteristics and characteristics of social relations. The feature concat strategy is used for feature fusion. The experimental results on real datasets show that the method in this paper is effective, and it is expected to propose a new solution for college students' mental health assessment.

1. Introduction

Psychological education [1, 2] is an indispensable part of college students' entrepreneurship education because the cultivation of college students' entrepreneurial psychological capital is of vital importance for guiding college students' mental healthy growth [3, 4], establishing entrepreneurial ideas, and planning for future development. From the perspective of college students' entrepreneurial behavior activities, "The psychological capital elements of college students' positiveness, learning ability, optimism, innovation, etc., shown in entrepreneurial activities are the key factors that determine the success of college students. In reality, some college students who have already embarked on the road of entrepreneurship will always encounter some new problem. When the problem cannot be solved, it will have a certain negative impact on their psychology. The specific manifestations are low self-esteem [5, 6], poor frustration [7], negative treatment [8–10], etc. College students can not only properly deal with their own career problems, but also affect other people by bringing new employment opportunities. Compared with traditional capital such as economic capital and human capital, the psychological quality of the response measures taken by college students in the special situation when facing entrepreneurship is more important.

Psychological quality [11, 12] refers to a more complex psychological phenomenon formed by combining related elements such as cognition, emotion, will and

behavior, and environment. Entrepreneurship psychology [13–15] refers to the relatively stable psychological characteristics and psychological qualities that people show in the process of entrepreneurship. Entrepreneurship psychology refers to the psychological ability, morality and personality, behavior habits, and other qualities that an individual needs when implementing a business. It can support the individual's planning and entrepreneurial goals, implement entrepreneurial behaviors, overcome entrepreneurial difficulties, expand the scale of entrepreneurship, and finally obtain entrepreneurship success. It can be observed that effective entrepreneurial psychology can provide a solid foundation for a successful business and assist college students in achieving their goals and realizing their own worth. As a result, the key to the growth of entrepreneurial education is the creation of entrepreneurial psychological education for college students.

Currently, college students' entrepreneurial psychology education [16, 17] focuses on the following outcomes: the entrepreneurial psychology education system, for starters, is out of date. In my country, entrepreneurship instruction for college students began late. Overall, entrepreneurial education (particularly psychological counseling) in most schools and universities is above a superficial level and lacks depth. Some colleges and universities will directly apply to undergraduate colleges in the practice phase. In-depth reflection on the psychological and behavioral features of college students lacks in schools or other entrepreneurial psychology education models, resulting in a lack of relevance in the curriculum. Second, effective teaching programs are in short supply. Some higher vocational colleges' entrepreneurial psychology teaching activities ignore the issue of student participation, making it impossible for students to gain adequate information.

The psychological quality of college students' entrepreneurship is positively influenced by continuous and effective mental health evaluation. This research investigates the current state and countermeasures of college students' entrepreneurial psychological education, based on the aforesaid theoretical framework. It can add to the theory of entrepreneurial psychological education for college students and create a theoretical framework for college students to develop strong entrepreneurial psychology and succeed as entrepreneurs.

The main contributions of this paper are as follows:

(1) A novel three-channel multifeature fusion network based on neural network technology is proposed to identify and predict the mental health problems of college students in an autonomous entrepreneurial environment.

(2) Multimodal data is used in this study. Long short-term memory (LSTM) network is used to extract behavioral features, convolutional neural networks are used to extract facial emotion features, and graph convolutional networks are used to extract social relationship features.

(3) For multimodal data, a novel three-channel network is proposed, and a feature concat strategy is for feature fusion.

The remaining part of the thesis is structured as follows: Section 2 demonstrates background knowledge, which mainly introduces the psychological performance of college students during their entrepreneurship. Section 3 presents the methods used in this article for psychological evaluation. The main model used for psychological evaluation is the LSTM network, and the multimodal feature fusion method is emphasized. Section 4 presents the experiment. It mainly includes the analysis of the experimental environment, data, evaluation indicators, and experimental results. Section 5 presents the conclusion.

2. Background

2.1. Entrepreneurship. The definition of entrepreneurship can be interpreted as the following two: one is "Entrepreneurship [18] which refers to a complex process in which people discover and seize opportunities to create new products and services and achieve wealth appreciation through the sale of products and services." The other is the theory that was put forward by Cole in 1965: Entrepreneurship is defined as "initiating, maintaining, and developing into the behavior of establishing a business for the purpose of achieving profit." Explaination according to the meaning of entrepreneurship: Entrepreneurship is a process in which entrepreneurs optimize and integrate the resources they own or through their efforts to create greater economic or social value. Entrepreneurship is a way of labor that requires entrepreneurs to operate and organize, use services and technology to think, reason, and judge. This is the theoretical basis for this article to study the psychological education of undergraduates' entrepreneurship, and it has clear guidance for solving the problem of psychological education of undergraduates' entrepreneurship. The above is about the definition and interpretation of the meaning of entrepreneurship. From the perspective of entrepreneurial behavior, broadly speaking, entrepreneurship should refer to all employment-creating behaviors. This is also the fundamental motivation for the government to support entrepreneurship. As small as roadside vendors, as large as listed companies, they should all belong to the category of entrepreneurship. The significance of this is to at least solve the entrepreneur's own employment problem and drive part of the employment within the scope of ability. From a narrow perspective, it should be a behavior that is innovative in certain aspects and regions and can create more employment opportunities.

2.2. Entrepreneurial Psychology. Human psychology mainly refers to the cognitive process, emotions, will, ability, and personality. Cognition refers to the process by which people learn and apply knowledge or the input, processing, and output of information. When humans process information input from the outside world, they can recognize the attributes, characteristics of things, and the relationships

between things, produce attitudes toward things, and trigger corresponding emotions and emotional experiences. Human beings can change the world in a planned and purposeful way. This is a manifestation of human conscious initiative and the fundamental difference between humans and animals. Will is the psychological process by which human beings consciously determine goals and consciously control and regulate their behavior in order to achieve goals. The various psychological characteristics formed when human beings learn and use knowledge or when processing input information will differ from person to person. These stable and often appearing psychological characteristics are the manifestation of a person's personality, which includes ability and personality. There are differences in human personalities, that is, differences in human abilities and personality. Cognitive process, emotion, will, ability, and personality are three important aspects of individual psychological phenomena. These three aspects are interrelated and interdependent and together constitute human psychology. Entrepreneurship psychology is a special psychological phenomenon manifested in a person's psychology in a special state, that is, in the course of entrepreneurial behavior, which is mainly a psychological characteristic. Entrepreneurship psychology refers to the psychological state of the individuals who engage in entrepreneurial behavior in the process of entrepreneurial activities that regulate and dominate the entrepreneurial behavior.

2.3. Entrepreneurship Psychology of College Students. Entrepreneurship psychology [19] of college students refers to the psychology that college students should have for entrepreneurship. For a university, it undertakes the task of cultivating more and better talents for society. For the development of the country, a large number of people with better quality and higher willpower, ideal ambitions, and confidence in starting a career Talent is needed. Therefore, in order to ensure that college students do not have a greater psychological burden in the process of starting a career, colleges and universities must not only teach college students entrepreneurship but also ensure that efforts are made in the cultivation of entrepreneurial psychology. Entrepreneurship is not easy, so entrepreneurial psychology has become an important step in the entrepreneurial process. No matter what kind of business it is, there is no way to avoid all kinds of difficulties when it just started, especially when it comes to fields that the predecessors have not set foot in. It is very difficult to persist at the end, which requires entrepreneurs. Only with a firm will and absolute confidence can we persist to the end and win victory. The current problems faced by college students are not enough. They have not stepped into society and do not know how to face and deal with the difficulties, so they will be relatively fragile. Therefore, colleges and universities must further improve the entrepreneurial psychological quality of college students. The long-term life of college students in the campus environment has formed a relatively single value judgment standard, and their own comprehensive quality is still in the process of rapid improvement, which also means the psychological activities and psychological qualities they have when facing entrepreneurial problems, etc. It still needs further guidance and training. The discussion of college students' entrepreneurial psychological problems, the analysis of the causes of the problems, the proposal of countermeasures, etc., are not only for the cultivation of their own entrepreneurial psychology, but also for the cultivation of their value, outlook on life, and outlook on the world. On the basis of perfection, it is further reflected in entrepreneurial psychology, forming a virtuous circle.

3. Methodology

The neural network technology-based [20–22] mental health evaluation model framework for college students in the autonomous entrepreneurial environment proposed in this paper mainly includes four stages: data preprocessing, multimodal feature extraction, feature fusion, and mental health prediction and recognition, as shown in Figure 1.

In Figure 1, the three features are first extracted. The LSRTM network is used to extract behavior features, the convolutional neural network is used to extract visual features, and the graph convolutional neural network is used to extract social relationship features. Second, use the feature connection strategy to fuse the three different features extracted. Finally, the features are classified and the evaluation results are obtained.

3.1. Multimodal Feature Extraction. In order to effectively evaluate the mental health of college students in the self-employed environment, it is necessary to collect various characteristic data reflecting mental health. This article innovatively considers multimodal data, including behavioral data, visual data (such as human faces), and social relationship data. The details are shown in Figure 2.

Behavioral data: It can describe the state and behavior of college students' psychological characteristics. From the perspective of psychology, college students are in an autonomous entrepreneurial environment. They are affected by various aspects such as family and economy.

Visual data: mainly relying on the facial data of college students collected by campus surveillance cameras. Through the presentation and analysis of facial expression features, the psychological state of college students can be identified.

Social relationship data: in psychology, social relationship refers to the mutual relationship generated by students' learning, social interaction, and other behaviors in various contexts such as school and society. In social forums, students' mutual concern and different degrees of intimacy can make different users connect. If a student is regarded as a node, and its active and passive attention behavior is regarded as a connection relation, a social network can be drawn for each student, and this network is also of great significance for the evaluation of students' mental health state.

3.2. LSTM Network. Scholars have developed an upgraded recurrent neural network (RNN) model containing long short-term memory units, dubbed the LSTM neural

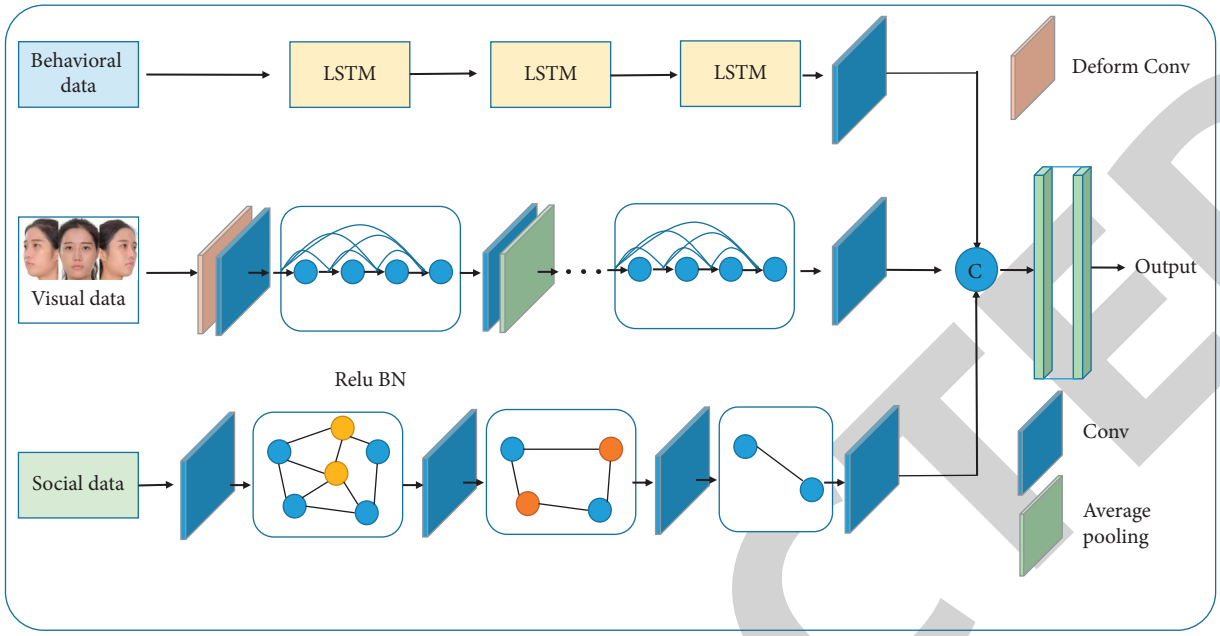

Figure 1: Schematic diagram of the overall framework of the proposed algorithm.

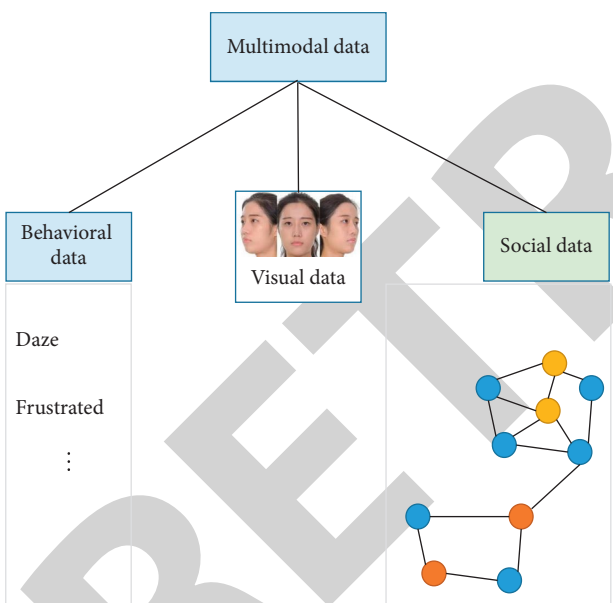

Figure 2: Schematic diagram of multimodal data.

network, to address the drawbacks of regular RNN neural networks. A sequence of recursively connected memory blocks makes up the LSTM neural network. Each memory block has three logic units: an input gate, an output gate, and a forget gate. The memory unit represents the neuron state's memory. The input and output gates are used to receive and output parameters, respectively, while the forget gate is used to determine if the historical information stored in the currently hidden layer node should be retained. The LSTM neural network can read, reset, and update historical data because of its cyclic feedback structure. Figure 3 depicts the schematic diagram.

The LSTM unit includes three gates: forget gate, input gate, and output gate, as well as two state vectors s and h. s is the internal state vector of LSTM and h is the output vector of LSTM. The forget gate determines the influence of the state vector s_{t-1} at the previous moment on the current state vector s_t, and the influence is controlled by the variable $f(t)$.

$$f(t) = \sigma\left(X_t W_f + h_{t-1} W_f + b_f\right), \tag{1}$$

where W_f is the forget gate's weight parameter, b_f is the forget gate's bias parameter, and σ is the activation function.

Through the new variable $g(t)$ and the control variable $i(t)$ generated by the nonlinear transformation, the input gate controls the degree of LSTM's acceptance of the input.

$$\begin{aligned} g(t) &= \tan h\left(X_t W_s + h_{t-1} W_s + b_s\right), \\ i(t) &= \sigma\left(X_t W_i + h_{t-1} W_i + b_i\right), \end{aligned} \tag{2}$$

where W_s and W_i are the input gate weight parameters, b_s and b_i are the input gate bias parameters, and tanh is the activation function. Under the control of the forget and input gate, LSTM updates the network state vector s_t.

$$s_t = f(t) * s_{t-1} + i(t) * g(t), \tag{3}$$

where $f(t) = 1$ and $i(t) = 1$ mean that the corresponding control door is fully opened, $f(t) = 0$ and $i(t) = 0$ mean that the corresponding control door is fully closed. The internal state vector s_t can be directly output as the state vector at the next moment, or it can be used to form an output variable h_t with the control variable of the output gate.

$$\begin{aligned} o(t) &= \sigma\left(X_t W_o + h_{t-1} W_o + b_o\right), \\ h_t &= o(t) * \tan h\left(s_t\right), \end{aligned} \tag{4}$$

where $o(t)$ represents the output gate control variable, when $o(t) = 1$, the state vector s_t is all used for output, when

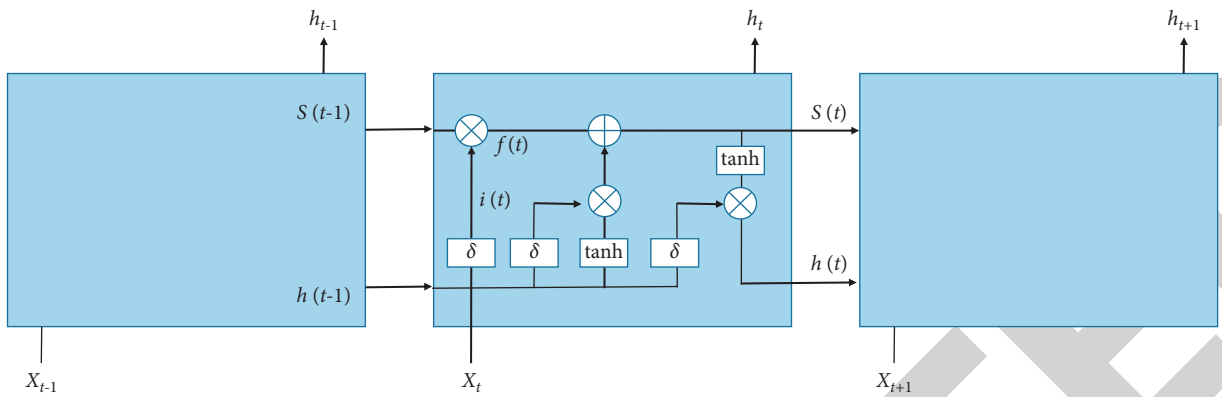

Figure 3: The structure of the LSTM neural network is depicted in this diagram.

$o(t) = 0$, the LSTM output is a vector of zero, W_o is the output gate weight parameter, b_o is the output gate offset parameter. Each LSTM neuron has an output value, but only the final output contains the feature information after the memory update on all previous timestamps. Therefore, LSTM neural network has its unique advantages in processing time series data. This article believes that behavioral data has long-term dependence. LSTM neural network can save historical information through a loop feedback structure and process and analyze time series data to predict the mental health of college students.

3.3. DenseXception Block. To extract facial emotion features from visual data, we propose a DenseXception block-based convolutional neural network, with each subnetwork consisting of five DenseXception blocks. The source picture is first warped and convolved to produce 64 deformation invariant feature maps, which are then passed through five DenseXception blocks in order. A 1×1 convolution is used as a conversion layer in the middle of each block to minimize the channel of the feature map by half. In addition, we only use a 2×2 average pooling layer after the first three blocks to maintain more spatial information in the feature map. The basic module for feature extraction is each DenseXception block. The original image information is fed into the deformed convolutional layer, which has a 3×3 convolution kernel, allowing the same item to appear in the image in various sizes, poses, angle changes, and even nonrigid deformations. A 1×1 conversion layer and a 2×2 average pool follow the first three DenseXception blocks. DenseNet's dense connection approach is used by the DenseXception block.

The original image is 64 pixels wide. The feature map will be quite vast and the quantity of calculation will be very large if the first DenseXception block's output channel is N and the size of the output feature map is $64 \times 64 \times N$. As a result, after the first three DenseXception blocks, we use the average pool to reduce the image size from 64×64 to 8×8. This significantly reduces the amount of computation required and increases the network's generalization ability. The conversion layer is only passed by the last two DenseXception blocks. The feature map is small enough at this point. No pooling operation is utilized in order to save enough space information.

Figure 4 shows the network structure diagram we created, which replaces DenseNet's convolutional layer with Xception. Each layer in DenseNet gets its input from the output of the layers before it. That is to say, for the L layer, there will be $(L(L+1)/2)$ connections in DenseNet. If the number of connections between these 5 Xception layers is 15, and the growth rate is R, the number of output features corresponding to the DenseXception block's input feature N equals $N + 5 \times R$. This dense connection method forms an implicit deep supervised learning by allowing each layer to get the gradient of the loss function straight from the original input feature map. The restricted network range, few parameters, high gradient, and characteristic information transmission efficiency, and ease of network training are all advantages of this structure. The deeper the network in a convolutional network, the more probable the gradient will vanish. Each layer of dense connections connects the input and the loss function directly, preventing gradient disappearance and increasing the network's depth.

As shown in Figure 4, the input channel count is $2N$, and the output channel count is M. To begin, reduce the number of channels to N and multiply by 1×1. Then, using deep separable convolution, N branches are obtained. Each branch's parameter is $3 \times 3 \times \mathrm{N} \times \mathrm{M}$. Finally, feature channels are created from the output of each branch's feature map. When we utilize classic 3×3 convolution and suppose that the input channel is 32 and the output channel is 64, the convolution parameter is $3333264 = 18432$. When using Xception, the 11 convolutional layer generation parameter is $113216 = 512$ for the same amount of input and output channels. As a result, the standard convolution parameters are approximately 17 times the Xception parameters under the same input and output conditions. As a result, Xception may drastically reduce the number of parameters in the network and the amount of computation required, successfully avoiding the overfitting problem. As a result, we were able to successfully extract facial emotion traits.

3.4. Graph Convolutional Neural Network. Although pure time series forecasting is sufficient to accurately fit the time series data of social relations, time series forecasting can only

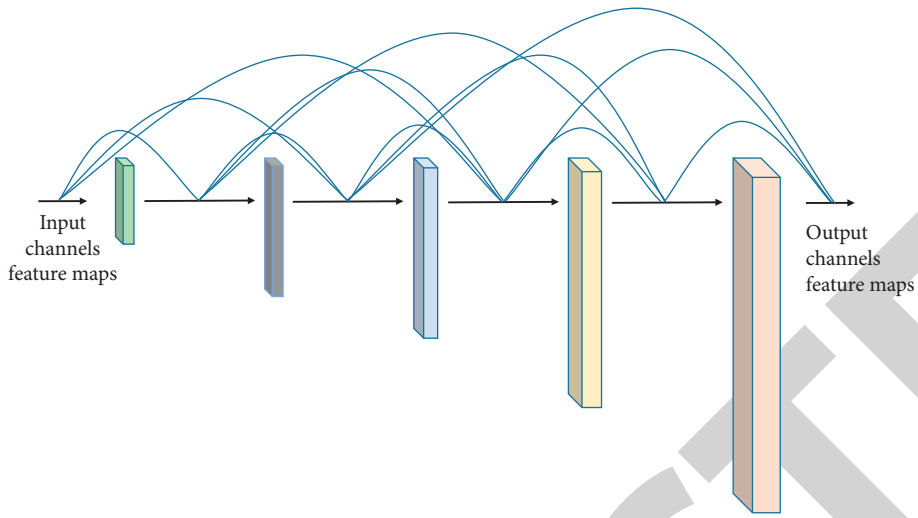

Figure 4: Schematic diagram of DenseXception.

consider time factors, not spatial distribution factors. The psychological problems of college students' entrepreneurship involve many social relationships. Therefore, this paper introduces graph convolutional neural networks to process social relationship data. The graph convolutional neural network is a method of automatically deep learning the graph data by considering the feature information of the node itself and the graph structure information at the same time. The graph convolutional neural network can learn the spatial and temporal features of the graph more efficiently. The operation principle of the graph convolutional neural network will be described in detail below.

Graph convolution uses the Adjacency matrix and Laplacian matrix to describe the node relationship of the graph. Among them, the adjacency matrix uses a digital square matrix to record whether there is an edge connection between each point, and the size of the number represents the weight of the edge. For graph $G = (V, E)$:

$$L = I_n - D^{-(1/2)} A D^{-(1/2)} \sim D^{-1} A, \tag{5}$$

where L is the regularized Laplacian matrix, A is the adjacency matrix of the graph, and D is the diagonal matrix.

$$D_{ij} = \sum_j \left(A_{ij}\right). \tag{6}$$

The graph convolution operation of the input signal X can be expressed as the following equation:

$$X_G f_\theta = \sum_{k=0}^{K-1} \left(\theta_k \left(D^{-1} A\right)^k\right) X, \tag{7}$$

where f_θ is the filter, θ is the parameter to be learned by the filter, and K is the maximum diffusion order, which is mainly used to describe the diffusion distance of a node to surrounding nodes. For example, the first-order means that the node is only connected to the surrounding nodes. The node has an influence, then the calculation equation of the graph convolutional layer is as follows:

$$\widehat{X} = \alpha\left(X_G f_\theta\right), \tag{8}$$

where X represents the input signal, $\widehat{X}$ is the output after the graph convolution, and α represents the activation function of the graph convolution. The main function of the graph convolutional layer is to capture the spatial information dependence of college students' social relations.

3.5. Feature Fusion. For the extracted features of multimodal data, this paper adopts the feature concat strategy to perform feature fusion, as shown in Figure 5.

It can be seen from Figure 5 that after extracting features from the three multimodal data, this paper adopts the feature concat strategy for feature fusion. In addition, for the fusion features, we use 2 fully connected layers to make the final prediction. If the predicted mental health status is higher than the alert threshold, psychological intervention and treatment should be carried out in time.

4. Experiments

4.1. Experimental Environments. We implemented our method with Python and PyTorch library and optimized it with Adam gradient descent algorithm, with a learning rate of 0.0001. All our training and testing are performed on the same GTX 2080TI, and the specific parameters are shown in Table 1.

4.2. Dataset. This article collected the behavioral data, visual data, and social relationship data of 49 college entrepreneurs of our school for 10 consecutive weeks, a total of 32,919 data. It is worth noting that these 49 creators were collected without their knowledge. However, after the event, we all obtained the approval of the observers to use their data for the research of this article. Therefore, we constructed the data set, the composition of which is shown in Table 2.

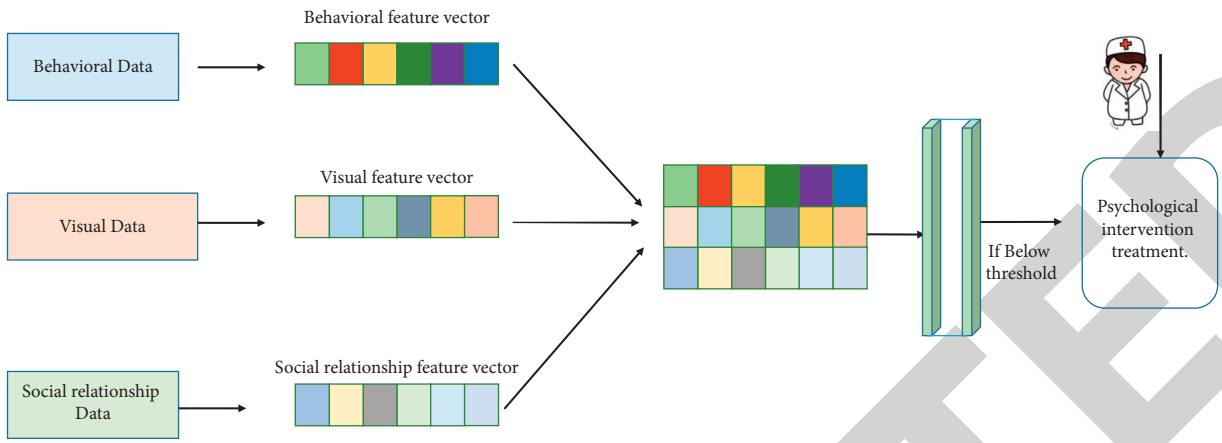

Figure 5: Schematic diagram of multimodal data feature fusion.

Table 1: Environment configuration.

Item	Parameter
CPU	Intel i9 9900k
RAM	32 GB
GPU	NVIDIA GTX 2080Ti
OS	Windows 10
Development tools	PyTorch 0.4, CUDA9.1, cuDNN7.6.5, Python3.6.5, Python-opencv, numpy
β_1	0.9
β_2	0.999
Learning rate	0.0001

Table 2: Data set division.

	Labelled	Unlabelled
Training set	28001	3527
Test set	1000	391

4.3. Evaluation Index. We use MSE to evaluate the performance of the proposed algorithm. The higher the accuracy of the model's prediction of experimental data, the smaller the value of MSE. The calculation equation of MSE is as follows:

$$\mathrm{MSE} = \frac{1}{n}\sum_{i=1}^{n}\left(\hat{y}_i - y_i\right)^2. \tag{9}$$

4.4. Experimental Results. The proposed technique is tested on real data sets in this part, and the experimental results are reported in Table 3. In addition, we divide the training set into three different magnitudes, 30 percent, 50 percent, 70 percent, and default, to more intuitively test the advanced nature of the proposed method.

It can be clearly seen from Table 3 that with the increase of the training set data, the error of the proposed algorithm is getting smaller and smaller. Moreover, when the training set uses 70% and 28001 training data, the error is the same. This shows the proposed algorithm. The algorithm value needs 70% to achieve the best performance, which proves the feature extraction ability of the three-channel network. In addition, the error rate of 3.69% also proves the effectiveness of the proposed algorithm.

Table 3: Experiment results.

Method	MSE (%)
30% training set	10.95
50% training set	5.69
70% training set	**3.69**
Ours (default)	**3.69**

4.5. Ablation Experiment with Multimodal Features. In order to further verify the advanced nature of the proposed algorithm, this section sets up an ablation experiment for feature extraction from multimodal data. We let B represent behavioral features, V represent visual features, and C represent social relationship features, then $B+V$, $B+C$, and $V+C$ represent the combined feature, and the results of the ablation experiment are shown in Table 4.

From Table 4, we can clearly see the impact of the three types of features on the performance of the proposed algorithm. First of all, we can see that the use of three multimodal features at the same time achieves the lowest error rate. Second, we find that for the prediction of mental health assessment, most of the existing methods use the B feature. However, the error of using the B feature is the largest. At the same time, in a single feature, the V feature has achieved relatively better performance, which proves the powerful ability of the computer vision method based on

Table 4: Ablation experiment results.

Method	MSE (%)
B	15.43
V	5.11
C	5.99
$B+V$	4.13
$B+C$	4.36
$V+C$	3.87
B + V + C (ours)	**3.69**

convolutional neural in facial emotion recognition. Similarly, the C feature has achieved suboptimal results. In addition, we found that combined features are better than single features, which further proves that it is effective to consider multiple modal features.

5. Conclusion

This paper proposes a method for evaluating and predicting the mental health of college students based on deep learning technology. The input feature data consists of three modalities: behavioral features, visual features, and social relationship features, and different deep learning techniques are used to process each modal feature. Specifically, for behavioral features, we use long and short-term memory networks to obtain deep context dependence. For visual features, we use convolutional neural networks. The network acquires facial emotion features and social relationship features, and we use graph convolutional networks to extract them. Finally, the feature connection strategy is used to fuse the above three features. Experiments verify that the new three-channel multifeature fusion network proposed in this paper has better performance. This also further shows that the network is suitable for the evaluation and prediction of the mental health of college students. However, because of the multimodal features used in this article, and the extraction of each model feature is based on deep learning technology. The time complexity of the proposed method is greatly increased. The improvement of this point is the direction of our follow-up research.

Data Availability

The dataset used to support the findings of this study are available from the corresponding author upon request.

Conflicts of Interest

All the authors do not have any conflicts of interest.

Acknowledgments

This study was supported by the Zhejiang Wanli University and also supported by the College Students' Ideological and political life project (a new exploration of college life and politics under the new situation: taking the "entrepreneurship into the community" of business school as an example) under the new situation under Grant SHSZ202007.

References

[1] S. Chai, B. Yao, L. Xu et al., "The effect of diabetes self-management education on psychological status and blood glucose in newly diagnosed patients with diabetes type 2," *Patient Education and Counseling*, vol. 101, no. 8, pp. 1427–1432, 2018.

[2] R. L. Mosher, N. A. Sprinthall, V. S. Atkins et al., "Psychological education: a means to promote personal development during adolescence," *The Counseling Psychologist*, vol. 2, no. 4, pp. 3–82, 1971.

[3] T. A. O. Xiangqi, "Research on the problems and countermeasures of mental health education for college students," *The Theory and Practice of Innovation and Enntrepreneurship*, vol. 3, no. 15, p. 160, 2020.

[4] D. P. Kraft, "Mens sana:the growth of mental health in the American college health association," *Journal of American College Health*, vol. 58, no. 3, pp. 267–275, 2009.

[5] W. J. Hale, J. K. Perrotte, M. R. Baumann, and R. T. Garza, "Low self-esteem and positive beliefs about smoking: a destructive combination for male college students," *Addictive Behaviors*, vol. 46, pp. 94–99, 2015.

[6] J. Clore and S. Gaynor, "Self-statement modification techniques for distressed college students with low self-esteem and depressive symptoms," *International Journal of Behavioral Consultation and Therapy*, vol. 2, no. 3, pp. 314–331, 2006.

[7] Y. H. Zang and L. Wu, "Mediation effect of interpersonal trust and mental resilience between positive mental health and frustration among poor college students," *Chinese Journal of School Health*, vol. 37, 2016.

[8] P. Pedrelli, M. Nyer, A. Yeung, C. Zulauf, and T. Wilens, "College students: mental health problems and treatment considerations," *Academic Psychiatry*, vol. 39, no. 5, pp. 503–511, 2015.

[9] S. Ketchen Lipson, S. M. Gaddis, J. Heinze, K. Beck, and D. Eisenberg, "Variations in student mental health and treatment utilization across US colleges and universities," *Journal of American College Health*, vol. 63, no. 6, pp. 388–396, 2015.

[10] S. M. Gaddis, D. Ramirez, and E. L. Hernandez, "Contextualizing public stigma: endorsed mental health treatment stigma on college and university campuses," *Social Science and Medicine*, vol. 197, pp. 183–191, 2018.

[11] R. C. Rosen and S. Althof, "Impact of premature ejaculation: the psychological, quality of life, and sexual relationship consequences," *The Journal of Sexual Medicine*, vol. 5, no. 6, pp. 1296–1307, 2008.

[12] J. Butler and J. Ciarrochi, "Psychological acceptance and quality of life in the elderly," *Quality of Life Research*, vol. 16, no. 4, pp. 607–615, 2007.

[13] M. Frese and M. M. Gielnik, "The psychology of entrepreneurship," *Annual Review of Organizational Psychology and Organizational Behavior*, vol. 1, no. 1, pp. 413–438, 2014.

[14] A. Omorede, S. Thorgren, and J. Wincent, "Entrepreneurship psychology: a review," *The International Entrepreneurship and Management Journal*, vol. 11, no. 4, pp. 743–768, 2015.

[15] M. J. Gorgievski and U. Stephan, "Advancing the psychology of entrepreneurship: a review of the psychological literature and an introduction," *Applied Psychology*, vol. 65, no. 3, pp. 437–468, 2016.

[16] T. M. Ndofirepi, "Relationship between entrepreneurship education and entrepreneurial goal intentions: psychological traits as mediators," *Journal of Innovation and Entrepreneurship*, vol. 9, no. 1, pp. 1–20, 2020.

Hindawi
Journal of Healthcare Engineering
Volume 2023, Article ID 9873297, 1 page
https://doi.org/10.1155/2023/9873297

Retraction

Retracted: Hippocampus Segmentation Method Based on Subspace Patch-Sparsity Clustering in Noisy Brain MRI

Journal of Healthcare Engineering

Received 5 December 2023; Accepted 5 December 2023; Published 6 December 2023

This article has been retracted by Hindawi, as publisher, following an investigation undertaken by the publisher [1]. This investigation has uncovered evidence of systematic manipulation of the publication and peer-review process. We cannot, therefore, vouch for the reliability or integrity of this article.

Please note that this notice is intended solely to alert readers that the peer-review process of this article has been compromised.

Wiley and Hindawi regret that the usual quality checks did not identify these issues before publication and have since put additional measures in place to safeguard research integrity.

We wish to credit our Research Integrity and Research Publishing teams and anonymous and named external researchers and research integrity experts for contributing to this investigation.

The corresponding author, as the representative of all authors, has been given the opportunity to register their agreement or disagreement to this retraction. We have kept a record of any response received.

References

[1] X. Ren, Y. Wu, and Z. Cao, "Hippocampus Segmentation Method Based on Subspace Patch-Sparsity Clustering in Noisy Brain MRI," *Journal of Healthcare Engineering*, vol. 2021, Article ID 3937222, 10 pages, 2021.

Hindawi
Journal of Healthcare Engineering
Volume 2021, Article ID 3937222, 10 pages
https://doi.org/10.1155/2021/3937222

Research Article

Hippocampus Segmentation Method Based on Subspace Patch-Sparsity Clustering in Noisy Brain MRI

Xiaogang Ren,[1,2] **Yue Wu**,[3] **and Zhiying Cao**[3]

[1]*Changshu Hospital of Chinese Medicine, Changshu 215516, Jiangsu, China*
[2]*School of Information and Control Engineering, China University of Mining and Technology, Xuzhou, Jiangsu 221116, China*
[3]*The Affiliated Changshu Hospital of Soochow University (Changshu No. 1 People's Hospital), Suzhou, Jiangsu 215500, China*

Correspondence should be addressed to Xiaogang Ren; lb20060005@cumt.edu.cn

Received 10 August 2021; Revised 10 September 2021; Accepted 16 September 2021; Published 25 September 2021

Academic Editor: Gu Xiaoqing

Since the hippocampus is of small size, low contrast, and irregular shape, a novel hippocampus segmentation method based on subspace patch-sparsity clustering in brain MRI is proposed to improve the segmentation accuracy, which requires that the representation coefficients in different subspaces should be as sparse as possible, while the representation coefficients in the same subspace should be as average as possible. By restraining the coefficient matrix with the patch-sparse constraint, the coefficient matrix contains a patch-sparse structure, which is helpful to the hippocampus segmentation. The experimental results show that our proposed method is effective in the noisy brain MRI data, which can well deal with hippocampus segmentation problem.

1. Introduction

The hippocampus is a decisive organization in the structure of human brain. Its function is to control memory and emotion and determine the spatial position [1]. As we all know, short-term memory is stored in the hippocampus. If the hippocampus is damaged, it will directly lead to partial or total irreversible loss of memory function [2]. The abnormal function and morphology of hippocampus may induce Alzheimer's disease [3], schizophrenia, temporal lobe epilepsy, severe depression, and other nervous system diseases [4]. Therefore, if the hippocampus can be accurately segmented from the brain tissue, it will be better to provide more accurate diagnostic basis for disease research, as shown in Figure 1 [5].

The difficulty of image segmentation is that there are many kinds of images with different quality, so it is impossible to establish a unified image segmentation standard [6]. How to segment the image quickly and effectively has always been the focus of image processing. So far, there is no general method of accurate image segmentation, but the cognition of image segmentation has become more and more clear, and many image segmentation methods have been produced. Different segmentation methods generally understand the problem of image segmentation from different perspectives.

The hippocampus has the characteristics of small size and irregular shape. The traditional segmentation method is prone to the wrong segmentation, and the segmentation speed is slow, which consumes a lot of time. In order to solve various problems in the process of hippocampus segmentation, the development of segmentation technology is mainly divided into manual segmentation, semiautomatic segmentation, and automatic segmentation [5]. Manual segmentation refers to experienced clinicians directly drawing the boundary of the hippocampus on the brain MRI image or drawing the boundary of the relevant tissues on the computer display through the mouse to form the region of interest. At present, the main purpose of hippocampus segmentation is to separate the interested objects from the brain MRI image background, so as to further analyze and recognize them quantitatively and understand the brain MRI image [5]. Due to the extremely complex diversity of medical images and the noise introduced in the brain MRI imaging equipment, there is a certain degree of noise in medical images, and some edges of the hippocampus object may not

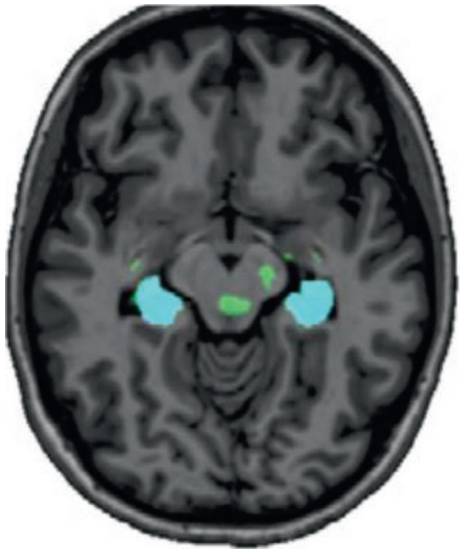

Figure 1: Example for hippocampus segmentation.

be clear [7]. Therefore, there is no general theory and method in hippocampus segmentation of brain MRI. The result of manual segmentation is usually regarded as the gold standard because of its high accuracy, but it is time-consuming and laborious at the same time [8]. The quality of the segmentation result completely depends on the operator's experience and knowledge, and the segmentation result is difficult to reproduce. Automatic segmentation means that the whole process of image segmentation is completely controlled by the computer and completely separated from the manual interference. Although this method can reproduce the segmentation results well, the computational complexity is also very large, and it requires high configuration of computer equipment. With the development of computer science and technology, the semiautomatic segmentation of human–computer combination model, also known as interactive segmentation method, comes into being [9]. It combines the experience of human knowledge with the powerful data processing, storage, and memory ability of computer and realizes image segmentation through human–computer interaction. However, the results of computer automatic segmentation are often not satisfactory, and the accuracy cannot meet the requirements of clinical application of medical images, while the manual segmentation, which relies too much on human experience, is also unacceptable in practical application [10]. The commonly used methods of hippocampal segmentation are threshold method, edge detection, region growing method, fuzzy clustering method [11, 12], graph theory-based max-flow/min-cut method, deformation model, neural network method, genetic algorithm, and wavelet transform method [13], where region growing segmentation based on seed points and deformation model methods are all interactive segmentation methods. Because of the complexity of human body structure, fuzzy edge, and uneven gray level, the medical image is more difficult to segment than nature image. Therefore, it is particularly important to study the hippocampus segmentation methods of medical images in depth.

At present, domestic and foreign scholars have made further research and exploration on the automatic hippocampus segmentation. Lu and Luo [14] proposed a segmentation method based on multi-atlas, which used similar weighted voting and label bias correction to achieve almost automatic segmentation of hippocampus. Wu et al. [15] used statistical model for automatic segmentation of hippocampus in brain MRI images, which is suitable for routine analysis of large-scale hippocampal formation. Some scholars have integrated the automatic segmentation technology of brain tissue and developed corresponding software, such as FSL and FreeSurfer [16]. The FSL is a tool library developed by the Oxford University for analyzing brain MRI. The tool library includes first toolkit, which can realize the automatic segmentation of brain structure and the segmentation of hippocampus, brain stem, nucleus accumbens, and other tissues. The FreeSurfer is developed by the world-famous Harvard Medical School and MIT, which can solve the problem of brain 3D MRI image data and automatically segment the cortex and subcutaneous nuclei by using the gold-standard prior probability information estimation.

Because of the weak edge of the object region in hippocampus MRI image, the existing active contour sequence segmentation models often show an edge-false problem. So, a contour transfer evolution based a segmentation method is proposed [17], which combines the region-based model and edge model based perfectly and transfers the growth edge of the object region in the current image to the adjacent image as its initial contour. As a result, the new model reduces iteration times and improves the accuracy of the segmentation results, but the performance of segmentation for a hippocampus with a small size and irregular shape is poor. The hippocampus segmentation method based on graph theory can make good use of multiscale redundancy features and has good segmentation effect. However, there is no unified method and standard for how to describe the image as a graph and how to extract it more accurately, and the representation of graph will affect the result of hippocampus segmentation [18].

In this paper, a novel image segmentation method based on subspace clustering is proposed, which regards the superpixel as the point of the image and chooses the matrix of the superpixel as the projection dictionary. By restraining the coefficient matrix with the block-sparse constraint, the coefficient matrix contains a patch-sparse structure, which is helpful to the hippocampus segmentation. The experimental results show that our proposed method is effective to the noisy brain MRI data, which can well deal with the hippocampus segmentation problem.

2. Related Works

2.1. Subspace Clustering. Subspace clustering, also known as subspace segmentation, assumes that the data are distributed in the union set of several low-dimensional subspaces, which is the process of classifying the data into their subspaces in some way [19]. Through subspace clustering, the data from the same subspace can be classified into one class, and the

relevant properties of the corresponding subspace can be extracted from the same kind of data. Subspace clustering is to classify the data belonging to the subspace S_i in the data matrix X to obtain a low-dimensional representation of the data and thereby obtain the dimension and base matrix of the subspace S_i. When the number of subspaces is one, the subspace clustering problem is equivalent to the principal component analysis. Through principal component analysis, the principal information of the data matrix can be obtained, so as to obtain the low-dimensional representation of these data. The most common method to solve the principal component analysis is singular value decomposition (SVD). When the number of subspaces is greater than one, the dimension and basis matrix of subspace are unknown, and the interaction between different subspaces makes the information obtained from the observation data inaccurate, which increases the difficulty of subspace clustering. Therefore, many scholars often assume that different subspaces are independent or noninteractive when building the subspace clustering models.

The process of subspace clustering is shown in Figure 2. There are many methods to realize subspace clustering, including algebraic method, iterative method, statistical method, and spectral clustering method [20]. The theoretical basis of each method is different, and there are also great differences in the solution process. However, the clustering results are obtained/solved by solving the representation coefficient of data matrix X under a specific base matrix. The representative method is to use the matrix decomposition method and spectral clustering method. In order to get the feature representation of data matrix X in subspace, X can be written as $X = DA$, where D represents the dictionary, the basis matrix can be obtained by training dictionary or using the iterative updating process, and A represents the representation coefficient matrix of data matrix X under dictionary D. By adding appropriate constraints to the coefficient matrix or dictionary, the data can be more accurately projected into its subspace. In this paper, we mainly studied the subspace clustering method based on spectral clustering for brain MRI hippocampus image, where the graph theory is taken as the theoretical basis and the data as the vertices in the graph. Therefore, the similarity between the vertices can be obtained by solving $X = DA$. Thus, the adjacency matrix of the graph is obtained, the Laplacian matrix of the graph is constructed, and the clustering result is obtained from the Laplacian matrix of the graph using the spectral clustering method, thereby obtaining the clustering result of the data.

The purpose of subspace clustering is to classify data from different subspaces into their corresponding subspaces [14]. The key point is to get the correct representation of the data in the subspace. The subspace clustering method is based on graph theory, using spectral clustering method to cluster data. The biggest difference among subspace clustering and traditional graph theory-based clustering and spectral clustering is that subspace clustering starts from the source of the data, focuses on the representation of the data in the subspace, and obtains more accurate data, while the subspace representation of data can also be used for data analysis and other processing. In the subspace clustering process, the data is regarded as the vertices in the graph, the weight matrix or adjacency matrix of the graph is obtained by solving the representation coefficient of the data in the subspace, and the final clustering result is obtained by using the spectral clustering method. The realization of a process is based on the mathematical theory of graph theory. The clustering process of data is transformed into the cutting process of the vertices of the graph. The connectivity of the graph is used to show the relationship between different classes.

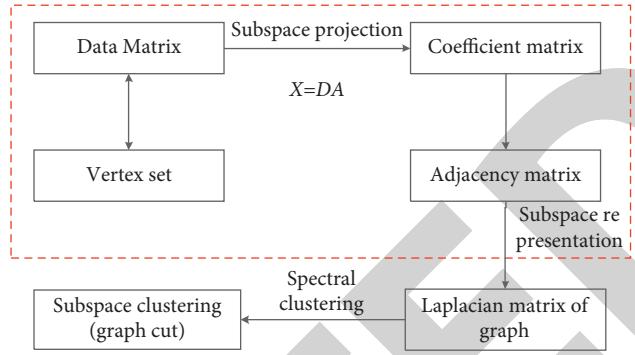

Figure 2: The process of subspace clustering.

2.2. Sparse Representation. Sparse representation is a research hotspot in the field of image processing recently. Its purpose is to better reveal the essential characteristics by using the sparse property of signal or image in a specific space [21]. The sparse representation of signal can be achieved by constructing appropriate dictionary and sparsity requirement of coefficients. In other words, the signal can be represented by as few atoms as possible in the dictionary. The obtained nonzero coefficients can represent the main structure and characteristics of the signal. In order to reveal the more essential characteristics and get a more sparse representation of the signal, many scholars have done a lot of work in the construction of dictionaries. Through dictionary construction, the signal has the basis of sparse representation, and the common method is to constrain the coefficients by l0 or l1 norm so as to get sparse coefficients. Sparse representation has achieved good results in many applications, such as compressed sensing, denoising, super-resolution reconstruction, and texture decomposition [22]. Sparse subspace clustering method combines sparse representation theory and subspace representation coefficients. The final result of subspace clustering is to classify the data in the same subspace. When the subspaces are independent of each other, the data belonging to a certain subspace is only composed of the baseline in this subspace. In other words, the representation coefficient of these data in other subspaces is zero. Therefore, as for high-dimensional data, the representation coefficients of data in low-dimensional subspace are sparse. The data in the same subspace only have representation coefficients in this subspace, which shows the same sparsity. By solving the sparsity constraint of

representation coefficients, the sparsity of data representation coefficients is highlighted, which provides support for the correct clustering.

According to the structural characteristics of the analyzed signal, any given observed signal $y \in R^N$ can be expressed in a parameterized way, which can construct the feature dictionary $D \in R^{N\times M}$. $d \in D$ is the atom in dictionary and $\|d\| = 1$. Therefore, the projection of y on the atoms in the dictionary can be written as $c = \langle y, d\rangle$. The standard formula of sparse representation problem can be denoted as follows:

$$x^* = \arg\min_x \|y - dx\|_2^2 + \lambda\|x\|_0, \tag{1}$$

where $\|x\|_0$ represents the number of nonzero elements in x; $\lambda > 0$ data, and each column x_i is an n-dimensional feature vector. These data come from the union of K independent subspaces $\{S_c\}_{c=1}^K$ with unknown dimension $\{r_c\}_{c=1}^K$. The purpose of subspace clustering is to reveal the subspace attributes of each data by clustering, and different classes correspond to different subspaces. If any data in the subspace can be represented as a linear combination of other data, the matrix Z can be used to construct the similarity matrix. In order to obtain the matrix Z, the following optimization problem can be solved:

$$\begin{cases} \min & \Omega(Z)_{Z,E} + \lambda\Phi(E), \\ s.t. & X = XZ + E, \end{cases} \tag{2}$$

where $\Omega(Z)$ and C are the constraints on Z; E is the error value or abnormal value; $\Phi(E)$ is the constraint function of E. In general, $\|E\|_F^2$ is used for Gaussian noise, and $\|E\|_1$ is used for abnormal value. λ is a trade-off parameter. The main difference between different clustering methods is the selection of $\Omega(Z)$. A suitable $\Omega(Z)$ is designed so that the matrix Z obtained from the model satisfies the properties of sparsity between classes and consistency within classes.

3. Subspace Patch Sparsity for Clustering Segmentation

3.1. Motivation. In Section 2, it is assumed that the data matrix can be denoted as $X = [X_1, X_2, \ldots, X_n] \in R^{M\times N}$, where $X_i \in R^{M\times n_i}$, $(i = 1, 2, \ldots, n)$, comes from n independent linear subspaces S_i. The subspace representation problem $X = XA$ has a solution with patch diagonal structure. For the previously mentioned subspace clustering problem, when the data is only represented by some atoms from the same subspace, the information of the data belonging to the same subspace can be easily obtained through the representation coefficient. When the data matrix is arranged via the matrix A, the representation is shown as the patch diagonal structure of the coefficient matrix. Theoretically, the coefficient matrix A has a patch diagonal structure, which means that the adjacency matrix W in the graph constructed by A also has a block diagonal structure. The patch diagonalization of the adjacency matrix indicates that the vertices in the same block constitute a connected subgraph and are not connected with other connected subgraphs, while the vertices in the connected subgraph are data in the same subspace. Therefore, the block diagonal structure of coefficient matrix plays an important role in subspace clustering.

In order to obtain the coefficient matrix with block diagonal structure, sparse subspace clustering and low-rank subspace clustering introduce sparse and low-rank constraints into subspace representation, respectively. The sparse clustering model measures the sparsity of the coefficients by l_1. The adaptive sparse representation makes the coefficient sparse matrix under the sparsity constraint block, which reflects the block diagonal structure. The low-rank subspace clustering model uses the kernel norm to constrain the rank of the coefficient matrix. The operation of the whole matrix makes the low-rank constraint better retain the global structure of the coefficient matrix than the sparse constraint. In addition, it is proved theoretically that the solution of the low-rank optimization problem has the block diagonal structure. Therefore, sparse and low rank can get the coefficient matrix with block diagonal structure. However, the coefficient matrix in sparse model has the block-sparse property, but the actual solution process is to calculate each column of coefficient separately, so the isolated calculation does not use the global patch-sparse structure of coefficient matrix.

Both sparse model and low-rank model constrain data in the same subspace. The sparse model takes advantage of the sparsity of data representation, while the low-rank model starts from the global structure of the matrix and makes full use of the correlation of the same subspace data. Combined with the idea of the sparse and low-rank model, the subspace representation of data should show sparsity between different subspaces. In other words, the patch representation of subspace is sparse, and the representation of different data should be closer in the same subspace, making full use of the correlation between data. Inspired by the previously mentioned analysis, this paper introduces the $l_{1,2}$ norm constraint to establish the patch-sparse subspace clustering model, which considers the global relationship of data in the subspace while calculating the sparsity of the coefficients.

3.2. Patch-Sparsity Model. Let $R = \{K_1, K_2, \ldots, K_n\}$ be a division of $\{1, 2, \ldots, n\}$, where K_i corresponds to the subscript of data in subspaceS_i. For a column vector x in data matrix X, the following model is constructed:

$$\begin{cases} \min & \sum_{K\in R} \|\alpha_k\|_2, \\ s.t. & x = Xa, \end{cases} \tag{3}$$

where a_k is a vector composed of elements whose subscripts belong to k in feature matrix a norm. Therefore, the solution of (3) can be equivalent to the solution of the following equation:

$$\min_\alpha \|Xa - x\|_2 + \lambda \sum_{K\in R} \|\alpha_K\|_2, \tag{4}$$

where λ is the regularization parameter and is typically set to 0.1.

For the sake of analysis, we can rewrite (4) as a matrix form, which can be denoted as follows:

$$\min_{A} \frac{1}{2}\|XA - X\|_F^2 + \lambda \sum_{j=1}^{N} \sum_{k\in R} \left\|\left(A_j\right)_k\right\|_2, \tag{5}$$

where $A = [A_1, A_2, \ldots, A_N] \in R^{N\times N}$, and $(A_j)_k$ is the vector of elements that are subscript to k.

In order to obtain the solution of the model, we deduce it according to the following steps. As for l_1 optimization problem $\min_{\alpha} \|D\alpha - x\|_2^2 + \lambda\|\alpha\|_1$, least absolute shrinkage and selection operator (LASSO) can be adopted to obtain the optimal result. As for l_2 optimization problem $\min_{\alpha} \|D\alpha - x\|_2^2 + \lambda\sum_{k\in R} w_k\|\alpha_k\|_2$, group LASSO can be adopted, where w_k is the number of elements in each group. As for $l_{1,2}$ optimization problem, some scholars introduced the block coordinate descent into group LASSO.

If the data patches, whose subscript set is K, are selected and other patches are fixed, (3) can be rewritten as follows:

$$\min_{\alpha_k} \frac{1}{2}\left\|X_K\alpha_K - x\right\|_2^2 + \lambda\left\|\alpha_K\right\|_2^2, \tag{6}$$

where k_i is a matrix composed of column vectors whose subscripts belong to K in X. Through the patches threshold method, we can get the following:

$$\alpha_k = \begin{cases} 0, & if\ \left\|X_K^T x\right\|_2 \le \lambda, \\ \left(X_K^T X_K + \delta\lambda I\right)^{-1} X_K^T x, & if\ \left\|X_K^T x\right\|_2 > \lambda, \end{cases} \tag{7}$$

where $\delta > 0$ and $\delta^{-1} = \|(X_K^T X_K + \delta\lambda I)^{-1} X_K^T x\|_2$ when $\|X_K^T x\|_2 > \lambda$ is given.

If δ can satisfy $\delta^{-1} = \|(X_K^T X_K + \delta\lambda I)^{-1} X_K^T x\|_2$, δ is the root of the equation $f(\delta) = 1$. If $X_K^T X_K = \begin{bmatrix} \sigma_1 & \cdots & 0 \\ \vdots & \ddots & \vdots \\ 0 & \cdots & \sigma_L \end{bmatrix}$ makes sense, we have

$$f(\delta) = \delta\left\|\left(X_K^T X_K + \delta\lambda I\right)^{-1} X_K^T x\right\|_2 = \sqrt{\sum_i \frac{\delta^2\left(X_K^T x\right)_i^2}{\left(\delta\lambda + \sigma_i\right)^2}}, \tag{8}$$

where is the number of elements in K. When $\delta = 0$, we can get $f(\delta) = 0$; if $\delta \longrightarrow \infty$ and $\|X_K^T x\|_2 > \lambda$, the following results can be obtained:

$$\lim_{\delta\longrightarrow\infty} f(\delta) = \lim_{\delta\longrightarrow\infty} \sqrt{\sum_i \frac{\left(X_K^T x\right)_i^2}{\left(\lambda + \sigma_i/\delta\right)^2}} = \sqrt{\sum_i \frac{\left(X_K^T x\right)_i^2}{\lambda}} > 1. \tag{9}$$

Thus, it is shown that there are solutions to $f(\delta) = 1$. It is assumed that the partition K is known, but in reality, the division $\mathfrak{R}$ is required to solve the subspace clustering problem. The closer the selection of division is to the real subspace division of the data, the closer the actual subspace representation is to the solution of equation (5). When $\mathfrak{R}$, equation (4) becomes an l_1 optimization problem, while equation (5) is transformed into a sparse model. It is worth noting that the division in $\mathfrak{R}$ often needs to be finer than the real division, which is to ensure that it is closer to the real division. Using some traditional clustering methods, such as k-means clustering, a preliminary division of the data can be obtained. In this paper, sparse agglomerative clustering (SAC) is adopted to determine the preliminary data division. In the construction of the block-sparse dictionary, the SAC algorithm can obtain the patch structure of the dictionary, which is the division of the dictionary atoms. The SAC algorithm introduces the index of the class and gradually merges the closest atoms to achieve the purpose of clustering. The clustering process does not need to define the number of classes but defines the upper bound of the number of elements in the class to limit the final clustering result.

4. Experimental Results and Analysis

4.1. Experimental Data and Configuration. In order to better show the advantages of the improved sparse subspace clustering segmentation method, this paper selects simulated brain MRI and real brain MRI data for simulation analysis. The real brain MRI data is 30 slices of 3D T1WI MRI images of adult male head with 3 mm slice provided by the Department of Radiology, West China Medical University. The simulation brain MRI is from the database BrainWeb, where BrainWeb provides standard segmentation results and is convenient for quantitative evaluation. It can help the validation of quantitative analyses of hippocampus.

The simulation platform uses MATLAB v7.8 (r2009a) and runs on core i5 processor with 8G memory and 2.94Ghz main frequency. The comparison algorithms used in this paper are sparse subspace clustering (SSC) [23], low-rank representation (LRR) [24], fuzzy GMM [25], LSM [26], and U-Net [27]. The first three models are the best algorithms in the traditional model, while U-Net is a semantic segmentation algorithm based on full convolution network, which is widely used in the field of natural image segmentation. In this paper, the contrast of brain MRI images is very low. The existing deep network algorithm is not adaptable. All comparison algorithms use the source code or executable file given by the author. It is worth noting that the test data selected in the experiment are the most challenging sequences available. In all experiments, all parameters of each algorithm are fixed to verify the robustness and stability of the proposed segmentation method. Therefore, in all experiments, if there is no special explanation, the parameters are set as follows: $c_0 = 2$, $u = 1$, $\lambda = 10$, $\nu = 0.05$, $\tau = 2$, and $\sigma = 1$.

In order to qualitatively evaluate the performance of all the comparison algorithms, we use false negative ratio (FNR), ratio of segmentation error (RSE), and dice similarity coefficient (DSC) to measure the segmentation accuracy. It is assumed that S_1 is denoted as the segmentation region obtained by each model and S_2 is the real boundary of a given image, so the previously mentioned three evaluation criteria are defined as follows:

$$\mathrm{FNR} = \frac{N(S_1/S_2)}{N(S_1)},$$

$$\mathrm{RSE} = \frac{N(S_1/S_2) + N(S_2/S_1)}{N(\Omega)}, \quad (10)$$

$$\mathrm{DSC} = \frac{2N(S_1 \cap S_2)}{N(S_1) + N(S_2)},$$

where $N(*)$ represents the number of pixels in the closed area. The closer the values of FNR and RSE are to zero and the closer the values of DSC are to one, the higher the image segmentation accuracy is.

4.2. Qualitative and Quantitative Analyses for Simulated Brain MRI. In order to better verify the effectiveness of the proposed method, it is tested on simulated brain MRI images and compared with the segmentation results of several classical algorithms. The data used in the experiment is from BrainWeb database. The test images were $T1$ weighted, 181×217 in size, and 1 mm in thickness. Before the experiment, extracranial tissues, such as blood vessels, cranium, and neuroticism, were removed and set as the background. In this paper, different slice images with added noise are selected as experimental data. Figure 3 shows the segmentation result processed by different algorithms.

Figure 3(a) shows the original brain MR image; the image in Figure 3(b) adds Gaussian noise with a variance of 10; Figure 3(c) shows the standard segmentation results; Figures 3(c)–3(h) show the corresponding segmentation results of the comparison algorithm. Through the qualitative comparison of segmentation results, SSC and LRR methods cannot get satisfactory segmentation results, and there are obvious false segmentation points in fuzzy GMM and LSM. In contrast, the proposed model gets the best segmentation results among the five methods, especially in the boundary region and detail texture region. It can be seen from the segmentation result that, with the increase of noise, the segmentation accuracy of each algorithm decreases gradually. This is because the noise has a certain impact on the segmentation accuracy of brain image. The greater the noise is, the greater the texture change of brain image is, and the regions with more detail information are prone to partial misclassification. By comparing the five segmentation algorithms, we can see that the proposed algorithm can get the highest segmentation accuracy in the brain MR images of hippocampus under different noise levels.

It can be seen from the result that our proposed model uses the improved coefficient matrix with the patch-sparse constraint on brain MRI image. It can not only successfully extract the hippocampus tissue but also remove many misclassification points. The segmentation effect is obviously better than the other five comparison algorithms. By comparing with the standard segmentation results, the segmentation accuracy of each algorithm under different noises is given in Table 1. The experimental data are obtained by averaging for each slice under the same noise. It can be seen from the table that fuzzy-GMM algorithm achieves better segmentation effect under some conditions, and the segmentation accuracy of the proposed model is the highest in most cases. With the increase of noise level, the difference of FNR and RSE value of our model is very small, while the decrease of other comparison algorithms is obvious. The experimental results show that the noise has a great influence on the segmentation accuracy of brain MR images, and the larger the noise are, the easier it is to produce wrong classification. However, according to the results in Table 1, the proposed model is less affected by noise.

The previously mentioned analysis shows that the segmentation accuracy is different under different noises. In order to facilitate intuitive analysis, we draw three curves to show the segmentation results of different algorithms in Figure 4. The FNR, RSE, and DSC indexes of our proposed algorithm are better than those of other algorithms, especially DSC. In the general segmentation algorithm, when the contrast of the image becomes worse or the noise becomes larger, it is more difficult to distinguish the boundary of LSM from the anatomical characteristics of brain tissue. Therefore, the combination of sparsity and low rank is more effective than the general single model, which can reduce the impact of noise on segmentation and retain the corresponding details.

4.3. Qualitative and Quantitative Analyses for Real Brain MRI. The real brain MRI data is 30 slices of 3D T1WI MRI images of adult male head with 3 mm slice provided by the Department of Radiology, West China Medical University. Table 2 shows the quantitative indicators of different algorithms. It can be seen that the segmentation performance for noisy images is not good. Although sparse and low-rank model is an effective processing strategy, it still has a shortcoming. First of all, the model requires sparse constraints on all image patches, which greatly reduces the real-time performance and improves the complexity of the model. The segmentation model proposed in this paper. LSM is an improved level-set model. From the analysis of segmentation effect, the traditional level-set method has the phenomenon of undersegmentation. This method only uses the gradient information of the image boundary, so the zero level-set curve is easy to stay in the nonobject region with large gradient value in the iterative process, which makes the final evolution result deviate from the real boundary of the hippocampus, and the hippocampus contour cannot be accurately segmented.

In order to quantitatively compare the segmentation performance on real brain MRI tissue, the real brain MRI database is used for experiments, which can provide the standard segmentation results, which is convenient to quantitatively evaluate the performance. $T1$ weighted brain MRI images with 1 mm slice thickness and 9% noise level are used as experimental data. In this paper, 20 slices in different positions are tested, and the segmentation result is shown. Due to the influence of space, we only give the segmentation results of our proposed algorithm, as shown in Figure 5. The segmentation results of fuzzy-GMM algorithm still contain a lot of noise. SSC algorithm, LRR algorithm, and proposed

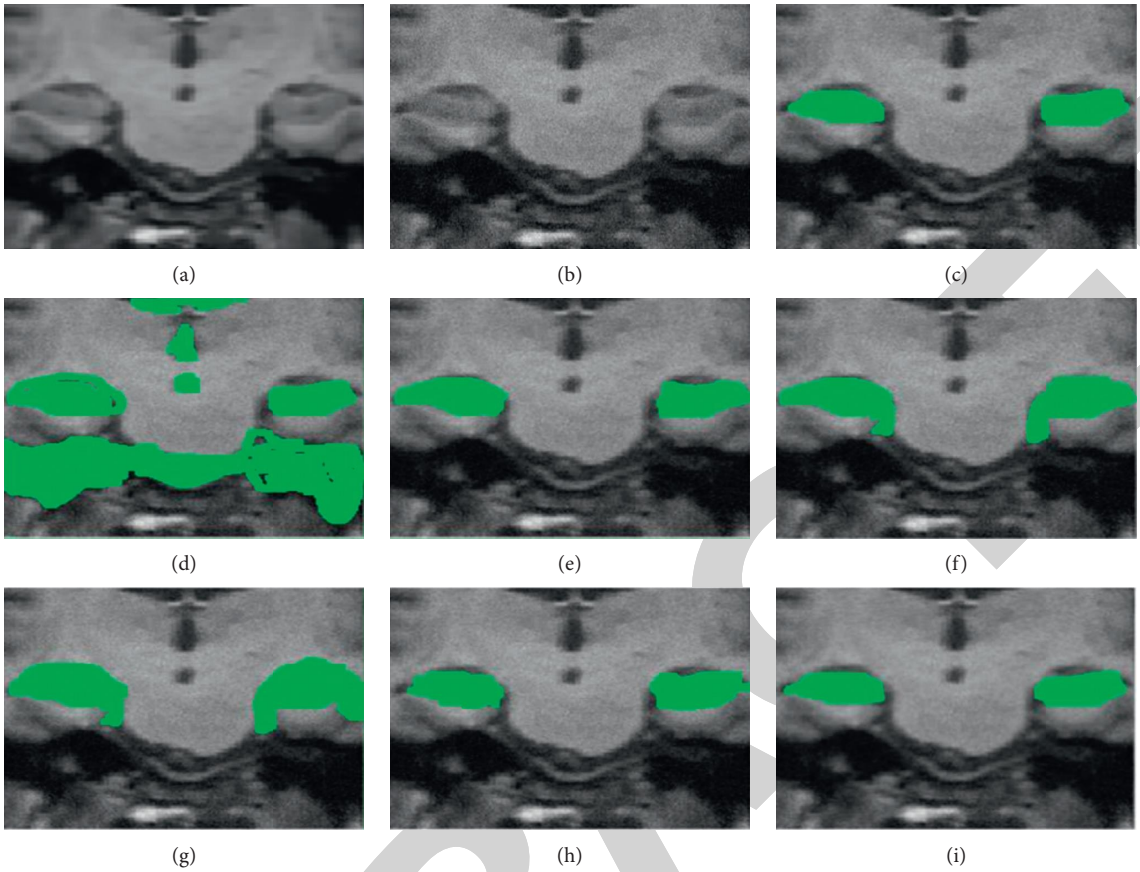

Figure 3: Segmentation result of different algorithms: (a) raw MRI, (b) noisy MRI, (c) benchmark result, (d) fuzzy-GMM, (e) LSM, (f) SSC, (g) LRR, (h) U-Net, and (i) proposed.

Table 1: Quantitative results for comparison models in different noises.

σ		SSC	LRR	Fuzzy GMM	LSM	U-Net	Proposed
5	FNR	0.461	0.407	0.461	0.512	0.523	0.453
	RSE	0.082	0.089	0.099	0.182	0.181	0.089
	DSC	0.761	0.808	0.891	0.782	0.831	0.903
10	FNR	0.357	0.543	0.504	0.516	0.621	0.707
	RSE	0.075	0.087	0.098	0.078	0.086	0.060
	DSC	0.682	0.836	0.718	0.805	0.816	0.836
20	FNR	0.316	0.593	0.623	0.485	0.707	0.718
	RSE	0.068	0.067	0.070	0.072	0.074	0.064
	DSC	0.579	0.531	0.690	0.734	0.752	0.792
30	FNR	0.297	0.282	0.317	0.378	0.322	0.252
	RSE	0.050	0.063	0.052	0.036	0.060	0.044
	DSC	0.508	0.471	0.523	0.658	0.680	0.697

algorithm in this paper all remove the interference of noise very well. In terms of details, the proposed algorithm is the most complete for the preservation of the hippopotamus in brain MRI image.

Figure 6 shows the segmentation results of the comparison algorithm on the real brain MRI images. Figure 6(a) is the original image; Figure 6(b) is the manually segmented hippocampus image; Figure 6(c) is the segmentation result obtained by the improved U-Net algorithm; Figure 6(d) is the segmentation result obtained by the fuzzy-GMM algorithm. The segmentation effect of our proposed subspace clustering segmentation is improved, and the segmentation result is the closest to that of manual annotation. The segmentation effect is the best, compared with other comparison algorithms in this paper. The sparse subspace clustering model SSC, low-rank subspace clustering model LRR, and block-sparse subspace in this paper are used.

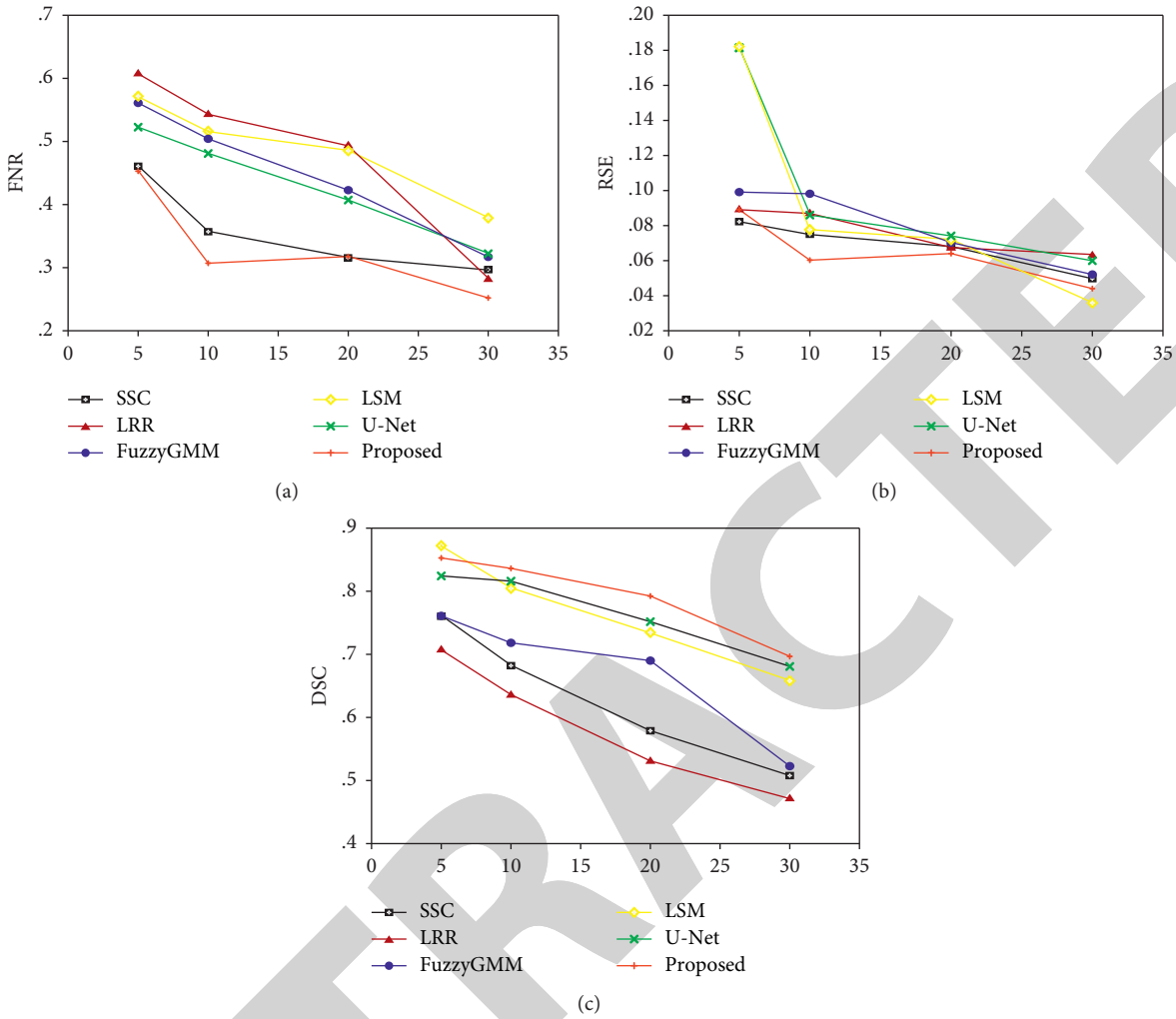

Figure 4: Segmentation curves for (a) FNR, (b) RSE, and (c) DSC indexes in different noises.

Table 2: Quantitative results for comparison models in real brain MRI.

	SSC	LRR	Fuzzy GMM	LSM	U-Net	Proposed
FNR	0.477	0.608	0.63	0.633	0.724	0.71
RSE	0.097	0.102	0.103	0.127	0.133	0.085
DSC	0.516	0.469	0.558	0.634	0.651	0.647

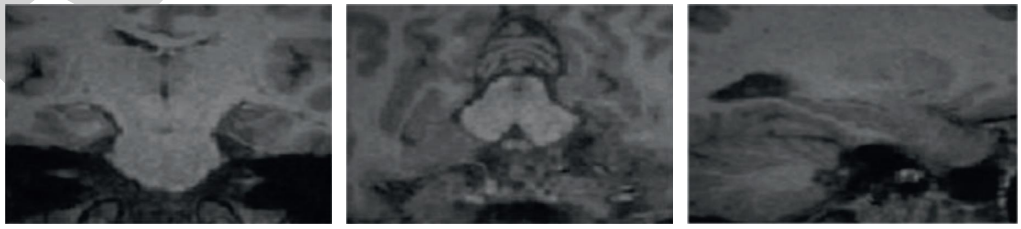

(a)

Figure 5: Continued.

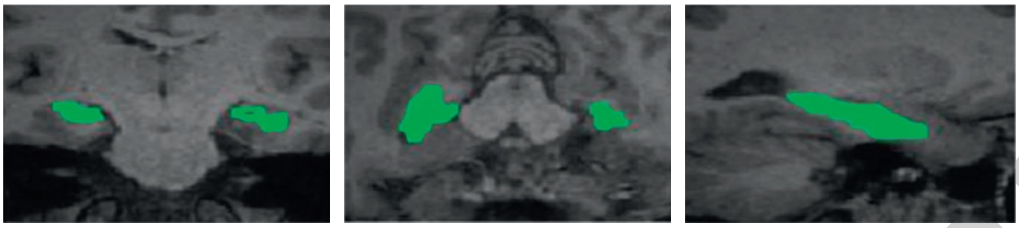

(b)

Figure 5: Segmentation results of our proposed algorithm. (a) Raw data; (b) segmentation results.

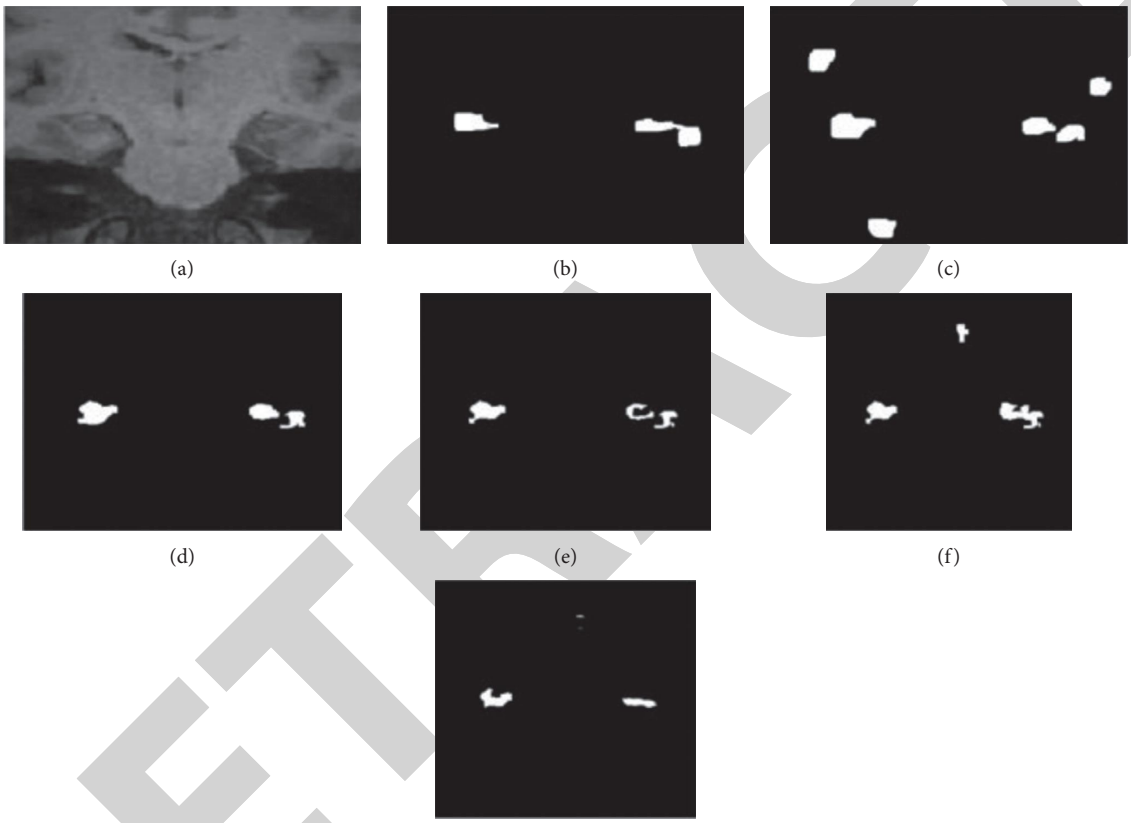

(a) (b) (c) (d) (e) (f) (g)

Figure 6: Segmentation results of different algorithms. (a) Raw data, (b) benchmark result, (c) U-Net, (d) fuzzy-GMM, (e) SSC, (f) LRR, and (g) proposed.

5. Conclusion

Since the hippocampus is of small size, low contrast, and irregular shape, a novel hippocampus segmentation method based on subspace patch-sparsity clustering in brain MRI is proposed to improve the segmentation accuracy, which regards the super pixel as the point of the image and chooses the matrix of the super pixel as the projection dictionary. By restraining the coefficient matrix with the patch-sparse constraint, the coefficient matrix contains a patch-sparse structure, which is helpful to the hippocampus segmentation. The experimental results show that our proposed method is effective in the noisy brain MRI data, which can well deal with hippocampus segmentation problem.

Data Availability

The labeled datasets used to support the findings of this study are available from the corresponding author upon request.

Conflicts of Interest

The authors declare no conflicts of interest.

Acknowledgments

This work was supported by the Health and Family Planning Commission of Changshu, under Grant csws201820.

Hindawi
Journal of Healthcare Engineering
Volume 2021, Article ID 1521013, 6 pages
https://doi.org/10.1155/2021/1521013

Research Article

A PLA2R-IgG4 Antibody-Based Predictive Model for Assessing Risk Stratification of Idiopathic Membranous Nephropathy

Xiaobin Liu,[1] Jing Xue,[2] Xiaoyi Guo,[2] Yijie Ding,[3] Yi Zhang,[4] Xiran Zhang,[2] Yiqing Huang,[2] Biao Huang,[5] Zhigang Hu,[6,7] Guoyuan Lu,[1] and Liang Wang[2]

[1]*Department of Nephrology, The First Affiliated Hospital of Soochow University, Suzhou 215006, China*
[2]*Department of Nephrology, The Affiliated Wuxi People's Hospital of Nanjing Medical University, Wuxi 214023, China*
[3]*Yangtze Delta Region Institute (Quzhou), University of Electronic Science and Technology of China, Quzhou 324000, China*
[4]*NHC Key Laboratory of Nuclear Medicine, Jiangsu Key Laboratory of Molecular Nuclear Medicine, Jiangsu Institute of Nuclear Medicine, Wuxi 214063, China*
[5]*College of Life Sciences and Medicine, Zhejiang Sci-Tech University, Hangzhou 310018, China*
[6]*Medical Laboratory, The Affiliated Wuxi Children's Hospital of Nanjing Medical University, Wuxi 214023, China*
[7]*Medical Laboratory, The Affiliated Wuxi People's Hospital of Nanjing Medical University, Wuxi 214023, China*

Correspondence should be addressed to Guoyuan Lu; snklgy@126.com and Liang Wang; wangliang_wuxi@126.com

Received 6 August 2021; Revised 19 August 2021; Accepted 20 August 2021; Published 31 August 2021

Academic Editor: Shengrong Gong

Background. Known as an autoimmune glomerular disease, idiopathic membranous nephropathy (IMN) is considered to be associated with phospholipase A2 receptor (PLA2R) in terms of the main pathogenesis. The quantitative detection of serum PLA2R-IgG and PLA2R-IgG4 antibodies by time-resolved fluoroimmunoassay (TRFIA) was determined, and the value of them, both in the clinical prediction of risk stratification in IMN, was observed in this study. *Methods*. 95 patients with IMN proved by renal biopsy were enrolled, who had tested positive for serum PLA2R antibodies by ELISA, and the quantitative detection of serum PLA2R-IgG and PLA2R-IgG4 antibodies was achieved by TRFIA. All the patients were divided into low-, medium-, and high-risk groups, respectively, which were set as dependent variables, according to proteinuria and renal function. Random forest (RF) was used to estimate the value of serum PLA2R-IgG and PLA2R-IgG4 in predicting the risk stratification of progression in IMN. *Results*. Out-of-bag estimates of variable importance in RF were employed to evaluate the impact of each input variable on the final classification accuracy. The variable of albumin, PLA2R-IgG, and PLA2R-IgG4 had high values (>0.3) of 0.3156, 0.3981, and 0.7682, respectively, which meant that these three were more important for the risk stratification of progression in IMN. In order to further assess the contribution of PLA2R-IgG and PLA2R-IgG4 to the model, we built four different models and found that PLA2R-IgG4 played an important role in improving the predictive ability of the model. *Conclusions*. In this study, we established a random forest model to evaluate the value of serum PLA2R-IgG4 antibodies in predicting risk stratification of IMN. Compared with PLA2R-IgG, PLA2R-IgG4 is a more efficient biomarker in predicting the risk of progression in IMN.

1. Introduction

Idiopathic membranous nephropathy (IMN), known as primary membrane nephropathy, is the most common cause of primary nephropathy syndrome in adults [1, 2], which is approximately 20%~30% of all the renal pathological biopsy reports [3]. IMN is usually manifested as nephropathy syndrome and depends on renal biopsy in diagnosis [4]. Although the study demonstrated that patients with IMN who received only symptomatic treatment had a relatively benign course, end-stage renal disease developed in 16% of the patients during a 5-year follow-up [5]. Therefore, it is critical to identify the degree of disease activity and progression risk in patients with IMN.

In 2009, Beck et al. [6] found 70% of the patients with IMN had antibodies against a conformation-dependent epitope in M-type phospholipase A2 receptor (PLA2R) which was present in normal podocytes and colocalized with

IgG4 in immune deposits in glomeruli. Currently, PLA2R antibodies have been confirmed to be major pathogenic antibodies in IMN [7], which are mainly IgG4, and the titer levels of anti-PLA2R antibodies are related to the activity of the disease [8, 9]. In 2019, Kidney Disease Improving Global Outcomes (KDIGO) recommended that quantitative detection and regular follow-up of anti-PLA2R antibodies would contribute to differential diagnosis and assessment of activity in IMN [10].

At present, the detection of sera anti-PLA2R antibodies normally applies indirect immunofluorescence assay (IIFA) and enzyme-linked immunosorbent assay (ELISA) [11]. IIFA is not a quantitative detection measure, while ELISA is characterized by low detection sensitivity [12]. In 2017, Huang et al. [13] developed an ultrasensitive quantitative assay, using time-resolved fluoroimmunoassay (TRFIA), for the detection of anti-PLA2R-IgG testing. Establishing the cutoff value for anti-PLA2R-IgG of 1990 ng/mL, the diagnostic sensitivity and specificity in IMN were 74% and 100%, respectively. Huang et al. [14] further tested anti-PLA2R-IgG4 and found that the diagnostic sensitivity and specificity in IMN were 90% and 100%, respectively when established the cutoff value for anti-PLA2R-IgG4 of 161.2 ng/mL.

In this study, we determined the quantitative detection of anti-PLA2R-IgG and -IgG4 antibodies by TRFIA and observed the value of them both in the clinical prediction of different risk-stratified IMN.

2. Materials and Methods

2.1. Subjects Selection. A total of 95 patients with IMN proved by renal biopsy, who had tested positive for serum PLA2R antibodies by ELISA, from the Affiliated Wuxi People's Hospital of Nanjing Medical University, were enrolled from January 2016 to December 2017. According to proteinuria <4 g/d, 4–8 g/d, and >8 g/d, with renal function taken into consideration, all the patients were divided into low-, medium-, and high-risk groups, respectively [15].

Blood samples were collected before renal biopsy and before the immunosuppressive therapy, which were left standing to clot thoroughly before centrifuging at 3000 rpm/min for 4 min to obtain serum, and sera were then stored at −80°C for pending analysis. All renal tissue specimens were examined using light microscope, immunofluorescence, and electron microscope. Pathological grading was performed by Ehrenreich and Churg standards [16].

Goat anti-human IgG antibodies were obtained from Jackson ImmunoResearch (USA), and mouse anti-human IgG4 antibodies were offered by Hytest (Finland). Europium labeling kits (1244-302) were purchased from Perkin Elmer (USA). The polystyrene microtiter plates were obtained from Nunc International (Denmark). The recombinant PLA2R antigen, series of standards of anti-human PLA2R-IgG and PLA2R-IgG4 were prepared in our laboratory as previously reported [13, 14]. All the buffer solutions were supplied from Jiangyuan Co. (China). The other reagents were of analytical grade and obtained from Sinopharm Chemical Reagent (China). An AutoDELFIA$_{1235}$ was purchased from Perkin Elmer (USA).

2.2. Anti-PLA2R-IgG and PLA2R-IgG4 Detection Procedure. Firstly, 100 μL of standards or diluted sera were pipetted to the microtiter plates fixed with 5 μg/mL of rPLA2R. The working dilutions of serum samples were 1 : 200 and 1 : 20 in the anti-PLA2R-IgG and anti-PLA2R -IgG4 assays, respectively. The mixture was reacted with continuously shaking at 25°C for 1 h. After the unreacted substances were removed by washing for 3 times, the plates were pipetted with europium-labelled goat anti-human IgG or mouse anti-human IgG4 antibodies, shaken for 1 h at 25°C, and then rinsed for 6 times. Finally, 96-well plates were added with 200 μL of enhancement solution, agitated for 5 min, and measured in AutoDELFIA$_{1235}$. The concentrations of serum samples of anti-PLA2R-IgG and anti-PLA2R-IgG4 were automatically calculated from the fluorescence of wells by AutoDELFIA$_{1235}$. According to the previous work [13, 14], the cutoff values were 1990 ng/mL and 161.2 ng/mL for anti-PLA2R-IgG and anti-PLA2R-IgG4, respectively.

2.3. Statistical Analyses. This work employed 38 features (variables) including pathological and clinical features to describe the patients' characters, which contained mean, standard deviation, and correlation coefficient of samples as shown in Table 1. The three groups (low-, medium-, and high-risk groups), which were divided according to proteinuria and renal function, were set as dependent variables. The results demonstrated that PLA2R-IgG (0.394) and PLA2R-IgG4 (0.524) had great correlation coefficients with the dependent variables. In our study, the number of patients in class 1, 2, and 3 (three types of risk stratification) was 45, 41, and 9, respectively.

2.4. Random Forest. In machine learning, the random forest (RF) [17] is a classifier that contains multiple decision trees, and the output category is determined by the mode of the category output by the individual trees. In this work, random forest was used as an analysis and classification tool to estimate the value of serum PLA2R-IgG and PLA2R-IgG4 in predicting the risk stratification of progression in IMN. Compared with k-nearest neighbor (KNN) and support vector machines (SVM) classifiers, it has the following advantages: (1) it can assess the importance of variables when determining categories; (2) when building a forest, it can produce an unbiased estimate of the generalized error internally; (3) for unbalanced classification data sets, it can balance errors; (4) the learning process is fast.

3. Results

3.1. Evaluation Measurements. The accuracy (ACC) is utilized to evaluate the performance of the RF model under 5-fold cross-validation (5-CV). The calculation method of ACC is as follows:

Table 1: The information of data set.

No.	Feature (variable)	Value	r^*
1	Age (years)	55.110 ± 15.110	0.175
2	Gender (males/females)	56/39	0.105
3	Renal tubular atrophy score	1.057 ± 0.721	0.080
4	Renal interstitial fibrosis score	1.100 ± 0.731	0.113
5	Renal interstitial lymphoplasmacytic infiltrate score	1.068 ± 0.861	0.187
6	Total score of renal tubular and interstitium	3.236 ± 2.138	0.136
7	Pathological stage of IMN	1.452 ± 0.495	0.009
8	IF IgA	0.220 ± 0.477	0.089
9	IF IgM	0.252 ± 0.635	0.034
10	IF IgG	2.789 ± 0.697	0.009
11	IF C1q	0.242 ± 0.488	0.098
12	IF C3	1.205 ± 0.738	−0.035
13	Renal tissue PLA2R antigen	0.952 ± 0.357	−0.031
14	SBP (mmHg)	133.389 ± 14.973	0.017
15	DBP (mmHg)	79.989 ± 9.079	−0.109
16	Serum C3 (mg/L)	894.305 ± 253.312	−0.008
17	Serum C4 (mg/L)	241.147 ± 87.192	0.058
18	Serum IgA (g/L)	5.206 ± 28.002	0.061
19	Serum IgG (g/L)	7.084 ± 2.891	−0.077
20	Serum IgM (g/L)	1.257 ± 0.637	−0.013
21	Serum albumin (g/L)	23.335 ± 8.233	−0.449
22	Hematuria (/uL)	102.377 ± 138.301	−0.014
23	Serum creatinine (umol/L)	83.664 ± 34.042	0.168
24	eGFR-EPI (ml/min)	86.535 ± 24.060	−0.189
25	BUN (mmol/L)	4.986 ± 1.929	0.172
26	Serum glucose (mmol/L)	5.142 ± 0.810	0.321
27	Serum lithic acid (umol/L)	344.676 ± 89.678	0.048
28	TG (mmol/L)	2.406 ± 1.471	0.415
29	TC (mmol/L)	7.119 ± 2.289	0.141
30	LDL-C (mmol/L)	3.902 ± 1.379	0.077
31	HDL-C (mmol/L)	1.323 ± 0.432	−0.110
32	WBC ($\times 10^9$/L)	8.577 ± 13.978	0.088
33	Hemoglobin (g/L)	122.204 ± 24.962	0.058
34	PLT ($\times 10^9$/L)	219 ± 65.409	−0.104
35	C-reactive protein (mg/L)	2.807 ± 3.167	0.057
36	ESR (mm/H)	53.589 ± 34.176	0.233
37	Serum PLA2R-IgG (ng/mL)	5243.957 ± 9282.902	0.394
38	Serum PLA2R-IgG4 (ng/mL)	1762.615 ± 2662.328	0.524

*denotes that each feature correlated with risk stratification of progression in IMN using Pearson correlation coefficient (r).

$$\text{whole ACC} = \frac{\sum_{i=1}^{c} TP^i}{M} \times 100\%,$$
$$\text{ACC}^i = \frac{TP^i}{M^i} \times 100\%, \quad (1)$$
$$M = \sum_{i=1}^{c} M^i,$$

where c denotes the number of classes. TP^i denotes the number of true positive (TP) in subclass i. M and M^i denote the number of whole test samples and subclass test samples. ACC^i denotes the accuracy in subclass i.

3.2. Relative Importance of Inputs in Estimating IMN. To evaluate the impact of each input variable on the final classification accuracy. We employed out-of-bag estimates of variable importance in RF. The RF stored the increase in mean square error (MSE) averaged over all trees in the ensemble and divided by the standard deviation taken over the trees, for each variable. So, we could get the importance scores of all input variables. In general, the larger the score, the more important it is for the prediction model. Figure 1 shows the results of relative importance for inputs. It could be seen from the figure that the 21-th (albumin), 37-th (PLA2R-IgG), and 38-th (PLA2R-IgG4) variables had high values (>0.3) of 0.3156, 0.3981, and 0.7682, respectively.

3.3. Comparison of PLA2R-IgG and PLA2R-IgG4. In order to further evaluate the contribution of PLA2R-IgG and PLA2R-IgG4 to the model, we constructed four different models, which contain both PLA2R-IgG and PLA2R-IgG4 variables, PLA2R-IgG variable, PLA2R-IgG4 variable, and no PLA2R-IgG and PLA2R-IgG4 variables. The relevant information of the models is shown in Table 2.

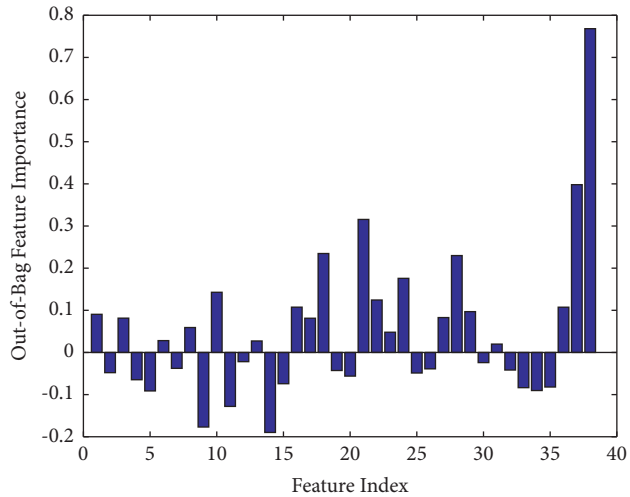

Figure 1: Relative importance for inputs.

Table 2: The information of models.

Model	Number of features (variables)	
Model 1	38	With PLA2R-IgG and PLA2R-IgG4
Model 2	37	With PLA2R-IgG and without PLA2R-IgG4
Model 3	37	Without PLA2R-IgG and with PLA2R-IgG4
Model 4	36	Without PLA2R-IgG and PLA2R-IgG4

The classification performance of the 4 models was verified by 5-fold cross-validation. And, the results are listed in Table 3. Obviously, when PLA2R-IgG and PLA2R-IgG4 were included, the prediction performance of the model (model 1) was the best, and the overall classification accuracy was 0.6743. In the overall ACC, the performance of model 2 (0.6422) was not better than model 3 (0.6639). This further verified that PLA2R-IgG4 is more important than PLA2R-IgG for classification accuracy. In addition, the performance of the model (model 4) was the worst (0.6290), when PLA2R-IgG4 and PLA2R-IgG were not contained at the same time. From the above test, it could be found that PLA2R-IgG and PLA2R-IgG4 were very helpful for classification. However, PLA2R-IgG4 could achieve better results than PLA2R-IgG.

In this study, we employed t-test to evaluate the significant differences of average ACC between different models. The results were list in Table 4, which show that the differences between model 1 and other three models were significant. Furthermore, the P value of model 3 and model 4 was 0.0022. This means that the PLA2R-IgG4 feature had a more significant performance improvement compared to the ordinary model (without PLA2R-IgG and PLA2R-IgG4).

Table 3: Comparison on four models via 5-fold cross-validation.

Model	Overall ACC	ACC^1	ACC^2	ACC^3
Model 1	0.6743	0.8	0.6583	0.1
Model 2	0.6422	0.7778	0.5833	0.2
Model 3	0.6639	0.7778	0.6806	0
Model 4	0.6290	0.7556	0.6306	0

ACC^1: the accuracy of class 1; ACC^2: the accuracy of class 2; ACC^3: the accuracy of class 3.

Table 4: Analysis of statistical significance for different methods via 5-fold cross validation (10 times).

	P value
Between model 1 and model 2	$6.355e-4$
Between model 1 and model 3	0.0085
Between model 1 and model 4	$1.8e-5$
Between model 2 and model 3	0.1142
Between model 2 and model 4	0.1510
Between model 3 and model 4	0.0022

4. Discussion

It is widely recognized that IMN is an autoimmune glomerular disease in which autoantibodies combine with antigens on glomerular podocytes and deposit in glomerular capillary walls [18]. With the discovery of M-type phospholipase A2 receptor (PLA2R) which was identified as the major target antigen, progress was made in understanding the pathogenesis of IMN [6]. Circulating anti-PLA2R antibodies not only contribute to distinguish primary membranous nephropathy from secondary membranous nephropathy in diagnosis but also conduce to monitor the immunological activity degree during the treatment period [19]. Accordingly, the quantitative detection of circulating anti-PLA2R antibodies is particularly important in diagnosis and treatment of IMN.

Among all the PLA2R-IgG antibodies, PLA2R-IgG4 antibodies are predominant [6, 18]. Lacking of mature commercial testing means TRFIA was employed in this study for the quantitative detection of anti-PLA2R-IgG4 antibodies. As a novel nonisotopic labeling technology, TRFIA has the advantages of high sensitivity (10^{-18} mol/L), wide monitoring range, and less susceptibility to matrix interference [14]. Our previous work discovered that using the cutoff value of 161.2 ng/mL, anti-PLA2R-IgG4 had higher sensitivity in diagnosis than anti-PLA2R-IgG by the cutoff value of 1990 ng/mL (90% versus 74%) [14]. Therefore, we speculate that, in addition to anti-PLA2R-IgG, anti-PLA2R-IgG4 may be an efficient biomarker in the assessment of the severity and prognosis of IMN too.

In recent years, machine learning methods have been widely used in medicine [20–22] and biology [23–25] to solve difficult data analysis problems for researchers. In our study, RF was employed to evaluate the importance of all the features (input variables). And, we found that the 21th (albumin), 37th (PLA2R-IgG), and 38th (PLA2R-IgG4) variables had high values (>0.3) of 0.3156, 0.3981, and 0.7682, respectively, which meant these three features were more important to the risk stratification of progression in IMN. At the same time, as shown in Figure 1, PLA2R-IgG4 manifested a better predictive value compared with PLA2R-IgG (0.7682 versus 0.3981). In addition, it could be seen from Table 3 that the prediction effect of the PLA2R-IgG4 feature (0.6639) was better than that of the PLA2R-IgG feature (0.6422). When both PLA2R-IgG4 and PLA2R-IgG features were input into the model, its prediction performance was the best (0.6743). The above test results further validated the importance of PLA2R-IgG4 and PLA2R-IgG in assessing the risk level model. In Table 4, we evaluated the significant differences between different models. Obviously, the difference between model 1 and other models was significant (P value < 0.05). Compared with model 4, model 3 also had significant difference (P value $= 0.0022$). It was obvious that PLA2R-IgG4 played an important role in improving the predictive ability of the model.

5. Conclusions

In this study, we evaluated the value of serum PLA2R-IgG4 antibodies in predicting risk stratification of IMN by establishing a random forest model. Compared with PLA2R-IgG, PLA2R-IgG4 is a more efficient biomarker in predicting the risk of progression in IMN. The study results are satisfactory, while disadvantages remain (1) there is lack of analysis about the value of serum PLA2R-IgG4 in the prediction of treatment effect; (2) the sample size needs to be further expanded to minimize the prediction bias. In the next work, we will expand the sample size and survey the predictive effect of serum PLA2R-IgG4 in the therapeutic regimen and prognosis of IMN.

Data Availability

The data used to support the research can be obtained from the corresponding authors according to the requirements of the institution.

Ethical Approval

The experimental protocol was established, according to the ethical guidelines of the Helsinki Declaration and was approved by the Human Ethics Committee (Wuxi People's Hospital Ethics Committee). This study had been approved by the ethics committee of the hospital (ethical approval no. kyl2016001).

Consent

Written informed consent for publication was obtained from all participants.

Conflicts of Interest

The authors declare that they have no conflicts of interest.

Authors' Contributions

They are joint first authors: Xiaobin Liu, Jing Xue, Xiaoyi Guo.

Acknowledgments

Thanks to the Department of Nephrology of Wuxi People's Hospital for collecting data in this study. This study was funded by the Top Talent Support Program for Young and Middle-Aged People of Wuxi Health Committee (HB2020008), Medical and Public Health Project of Wuxi Sci-Tech Development Fund (WX18 II AN047), the Scientific research project of Wuxi Health Committee (MS201927), the Scientific research project of Wuxi Health Committee (Z201914), Major projects of precision medicine of Wuxi health Committee (J202001), Maternal and Child Health Research Project of Jiangsu Province (F202033), the Scientific Research Projects of Jiangsu Provincial Health Commission (LGY201801), and Jiangsu Province "333" Project (BRA2020142).

References

[1] J. M. Hofstra and J. F. M. Wetzels, "Management of patients with membranous nephropathy," *Nephrology Dialysis Transplantation*, vol. 27, no. 1, pp. 6–9, 2012.

[2] F. C. Fervenza, S. Sethi, and U. Specks, "Idiopathic membranous nephropathy: diagnosis and treatment," *Clinical Journal of the American Society of Nephrology*, vol. 3, pp. 905–919, 2008.

[3] X. Pan, J. Xu, H. Ren et al., "Changing spectrum of biopsy-proven primary glomerular diseases over the past 15 Years: a single-center study in China," *Contributions to Nephrology*, vol. 181, pp. 22–30, 2013.

[4] K. Zuo, Y. Wu, S.-J. Li, F. Xu, C.-H. Zeng, and Z.-H. Liu, "Long-term outcome and prognostic factors of idiopathic membranous nephropathy in the Chinese population," *Clinical Nephrology*, vol. 79, pp. 445–453, 2013.

[5] A. Schieppati, L. Mosconi, A. Perna et al., "Prognosis of untreated patients with idiopathic membranous nephropathy," *New England Journal of Medicine*, vol. 329, no. 2, pp. 85–89, 1993.

[6] L. H. Beck, R. G. Bonegio, G. Lambeau et al., "M-type phospholipase A2 receptor as target antigen in idiopathic membranous nephropathy," *New England Journal of Medicine*, vol. 361, pp. 11–21, 2009.

[7] J. N. Chi, T. S. Lai, C. F. Wu et al., "The relationship of anti-phospholipase A2 receptor antibody and C5a complement with disease activity and short-term outcome in idiopathic membranous nephropathy," *Journal of the Formosan Medical Association*, vol. 118, no. 5, pp. 898–906, 2019.

[8] S. Provatopoulou, D. Kalavrizioti, M. Stangou et al., "Circulating anti-phospholipase A2 receptor antibodies as a diagnostic and prognostic marker in Greek patients with idiopathic membranous nephropathy-a retrospective cohort study," *Romanian Journal of Internal Medicine*, vol. 57, no. 2, pp. 141–150, 2019.

[9] A. S. Bomback, "Management of membranous nephropathy in the PLA2R era," *Clinical Journal of the American Society of Nephrology*, vol. 13, no. 5, pp. 784–786, 2018.

[10] J. Floege, S. J. Barbour, D. C. Cattran et al., "Management and Treatment of Glomerular diseases (part1):Conclusions from a Kidney Disease: Improving Global Outcomes (KDIGO)," *Nephrology (Saint-Petersburg)*, vol. 24, no. 2, pp. 22–41, 2020.

[11] W. Schlumberger, N. Hornig, S. Lange et al., "Differential diagnosis of membranous nephropathy with autoantibodies to phospholipase A2 receptor 1," *Autoimmunity Reviews*, vol. 13, no. 2, pp. 108–113, 2014.

[12] G. Cheng, J. Liu, A. Gilbert et al., "Serum phospholipase A2 receptor antibodies and immunoglobulin G subtypes in adult idiopathic membranous nephropathy: clinical value assessment," *Clinica Chimica Acta*, vol. 490, pp. 135–141, 2019.

[13] B. Huang, L. Wang, Y. N. Cao et al., "Improvement of idiopathic membranous nephropathy diagnosis with ultrasensitive quantitative detection of anti-phospholipase A2 receptor," *The Journal of Allergy and Clinical Immunology*, vol. 139, no. 6, pp. 1988–1990 e2, 2017.

[14] B. Huang, Y. Zhang, L. Wang et al., "Phospholipase a2 receptor antibody IgG4 subclass improves sensitivity and specificity in the diagnosis of idiopathic membranous nephropathy," *Kidney Blood Press Res.*vol. 44, no. 4, pp. 848–857, 2019.

[15] C. Daniel, "Cattran.Idiopathic membranous glomerulonephritis," *Kidney International*, vol. 59, pp. 1983–1994, 2001.

[16] P. H. Nachman, J. C. Jennette, and R. J. Falk, "Membranous glomerulopathy," *Brenner BM. Brenner and Rector's the Kidney*pp. 1121–1131, Saunders, Boston, MA, USA, 9th edition, 2012.

[17] B. Leo, "Random forests," *Machine Learning*, vol. 45, no. 1, pp. 5–32, 2001.

[18] L. H. Beck and D. J. Salant, "Membranous nephropathy: from models to man," *Journal of Clinical Investigation*, vol. 124, no. 6, pp. 2307–2314, 2014.

[19] R. Ayalon and L. H. Beck, "Membranous nephropathy: not just a disease for adults," *Pediatric Nephrology*, vol. 30, no. 1, pp. 31–39, 2015.

[20] X. Y. Guo, W. Zhou, B. Shi et al., "An efficient multiple kernel support vector regression model for assessing dry weight of hemodialysis patients," *Current Bioinformatics*, vol. 16, pp. 284–293, 2021.

[21] J. Gao, L. Zhang, G. Yu, G. Qu, Y. Li, and X. Yang, "Model with the GBDT for colorectal adenoma risk diagnosis," *Current Bioinformatics*, vol. 15, pp. 971–979, 2020.

[22] Y. Jiang, Y. Zhang, C. Lin, D. Wu, and C. T. Lin, "EEG-based driver drowsiness estimation using an online multi-view and transfer TSK fuzzy system," *IEEE Transactions on Intelligent Transportation Systems*, vol. 22, no. 3, pp. 1752–1764, 2021.

[23] H. Wang, J. Tang, Y. Ding, and F. Guo, "Exploring associations of non-coding RNAs in human diseases via three-matrix factorization with hypergraph-regular terms on center kernel alignment," *Briefings in Bioinformatics*, 2021.

[24] Y. Jiang, X. Gu, D. Wu et al., "A novel negative-transfer-resistant fuzzy clustering model with a shared cross-domain transfer latent space and its application to brain CT image segmentation," *IEEE/ACM Transactions on Computational Biology and Bioinformatics*, vol. 18, no. 1, pp. 40–52, 2021.

[25] Y. Jiang, K. Zhao, K. Xia et al., "A novel distributed multitask fuzzy clustering algorithm for automatic MR brain image segmentation," *Journal of Medical Systems*, vol. 43, no. 5, 118 pages, 2019.